

UC Davis

Research Reports

Title

Calibration of Incremental-Recursive Flexible Damage Models in CalME Using HVS Experiments

Permalink

<https://escholarship.org/uc/item/59m8m9m1>

Authors

Ullidtz, Per
Harvey, John T
Tsai, Bor-Wen
[et al.](#)

Publication Date

2005-06-01

Peer reviewed

April 2006

Research Report: UCPRC-RR-2005-06

Calibration of Incremental-Recursive Flexible Damage Models in *CalME* Using HVS Experiments

Authors:

Per Ullidtz, Dynatest Consulting Inc
John Harvey, UC Davis
Bor-Wen Tsai, UC Berkeley
Carl Monismith, UC Berkeley

**This work was completed as part of Partnered Pavement
Research Program Strategic Plan Element 4.1:**

“Development of the First Version of a Mechanistic-Empirical Pavement Rehabilitation,
Reconstruction and New Pavement Design Procedure for Rigid and Flexible Pavements
(pre-Calibration of AASHTO 2002)”

PREPARED FOR:

California Department of Transportation
Division of Research and Innovation
Office of Roadway Research

PREPARED BY:

University of California
Pavement Research Center
Berkeley and Davis



DOCUMENT RETRIEVAL PAGE		Report No: UCPRC-RR-2005-06		
Title: Calibration of Incremental-Recursive Flexible Damage Models in <i>CalME</i> Using HVS Experiments				
Authors: Per Ullidtz, Dynatest Consulting Inc.; John Harvey, UC Davis; Bor-Wen Tsai, UC Berkeley; and Carl Monismith, UC Berkeley				
Prepared for: California Department of Transportation Division of Research and Innovation Office of Roadway Research		FHWA No.: F/CA/RR/2006/49		Date: Stage 5, May 2007
Contract number: UCPRC-RR-2005-06		Client Reference No: UCPRC-RR-2005-06		Status: Final, Caltrans approved
<p>Abstract: Caltrans is in the process of implementing Mechanistic-Empirical design procedures. All mechanistic-empirical methods must be validated/calibrated against the behavior of real pavements. This should be done before implementing models in design methods to ensure that designs will be reasonable. The Heavy Vehicle Simulator (HVS) provides a first step in this validation/calibration process. The short test section can be carefully constructed with well characterized materials and instrumented to measure the pavement response. The climatic conditions may be controlled or monitored closely and all load applications are known exactly. The pavement may also be tested until it fails. The HVS may be seen as “large scale” laboratory equipment, between the “small scale” laboratory equipment (triaxial tests, bending tests etc.) and the reality of real pavements, which have uncertainties regarding materials, loads and climatic conditions. The two HVSs owned by Caltrans have been used on 27 flexible pavement test sections, with varying combinations of asphalt and granular layers. Temperature control was used during the tests. Most sections have been instrumented with Multi-depth Deflectometers (MDDs) to compare the measured pavement deflections (at several depths) to the deflections predicted by mechanistic methods, during the full duration of tests carried to “failure” (in terms of rutting or cracking). Results from mechanistic models have been compared with the deflection measurements and performance as a first step prior to empirical calibrations with field results. The complete time history of each test has been compared rather than just the beginning and end measurements. This report presents the validation of the mechanistic models for asphalt fatigue and for permanent deformation with the HVS test results.</p>				
Keywords: Mechanistic-empirical, full-scale-testing, calibration, response, performance, flexible pavement .				
Proposals for implementation: None				
Related documents: Kannekanti, V., and Harvey, J. June 2005. <i>Sensitivity Analysis of 2002 Design Guide Rigid Pavement Distress Prediction Models</i> . Draft report prepared for the California Department of Transportation. Pavement Research Center, Institute of Transportation Studies, University of California Berkeley, University of California Davis. UCPRC-RR-2005-01				
Signatures:				
P. Ullidtz Principal Author	J. Harvey Co-principal Investigator	C. L. Monismith Co-principal Investigator	D. Spinner Editor	M. Samadian Caltrans Contract Mgr.

DISCLAIMER

The contents of this report reflect the views of the authors who are responsible for the facts and accuracy of the data presented herein. The contents do not necessarily reflect the official views or policies of the State of California or the Federal Highway Administration. This report does not constitute a standard, specification, or regulation.

EXECUTIVE SUMMARY

The first step in a mechanistic-empirical (ME) pavement design or evaluation is to calculate pavement response — in terms of stresses, strains, and/or displacements — using a mathematical (or mechanistic) model. In the second step, the calculated response is used as a variable in empirical relationships to predict structural damage (decrease in moduli or cracking) and functional damage (rutting and roughness) to the pavement.

Both of these steps must be reasonably correct. If the calculated response bears little resemblance to the pavement's actual response, there is no point in trying to use the calculation to predict future damage to the pavement. In other words, only if the calculated response is reasonably correct does it make sense to try to relate the damage to the pavement response.

This study's purpose was to evaluate the overall trends of the damage models in the draft software package called *CalME* against those of Heavy Vehicle Simulator (HVS) tests for which data was available. The report presents simulations of HVS tests using the set of distress models included in *CalME*. These models are for the typical flexible pavement distresses observed in California: asphalt fatigue, asphalt rutting, unbound layers rutting, and reflection cracking. An Incremental-Recursive approach (see item 4 below) was used for the simulations included in this report because this approach can accurately indicate pavement condition at different points during a pavement's life.

Approaches Included in *CalME*

CalME software provides the user with four approaches to evaluating or designing a flexible pavement structure:

1. Caltrans' current methods: the R-value method for new flexible structures and the deflection reduction method used by Caltrans for overlay thickness design for existing flexible pavements.
2. "Classical" Mechanistic-Empirical (ME) Design, which is based largely on the Asphalt Institute Method which uses very simple methods to characterize materials, climate, and traffic inputs.
3. An Incremental approach, which is a standard Miner's Law approach that permits damage calculation for the axle load spectrum and expected temperature regimes, but without updating of the material's properties through the life of the project. This is an approach similar to the one for cracking of asphalt included in the NCHRP 1-37A Pavement Design Guide, also referred to as the Mechanistic-Empirical Design Guide (MEPDG). This type of approach is calibrated against an end failure state (such as, 25 percent cracking of the wheelpath) and it assumes a linear accumulation of damage to get to that state.
4. An Incremental-Recursive approach in which the materials properties of the pavement — in terms of damage and aging — are updated as the pavement life simulation progresses.

The current Caltrans methods and the Classical method are very fast in terms of computational time, and user input is highly simplified. In *CalME* both of these options perform a "design" function, calculating and presenting pavement structures that meet the design requirements for the design traffic, materials, and climate.

For design practice the Classical and Caltrans methods should be used to produce a set of potential pavement sections. The Incremental-Recursive method should then be run to check the lowest-cost alternative designs in the set to be certain that they meet design requirements. Once the final design has been selected, its Incremental-Recursive output provides a prediction of the pavement condition across its entire life. The prediction of the pavement's condition through its life from the Incremental-Recursive output can be used as the first prediction for use in a pavement management system.

Use of Heavy Vehicle Simulator Data to Evaluate Models

The Incremental-Recursive models included in *CalME* were used to predict performance for all twenty-seven of the flexible pavement HVS tests performed so far as part of the Accelerated Pavement Testing (APT) program operated for the California Department of Transportation (Caltrans) by the University of California Pavement Research Center (UCPRC). The HVS test data in this report come from tests performed between the years 1995 and 2004. The HVS response data and corresponding laboratory test data were extracted from the UCPRC HVS database.

During HVS testing, pavement response - in terms of deflections at the surface and/or at multiple depths - may be measured. A Road Surface Deflectometer (RSD) measures deflections at the surface and is similar to the Benkelman Beam used to develop the current Caltrans overlay design method in the 1950s. A Multi-depth Deflectometer (MDD) measures deflections at multiple depths.

In order to accurately predict the gradual degradation of a pavement, the response model must predict measured deflections with reasonable accuracy. Although a model might predict deflections correctly, this ability does not guarantee that the model can also accurately predict the stresses and strains in all the pavement layers. However, the opposite is true: if a model predicts deflections incorrectly it will also produce incorrect stress and strain predictions. Therefore when attempting to calibrate ME models from HVS tests, the research team's first concern was to make sure that resilient deflections were predicted reasonably well for the duration of the test and for all load levels. This prediction depended on the moduli of all the pavement layers and on the changes to the moduli caused by fatigue damage, slip between asphalt layers, non-linear elastic characteristics of unbound layers, and the effect of confinement on granular layers. Once reasonably good agreement was achieved between the measured and the calculated deflections then the permanent deformation models could be calibrated with confidence.

Differences in boundary conditions, strain levels, and loading times, all of which can produce varied effects in materials, result in differing moduli values. In this study, methods used for determining moduli (also referred to as "stiffness") values included backcalculation from Falling Weight Deflectometer (FWD) and MDD data, and direct measurement — employing laboratory triaxial testing for unbound materials and flexural frequency sweep testing for asphaltic materials. Stiffnesses for the study's asphalt materials were taken primarily from flexural frequency sweep data. Stiffnesses for the unbound layers came primarily from MDD data backcalculation.

In practice the FWD is seen by the research team as the primary tool for stiffness measurement of all layers already constructed because it is used in the field on the full pavement system; this is thought to be appropriate because the boundary conditions are those of real pavement, and most Caltrans' work will be rehabilitation and reconstruction with at least some layers already in place. The research team saw the flexural beam test as the primary means for measuring the stiffness and fatigue characteristics of asphalt overlay materials for new layers. For new pavement construction, a combination of FWD testing on existing pavements and triaxial testing can be used to develop a database of stiffnesses of unbound granular layers and subgrades based on different characteristics, such as Unified Soil Classification System (USCS) classification.

The purpose of this study was to evaluate the overall trends of the *CalME* damage models against those of the HVS test results. This was accomplished by comparing deflections calculated using moduli determined from initial measurements and *CalME* damage calculations with measured deflections under HVS loading. The results presented in this report verify that, overall, the *CalME* damage trends for deflection and permanent deformation under loading are correct.

During HVS testing, deflections often increase markedly, sometimes becoming more than twice as high at the end of the test as they were at the beginning because of damage to the asphalt concrete caused by the repeated wheel loads. However, the flexible pavement design model of the NCHRP 1-37A Design Guide does not consider any decrease in the asphalt modulus as a result of fatigue damage (except for rehabilitation designs). In fact, the NCHRP 1-37A Design Guide includes a model for aging that predicts a continuous increase in the stiffness of the asphalt concrete layers across the life of the pavement, which results in increased stiffness and smaller predicted deflections as the pavement is subjected to trafficking. While the

aging is potentially important, the effect of updating stiffness for aging and not updating it for fatigue damage results in calculation of very unrealistic elastic responses in the pavement during its life. This makes it impossible to use the model to simulate an HVS test and, inversely, to use HVS tests to calibrate the model, except for pavements with extremely thick asphalt concrete layers where little fatigue should develop.

Results of HVS Test Simulation Using *CalME*

The series of HVS tests in this report are grouped here by goals, which are defined as follows:

- Goal 1, a comparison of new pavement structures with and without asphalt-treated permeable base (ATPB) layer under dry conditions, moderate temperatures, 20°C (HVS Sections 500RF, 501RF, 502CT, 503RF)
- Goal 3 Cracking, a comparison of reflection cracking performance of ARHM-GG (the acronym ARHM, asphalt rubber hot-mix gap-graded, refers to the material specification at the time of construction in April 1997.) and dense-graded asphalt concrete (DGAC) overlays placed on the cracked Goal 1 sections, dry conditions, 20°C (HVS Sections 514RF, 515RF, 517RF, 518RF)
- Goal 3 Rutting, a comparison of rutting performance of ARHM-GG and DGAC overlays of previously untrafficked areas of Goal 1 pavements, dry conditions, 40°C or 50°C at 50-mm depth, four different tire/wheel types (HVS Sections 504RF, 505RF, 506RF, 507RF, 508RF, 509RF, 510RF, 511RF, 512RF, 513RF)
- Goal 5, a comparison of new pavement structures with and without ATPB layer under wet conditions (water introduced into base layers), moderate temperatures, 20°C (HVS Sections 543RF, 544RF, 545RF)
- Goal 9, initial cracking of asphalt pavement with six replicate sections in preparation for later overlay, new pavement, ambient rainfall, 20°C (HVS Sections 567RF, 568RF, 569RF, 571RF, 572RF, 573RF)

CalME models that the simulations evaluated included:

- A stiffness model for asphalt concrete modulus as a function of reduced time based on the model used in NCHRP 1-37A Design Guide, with some adjustments based on field observations;
- An asphalt concrete fatigue model that predicts damage, in terms of decrease in modulus, as a function of load repetitions, tensile strain, and stiffness, using parameters from flexural beam testing;
- An ability to model partial bonding between asphalt concrete layers;
- A model that adjusts the stiffness of unbound layers as a function of the combined bending resistance (a function of their stiffness and thickness) of the layers above them;
- A model that adjusts the stiffness of unbound layers as a function of load level, with an increased load level increasing the moduli for the granular layers and decreasing modulus for the subgrade (clay);
- A permanent deformation model for asphalt concrete as a function of permanent shear strain near the pavement surface beneath the edge of a tire, with permanent shear strain predicted by the calculated elastic shear strain and elastic shear stress;
- A permanent deformation model for unbound layers as a function of the vertical strain at the top of each layer; and
- A reflection cracking model based on tensile strain calculated using a regression equation developed from a large number of Finite Element analyses and the same damage parameters developed for asphalt concrete fatigue.

Response Models

During most of the HVS tests, resilient deflections were measured using the RSD and the MDD. The following figure summarizes the measured deflections with those calculated using *CalME* damage models for all of the sections in terms of the ratio of the initial deflections before HVS loading to the final deflections at the end of the loading.

Assumptions made regarding differences between moduli from different measurement methods, shift factors, slip between layers, and non-linear elasticity of unbound layers to obtain reasonably good agreement between measured resilient deflections and those calculated with *CalME* are discussed in the report.

The observed behavior of the aggregate base (AB) and subbase layers under HVS loading contradicts the commonly accepted wisdom for granular materials, which is based primarily on triaxial testing. The observed behavior is discussed in the report and is modeled in *CalME*.

Using these assumptions, it was possible to model resilient deflections reasonably well for the full history of all of HVS test sections using the layered elastic analysis program (LEAP) response model.

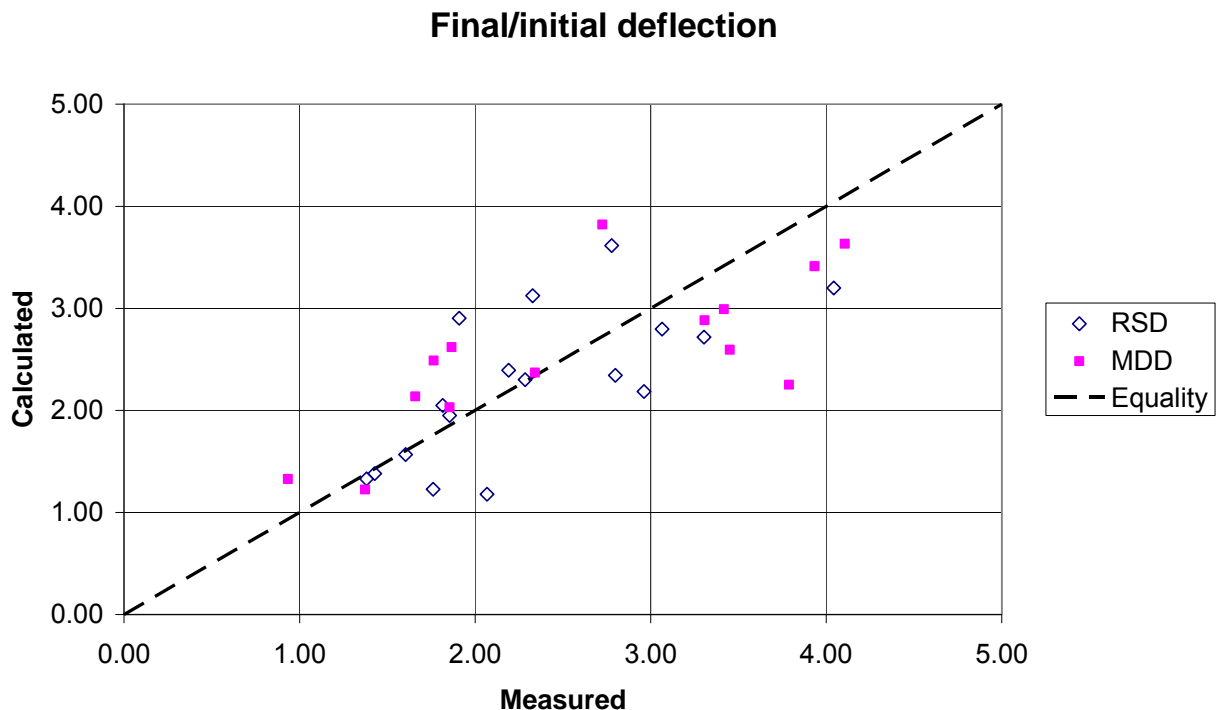


Figure ES-1. Ratio of initial to final deflection.

Damage of Asphalt Materials

Controlled strain fatigue tests conducted on beams were used to derive model parameters for the decrease in modulus for all the asphalt materials — except for the ATPB, where laboratory tests were not available. Working under the assumptions used in the modeling and using a shift factor with these damage models produced the correct changes in resilient deflections during all the HVS tests.

For reflection cracking, a simple model was used to calculate the strains in an overlay caused by existing cracking in the original top layer. Using this model and the laboratory fatigue model, reasonably correct resilient deflections were also predicted.

Relating visual cracking to the calculated asphalt damage proved to be difficult, and no single relationship could be derived. Goal 1 and Goal 5 showed differences between the drained and the undrained sections; for Goal 3 Cracking, the increase in visual cracking was quicker than for Goal 1 and Goal 5; and for Goal 9, visual cracking occurred at much less calculated damage than for the other experiments.

It is possible that the relationship between visual cracking and calculated damage depends on the thickness of the asphalt layers, and that reflection cracks and cracks in new pavements develop differently. It is also possible that the development of visual cracking depends on factors that the simulations did not consider.

No single relationship could be established between the relative increase in deflection and the amount of surface cracking (shown in the following figure), but it may be noted that visible cracking was not observed until deflection had increased by 50 percent or more.

Cracking versus relative deflection

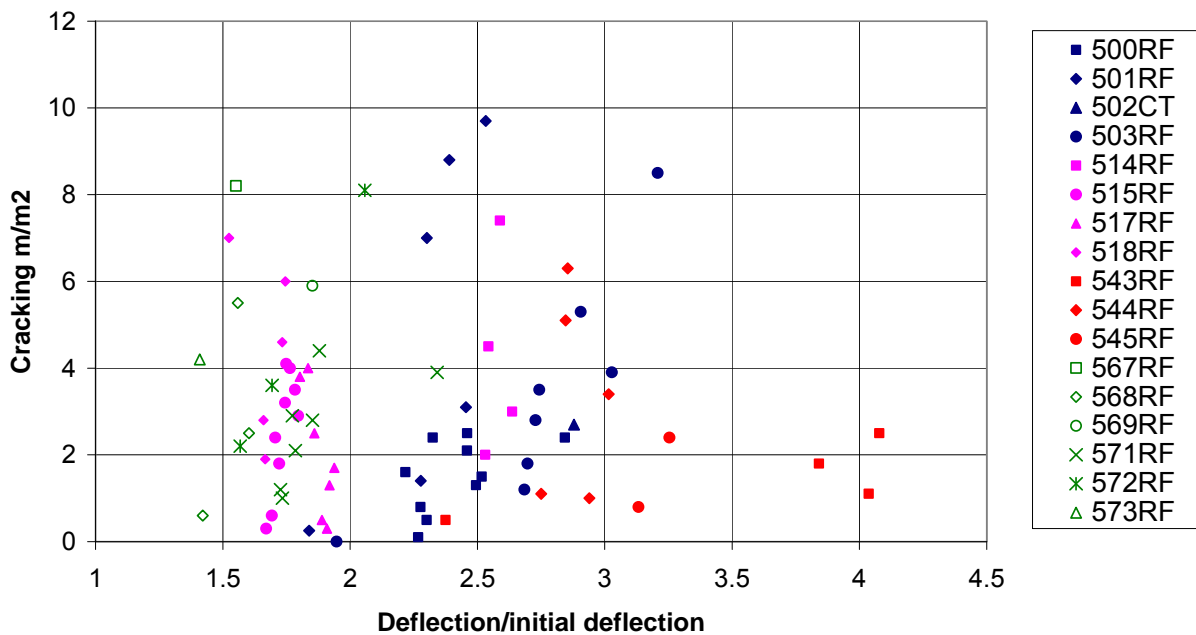


Figure ES-2. Cracking versus increase in deflection.

Permanent Deformation of Asphalt

The following figure shows the measured and predicted final permanent deformation of the asphalt layers from Goal 1, Goal 3, and Goal 5, where data were available. Permanent deformation was calculated for the upper 100 mm of the asphalt layer(s).

Permanent deformation in AC (pro rated)

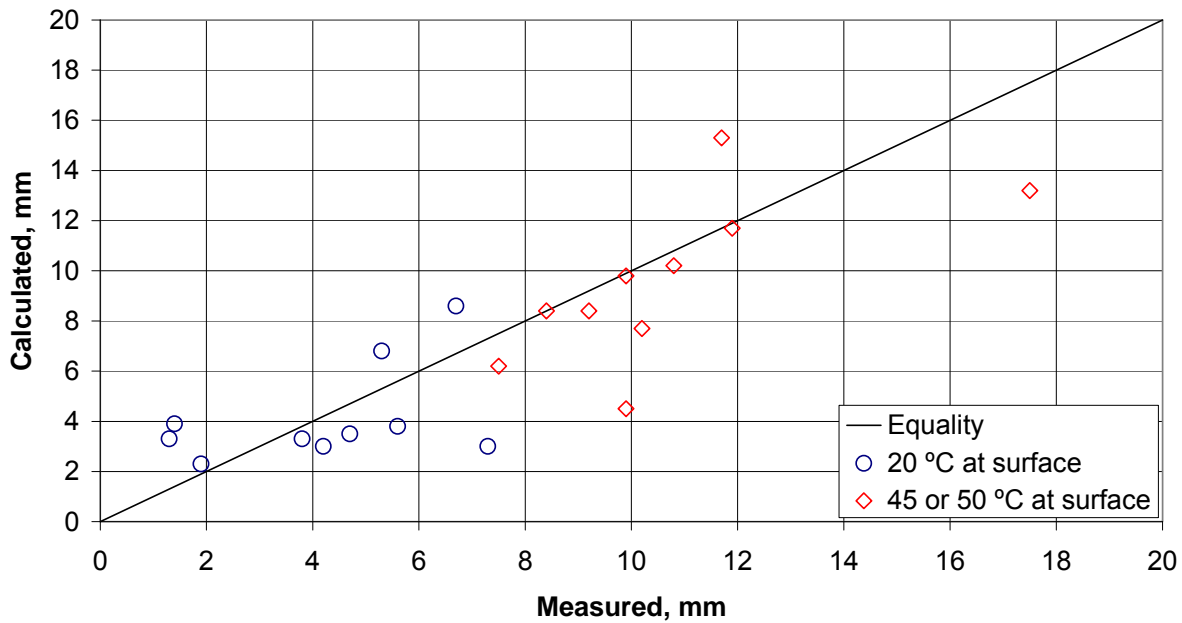


Figure ES-3. Measured and predicted final permanent deformation of asphalt.

In Figure ES-3, the 20°C outlier point with a measured deformation greater than the calculated one is Section 543RF, which was a wet, drained test where the ATPB stripped and collapsed. The two relatively low values at high temperatures are from the test with a bias-ply dual tire and from the test with an aircraft tire. The correlation coefficient between measured and calculated values is 0.82 and the standard error of estimate is 2.2 mm.

The parameters for predicting permanent shear strain were based on Repeated Simple Shear Tests at Constant Height (RSST-CH).

Permanent Deformation of Granular Layers

The permanent deformation of the granular layers for Goal 1, Goal 3, and Goal 5 are shown with average measured values in Figure ES-4. It should be noted that the permanent deformations are rather small except for Section 543RF, the wet drained section, where the permanent deformation includes part of the ATPB.

Permanent deformation of granular layers

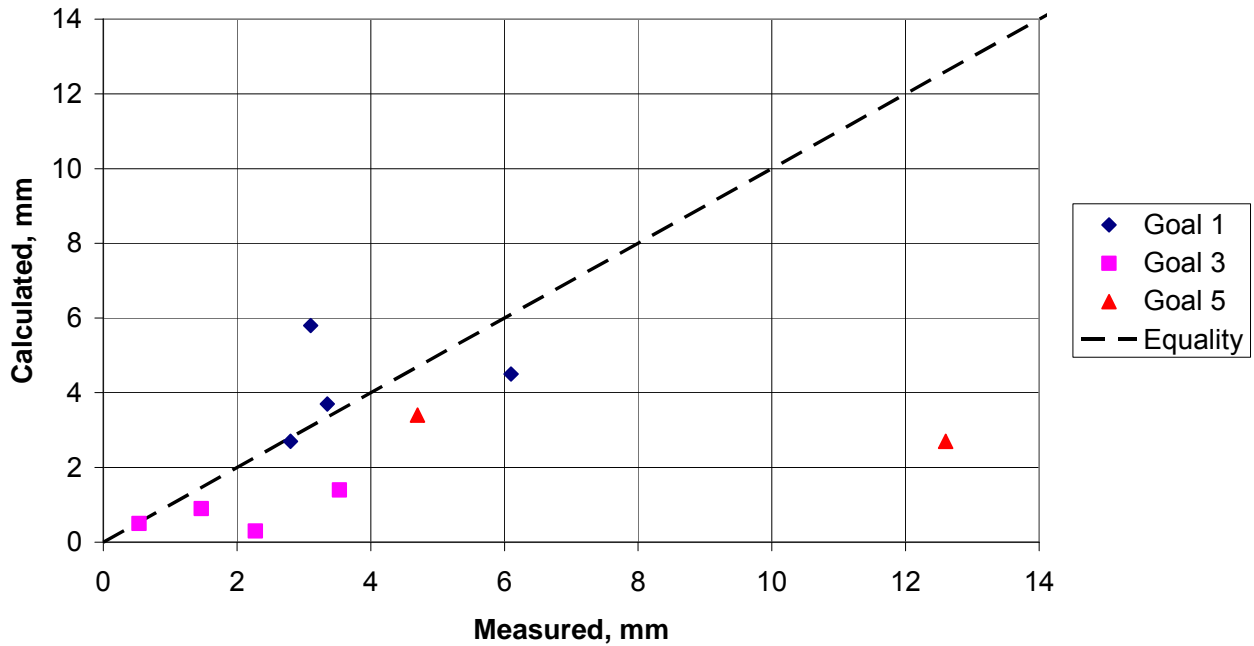


Figure ES-4. Final permanent deformation of granular layers.

Permanent deformation was calculated both at the top of the AB and at the top of the aggregate subbase (ASB). The two materials are rather similar and might have been treated as a single layer.

Permanent Deformation of Subgrade

The final permanent deformation of the subgrade is even smaller than that of the granular layers, with a maximum measured value of less than 2 mm. In addition, the data scatter is as large as that of the granular layers, with an average coefficient of variation of 70 percent. This is far from ideal for the calibration of a subgrade permanent deformation model. The mean measured and predicted final deformations are shown in Figure ES-5. The subgrade and granular results indicate that rutting of the unbound layers is probably not a major concern for existing Caltrans pavements that need rehabilitation unless there is poor drainage or significant amounts of water are entering cracks in the asphalt layers.

Permanent deformation of subgrade

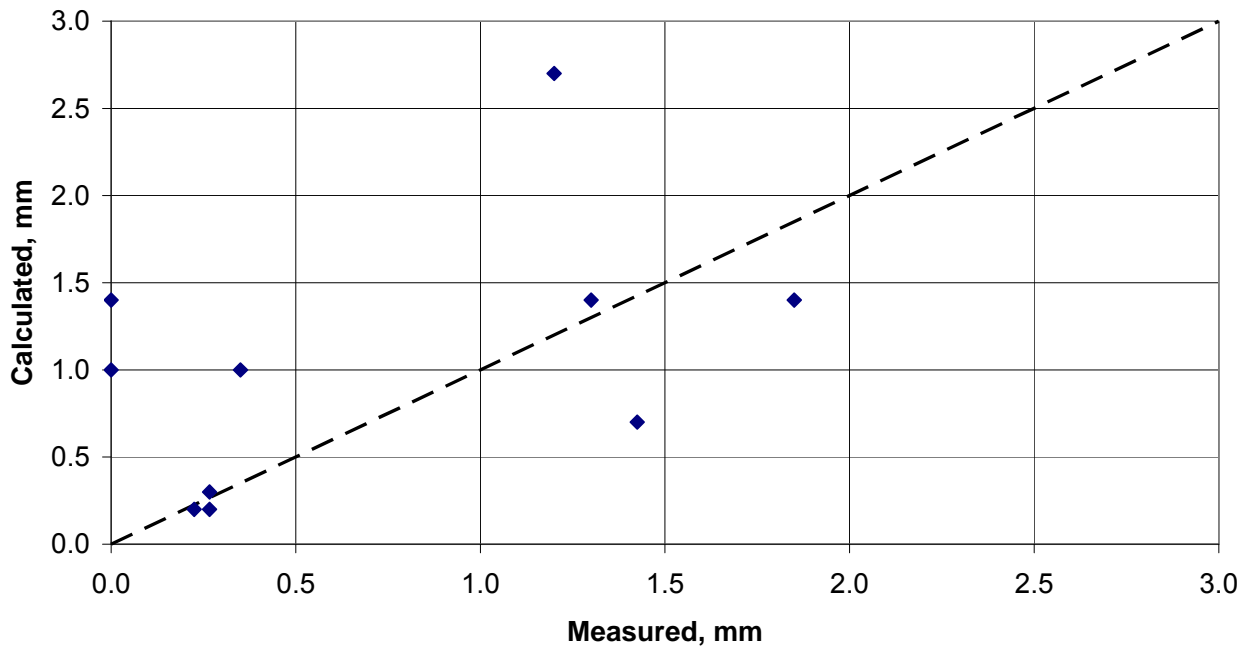


Figure ES-5. Final permanent deformation of the subgrade.

Total Permanent Deformation at Pavement Surface

Figure ES-6 shows the final calculated permanent deformation at the pavement surface versus the measured final deformation averaged from profilometer measurements along the HVS test area.

Calculated final permanent deformations that underestimated the measured final permanent deformations were worst for the Goal 5 sections in which water was dripped into the base layers, especially for the drained section, 543RF in which the ATPB stripped.

The correlation coefficient between measured and calculated deformations is 0.61 and the standard error of estimate is 2.6 mm.

Conclusions and Recommendations

The overall results from this study indicate that Incremental-Recursive models provide reasonable results when predicting the response and performance of pavement under HVS loading. However, now that the models have been shown to match the mechanics of the flexible pavements under HVS loading, additional work remains to be done before these models can be used for pavement design and performance prediction.

There are significant differences between HVS testing and field results, and the approach used in this study has limitations because of those differences. These include the effects of age and of seasonal variation that have not been quantified in the simulations because HVS tests are of relatively short duration and are performed, to varying degrees, in controlled environments. Field calibration is required to evaluate the response difference between the field pavement and the Incremental-Recursive simulation that should be attributed to aging and seasonal effects. It is likely that the effects of aging can be dealt with using shift factors.

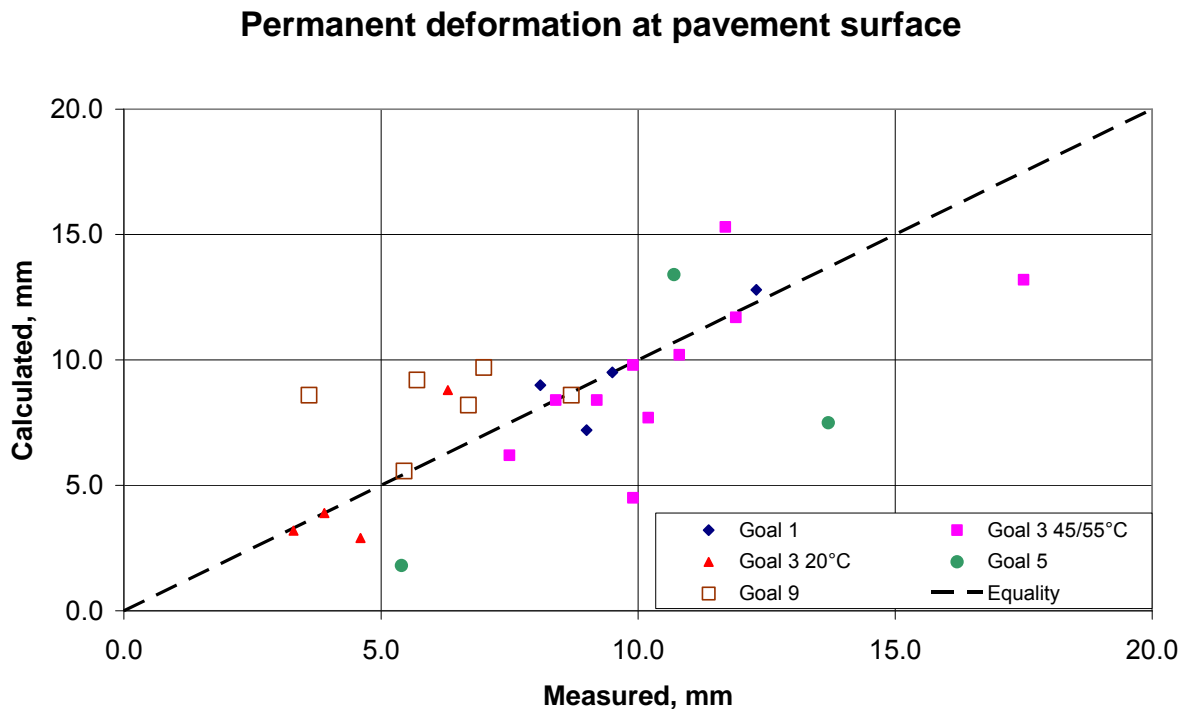


Figure ES-6. Final permanent deformation at the pavement surface.

The effects of rest periods between loadings and of faster traffic have also not been included in the calibration. It is expected that different shift factors will result because of rest periods and different trafficking patterns.

Lastly, moduli from frequency sweep data, triaxial tests, FWD tests, and MDD deflections used in this study are similar but they are not identical. The NCHRP 1-37A Design Guide study proposes relying primarily on triaxial testing to characterize the stiffness of flexible pavement layers and the permanent deformation parameters of asphaltic materials.

Recommendations are made in this report for the most practical and economical methods for characterizing materials based on the understanding that the majority of Caltrans' work over the next several decades will be rehabilitation and reconstruction, with some addition of lane capacity.

Recommendations are also made regarding the next steps to develop the *CalME* models. These include:

1. Perform a sensitivity analysis using "typical" values for properties and climate in the database established to date, and compare the results from the Classical, Incremental, and Incremental-Recursive methods included in *CalME* to evaluate reasonableness of sensitivity across the three methods.
2. Simulate mainline highway case studies and test track data (such as WesTrack and NCAT track) using the recommended methods for characterizing flexible pavement materials in conjunction with the Incremental-Recursive models in *CalME*, and compare the simulated and measured results, as was done for the HVS results presented in this report. This step will provide validation for the models

3. Address the variability of the input parameters (moduli, thicknesses, traffic loading, etc.) and uncertainty on the damage models. Several approaches should be considered, including the approach used in the NCHRP 1-37A method.
4. Make final decisions regarding use of cemented layers in the flexible pavement structure, then calibrate. It is generally recommended that “semi-rigid” pavements, in which asphalt concrete is placed directly on cement-treated base (CTB) or lean concrete base (LCB), not be used because of the relatively quick reflection of shrinkage cracks. However, because Caltrans has used semi-rigid pavements in the past and they remain in the current design method, it is therefore important to have models for the response and performance of these layers. The models in the NCHRP 1-37A Report should be the starting point for such a validation-and-calibration exercise.

TABLE OF CONTENTS

Executive Summary	iv
Approaches Included in <i>CalME</i>	iv
Use of Heavy Vehicle Simulator Data to Evaluate Models	v
Results of HVS Test Simulation Using <i>CalME</i>	vi
Response Models	vii
Damage of Asphalt Materials	vii
Permanent Deformation of Asphalt	viii
Permanent Deformation of Granular Layers	ix
Permanent Deformation of Subgrade	x
Total Permanent Deformation at Pavement Surface	xi
Conclusions and Recommendations	xi
List of Figures	xvii
List of Tables	xxv
1.0 Introduction	1
1.1 Models and Approaches Included in <i>CalME</i>	1
1.1.1 Validation Using Heavy Vehicle Simulator Data	2
1.2 HVS tests	4
1.2.1 Goal 1 and Goal 3 Tests	4
1.2.2 Goal 5 Tests	6
1.2.3 Goal 9 Tests	7
1.3 Response and Damage Models	8
1.3.1 Asphalt Modulus	8
1.3.2 Fatigue	21
1.4 Weak Bonding	24
1.5 Unbound Layers	25
1.5.1 Triaxial Tests	25
1.5.2 Influence of Stiffness of Layers above an Unbound Layer	26
1.5.3 Influence of Load Level	39
1.6 Permanent Deformation	40
1.6.1 Asphalt	40
1.6.2 Unbound Materials	47
1.7 Reflection Cracking	48
2.0 Goal 1 Cracking Test Simulations	50
2.1 Goal 1 Resilient Deformations	50

2.1.1	Section 501RF Resilient Deflections (Undrained).....	50
2.1.2	Section 503RF Resilient Deflections (Undrained).....	56
2.1.3	Section 500RF Resilient Deflections (Drained).....	60
2.1.4	Section 502CT Resilient Deflections (Drained).....	65
2.2	Visual Cracking Versus Damage of the Top Asphalt Layer, Goal 1	69
2.3	Goal 1 Permanent Deformation.....	72
2.3.1	Section 501RF Permanent Deformations.....	73
2.3.2	Section 503RF Permanent Deformations.....	75
2.3.3	Section 500RF Permanent Deformations.....	77
2.3.4	Section 502CT Permanent Deformations.....	79
3.0	Goal 3 Reflection cracking tests.....	81
3.1	Resilient Deflections	81
3.1.1	Section 517RF DGAC on Section 501RF Resilient Deflections	81
3.1.2	Section 518RF ARHM on Section 503RF Resilient Deflections.....	86
3.1.3	Section 514RF DGAC on Section 500RF Resilient Deflections	91
3.1.4	Section 515RF ARHM on Section 502CT Resilient Deflections	96
3.2	Visual Cracking Versus Damage of the Overlay, Goal 3, 20°C.....	101
3.3	Permanent Deformation Goal 3, 20°C.....	104
3.3.1	Section 517RF 75-mm DGAC Permanent Deformations	105
3.3.2	Section 518RF 38-mm ARHM Permanent Deformation.....	107
3.3.3	Section 514RF 75-mm DGAC Permanent Deformations	109
3.3.4	Section 515RF 38-mm ARHM Permanent Deformations	112
4.0	Goal 3 Rutting experiments.....	114
4.1	Section 504RF No Overlay, Wide-Base Single Tire.....	115
4.2	Section 505RF DAGC Overlay, Bias-Ply Dual Tire.....	117
4.3	Section 506RF DGAC Overlay, Radial Dual Tire	119
4.4	Section 507RF DGAC Overlay, Wide-Base Single Tire	121
4.5	Section 508RF ARHM Overlay, Wide-Base Single Tire.....	123
4.6	Section 509RF ARHM Overlay, Radial Dual Tire	125
4.7	Section 510RF ARHM Overlay, Radial Dual Tire	127
4.8	Section 511RF ARHM Overlay, Wide-Base Single Tire.....	129
4.9	Section 512RF DGAC Overlay, Wide-Base Single Tire	131
4.10	Section 513RF DGAC Overlay, Aircraft Tire.....	133
5.0	Goal 5 Wet conditions.....	135
5.1	Section 543RF ARHM Overlay, Drained	136
5.2	Section 544RF ARHM Overlay, Undrained	145

5.3	Section 545RF DGAC Overlay, Undrained	153
5.4	Visual Cracking versus Damage of the Top Asphalt Layer, Goal 5	160
6.0	Goal 9 Modified Binder (MB) road, initial tests	162
6.1	Materials Characterization	162
6.2	Section 567RF MB Road	169
6.3	Section 568RF MB Road	173
6.4	Section 573RF MB Road	176
6.5	Section 571RF MB Road	179
6.6	Section 572RF MB Road	183
6.7	Section 569RF MB Road	186
6.8	Visual Cracking Versus Damage of the Top Asphalt Layer, Goal 9	190
7.0	Summary and recommendations	191
7.1	Shift Factors and Damage Equations Used in Simulations	191
7.2	Response Model	192
7.3	Damage of Asphalt Materials	197
7.4	Permanent Deformation of Asphalt	199
7.5	Permanent Deformation of Granular Layers	201
7.6	Permanent Deformation of Subgrade	203
7.7	Total Permanent Deformation at Pavement Surface	205
7.8	Recommendations	207
8.0	References	209
9.0	Appendix	212
9.1	Glossary	212
9.2	List of Units	214
9.3	List of Parameters in Equations	214
9.4	Parameter Values Used in Simulations	216
9.5	Section 569RF Simulated with a CTB Model from an HVS Nordic Experiment	217

LIST OF FIGURES

Figure ES-1. Ration of final to initial deflectionvii

Figure ES-2. Cracking versus increase in deflectionviii

Figure ES-3. Measured and predicted final permanent deflection of asphaltix

Figure ES-4. Final permanent deformation of granular layersx

Figure ES-5. Final permanent deformation of the subgradexi

Figure ES-6. Final permanent deformation at the pavement surfacexii

Figure 1. Layout of 20°C test sections. Goal 3 rutting sections are distributed in the area between the 20°C test sections. 4

Figure 2. Drip watering system for Goal 5 tests. 7

Figure 3. Layout of Goal 9 test sections. 9

Figure 4. Example of modulus versus reduced time relationship. 10

Figure 5. Modulus versus temperature for different viscosity versus temperature relationships..... 12

Figure 6. Frequency sweep data for Goal 1 and Goal 3 materials compared to models. 13

Figure 7. Example of input parameters for the modulus-versus-reduced time relationship for the AC bottom layer. 21

Figure 8. Example of damage versus number of load applications. 23

Figure 9. Example of Equation 6 damage parameters of AC bottom layer (Goal 1). 24

Figure 10. Simple Drucker-Prager failure condition..... 28

Figure 11. E_{AC} 10,000 MPa, no slip, 40 kN load. 29

Figure 12. E_{AC} 10,000 MPa, slip, 40 kN. 30

Figure 13. E_{AC} 2,000 MPa, slip, 40 kN. 31

Figure 14. E_{AC} 2,000 MPa, slip, 100 kN load. 33

Figure 15. Displacement field in particulate sample..... 34

Figure 16. Displacement field in elastic solid (FEM). 35

Figure 17. Modulus of Layer 2 as a function of the stiffness of the asphalt layers, for the undrained sections. 36

Figure 18. Modulus of Layer 2 as a function of the stiffness of the asphalt layers, for the drained sections. ... 37

Figure 19. Modulus of subgrade as a function of the stiffness of the pavement layers. 37

Figure 20. Results of RSST-CH tests. [Note: FMFC indicates field-mixed field compacted specimen taken by coring the pavement. AV5.5 indicates cores with approximately 5.5 percent air-voids. Each title in the legend indicates the RSST-CH test temperature (40, 50, or 60 °C) and average shear stress (MPa).] 42

Figure 21. Normalized plastic strain versus number of load repetitions. (Note: legend is the same as in Figure 20). 44

Figure 22. Average values for Figure 21 curves..... 45

Figure 23. Best fitting Gamma function. (Note: legend is the same as in Figure 20 and Figure 21. 46

Figure 24. Input parameters for permanent deformation (rutting) of subgrade in second column. 48

Figure 25. Comparison of fitted vs. calculated strain for AC-on-AC overlay, 2D. 49

Figure 26. Section 501RF pavement structure. 51

Figure 27. Section 501RF temperatures during testing. 52

Figure 28. Section 501RF 40 kN top modules deflection. 52

Figure 29. Section 501 RF 40 kN resilient compression of pavement layers. 53

Figure 30. Section 501RF 40 kN deflection of subgrade. 53

Figure 31. Section 501RF 100 kN deflection of top modules. 54

Figure 32. Section 501RF 100 kN resilient compression of pavement layers. 54

Figure 33. Section 501RF 100 kN deflection of subgrade. 55

Figure 34. Section 501RF calculated moduli at 40 kN and actual temperature. (Note: in this and all other figures showing change in elastic moduli (E) under loading the lines are plotted for the modulus of each layer, i.e., E1 is the modulus of the first layer, E2 is the modulus of the second layer, etc.)..... 55

Figure 35. Section 503RF pavement structure. 56

Figure 36. Section 503RF temperatures during testing. 56

Figure 37. Section 503RF 40 kN deflection of top modules. 57

Figure 38. Section 503RF 40 kN compression of pavement layers. 57

Figure 39. Section 503RF 40 kN deflection of subgrade. 58

Figure 40. Section 503RF 100 kN deflection of top modules. 58

Figure 41. Section 503RF 100 kN resilient compression of pavement layers. 59

Figure 42. Section 503RF 100 kN deflection of subgrade. 59

Figure 43. Section 503RF calculated layer moduli at 40 kN and actual temperature. 60

Figure 44. Section 500RF pavement structure. 60

Figure 45. Section 500RF temperatures during testing. 61

Figure 46. Section 500RF 40 kN deflection of top modules. 61

Figure 47. Section 500RF 40 kN resilient compression of pavement layers. 62

Figure 48. Section 500RF 40 kN deflection of subgrade. 62

Figure 49. Section 500RF 100 kN deflection of top modules. 63

Figure 50. Section 500RF 100 kN compression of pavement layers. 63

Figure 51. Section 500RF 100 kN deflection of subgrade. 64

Figure 52. Section 500RF calculated moduli at 40 kN and actual temperature. 64

Figure 53. Section 502CT pavement structure. 65

Figure 54. Section 502CT 40 kN deflection on top of AC. 65

Figure 55. Section 502CT 40 kN compression of pavement layers. 66

Figure 56. Section 502CT 40 kN deflection of subgrade. 66

Figure 57. Section 502CT 100 kN deflection at top of AC. 67

Figure 58. Section 502CT 100 kN resilient compression of pavement layers..... 67

Figure 59. Section 502CT 100 kN deflection of subgrade..... 68

Figure 60. Section 502CT calculated moduli at 40 kN and 20°C..... 68

Figure 61. Cracking versus relative decrease in modulus of top AC layer for Goal 1..... 69

Figure 62. Goal 1, cracking versus increase in deflection. 70

Figure 63. Permanent compression of AC layers. 73

Figure 64. Permanent compression of granular layers..... 73

Figure 65. Permanent deformation of subgrade..... 74

Figure 66. Permanent deformation at pavement surface..... 74

Figure 67. Permanent compression of AC layers. 75

Figure 68. Permanent compression of granular layers..... 75

Figure 69. Permanent deformation of subgrade..... 76

Figure 70. Permanent deformation at pavement surface..... 76

Figure 71. Permanent deformation of the AC layers. 77

Figure 72. Permanent compression of the granular layers..... 77

Figure 73. Permanent deformation of the subgrade..... 78

Figure 74. Permanent deformation at pavement surface..... 78

Figure 75. Permanent compression of the AC layers..... 79

Figure 76. Permanent deformation of granular layers. 79

Figure 77. Permanent deformation of subgrade..... 80

Figure 78. Permanent deformation at surface of pavement. 80

Figure 79. Section 517RF pavement structure..... 82

Figure 80. Section 517RF AC temperature during testing..... 82

Figure 81. Section 517RF 40 kN deflection of top modules..... 83

Figure 82. Section 517RF 40 kN compression of pavement layers..... 83

Figure 83. Section 517RF deflection of subgrade..... 84

Figure 84. Section 517RF 100 kN top modules deflection. 84

Figure 85. Section 517RF 100 kN compression of pavement layers. 85

Figure 86. Section 517RF 100 kN deflection of subgrade..... 85

Figure 87. Section 517RF calculated moduli at 40 kN and actual temperature..... 86

Figure 88. Section 518RF pavement structure..... 86

Figure 89. Section 518RF AC temperature during testing..... 87

Figure 90. Section 518RF 40 kN top modules deflection..... 87

Figure 91. Section 518RF 40 kN resilient compression of pavement layers. 88

Figure 92. Section 518RF 40 kN deflection of subgrade..... 88

Figure 93. Section 518RF 100 kN top modules deflection..... 89

Figure 94. Section 518RF 100 kN compression of pavement layers. 89

Figure 95. Section 518RF 100 kN deflection of subgrade. 90

Figure 96. Section 518RF calculated moduli at 40 kN and actual temperature. 90

Figure 97. Section 514RF pavement structure. 91

Figure 98. Section 514RF AC temperature during testing. 91

Figure 99. Section 514RF 40 kN top modules deflection. 92

Figure 100. Section 514RF 40 kN compression of pavement layers, MDD1 and MDD2. 92

Figure 101. Section 514RF 40 kN compression of pavement layers, MDD3 and MDD4. 93

Figure 102. Section 514RF 40 kN deflection of subgrade. 93

Figure 103. Section 514RF 100 kN top modules deflection. 94

Figure 104. Section 514RF 100 kN compression of pavement layers, MDD1 and MDD2. 94

Figure 105. Section 514RF 100 kN compression of pavement layers, MDD3 and MDD4. 95

Figure 106. Section 514RF 100 kN deflection of subgrade. 95

Figure 107. Section 514RF calculated moduli at 40 kN and actual temperature. 96

Figure 108. Section 515RF pavement structure. 96

Figure 109. Section 515RF AC temperature during testing. 97

Figure 110. Section 515RF 40 kN top modules deflection. 97

Figure 111. Section 515RF 40 kN resilient compression of pavement layers. 98

Figure 112. Section 515RF 40 kN deflection of subgrade. 98

Figure 113. Section 515RF 100 kN top modules deflection. 99

Figure 114. Section 515RF 100 kN compression of pavement layers. 99

Figure 115. Section 515RF 100 kN deflection of subgrade. 100

Figure 116. Section 515RF calculated moduli at 40 kN and actual temperatures. 100

Figure 117. Cracking in overlay versus relative decrease in modulus of overlay, Goal 3. 101

Figure 118. Goal 3, 20°C, cracking versus increase in deflection. 102

Figure 119. Section 517RF permanent deformation of AC layers. 105

Figure 120. Section 517RF permanent deformation of granular layers. 105

Figure 121. Section 517RF permanent deformation of subgrade. 106

Figure 122. Section 517RF permanent deformation at pavement surface. 106

Figure 123. Section 518RF permanent deformation of AC layers. 107

Figure 124. Section 518RF permanent deformation of granular layers. 107

Figure 125. Section 518RF permanent deformation of subgrade. 108

Figure 126. Section 518RF permanent deformation at pavement surface. 108

Figure 127. Section 514RF permanent deformation of AC layers. 109

Figure 128. Section 514RF permanent deformation of granular layers, MDD1 and MDD2. 109

Figure 129. Section 514RF permanent deformation of granular layers, MDD3 and MDD4. 110

Figure 130. Section 514RF permanent deformation of subgrade. 110

Figure 131. Section 514RF permanent deformation at pavement surface. 111

Figure 132. Section 515RF permanent deformation of AC layers..... 112

Figure 133. Section 515RF permanent deformation of granular layers..... 112

Figure 134. Section 515RF permanent deformation of subgrade. 113

Figure 135. Section 515RF permanent deformation of the pavement surface..... 113

Figure 136. Section 504RF pavement structure..... 115

Figure 137. Section 504RF permanent deformation at pavement surface from profilometer..... 115

Figure 138. Section 504RF calculated permanent deformation of pavement layers..... 116

Figure 139. Section 505RF pavement structure..... 117

Figure 140. Section 505RF temperatures during testing..... 117

Figure 141. Section 505RF permanent deformation at pavement surface from profilometer..... 118

Figure 142. Section 505RF calculated permanent deformation of pavement layers..... 118

Figure 143. Section 506RF pavement structure..... 119

Figure 144. Section 506RF temperatures during testing..... 119

Figure 145. Section 506RF permanent deformation at pavement surface from profilometer..... 120

Figure 146. Section 506RF calculated permanent deformation of pavement layers..... 120

Figure 147. Section 507RF pavement structure..... 121

Figure 148. Section 507RF temperatures during testing..... 121

Figure 149. Section 507RF permanent deformation at pavement surface from profilometer..... 122

Figure 150. Section 507RF calculated permanent deformation of pavement layers..... 122

Figure 151. Section 508RF pavement structure..... 123

Figure 152. Section 508RF temperatures during testing..... 123

Figure 153. Section 508RF permanent deformation at pavement surface from profilometer..... 124

Figure 154. Section 508RF calculated permanent deformation of pavement layers..... 124

Figure 155. Section 509RF pavement structure..... 125

Figure 156. Section 509RF temperatures during testing..... 125

Figure 157. Section 509RF permanent deformation at pavement surface from profilometer..... 126

Figure 158. Section 509RF calculated permanent deformation of pavement layers..... 126

Figure 159. Section 510RF pavement structure..... 127

Figure 160. Section 510RF temperatures during testing..... 127

Figure 161. Section 510RF permanent deformation at pavement surface from profilometer..... 128

Figure 162. Section 510RF calculated permanent deformation of pavement layers..... 128

Figure 163. Section 511RF pavement structure..... 129

Figure 164. Section 511RF temperatures during testing..... 129

Figure 165. Section 511RF permanent deformation at the pavement surface. 130

Figure 166. Section 511RF calculated permanent deformation of the pavement layers.....	130
Figure 167. Section 512RF pavement structure.....	131
Figure 168. Section 512RF temperatures during testing.....	131
Figure 169. Section 512RF permanent deformation at pavement surface from profilometer.....	132
Figure 170. Section 512RF calculated permanent deformation of the pavement layers.....	132
Figure 171. Section 513RF pavement structure.....	133
Figure 172. Section 513RF permanent deformation at pavement surface from profilometer.....	134
Figure 173. Section 513RF calculated permanent deformation of pavement layers.....	134
Figure 174. Cores from trafficked area of Section 543RF after HVS loading show stripping and disintegration of ATPB, as well as signs of moisture damage between the the three lifts of asphalt concrete (Bejarano et al. 2003).....	135
Figure 175. Section 543RF pavement structure.....	136
Figure 176. Section 543RF temperatures during testing.....	137
Figure 177. Section 543RF Road Surface Deflectometer, at 40 kN.....	137
Figure 178. Section 543RF Road Surface Deflectometer, at 100 kN.....	138
Figure 179. Section 543RF 40 kN top module.....	138
Figure 180. Section 543RF 40 kN top of aggregate base.....	139
Figure 181. Section 543RF 40 kN top of aggregate subbase.....	139
Figure 182. Section 543RF 40 kN deflection of subgrade (850 mm depth).....	140
Figure 183. Section 543RF 100 kN top module.....	140
Figure 184. Section 543RF 100 kN top of aggregate base.....	141
Figure 185. Section 543RF 100 kN top of aggregate subbase.....	141
Figure 186. Section 543RF 100 kN deflection of subgrade (850 mm depth).....	142
Figure 187. Section 543RF Permanent deformation of asphalt layers.....	142
Figure 188. Section 543RF permanent deformation of granular layers plus top of subgrade.....	143
Figure 189. Section 543RF permanent deformation in subgrade (850 mm depth).....	143
Figure 190. Section 543RF permanent deformation at pavement surface.....	144
Figure 191. Section 543RF calculated layer moduli, at 40 kN and actual temperatures.....	144
Figure 192. Section 544RF pavement structure.....	145
Figure 193. Section 544RF temperatures during testing.....	145
Figure 194. Section 544RF Road Surface Deflectometer, at 40 kN.....	146
Figure 195. Section 544RF Road Surface Deflectometer, at 100 kN.....	146
Figure 196. Section 544RF 40 kN top module.....	147
Figure 197. Section 544RF 40 kN top of aggregate base.....	147
Figure 198. Section 544RF 40 kN top of aggregate subbase.....	148
Figure 199. Section 544RF 100 kN top module.....	148

Figure 200. Section 544RF 100 kN top of aggregate base. 149

Figure 201. Section 544RF 100 kN top of aggregate subbase. 149

Figure 202. Section 544RF Permanent deformation of asphalt layers. 150

Figure 203. Section 544RF permanent deformation of aggregate base. 150

Figure 204. Section 544RF permanent deformation on top of basecourse. 151

Figure 205. Section 544RF permanent deformation at pavement surface. 151

Figure 206. Section 544RF calculated moduli of pavement layers. 152

Figure 207. Section 545RF pavement structure. 153

Figure 208. Section 545RF temperatures during testing. 153

Figure 209. Section 545RF Road Surface Deflectometer, at 40 kN. 154

Figure 210. Section 545RF Road Surface Deflectometer, 100 kN. 154

Figure 211. Section 545RF 40 kN top module. 155

Figure 212. Section 545RF 40 kN top of aggregate base. 155

Figure 213. Section 545RF 40 kN top of aggregate subbase. 156

Figure 214. Section 545RF 100 kN top module. 156

Figure 215. Section 545RF 100 kN top of aggregate base. 157

Figure 216. Section 545RF 100 kN top of aggregate subbase. 157

Figure 217. Section 545RF permanent deformation of asphalt layers. 158

Figure 218. Section 545RF permanent deformation of aggregate base. 158

Figure 219. Section 545RF permanent deformation at pavement surface. 159

Figure 220. Section 545RF calculated moduli of pavement layers. 159

Figure 221. Visual cracking versus relative decrease in modulus of layer 1, Goal 5 Wet conditions. 160

Figure 222. Goal 5, cracking versus increase in deflection. 161

Figure 223. MB road, AC modulus-versus-reduced time parameters from frequency sweep. 162

Figure 224. Moduli from FWD compared to frequency sweep tests, Goal 9 (MB road). 163

Figure 225. MB road, damage parameters for AC in first column. 165

Figure 226. MB road, backcalculated modulus of AB versus time. 166

Figure 227. MB road, modulus of AB versus stiffness of AC. 166

Figure 228. MB road, subgrade modulus versus stiffness of pavement layers. 167

Figure 229. Section 567RF pavement structure. 169

Figure 230. Section 567RF load levels. 169

Figure 231. Section 567RF temperatures during testing. 170

Figure 232. Section 567RF Road Surface Deflectometer. 170

Figure 233. Section 567RF MDDs at 90mm and 330 mm. 171

Figure 234. Section 567RF permanent deformation of MDDs. 171

Figure 235. Section 567RF permanent deformation at pavement surface from profilometer. 172

Figure 236. Section 567RF calculated moduli at 40 kN and actual temperature..... 172

Figure 237. Section 568RF pavement structure..... 173

Figure 238. Section 568RF temperatures during testing..... 173

Figure 239. Section 568RF Road Surface Deflectometer..... 174

Figure 240. Section 568RF permanent deformation at pavement surface from profilometer..... 174

Figure 241. Section 568RF calculated layer moduli at 40 kN and actual temperature..... 175

Figure 242. Section 573RF pavement structure..... 176

Figure 243. Section 573RF temperatures during testing..... 176

Figure 244. Section 573RF Road Surface Deflectometer..... 177

Figure 245. Section 573RF permanent deformation at pavement surface from profilometer..... 177

Figure 246. Section 573RF calculated layer moduli at 40 kN and actual temperature..... 178

Figure 247. Section 571RF pavement structure..... 179

Figure 248. Section 571RF temperatures during testing..... 179

Figure 249. Section 571RF Road Surface Deflectometer..... 180

Figure 250. Section 571RF MDDs at 90 mm, 300 mm, and 525 mm. 180

Figure 251. Section 571RF permanent deformation of MDDs..... 181

Figure 252. Section 571RF permanent deformation at the pavement surface. 181

Figure 253. Section 571RF calculated layer moduli at 40 kN and actual temperature..... 182

Figure 254. Section 572RF pavement structure..... 183

Figure 255. Section 572RF temperatures during testing..... 183

Figure 256. Section 572RF Road Surface Deflectometer..... 184

Figure 257. Section 572RF permanent deformation at the pavement surface. 184

Figure 258. Section 572RF calculated layer moduli at 40 kN and actual temperature..... 185

Figure 259. Section 569RF pavement structure..... 186

Figure 260. Section 569RF temperatures during testing..... 186

Figure 261. Section 569RF Road Surface Deflectometer..... 187

Figure 262. Section 569RF MDDs at 90 mm, 300 mm, and 525 mm 187

Figure 263. Section 569RF permanent deformation of MDDs..... 188

Figure 264. Section 569RF permanent deformation at pavement surface from profilometer..... 188

Figure 265. Section 569RF calculated layer moduli at 40 kN and actual temperature..... 189

Figure 266. Cracking versus relative decrease in modulus of AC layer for Goal 9 (MB road)..... 190

Figure 267. Goal 9 (MB road), Cracking versus increase in deflection (RSD) 190

Figure 268. Ratio of final over initial deflection. 195

Figure 269. Cracking versus calculated decrease in modulus of top layer. 197

Figure 270. Cracking versus increase in deflection. 198

Figure 271. Measured and predicted final permanent deformation of asphalt..... 199

Figure 272. Final permanent deformation of granular layers. 201

Figure 273. Final permanent deformation of the subgrade. 203

Figure 274. Final permanent deformation at the pavement surface (profile data). 205

Figure 275. Modulus of AB layer backcalculated from FWD tests in center line. 217

Figure 276. Pavement structure for Section 569RF. 219

Figure 277. Damage parameters used for DGAC of Section 569RF. 219

Figure 278. Damage parameters used for CTB of Section 569RF. 220

Figure 279. Section 569RF Road Surface Deflectometer. 220

Figure 280. Section 569RF MDD resilient deflections. 221

Figure 281. Section 569RF permanent MDD deformations. 221

Figure 282. Section 569RF average permanent deformation from pavement profile. 222

LIST OF TABLES

Table 1. Summary List of HVS Tests 3

Table 2. Design Thicknesses for Goal 1 Sections 5

Table 3. As-built Thicknesses for Goal 5 Sections 6

Table 4. As-built Thicknesses of Goal 9 Sections 8

Table 5. Influence of Slip Value in LEAP on Calculated Vertical Deflections and Horizontal Strains 25

Table 6. Triaxial Tests on Subgrade. 26

Table 7. Triaxial Tests on Aggregate Base (AB) 26

Table 8. Layer Thicknesses Used for FWD Backcalculation. 36

Table 9. Moduli Parameters from FWD 38

Table 10. Moduli Parameters from Calibration to MDD Deflections. 38

Table 11. Initial Moduli Used in HVS Simulations (MPa). 39

Table 12. Summary of Moduli (MPa). 39

Table 13. Parameters Used in Equation 20 41

Table 14. AC on AC, 2D Structural Parameter Combinations 49

Table 15. Initial Moduli MPa (1.8 km/h, 40 kN, Actual Temperature) for Each Section. 71

Table 16. Final Moduli MPa (1.8 km/h, 40 kN, Actual Temperature) for Each Section. 71

Table 17. Percentage Decrease in Layer Moduli for Each Section. 72

Table 18. Damage Parameter for Asphalt Layers at End of Test for Each Section 72

Table 19. Initial Damage Parameters for “Old” Asphalt Overlay Sections 81

Table 20. Layered Moduli at Start of Test, MPa 103

Table 21. Layer Moduli at End of Test, MPa 103

Table 22. Percentage Decrease in Moduli 104

Table 23. Initial Permanent Deformations, Goal 3, in mm 104

Table 24. Tire Types and Pressure, MPa	114
Table 25. Estimated Temperatures for Section 513RF	133
Table 26. Parameters for FWD Moduli versus Reduced Time, Goal 9	164
Table 27. MB Road, Stiffness Parameters for AB	167
Table 28. Summary of Damage Equations and Shift Factors Used in All Simulations	192
Table 29. Measured and Calculated Road Surface Deflectometer Deflections (RSD), in mm	193
Table 30. Measured and Calculated Deflections of the Top Multi-depth Deflectometer (MDD), in mm	194
Table 31. Final Permanent Deformation of Asphalt, in mm	200
Table 32. Final Permanent Deformation of Granular Layer, in mm	202
Table 33. Parameters used for Granular Materials in Equation (29)	202
Table 34. Final Permanent Deformation of Subgrade, in mm	204
Table 35. Parameters Used for Subgrade in Equation (29)	204
Table 36. Final Permanent Deformation at the Pavement Surface, in mm	206

1.0 INTRODUCTION

The first step in creating a Mechanistic-Empirical (ME) pavement design or evaluation is to calculate pavement response — in terms of stresses, strains, and/or displacements — using a mathematical (or mechanistic) model. In the second step, the calculated response is used as a variable in empirical relationships to predict structural damage (decrease in moduli or cracking) and functional damage (rutting and roughness) to the pavement.

Both of these steps must be reasonably correct. If the calculated response bears little resemblance to the pavement's actual response, there is no point in trying to use the calculation to predict future damage to the pavement with the empirical relationship. In other words, only if the calculated response is reasonably correct does it make sense to try to relate the damage to the pavement response.

1.1 Models and Approaches Included in *CalME*

This report presents the modeling of several series of flexible pavement Heavy Vehicle Simulator (HVS) tests using the set of distress models included in the draft software package, *CalME*. These models are for the flexible pavement distresses typically observed in California: asphalt fatigue, asphalt rutting, unbound layers rutting and reflection cracking.

CalME software provides the user with four approaches for evaluating or designing a flexible pavement structure:

- Caltrans current methods, the R-value method for new flexible structures, and the deflection reduction method for overlay thickness design for existing flexible structures.
- “Classical” Mechanistic-Empirical (ME) design, largely based on the Asphalt Institute method. This method uses a standard Equivalent Single Axle Load (ESAL) for the traffic load, one temperature to characterize the entire range of temperatures the asphalt concrete (AC) layer will experience, and the Asphalt Institute fatigue and unbound layers rutting equations, with an adjustment for air-void content and binder content in the asphalt concrete.
- An Incremental method, using the typical Miner's Law approach, permitting damage calculation for the axle-load spectrum and expected temperature regimes, but with no updating of materials properties through the life of the project. This is similar to the approach included in the NCHRP 1-37A Design Guide, also referred to as the Mechanistic-Empirical Pavement Design Guide (MEPDG). This type of approach is calibrated against an end failure state, such as 25 percent cracking of the wheelpath, and it assumes a linear accumulation of damage to get to that state.
- An Incremental-Recursive method in which the materials properties for the pavement are updated in terms of damage as the simulation of the pavement life progresses. The Incremental-Recursive approach was used for the simulations included in this report, and is the only approach that can provide an accurate indication of pavement condition at different points during the pavement's life.

The research team proposes that pavement designers should begin their designs by applying either an existing Caltrans method or the Classical method. In *CalME* both of these options perform a “design” function, calculating and presenting pavement structures that meet design requirements for a predetermined number of traffic loads. Then, the lowest cost alternatives in the set of candidate pavement structures meeting the design requirements with either of these methods should be checked by the designer with the more comprehensive and precise Incremental-Recursive method to be certain that they meet the design requirements. Once a final design has been selected, its Incremental-Recursive output can be used to provide a prediction of the pavement's condition across its entire life.

Some distresses and some materials are not considered in either the Caltrans or Classical methods, and can only be evaluated using the Incremental-Miner's Law approach or the Incremental-Recursive approach.

1.1.1 Validation Using Heavy Vehicle Simulator Data

The Incremental-Recursive models included in *CalME* were used to predict the performance of all the flexible pavement HVS tests performed to date as part of the Accelerated Pavement Testing (APT) program operated for the California Department of Transportation (Caltrans) by the University of California Pavement Research Center (UCPRC).

The HVS test data presented in this report come from tests performed between 1995 and 2004. The HVS response data and the corresponding laboratory test data were extracted from the UCPRC HVS database.

HVS tests measure pavement response in terms of deflections, either at the pavement surface, using a Road Surface Deflectometer (RSD), at multiple depths, using a Multi-depth Deflectometer (MDD), or both. The RSD is very similar to the Benkelman Beam used in the development of the Caltrans new flexible pavement and overlay design methods in the 1950s. In predicting the gradual degradation of the pavement it is important that the response model provides a reasonably accurate prediction of measured deflections. Although a correct prediction of deflections by the response model is no guarantee that it can also correctly predict the stresses and strains in all of the pavement layers, the opposite is true: if the model inaccurately predicts deflections, it will also provide inaccurate predictions of stresses and strains.

Therefore, in trying to calibrate the ME models from HVS testing, the research team's first concern was to make sure that the model predicted resilient deflections reasonably well for the duration of the test and for all load levels. This prediction depended on the moduli (often referred to as "stiffnesses" in this report and in the literature) of all of the pavement layers and on the changes to these moduli caused by fatigue damage, slip between asphalt layers, non-linear elastic characteristics of the unbound layers, and the effect of confinement on granular layers. Once reasonable agreement was achieved between the measured resilient deflections and the calculated ones, then models of permanent deformation could be calibrated with some confidence.

There are different methods for determining moduli and there are often differences in the results from each method (which should be expected based on the literature.) The methods used in this study included backcalculation of moduli for all layers from Falling Weight Deflectometer (FWD) and MDD deflection data, and direct measurement of moduli in the laboratory using triaxial tests for unbound materials and flexural frequency sweep tests for asphaltic materials. Differences in measured moduli across the different methods are due to variations in boundary conditions, strain levels, and loading times between the different measurement methods, the effects of which vary among materials. The FWD does not fit under the HVS, so there is no FWD data during an HVS test, there is only FWD data from before the HVS was placed on the pavement and from after the HVS was taken off the trafficked section. The simulations in this report primarily relied on stiffnesses for the asphalt materials taken from flexural frequency sweep data, and stiffnesses for the unbound layers taken from backcalculation of MDD deflection data.

In practice, the research team views backcalculation using deflections from the FWD as the primary tool for obtaining the stiffnesses of layers in existing pavements, as opposed to laboratory testing of materials samples taken from the already constructed pavement. FWD deflections and backcalculation take into consideration the stiffness of the layers as they occur in the constructed pavement structure, including the effects of boundary conditions, water and temperature conditions, previous traffic and environmental conditioning, and interaction between layers acting as a system in the in-place pavement structure. This is important because most of Caltrans future work will be rehabilitating and reconstructing pavements already in service.

The research team sees the flexural beam test as the primary tool for measuring the stiffness and the fatigue characteristics of asphalt overlay materials for new layers. For new pavement construction, the team sees the use of databases of moduli for granular bases and subbases and for subgrades backcalculated from FWD tests on existing pavements, with the materials referenced by characteristics such as the Unified Soil Classification System (USCS) classification and relative density. The databases should also include some laboratory triaxial tests for these materials, for comparison with any new base, subbase, and subgrade materials

for which there is no previous FWD testing, and for which laboratory triaxial testing must be used to measure stiffness.

The purpose of this study was to compare the overall trends shown by the damage models in simulations of the HVS tests against the actual trends measured in the same HVS tests. Asphalt concrete stiffnesses from flexural frequency sweep data were used in the simulations of the HVS tests, and the stiffnesses of the underlying moduli were adjusted from their initial values as the asphalt concrete stiffness changed with damage so they would match the measured and calculated deflections. The results presented herein show that, overall, the damage trends for deflection and permanent deformation under loading were verified.

During HVS testing, deflections often increase markedly, with deflection sometimes rising more than twice as high at the end of the test than they were at the beginning. The flexible pavement design model of the NCHRP 1-37A Design Guide (NCHRP 2004) does not consider any decrease in the asphalt concrete modulus as a result of fatigue damage (except for rehabilitation designs). In fact, the NCHRP 1-37A Design Guide includes a model for aging that predicts a continuous increase in the stiffness of asphalt concrete layers across the life of the pavement, resulting in smaller predicted deflections as the pavement is subjected to trafficking. While aging is potentially important, the effect of updating stiffness for aging and not updating it for fatigue damage results in the calculation of unrealistic elastic responses during the pavement life. This may be acceptable for pavements with extremely thick asphalt concrete layers where little fatigue should occur, but it is impossible to use the model to simulate an HVS test and, inversely, to use HVS tests to calibrate the model.

The HVS test series in this report were grouped by “goals,” which are defined as follows:

Table 1. Summary List of HVS Tests

Goal	General Conditions	HVS Test Numbers	Original Report References
Goal 1: Comparison of structures with and without ATPB layer under dry conditions, moderate temperatures	New pavement, dry conditions, 20°C	500RF, 501RF, 502CT, 503RF	14, 15, 16, 17, 18
Goal 3 Cracking: Comparison of reflection cracking performance of ARHM-GG and DGAC overlays	Overlays of cracked Goal 1 sections, dry conditions, 20°C	514RF, 515RF, 517RF, 518RF	8, 11, 13
Goal 3 Rutting: Comparison of rutting performance of ARHM-GG and DGAC overlays	Overlays of previously untrafficked areas of Goal 1 pavements, dry conditions, 40°C or 50°C at 50-mm depth, four different tire/wheel types	504RF, 505RF, 506RF, 507RF, 508RF, 509RF, 510RF, 511RF, 512RF, 513RF	7, 10
Goal 5: Comparison of structures with and without ATPB layer under wet conditions, moderate temperatures	New pavement, wet conditions, 20°C	543RF, 544RF, 545RF	2, 3, 4, 5, 13
Goal 9: Initial cracking of asphalt pavement in preparation for later overlay	New pavement, ambient rainfall, 20°C	567RF, 568RF, 569RF, 571RF, 572RF, 573RF	1

ATPB: Asphalt-treated permeable base.

ARHM-GG: Asphalt-rubber hot-mix gap-graded.

DGAC: Dense-graded asphalt concrete.

The Goal 1, 3, and 5 tests were performed inside a metal shed built over native subgrade. The shed provided protection from sun, wind, and rain; however, changes in subgrade water content and the depth to the water table were recorded during HVS tests. Goal 9 tests were performed on a road with no cover other than what the HVS and its temperature cabinet provided.

The remainder of this chapter presents the general descriptions of the HVS tests and the models used to simulate them.

1.2 HVS tests

1.2.1 Goal 1 and Goal 3 Tests

Figure 1 shows the layout of the Goal 1 and Goal 3 cracking sections.

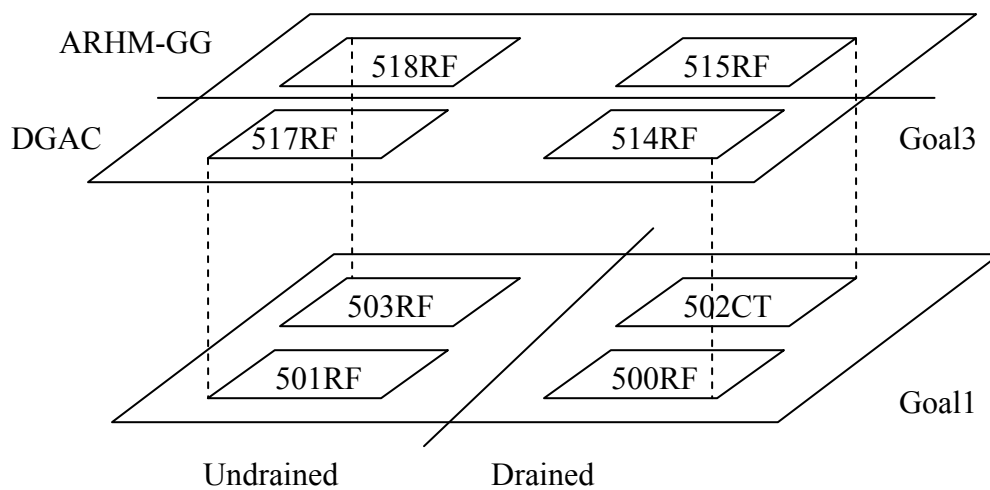


Figure 1. Layout of 20°C test sections. Goal 3 rutting sections are distributed in the area between the 20°C test sections.

All the sections in Goal 1 had two layers of asphalt concrete (AC), an aggregate base (AB), and an aggregate subbase (ASB). In the two drained sections, part of the AB layer thickness was replaced by an asphalt-treated permeable base (ATPB) at a ratio of 1.4:1.1. A constant temperature of about 20°C was maintained during Goal 1. The design layer thicknesses are shown in Table 2.

Table 2. Design Thicknesses for Goal 1 Sections

Layer	Undrained (mm)	Drained (mm)
AC top lift	61	61
AC bottom lift	76	76
ATPB	None	76
AB	274	182
ASB	229	229

The subgrade was clay, with varying plasticity across the pavements.

Goal 3 was an overlay study with an asphalt rubber hot-mix gap-graded (ARHM-GG) (the acronym ARHM, asphalt rubber hot-mix gap-graded, refers to the material specification at the time of construction in April 1997.) concrete and a dense-graded asphalt concrete (DGAC). The four Goal 3 Cracking tests were performed at the same temperature as Goal 1 (20°C), with similar wheel types and loads. For these tests the design thickness of the DGAC overlay (75 mm) was approximately twice as thick as that of the ARHM (40 mm), and the overlays were placed over the four previously cracked Goal 1 sections. The remainder of Goal 3 was done at higher temperatures, with the two overlays placed on previously untested areas of the Goal 1 pavement, and several overlay thicknesses, tire types, and wheel loads used in the testing. (Table 1 provides the reference numbers for the reports containing the details regarding thickness, tire types, and wheels loads.)

All the HVS tests at 20°C started with a wheel load of 40 kN, which was increased stepwise to 100 kN. Most of the load applications were at 100 kN. Bias-ply tires on a dual wheel were used for the Goal 1 tests. The same radial tires on a dual wheel were used for the Goal 3 Cracking tests, and the Goal 5 and Goal 9 tests. Various tires and wheels were used for the Goal 3 Rutting tests, with the load for the entire duration of all but one test fixed at 40 kN. [De Beer and Fisher (1997) describe the details of the tire contact stresses measured.] For all the tests except the Goal 3 Rutting tests, the wheel load was a dual wheel with a centerline distance of 305 mm and an assumed tire pressure of 690 kPa for all load levels. It was assumed that the wheels distributed the load over two circular areas; this assumption was reasonably correct for the low load level (40 kN) but not for the high load level (100 kN, where the actual load distribution was closer to two rectangles with one side twice the length of the other).

All the 20°C sections were instrumented with MDDs. Each section in Goal 1 had two MDDs. Each section had two additional MDDs installed for Goal 3 testing. All MDD anchor depths were assumed to be 3,000 mm. Not all MDD modules functioned for the duration of the tests.

The as-constructed layer thicknesses given in Harvey et al. (1999) were used for the analyses of the Goal 1 and Goal 3 results presented in this report. As-built layer thicknesses given in Bejarano et al. (2003) and Bejarano et al. (2005) were used to analyze the Goal 5 and Goal 9 results respectively. The remaining data was imported from the UC Pavement Research Center database, taken from a subset database named *PRC-HVS.mdb*.

Although actual wheel speeds varied, they were assumed to be 7.6 km/h during HVS testing and 1.8 km/h during deflection measurement on the MDDs. All tests other than the Goal 3 Rutting tests were performed with bidirectional loading. The Goal 3 Rutting tests were performed with unidirectional loading.

The temperature of the test sections was controlled by a “temperature control box.” The actual temperatures of the asphalt layers were recorded and used in the simulations.

Poisson’s ratio was assumed to be 0.35 for all layers.

1.2.2 Goal 5 Tests

The Goal 5 tests were performed on the overlay structures of Goal 3 in locations where the overlay had not been placed on previously trafficked and cracked Goal 1 pavement. The designed structures were:

- Section 543RF drained with ATPB and 40-mm ARHM-GG wearing surface,
- Section 544RF undrained (no ATPB) and 40-mm ARHM-GG wearing surface, and
- Section 545RF undrained (no ATPB) and 75-mm DGAC wearing surface.

The structures' as-built thicknesses are shown in Table 3.

Table 3. As-built Thicknesses for Goal 5 Sections

Layer	Section 543RF (mm)	Section 544RF (mm)	Section 545RF (mm)
Wearing course	36	51	90
AC (two lifts combined)	140	149	143
ATPB	64	none	none
AB	180	272	259
ASB	223	205–310	206–280

All of the test sections had a 2 percent transverse gradient and an approximate 0.5 percent longitudinal gradient in all the layers above the subbase. Holes with a diameter of 38 mm were drilled through the asphalt concrete layers on the uphill side of the three HVS test sections, and a drip watering system was installed to continuously put water into the pavement. Holes were drilled into the top of the ATPB layer of Section 543RF so that water entered into that layer. Sections 544RF and 545RF had holes drilled into the top of their aggregate bases, and water entered those layers. The water flow was greater into Section 543RF because of the initial high permeability of its ATPB layer. Considerably less water flowed into the other two sections because of the relative impermeability of their AB layer. Figure 2 shows the drip watering system. Each pavement section had water introduced into it for more than a month prior to HVS loading. This allowed the section to reach an approximate steady-state moisture condition.

Goal 5 testing used the same dual-wheel, radial tire configuration as Goal 3 testing. Similar loading patterns and the same temperature control provided a basis for comparing the results from Goal 3 and Goal 5 tests to the result of Goal 1 (dry condition) testing. In addition, two MDDs were installed in each pavement section, with depths similar to those used for Goal 1.

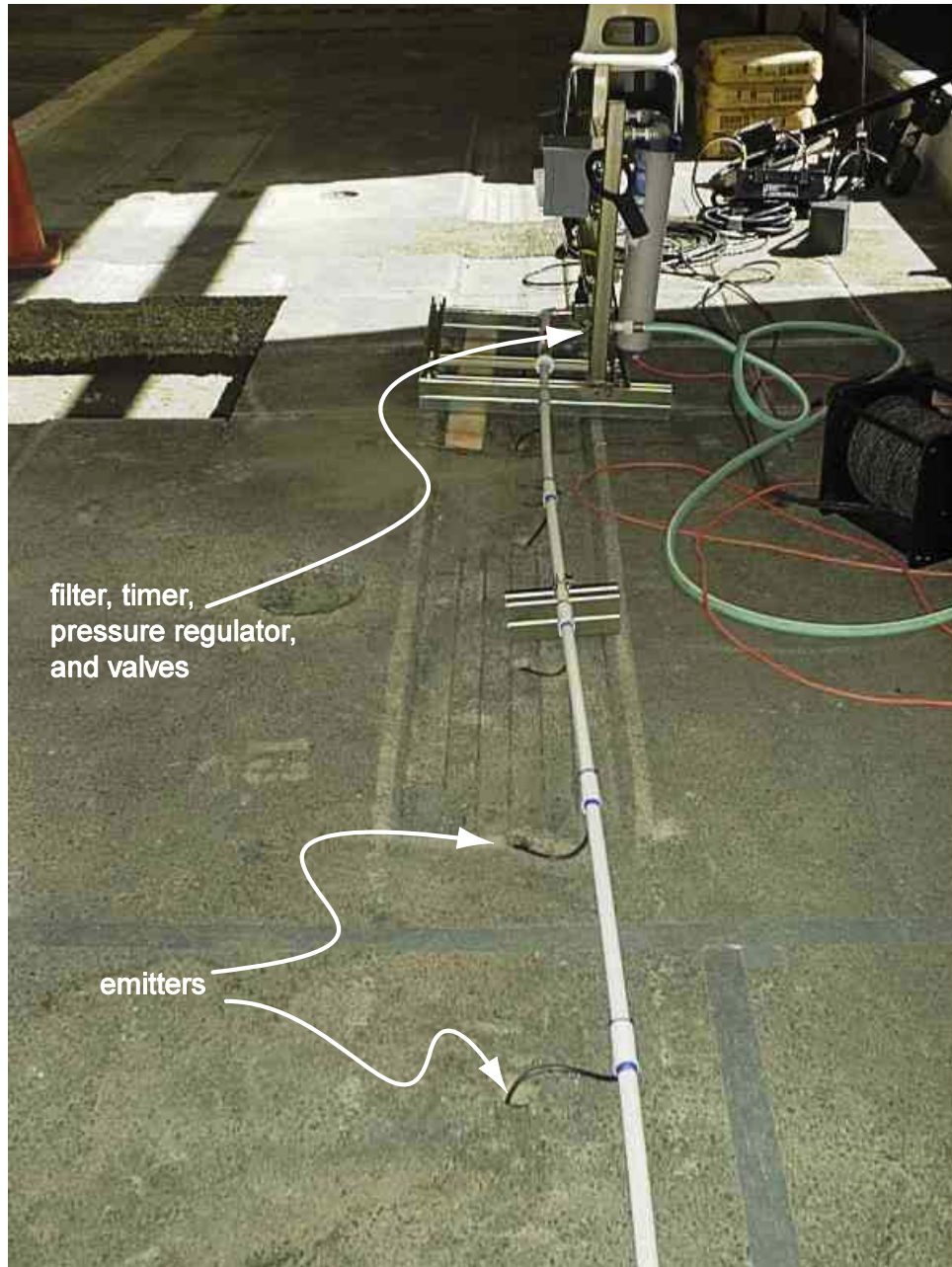


Figure 2. Drip watering system for Goal 5 tests.

1.2.3 Goal 9 Tests

Six HVS tests were performed on what were designed to be identical pavement structures. The primary purpose of the six tests was to provide fatigue-cracked sections for subsequent placement of different kinds of overlay for HVS reflection cracking tests; these would be similar to the work performed in the Goal 3 cracking tests.

The pavements were built so that they aligned with an existing access road. When the existing structure was removed, its subgrade was compacted to state standards. (Figure 3 shows the layout of the six

test sections.) The structures' design thicknesses were: 410 mm of AB with 90 mm of dense-graded asphalt concrete (DGAC). (Table 4 shows the as-built thicknesses.)

The dual-wheel and radial tire configuration used for the Goal 3 tests was used for Goal 9. Loads were generally lower than those used during Goals 1, 3, and 5 to minimize rutting. Temperatures were maintained close to 20°C, as on the other cracking tests.

Two MDDs were placed in each test section. However, most of the MDD modules below the surface either never functioned or failed during the test.

Table 4. As-built Thicknesses of Goal 9 Sections

Layer	567RF	568RF	569RF	571RF	572RF	573RF
AC	78	80	81	82	78	76
AB	352	349	337	352	349	337

1.3 Response and Damage Models

Response and damage models are presented in this section, and they are discussed in terms of the materials properties common to the Goal 1, 3, and 5 tests. The materials properties of the Goal 9 tests are discussed with the description of the simulations for those tests later in this report.

1.3.1 Asphalt Modulus

Asphalt modulus was determined as a function of temperature and loading time, using the NCHRP 1-37A Design Guide model (NCHRP 2004):

$$\log(E) = \delta + \frac{\alpha}{1 + \exp(\beta + \gamma \log(tr))} \quad (1)$$

where E is the modulus in MPa,
 tr is reduced time in sec,
 α , β , γ , and δ are constants, and
 logarithms are to base 10.

Reduced time is found from:

$$tr = It \times \left(\frac{visc_{ref}}{visc} \right)^{aTg} \quad (2)$$

where It is the loading time (in sec),
 $visc_{ref}$ is the binder viscosity at the reference temperature,
 $visc$ is the binder viscosity at the present temperature, and
 aTg is a constant.

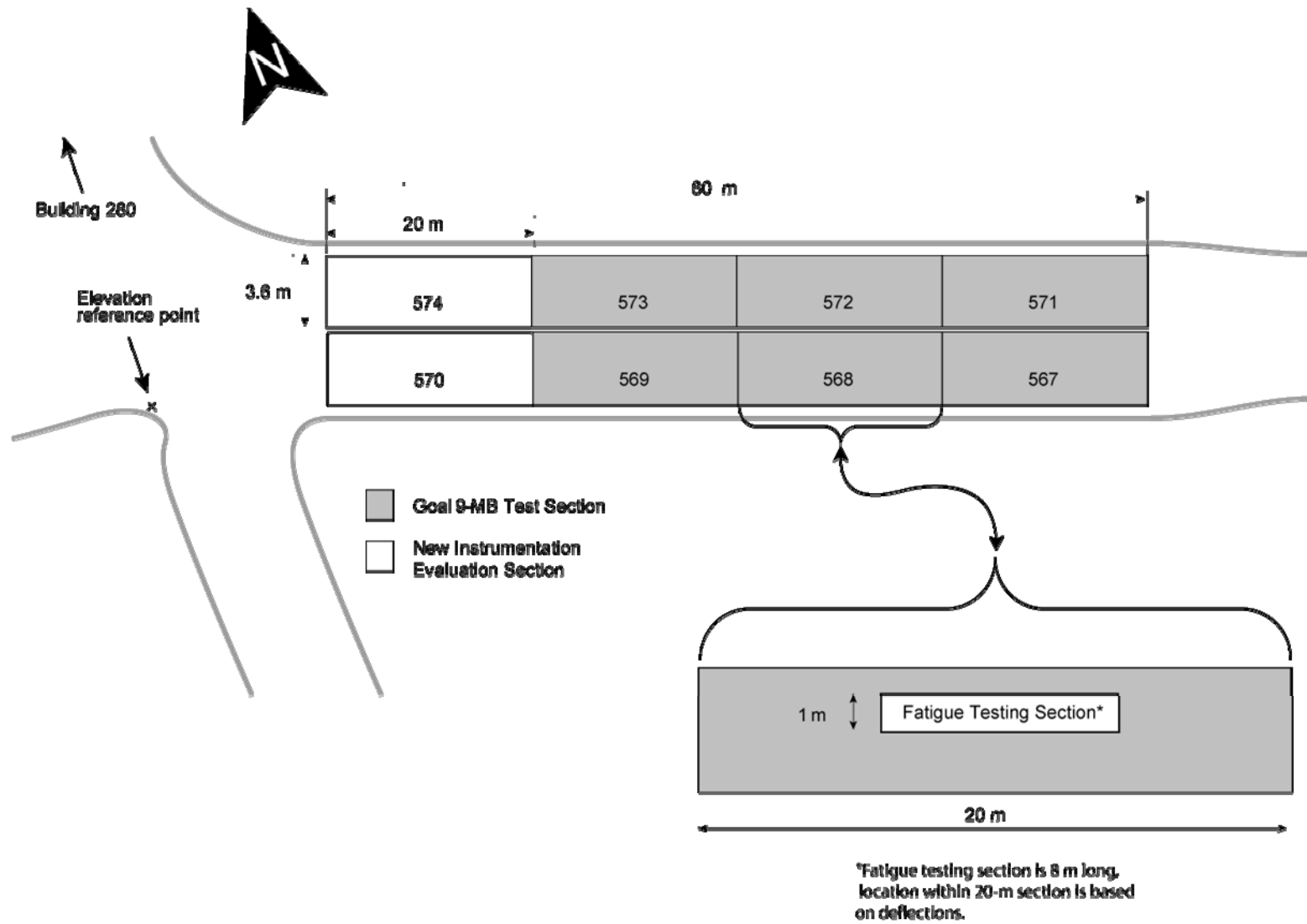


Figure 3. Layout of Goal 9 test sections.

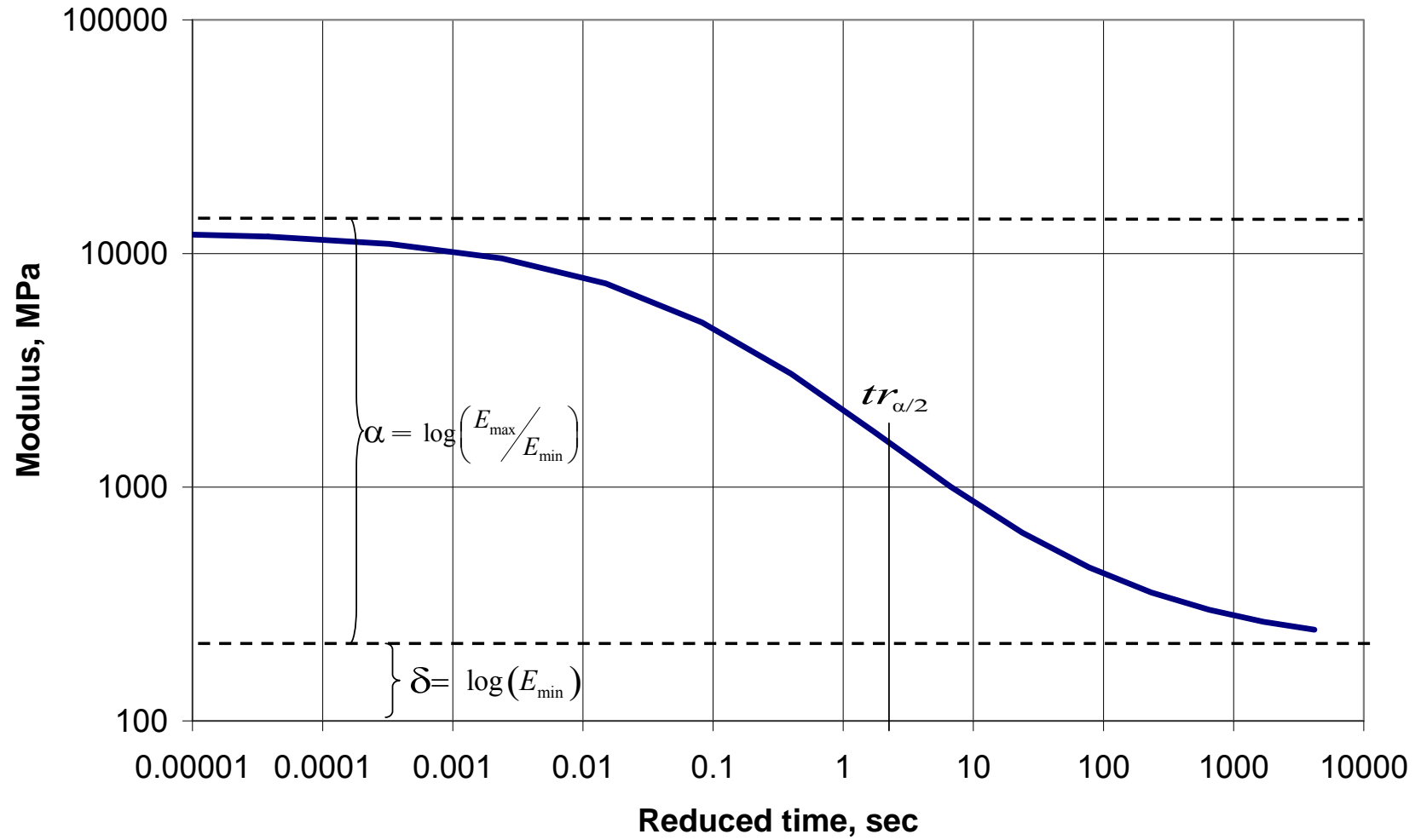


Figure 4. Example of modulus versus reduced time relationship.

Equation 1 may also be written:

$$\log(E) = \delta + \frac{\alpha}{1 + \left(\frac{tr}{tr_{\alpha/2}}\right)^{\gamma'}} = \log(E_{\min}) + \frac{\log\left(\frac{E_{\max}}{E_{\min}}\right)}{1 + \left(\frac{tr}{tr_{\alpha/2}}\right)^{\gamma'}} \quad (3)$$

where $\gamma' = \frac{\gamma}{\ln(10)}$ and $tr_{\alpha/2} = \exp\left(\frac{-\beta}{\gamma} \times \ln(10)\right)$

$tr_{\alpha/2}$ is the reduced time corresponding to $\log(E) = \delta + \alpha/2$, as indicated in Figure 4. Equation 1 is normally used with frequency sweep data to characterize the master curve. The form of the master curve equation shown in Equation 2 provides some insight, and can be used if E_{\max} and E_{\min} were known. E_{\max} is related to the limiting stiffness of asphalt binder at temperatures below the glass transition temperature. E_{\min} appears to depend on the boundary conditions under which it was measured, with different values coming from backcalculation of in-situ pavements and beam fatigue tests.

From Equation 2 it can be seen that changing $tr_{\alpha/2}$ will shift the curve left or right and changing γ' will change the curvature.

The loading time is determined from the speed of the wheel (input on the incremental design screen in *CalME*) and from the depth at which the loading time is desired.

Loading time is a rather uncertain notion, as it will vary for different types of responses. For example, the loading time for transverse strain will be much longer than it is for longitudinal strain because of the actual shape of the contact area of the tire on the pavement, which is longer in the longitudinal direction than the transverse direction. The reason for the longer loading time for transverse strain is that the transverse strain is tangential to the load, whereas the longitudinal is radial and therefore has a sign change. The loading time is calculated from $(200 \text{ mm} + 2 \times \text{depth}) / (\text{wheel speed in mm/sec})$. The reference loading time is 0.015 sec (15 msec, roughly corresponding to the loading time of a standard FWD, where loading time refers to a creep test), and the reference temperature is 20°C.

The NCHRP 1-37A Design Guide makes use of an “effective depth” based on the equivalent thickness of the layers, which results in longer loading times. The guide, however, then converts loading time into frequency, using $f = 1/lt$, rather than $f = 1/(2\pi lt)$, more than compensating for the longer loading time (unless loading time is defined differently, i.e., it is not based on a creep test).

Viscosity is found from:

$$\log(\log(\text{visc cPoise})) = A + VTS * \log(t_K) \quad (4)$$

where t_K is the temperature (in °K), and
 A and VTS are constants, and
 $cPoise$ indicates units of centipoise

For all of the asphalt materials in this report a value of $A = 9.6307$ [10.5254 with temperature in °R (degrees Rankine)] and $VTS = -3.5047$ were used. These values correspond (according to the NCHRP 1-37A Design Guide) to an asphalt with a penetration grade of 40–50.

If the minimum modulus, E_{\min} , the maximum modulus, E_{\max} , and the modulus at two different temperatures are known, the viscosity versus temperature relationship (Equation 4) will have very little influence on the modulus versus temperature relationship. This can be seen in Figure 5, where the resulting modulus versus temperature relationship is shown for asphalts with penetration grades from 40–50 to 200–300 and for a PG64-22 grade asphalt.

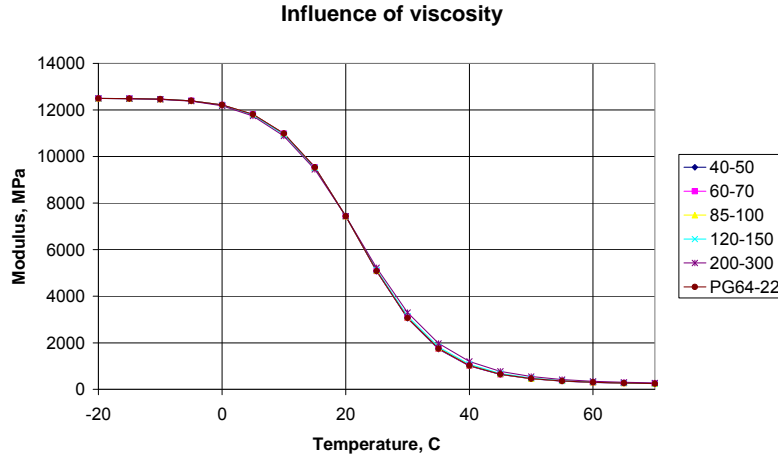


Figure 5. Modulus versus temperature for different viscosity versus temperature relationships.

The constants δ , β , γ , and aTg , and the modulus at the reference temperature (20°C) were derived from flexural frequency sweep tests. The constant a is calculated by the program. The frequency sweep tests were available for the top and bottom asphalt layers of Goal 1 and for the overlays in Goal 3.

The fit between frequency sweep data and model data is shown in Figure 6. In fitting the model to the frequency sweep data it was assumed that the minimum modulus (10^0) was 200 MPa ($\delta = 2.3010$). In the frequency sweep test the measured modulus was considerably lower. However, based on FWD testing, it was assumed that an asphalt layer's modulus, even at very low frequencies and high temperatures, had a minimum value greater than the one measured in the frequency sweep test on a flexural beam. This variance is attributable to the differences in boundary conditions between a laboratory test, such as a flexural beam frequency sweep and the same material when it is part of a layered pavement structure in the field. Specifically, a flexural beam is suspended in space without confinement in a flexural frequency sweep test. In contrast, the same asphalt concrete material, confined below and on its sides when it is part of a pavement layer, has its modulus increased. (In this confined condition, the aggregate in the asphalt concrete, which has its own relatively unchangeable high modulus, also has a large compressive stress component applied to it.)

Figure 7 shows an example of the input parameters for the AC bottom layer. A modulus-versus-reduced time relationship was assumed for the ATPB, based largely on laboratory triaxial testing. The ATPB had a modulus of 1144 MPa at a temperature of 20 C and a loading time of 0.015 sec. A minimum modulus of 200 MPa was assumed.

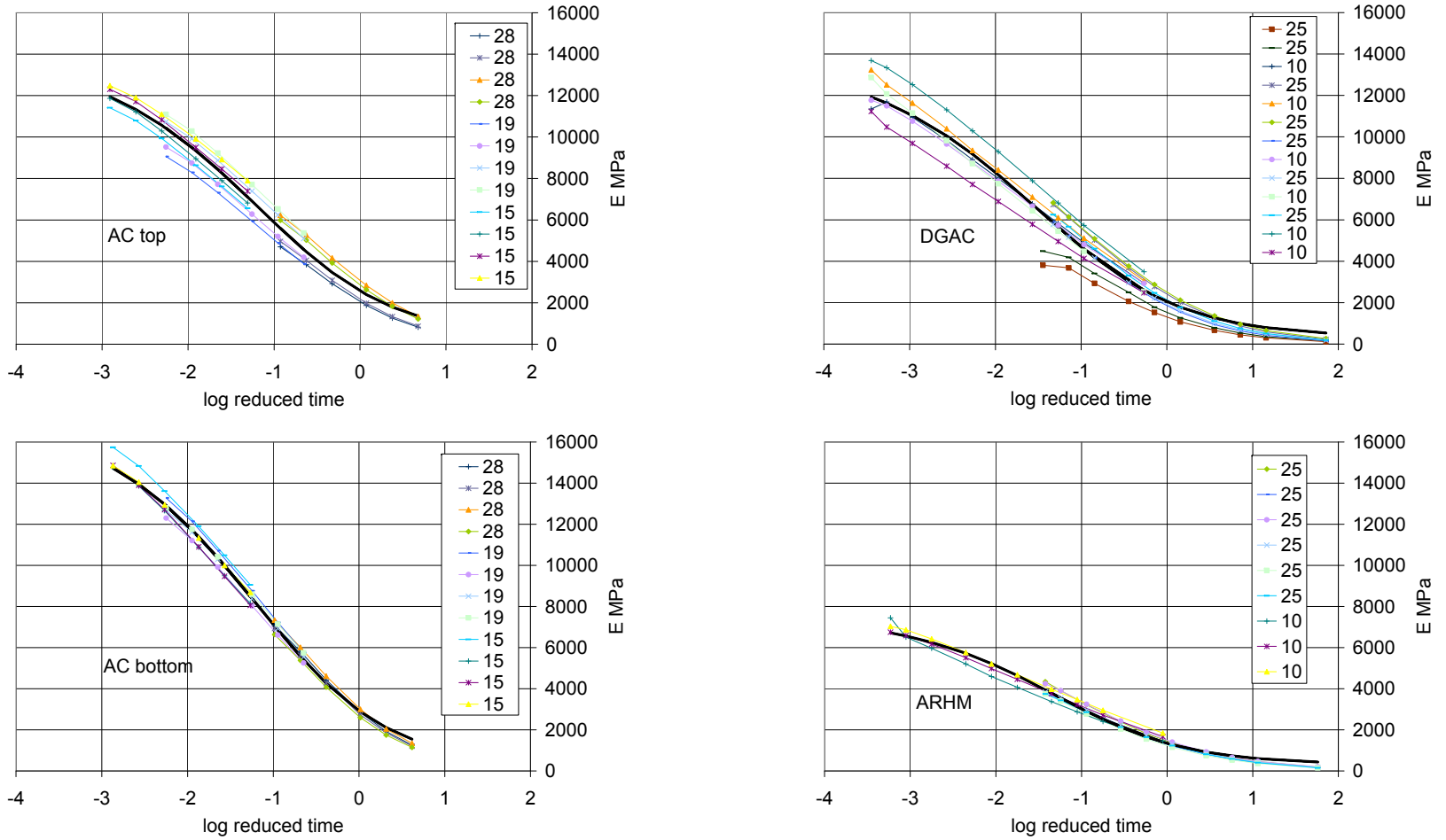


Figure 6. Frequency sweep data for Goal 1 and Goal 3 materials compared to models.

Figure 7. Example of input parameters for the modulus-versus-reduced time relationship for the AC bottom layer.

1.3.2 Fatigue

The modulus of damaged asphalt was calculated as:

$$\log(E) = \delta + \frac{\alpha \times (1 - \omega)}{1 + \exp(\beta + \gamma \log(tr))} \quad (5)$$

where the damage, ω , was calculated from:

$$\omega = A \times MN^\alpha \times \left(\frac{\mu\varepsilon}{200 \mu\varepsilon} \right)^\beta \times \left(\frac{E}{3000 \text{ MPa}} \right)^\gamma \times \exp(\delta \times t) \quad (6)$$

where E is the modulus of damaged material,

MN is the number of load repetitions in millions ($N/10^6$),

$\mu\varepsilon$ is the strain in μstrain ,

t is the temperature in $^\circ\text{C}$, and

α , β , γ , and δ are constants (these constants are the same as the constants in Equations 1 through 5, and different in Equation 6).

The initial (intact) modulus, E_i , corresponds to a damage, ω , of 0, and the minimum modulus, $E_{min}=10^\delta$, to a damage of 1.

Equation 5 leads to:

$$\log(E) - \delta = (\log(E_i) - \delta) \times (1 - \omega), \text{ or}$$

$$\frac{E}{E_i} = \left(\frac{E_{min}}{E_i} \right)^\omega, \text{ or} \tag{7}$$

$$\omega = \frac{\log\left(\frac{E_i}{E}\right)}{\log\left(\frac{E_i}{E_{min}}\right)}$$

The NCHRP 1-37A Design Guide calculates the modulus of damaged asphalt, for rehabilitation purposes, using Equation (5), but at the same time the Guide defines ω as the relative decrease in modulus (although this is mistakenly indicated as E/E_i in the report for the Guide). This definition of ω included in the NCHRP 1-37A Design Guide is inconsistent with Equation 5, as shown in Equation (7)

The one-stage Weibull distribution, Equation (8), could be used instead of Equation 6:

$$SR = \exp\left(-\alpha \times N^\beta\right) \tag{8}$$

where SR is the stiffness reduction ($= E/E_i$),
 N is the number of load applications, and
 α and β are constants, different from those used in previous equations.

Combining Equations (7) and (8) one gets:

$$\omega = \frac{\ln\left(\frac{E}{E_i}\right)}{\ln\left(\frac{E_{min}}{E_i}\right)} = \frac{\ln(SR)}{\ln\left(\frac{E_{min}}{E_i}\right)} = \frac{-\alpha \times N^\beta}{\ln\left(\frac{E_{min}}{E_i}\right)} = \frac{\alpha}{\ln\left(\frac{E_i}{E_{min}}\right)} \times N^\beta \tag{9}$$

which has the same format as Equation 6. In the present version of *CalME* (September 2006) it is assumed that α and β can be written in the format:

$$\alpha = \exp(\alpha A + \alpha B \times t + \alpha C \times \ln(w) + \alpha D \times t \times \ln(w))$$

$$\beta = \beta A + \beta B \times t + \beta C \times \ln(w) \tag{10}$$

where t is the temperature in °C,
 w is the internal energy density ($\frac{1}{2} \times \epsilon^2 \times E$),
 and αA , αB , αC , αD , βA , βB , and βC are constants fit from the beam fatigue data.

Fatigue parameters were determined for the AC top and AC bottom of Goal 1 and for the DGAC and ARHM overlays of Goal 3, based on four-point bending beam tests at 10 Hz under controlled strain.

In determining the fatigue parameters it was assumed that for Equation 6 that β was equal to two times γ . This reduces the number of parameters to be determined by one, and it ensures that the damage is a function of the internal energy density ($\frac{1}{2} \times \epsilon^2 \times E$).

The parameters were determined by minimizing the root-mean square (RMS) difference between the calculated relative modulus (E/E_i) and the experimental data for values of $E/E_i > 0.3$, the stiffness ratio to which most of the beam fatigue tests were carried out.

An example of damage versus number of load applications is shown in Figure 8 which shows the damage at a temperature of 20°C for a constant strain of 400 μ strain. The four materials are surprisingly similar with respect to damage.

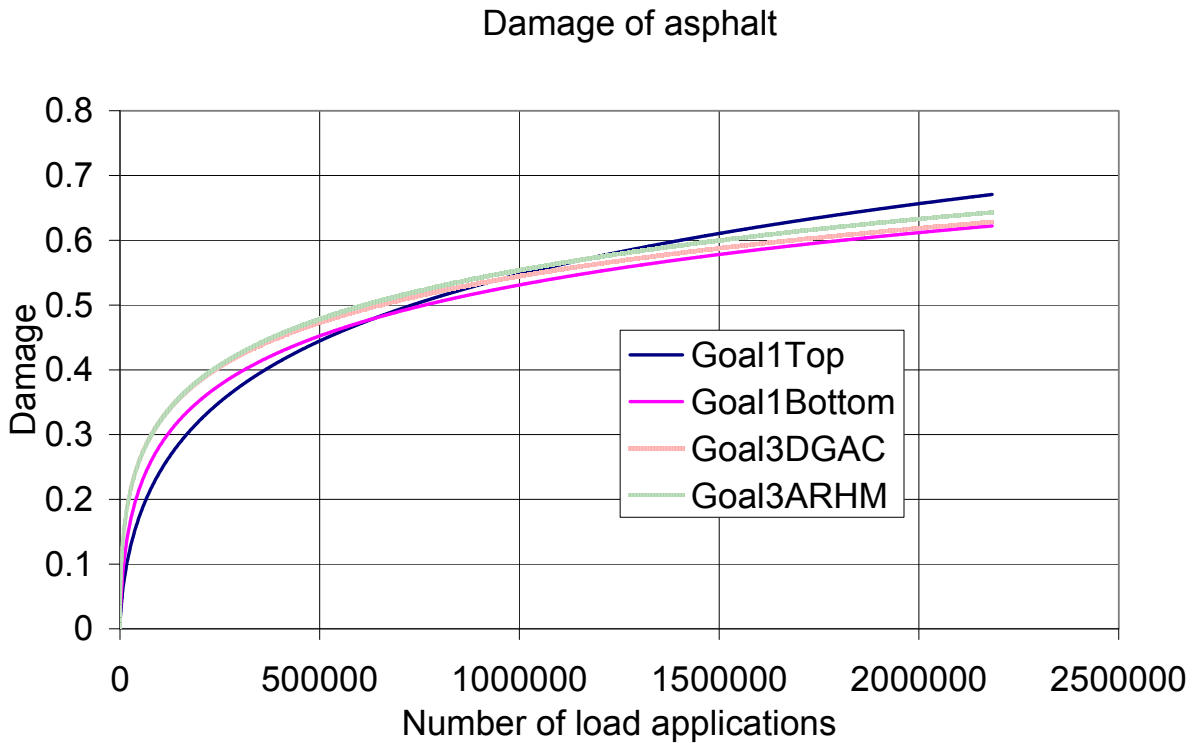


Figure 8. Example of damage versus number of load applications.

For ATPB a damage function (Equation 6) was chosen based on the damage function for the bottom lift of Goal 1, but with a value of A about fifty times as high.

Figure 9 shows an example of the damage parameters for Equation 6 for the AC bottom lift of Goal 1. The parameters of interest here are the values of the first column (under the heading “Fatigue, dE/E_i ”). The response type is the horizontal tensile strain at the bottom of the layer (the minor principal strain) indicated by the Response type “e”. The parameters A , α , Reference strain ($Resp_{ref}$), β , Reference modulus (E_{ref}), γ , and δ are given. The parameter Std A is a Standard Deviation factor on A that is used in the Monte Carlo simulations, which are not used in this report. The number of *in situ* load applications is divided by the Shift Factor given at the bottom of the column to allow for differences between laboratory testing and field conditions. A Shift Factor of 3 was used for all materials, i.e., three HVS loads were assumed to give the same damage as one laboratory load.

Name: DGACVHVS1B R value: 0 Gravel factor: 1.46 Cancel Save as default Save to project only

Modulus Classical Incremental **Recursive** Environment

Damage = $A * MN^{\alpha} * (\text{response/reference response})^{\beta} * (E/\text{reference modulus})^{\gamma}$, MN million passages
AC shear, rd mm = $A * MN^{\alpha} * \exp(\beta * \text{shear stress MPa/reference shear stress}) * (\text{elastic shear microstrain})^{\gamma}$

	Fatigue, dE/Ei	Permanent deformation, mm	Crushing, dE/Ei	Roughness, IRI m/km
Response type	e	e	z	e
A	0.001245	1.1	0	0.3
Sdf A	1.1	1.1	1.1	1.1
alfa	0.8399	0.333	0.6	0.2
Respref	-200	1000	1.53	1000
beta	3.9718	1.333	7.69	1.333
Eref	3000	40	10000	40
gamma	1.9859	0.333	-15.4	-1
delta	0.1913			
Shift factor	3			

Figure 9. Example of Equation 6 damage parameters of AC bottom layer (Goal 1).

1.4 Weak Bonding

Weak bonding between the top and bottom asphalt lifts of Goals 1, 3, and 5 was found for certain areas of the HVS test sections. It appeared that the top AC layer had moved horizontally with respect to the bottom AC layer. During forensic studies a brown discoloration and scratch marks were observed on the surfaces of the materials at the interface where slip had apparently occurred. Cores showed no bonding at the interface.

The layered elastic analysis program (LEAP) option of *CalME* has a parameter that controls the degree of bonding between two layers, referred to as “slip” in LEAP if less than full bonding and “stick” if full bonding. Full bond corresponds to a high value (10^5 is used in *CalME*), and a value of 0 corresponds to full slip (i.e., there is no bond between the layers). The logarithm of this parameter is decreased linearly until the final slip is reached, as a function of the number of loads in ESALs. The number of ESALs corresponding to final slip is not known, but the shape of the deflection-versus-number of loads curve can serve as a guide.

The LEAP program treats the pavement structure as a continuum, which means that the two materials above and below the slip interface will be in contact for all points of the interface. This is not a completely realistic assumption, but with the present response models it cannot be changed. [A three-dimensional Finite Element Model (FEM) would be required to change that assumption.]

It is likely that this incorrect modeling of the slip interface will have different effects on deflections, on horizontal strains at the interface, and on the shear stress and strain at a depth of 50 mm. (This depth is used for calculating the permanent deformation of the AC layer. This is described later). For deflection and shear

stress, it is likely that friction between the two layers immediately under the wheel will result in only a partial slip occurring because of the high compressive normal force, whereas the maximum horizontal strains may well correspond to a condition closer to full slip.

Table 5 Influence of Slip Value in LEAP on Calculated Vertical Deflections and Horizontal Strains

Slip Value	0-10 ⁻⁴	10 ⁻³	10 ⁻²	10 ⁻¹	1	10	10 ²	10 ³	10 ⁴	10 ⁵
d 0 mm*	0.526	0.526	0.525	0.517	0.473	0.396	0.370	0.367	0.367	0.367
d 625 mm*	0.276	0.276	0.276	0.272	0.253	0.228	0.220	0.220	0.219	0.219
Ex top*	230	230	229	222	182	83	14	0	-2	-2
Ex bottom*	232	232	232	232	226	196	168	162	161	161

*Note: d 0 mm is vertical deflection at surface, d 625 mm is vertical deflection at 625 mm depth, Ex top is horizontal strain at the bottom of the top asphalt layer, Ex bottom is the horizontal strain at the bottom of the bottom asphalt layer.

Table 5 shows an example, taken from Section 501RF, of the influence of the slip value on the deflection at the surface (d 0 mm) and the deflection of the subgrade (d 625 mm), and the horizontal strain at the bottom of the top AC layer (Ex top, tensile as positive) and at the bottom of the bottom AC layer (Ex bottom).

A slip value of 0.0001 was chosen for the main simulations. This corresponds to full slip between the layers. At the interface with full slip the shear stress will be zero. The shear stress used for calculating permanent deformation in the asphalt is at a depth of 50 mm, which is only slightly above the interface. When full slip develops, the shear stress at depth 50 mm will therefore decrease considerably. As was mentioned above, this may not be realistic, so a second simulation was carried out with full bonding to determine the permanent deformation of the asphalt. During this simulation the stiffness factors for the unbound layers and the shift factor for asphalt fatigue were adjusted to assure that the pavement deflection history was still correct. These simulations with no slip were only used for determining the permanent deformation of the asphalt.

1.5 Unbound Layers

1.5.1 Triaxial Tests

Table 6 shows the results of triaxial tests on the subgrade material (Harvey et al. 1996). Two specimens were tested, compacted at different density and moisture content (MC) and either soaked or saturated. The tests were done at a confining stress of 7 kPa, which is close to the static confining stress at the top of the subgrade. The parameters C and n are defined by the equation:

$$E = C \times \left(\frac{\sigma_d}{0.1 \text{ MPa}} \right)^n \quad (11)$$

where E is the modulus, and
 σ_d is the deviator stress.

The column “E(30 kPa)” indicates the modulus, at a deviator stress of 30 kPa, which is a typical stress at the top of the subgrade under a 40 kN dual wheel load.

Table 6. Triaxial Tests on Subgrade

Density	MC%	Condition	C	n	E(30 kPa)
2.06 g/cm ³	22.4	Soaked	36.2	-0.34	55 MPa
2.12 g/cm ³	15.8	Soaked	66.5	-0.32	98 MPa
2.12 g/cm ³	15.8	Saturated	41.5	-0.27	57 MPa

Triaxial tests were done on one AB specimen, with the results shown in Table 7. The sample was compacted to a density of 2.47 g/cm³ at a MC of 5.5 percent. The top of the specimen was exposed for ten days to simulate the effects of exposure to air on the test section. The moisture content dropped from 5.5 percent to 2.9 percent during the ten days. After testing the specimen was saturated and tested again.

Table 7. Triaxial Tests on Aggregate Base (AB)

Condition	k ₁	k ₂	E(50 kPa)
Exposed	481	0.16	430 MPa
Saturated	201	0.49	143 MPa

The constants k_1 and k_2 are defined by the equation

$$E = k_1 \times \left(\frac{\theta}{0.1 \text{ MPa}} \right)^{k_2} \quad (12)$$

where E is the modulus, and
 θ is the bulk stress.

The column “E(50 kPa)” indicates the modulus at a bulk stress of 50 kPa. According to the theory of elasticity, the bulk stress in the AB and ASB would vary from more than 100 kPa to negative values when the confining pressure is less than zero (the granular layers are in tension).

1.5.2 Influence of Stiffness of Layers above an Unbound Layer

The increase in deflection during the HVS loading cannot be fully explained by the development of slip between the two Goal 1 asphalt layers and the decrease in asphalt modulus from damage. However, the increase in deflection must be caused at least partly by an additional decrease in the moduli of the unbound layers. This is obvious from the resilient MDD deflections and it is consistent with FWD backcalculation results for the HVS test sections and for pavements tested by the research team at several seasonal monitoring sites in the state. These tests showed that the moduli of some of the unbound layers varied with the modulus of the asphalt, and that they decreased with decreased asphalt stiffness (e.g., when it was caused by increasing temperature).

This decrease in the modulus of the unbound layers with decreasing stiffness of the asphalt layers could be caused by the non-linear characteristics of the unbound materials. The modulus of an unbound material will increase with increasing confining stress and decrease with increasing deviator stress (see the results of the triaxial tests above as an example). For Level 1 input of material parameters in the NCHRP 1-37A Design Guide, the following relationship describes the stress dependency of unbound material:

$$M_R = k_1 \times \left(\frac{\theta}{p_a} \right)^{k_2} \times \left(\frac{\tau_{oct}}{p_a} + 1 \right)^{k_3} \quad (13)$$

where p_a is atmospheric pressure (0.1 MPa),
 θ is the bulk stress (equal to the first stress invariant), and
 τ_{oct} is the octahedral shear stress.
 The constants k_1 , k_2 , and k_3 are determined from triaxial testing.

However, it seems reasonable to assume that the modulus should also be a function of the strength of the material. At a stress condition close to failure, the modulus must presumably be low. With a simple, 2D Drucker-Prager model, “failure” may be given by (see Figure 10):

$$q = k + p \times \tan(\alpha) \quad (14)$$

where p is the mean normal stress (or hydrostatic pressure = $\theta/3$),
 k is the strength at pure shear ($p = 0$), and
 q is the deviator stress (= $3/\sqrt{2} \times \tau_{oct}$).

The modulus will be increasing with increasing p , and it seems reasonable to assume that it will decrease the closer the stress state gets to failure:

$$E = k_1 \times \left(\frac{p + p_0}{p_a} \right)^{k_2} \times \left(1 - \frac{q}{(p + p_0) \times \tan(\alpha)} \right)^{k_3} \quad (15)$$

where $p_0 = k/\tan(\alpha)$.

According to the model, when failure is reached the modulus will be 0. This equation could also be given in terms of the first stress invariant, $I_1 = 3 \times p$, and the square root of the second deviator stress invariant, $\sqrt{J_2} = q/\sqrt{3}$.

To study the effects of this relationship, a few calculations were carried out using an axial symmetric Finite Element program. A structure with three asphalt layers — of 70 mm, 10 mm, and 70 mm — was assumed. With full bonding, the modulus of the 10-mm thick intermediate layer was assumed to be the same as for the other two asphalt layers; slip was modeled by reducing the modulus of the thin layer to 10 MPa. This would result in incorrect deflections, but should have worked reasonably well for stresses and strains (the only response of interest here). The asphalt layers were followed by a 400-mm thick granular layer on a subgrade with constant modulus of 100 MPa.

For the granular layer the following parameters were assumed:

$$E = 300 \text{ MPa} \times \left(\frac{p + 0.044 \text{ MPa}}{0.1 \text{ MPa}} \right)^{0.6} \times \left(1 - \frac{q}{(p + 0.044 \text{ MPa}) \times 2.27} \right)^2 \quad (16)$$

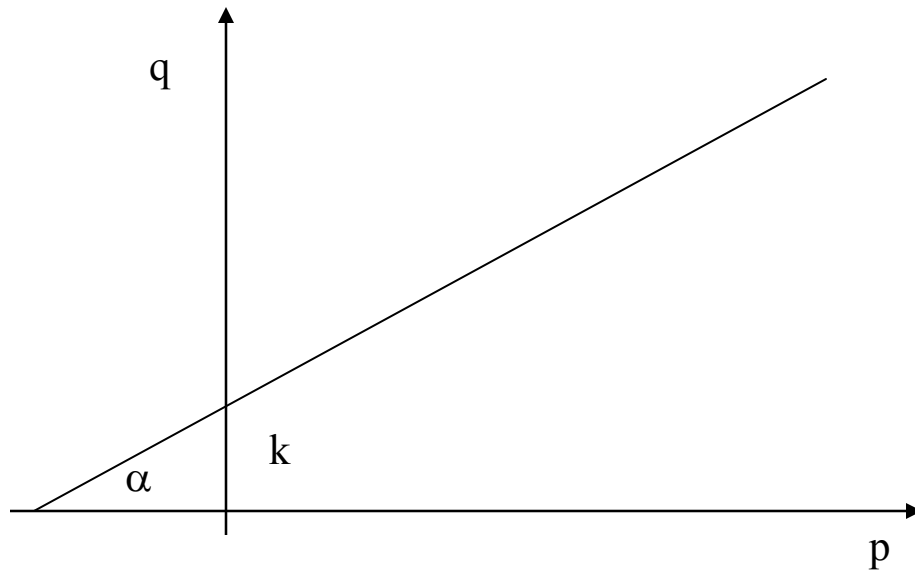


Figure 10. Simple Drucker-Prager failure condition.

The values of p_o and $\tan(\alpha)$ in Equation 15 were taken from a test reported by Hornych and Gérard (1999). The remaining values were estimates.

In the first calculation, all of the asphalt layers were assumed to have a modulus of 10,000 MPa (no slip).

Figure 11 shows the modulus variation in the granular material on a color scale from 100 MPa (red) to 150 MPa (blue). The modulus is lowest at the center of the load and at the top of the granular layer (127 MPa).

Introducing a slip between the two asphalt layers results in the moduli shown in Figure 12.

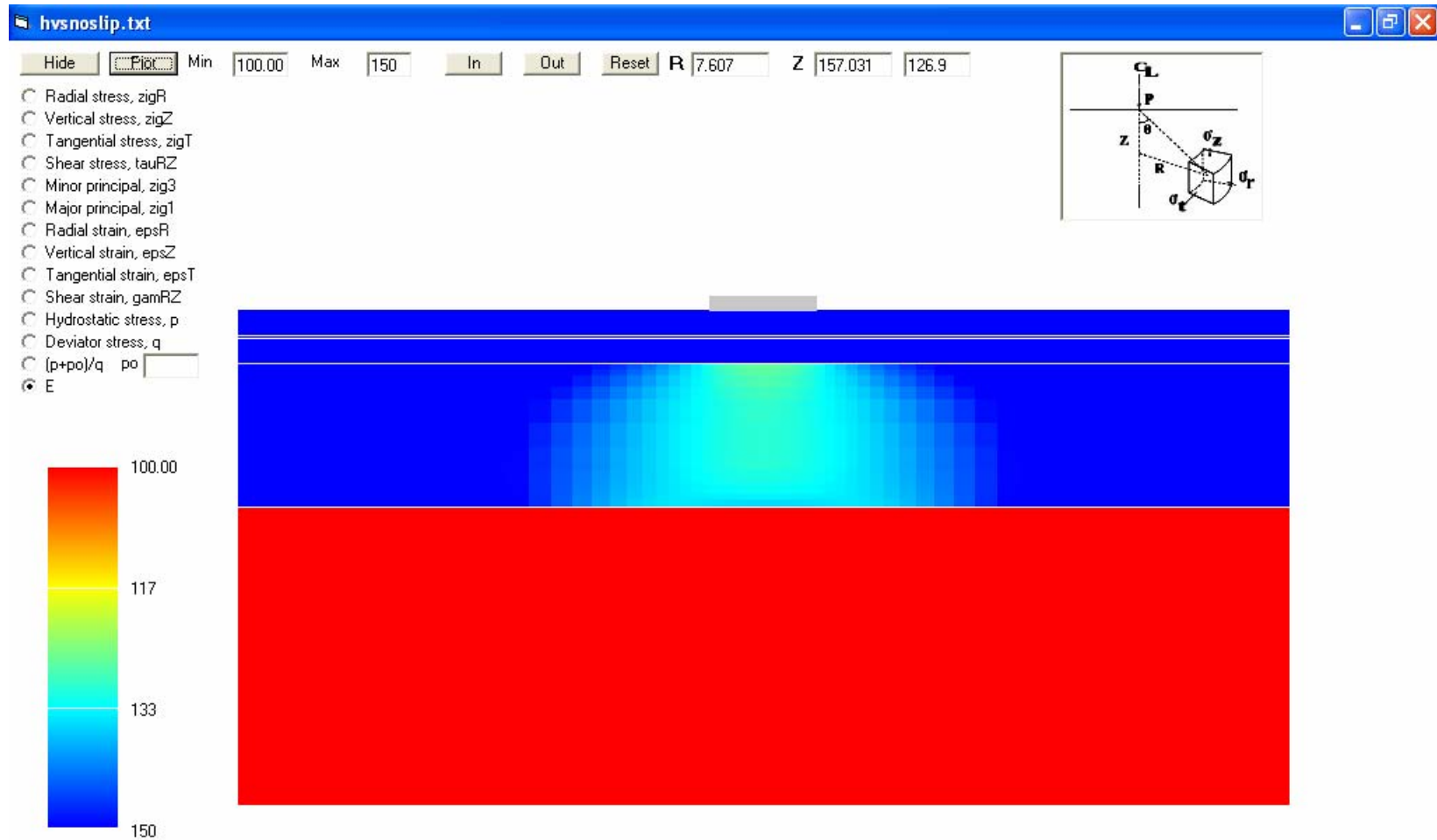


Figure 11. E_{AC} 10,000 MPa, no slip, 40 kN load.

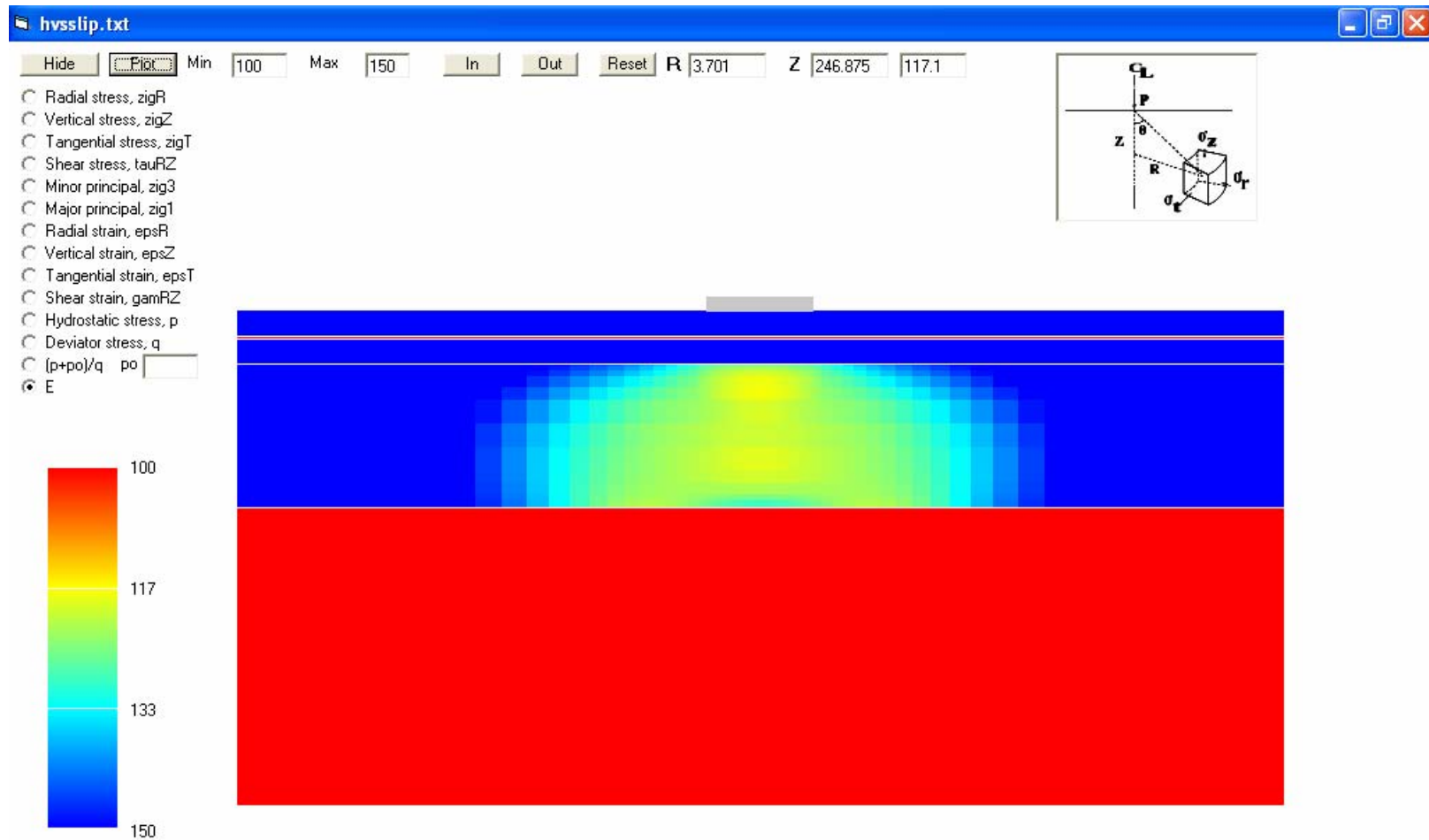


Figure 12. E_{AC} 10,000 MPa, slip, 40 kN.

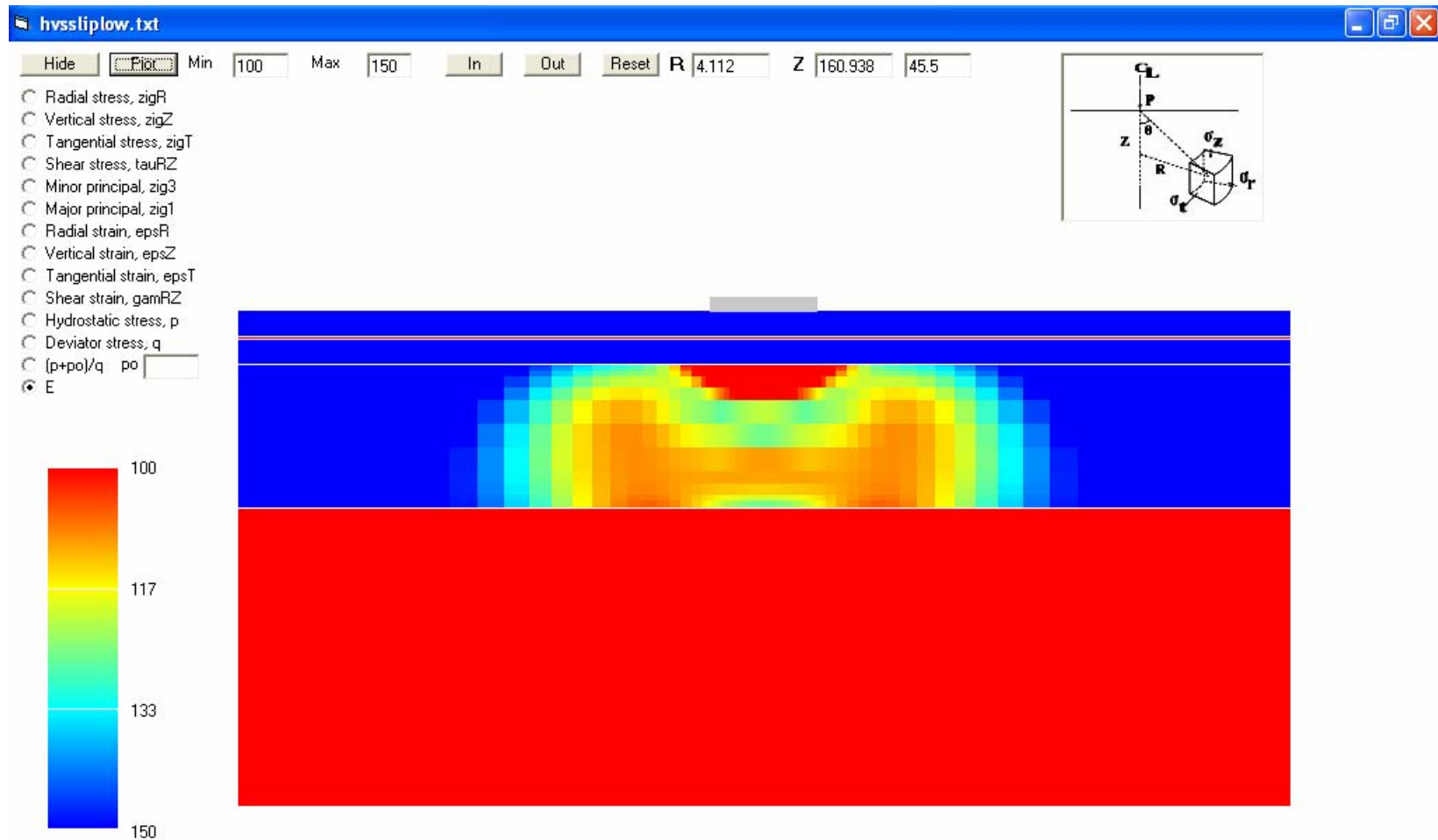


Figure 13. E_{AC} 2,000 MPa, slip, 40 kN.

The modulus of the granular material decreases at the center of the load, indicating that the effect of the deviator stress is more important than the effect of the confining stress.

Decreasing the modulus of the two asphalt layers to 2,000 MPa results in an even lower modulus of the granular layer, as seen in Figure 13. This decrease in modulus of the granular layer with development of slip and with a decrease in the modulus of the asphalt layers is in good agreement with the observed changes during HVS and FWD testing.

Increasing the load from 40 kN to 100 kN, however, causes a further decrease in the modulus of the granular layer, as shown in Figure 14. This is contrary to the change observed during HVS testing, where an increase in the load from 40 kN to 100 kN resulted in an increase in the modulus of the granular layers.

Therefore it is doubtful whether the changes in the modulus of the granular layers can be explained solely by the stress dependence of the material. It may be necessary to include the particulate nature of the material, for example, by using the Distinct Element Method, an example of which was given by Ulliditz (2002). The Distinct Element Method was used with a 1000×2000 mm “box” filled with 3,662 particles. The particles had been compacted in two layers to a thickness of 830 mm for the lower layer and 100 mm for the upper layer. Particle size distribution and angularities were different for the two layers. In the upper layer, cohesion is assumed between the particles, as well as a permissible tensile force (of 20 N at each contact point). In Figure 15, the vectors from the centers of the particles show the displacement during the first 8 msec of loading on a 150-mm plate at the surface of the sample. All contacts were intact at this low load.

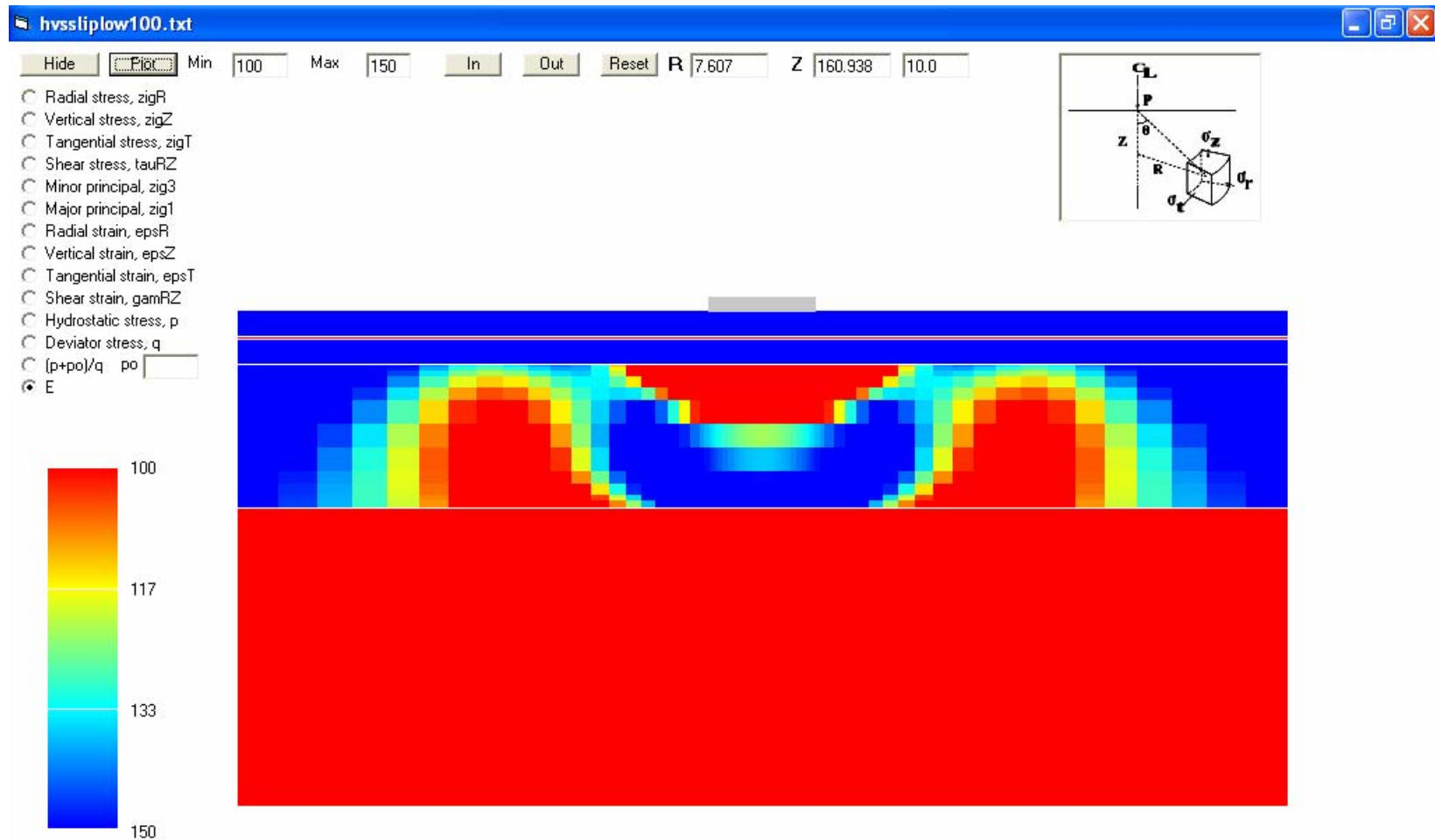


Figure 14. E_{AC} 2,000 MPa, slip, 100 kN load.

The displacement field is quite different from what would have been obtained in an elastic solid, with a great deal of particle rotation and uplift away from the load. Figure 16 shows an example from a Finite Element calculation, with the same proportions and the same center-line deflection. In the elastic solid most of the displacement is downward with only a slight rotation away from the load.

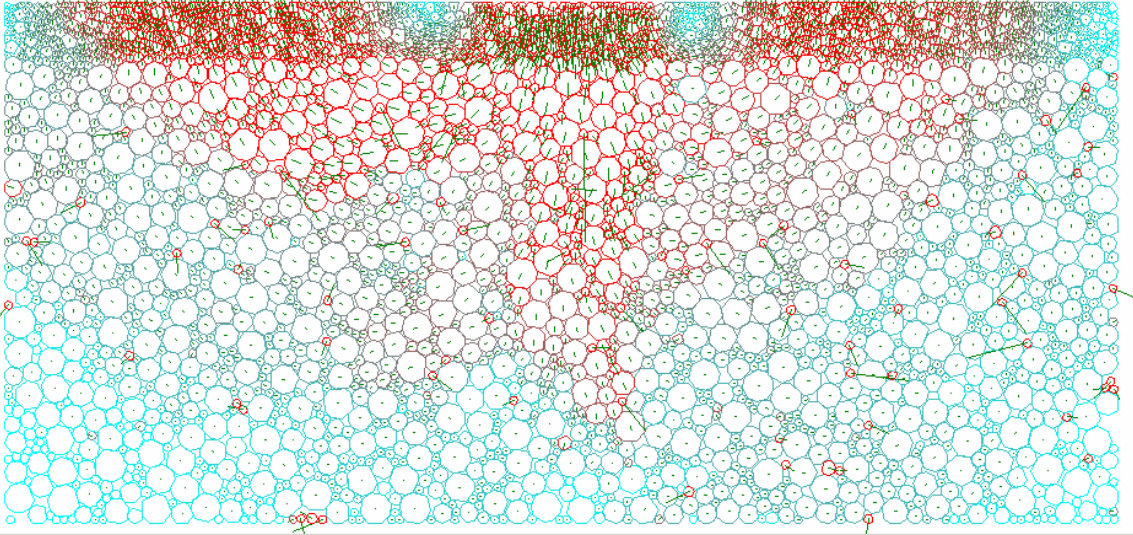


Figure 15. Displacement field in particulate sample.

This suggests that the stiffness of the upper layer may be important to the displacement of the granular material and thus to the (apparent) stiffness of the material. The upper layer acts as a plate controlling the upward and outward rotation of the particles away from the load. The Discrete Element Method analysis suggests that a stiffer plate (the asphalt layers) over the granular layers would tend to decrease the displacements of the granular particles, thus increasing their effective stiffness. HVS and FWD tests have indicated that the granular layer stiffness decreases as the asphalt layers stiffness decreases, whether that decrease is temporary (caused by temperature change) or permanent (caused by fatigue damage).

However, in order to simulate HVS testing, it is essential that deflections be predicted correctly. To do this, changes in moduli must be modeled. A procedure for doing so was developed and used for this report. The procedure, based on the observations discussed earlier, is described below.

The stiffness reduction of the unbound layers was assumed to be a fraction of the decrease in the stiffness of the layers above the one under consideration, this fraction is referred to as the “stiffness factor” in this report. The decrease in stiffness of the unbound layers was treated as “apparent” (and temporary) damage (i.e., it would disappear if the stiffness of the layers above recovered, such as in the case of changing temperature). If the reference stiffness of the layers above a certain layer is S_{ref} and the present stiffness is S , then the apparent damage is calculated as:

$$Apparent\ damage = \left(1 - \frac{S}{S_{ref}}\right) \times Stiffness\ factor \quad (17)$$

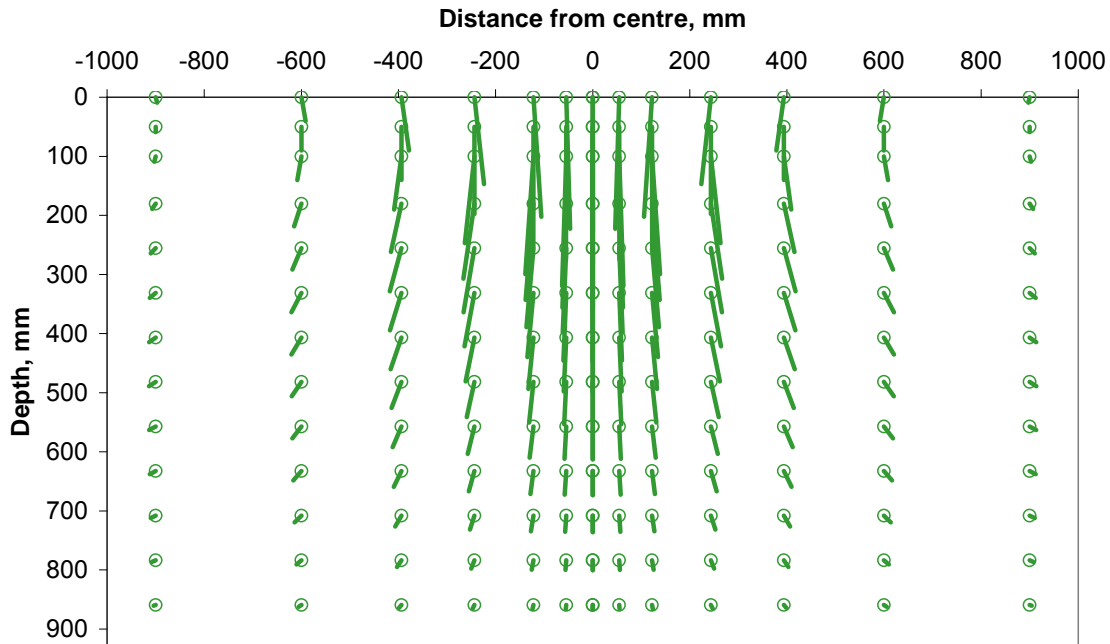


Figure 16. Displacement field in elastic solid (FEM).

The moduli of the unbound materials were calculated from the equation:

$E = E_o \times (1 - (1 - S / S_{ref}) \times \text{Stiffness factor})$, with

$$S = \left(\sum_{1}^{n-1} h_i \times \sqrt[3]{E_i} \right)^3 \quad (18)$$

where E_o is the modulus (of layer n) when the combined stiffness of the layers above (S) is equal to the reference stiffness (S_{ref}).

A reference stiffness of 3500^3 N/mm was used for all unbound materials. (For practical reasons, the input to the program is the cube root of the reference stiffness, or, in this case, 3500.) For the stiffness calculation in Equation (18), the layers are assumed to be fully bonded. If two layers are debonded, the combined stiffness is calculated as $h_1^3 \times E_1 + h_2^3 \times E_2$. A full bond is assumed if the slip value is more than 100; a full slip is assumed when the value is less than 0.01. A logarithmic interpolation is used between these two values.

FWD tests were carried out on September 29, 1995, in the lines of the HVS test sections of Goal 1 (with the exception of the Section 500RF test area where testing was ongoing), with asphalt temperatures of 20–22°C. Layer moduli were backcalculated using *Elmod5* software and the following layer thicknesses were assumed:

Table 8. Layer Thicknesses Used for FWD Backcalculation

HVS Test Section	Layer 1	Layer 2
500RF	225 mm	320 mm
501RF	150 mm	490 mm
502CT	225 mm	400 mm
503RF	150 mm	580 mm

All of the asphalt bound layers (including ATPB) were combined into Layer 1 and the two granular layers into Layer 2. Drop 2 of the FWD tests, with a peak contact stress of about 0.6 MPa, was used.

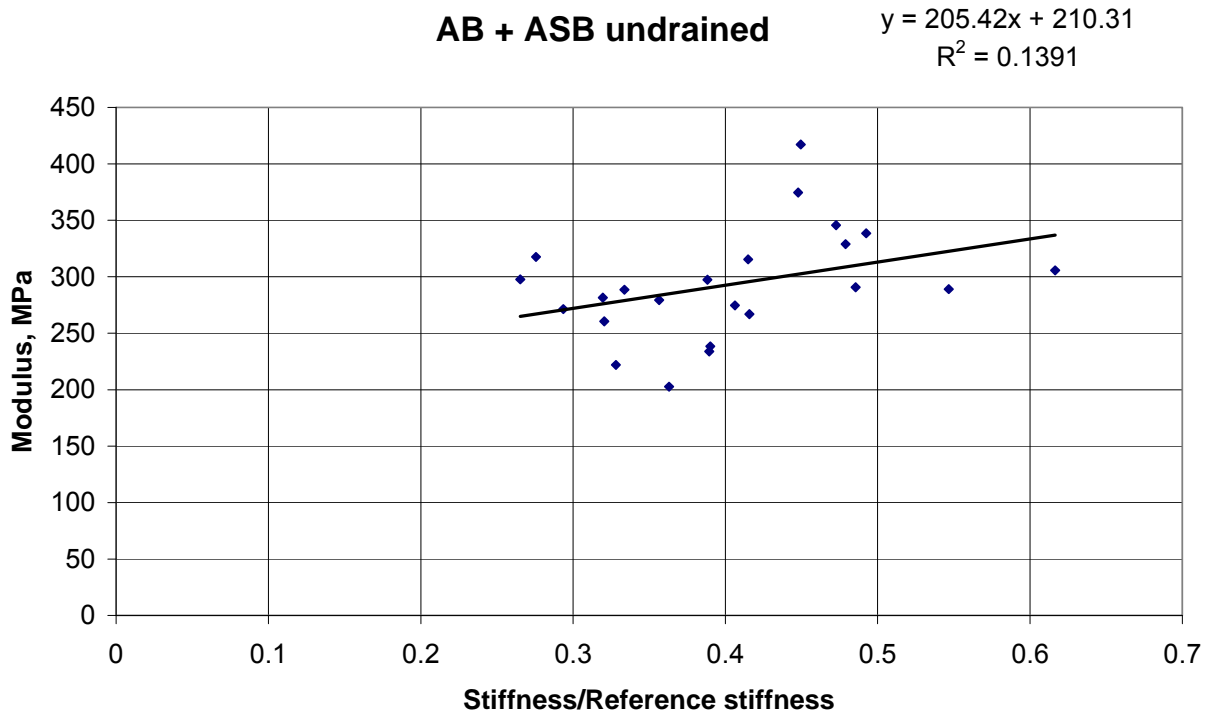


Figure 17. Modulus of Layer 2 as a function of the stiffness of the asphalt layers, for the undrained sections.

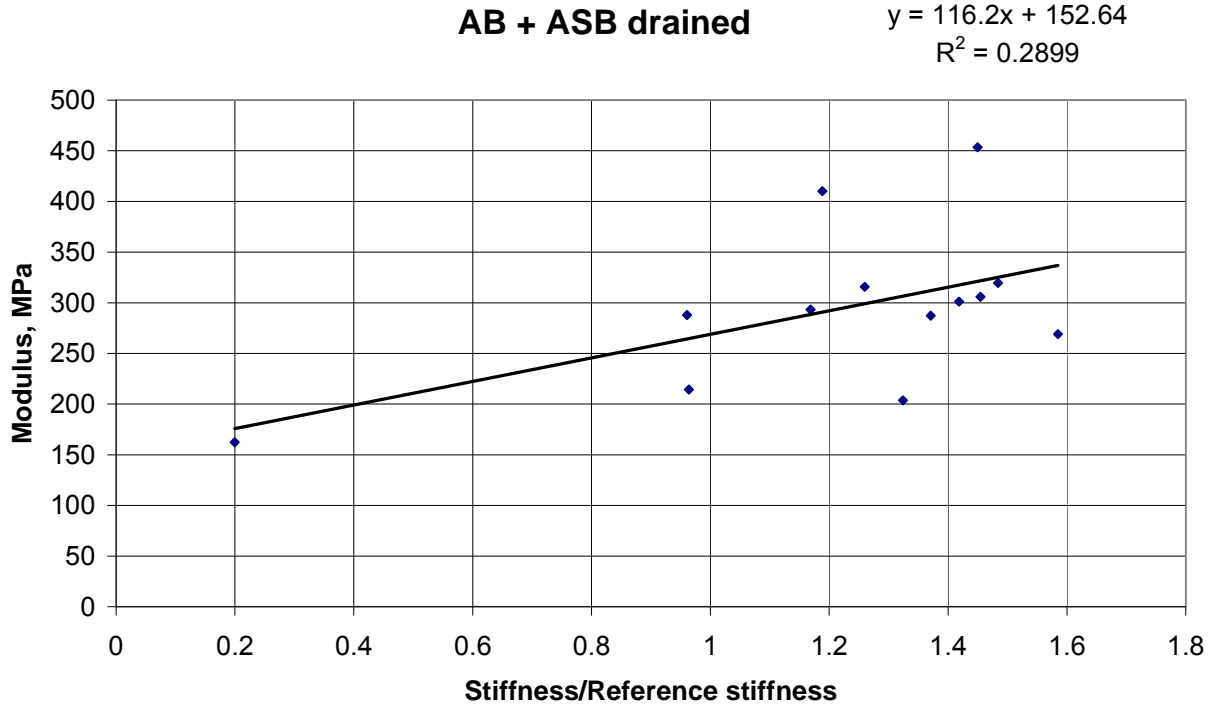


Figure 18. Modulus of Layer 2 as a function of the stiffness of the asphalt layers, for the drained sections.

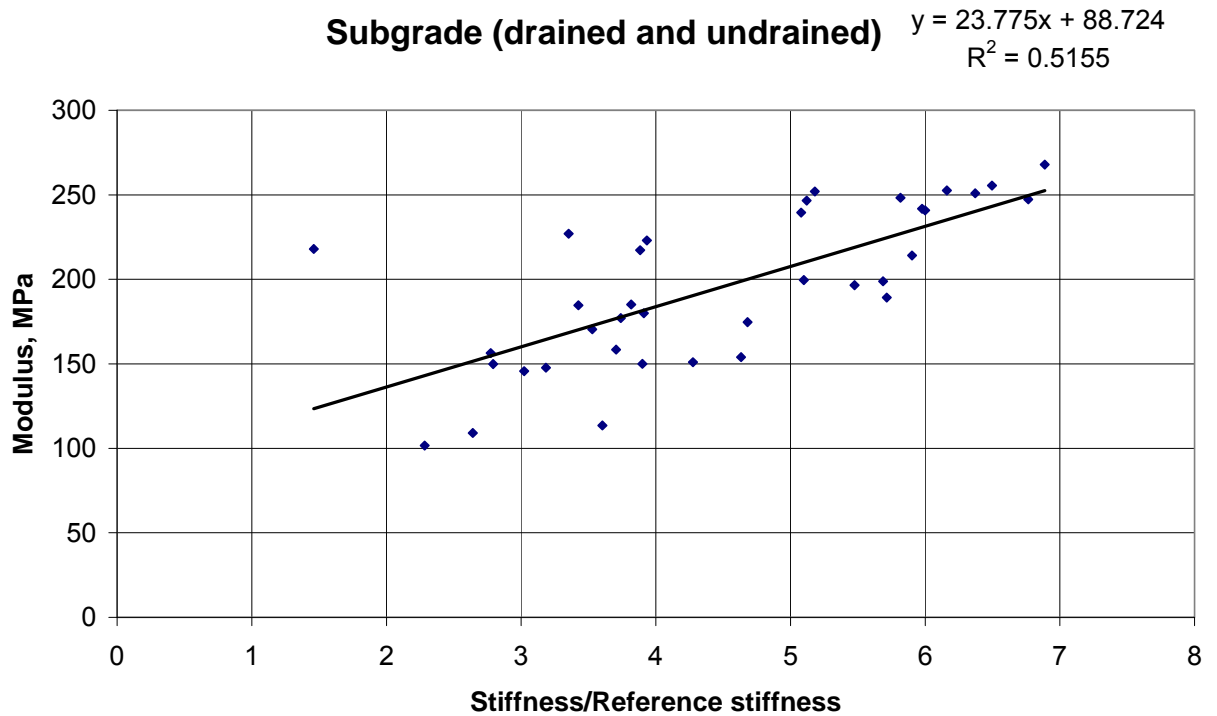


Figure 19. Modulus of subgrade as a function of the stiffness of the pavement layers.

In Figure 17 through Figure 19, the moduli of the unbound layers are shown as functions of the stiffness ratio of the layers above. The correlation between stiffness ratio and modulus is not very good, but if the best fitting lines are used anyway, the stiffness parameters shown in Table 9 result.

Table 9. Moduli Parameters from FWD

Layer	Eo, MPa	Stiffness Factor
AB + ASB undrained	416	0.49
AB + ASB drained	269	0.43
Subgrade	112	0.21

Based on the calibration using Section 501RF the parameters shown in Table 10 were chosen:

Table 10. Moduli Parameters from Calibration to MDD Deflections

Material	Eo, MPa	Stiffness Factor
Aggregate base	165	0.4
Aggregate subbase	115	0.3
Subgrade	60	0.2

These values were used for all of the tests of Goals 1, 3, and 5, except for the subgrade of Section 502CT (and the corresponding overlay section, 515RF), where a value of 102 MPa was used in order to get a more correct initial subgrade deflection. In the simulations with full bond, factors of 0.55, 0.45, and 0.3 were used to compensate for the lack of slip. This was to ensure correct deflections during the simulation, where only the permanent deformation of the asphalt was determined.

The initial moduli used in the HVS simulations for Goal 1 and Goal 3 appear in Table 11. The moduli correspond to a 40 kN wheel load, a loading time of 0.015 sec., and a temperature of 20°C. The moduli are given in MPa.

Table 11. Initial Moduli Used in HVS Simulations (MPa)

Section	Overlay	AC top	AC bottom	ATPB	AB	ASB	Subgrade
501RF		9038	11173		149	161	103
503RF		9038	11173		165	182	134
500RF		9038	11173	1144	199	186	105
502CT		9038	11173	1144	197	184	199
517RF	7653	1968	2733		162	177	113
518RF	4755	1968	2733		133	140	102
514RF	7653	2881	4997	807	242	227	125
515RF	4755	2881	4997	808	175	164	178

Table 12 gives a summary of the moduli determined by different methods. The range of moduli is given in MPa.

Table 12. Summary of Moduli (MPa)

Material	Triaxial	FWD	MDD
AB-ASB	140-430	200-400	120-240
Subgrade	55-100	100-150	100-200

It may be noted that asphalt moduli from the master curve developed from backcalculated FWD deflections were lower than those from the master curve developed from measured moduli in frequency sweep tests, after the minimum modulus of the frequency sweep-derived master curve had been set at a value of 200 MPa (note see Figure 224 for similar occurrence with the Goal 9 master curve for the underlying asphalt concrete). The larger asphalt moduli from the frequency sweep tests were used when backcalculating the moduli of the unbound materials using MDD deflections. The unbound layers' moduli backcalculated from the MDD deflections would have been larger if the FWD asphalt moduli had been used with the MDD deflections instead of the frequency sweep moduli.

1.5.3 Influence of Load Level

During testing, MDD deflections were measured under different wheel loads. This showed that the moduli of the unbound layers were not constant; they changed with the load level. Because of the effect of the stiffness of the layers above the unbound layers, this non-linearity could not be treated as a function of the stress condition in the material (because of the influence of the stiffness of the above layers). Instead, it had to be treated as a function of the load level. The modulus at load level P was calculated as:

$$E_P = \left(\frac{P}{40 \text{ kN}} \right)^\alpha \times E_{40\text{kN}} \quad (19)$$

The power α was 0.6 for the granular layers and -0.3 for the subgrade. Both are typical values for granular and cohesive materials, respectively.

The permanent deformation of the materials is a function of the resilient pavement response but, with the models used here, the response is independent of the permanent deformation. The parameters controlling resilient response can, therefore, be determined without considering permanent deformations, as was done in the sections above. Once the calculated response appears to be correct, the parameters controlling the permanent deformations may be calibrated.

1.6 Permanent Deformation

1.6.1 Asphalt

A shear-based approach, developed by Deacon et al. (2002), for predicting rutting of the asphalt layer was used in a first attempt. Rutting in the asphalt is assumed to be controlled by shear deformation. The computed values of shear stress, τ , and elastic shear strain, γ^e , at a depth of 50 mm beneath the edge of the tire are used for the rutting estimates.

Rutting in the AC layer due to the shear deformation is determined from the following:

$$rd_{AC} \text{ mm} = K \times \gamma^i = A \times MN^\alpha \exp\left(\frac{\beta \times \tau}{resp_{ref}}\right) \times (\gamma^e)^\gamma \quad (20)$$

where rd_{AC} mm is the vertical rut depth in the asphalt concrete

γ^i = permanent (inelastic) shear strain at 50 mm depth,

τ = shear stress determined at this depth using elastic analysis,

γ^e = corresponding elastic shear strain (m/m),

K is a value relating permanent shear strain to rut depth (mm), and

A , α , β , $resp_{ref}$, and γ are constants.

The purpose of $resp_{ref}$ is to make the right side of the equation unitless. Atmospheric pressure (0.1 MPa) was selected as the value for $resp_{ref}$, and γ was assumed to be 1. Two Repeated Simple Shear Tests at Constant Height (RSST-CH) were available for the top layer of Goal 1 (for the initial simulations), both at 40°C and at a shear stress of approximately 70 kPa. From these tests $A/K = 49.3$ and $\alpha = 0.208$ could be derived. The constant β was set at 1.03 based on the experiments by Deacon et al. (2002). The research team determined A/K and α by importing the results of the RSST-CH (number of load applications, shear stress, resilient shear strain, temperature, and permanent shear strain) into a spreadsheet. The tests were then modeled using the right part of Equation (20) (the permanent strain part). The RMS difference between the measured and calculated permanent strain was calculated. *Excel's* "Solver" was used to minimize this difference by changing A/K and α .

The constant A was determined from a simulation of Section 501RF with full friction at the first interface. The fatigue shift factor and the stiffness factors for the unbound layers were adjusted, as mentioned above, in order to get the correct resilient deflections during the full test period. In determining A the first 500,000 load applications were used, as the measured data showed an unexplained 1-mm increase in the permanent deformation of the AC layers from 550,000 to 600,000 load repetitions.

For Goal 1, A was found to be about 400, which corresponded to a K value of 8.1.

It should be noted that the modulus of the asphalt decreased due to damage during the test. In the initial attempt, the shear stress and shear strain were calculated using the modulus of the damaged material. A

decrease in modulus caused by damage could have influenced the permanent deformation in the AC differently from a similar modulus decrease due to an increase in temperature.

The parameters used in the first set of simulations and in the simulation of the underlying pavement of Goal 9 are given in Table 13.

Table 13. Parameters Used in Equation 20

Test	Material	A	α
Goal 1	DGAC1	400	0.208
Goal 3, 20°C	DGAC3	700	0.208
	ARHM	400	0.208
Goal 3, 45°C	DGAC1	700	0.208
	DGAC3	1500	0.17
	ARHM	1500	0.17
Goal 5	DGAC3	700	0.208
	ARHM	400	0.208

In general the parameters gave a good fit to the measured permanent deformations, although there were problems with thin overlays, less than 50 mm thick, where no permanent deformation was determined.

As can be seen, the parameters used are not totally consistent. Because of the problem with thin layers the approach was modified using additional RSST-CH test data as explained below.

Figure 20 shows the results of ten RSST-CH for field mix, field compacted (FMFC) specimens from the dense-graded asphalt concrete (DGAC) of Goal 3. The air-void content for these specimens was close to 5.5 percent. Testing was done at 40°C, 50°C, and 60°C. The applied shear stress was reasonably constant at 70 kPa.

The value of α in Equation (20) corresponds to the slope of the curves in Figure 20. It is quite evident that the slope is not constant. Even if only the values above 100 load applications are included, there is still a considerable variation, both with the number of load applications for each curve and between the curves.

Two approaches were tried in order to get a better relationship between the plastic shear strain and the number of load applications: a Weibull function and a Gamma function.

Goal 3 DGAC FMFC AV5.5

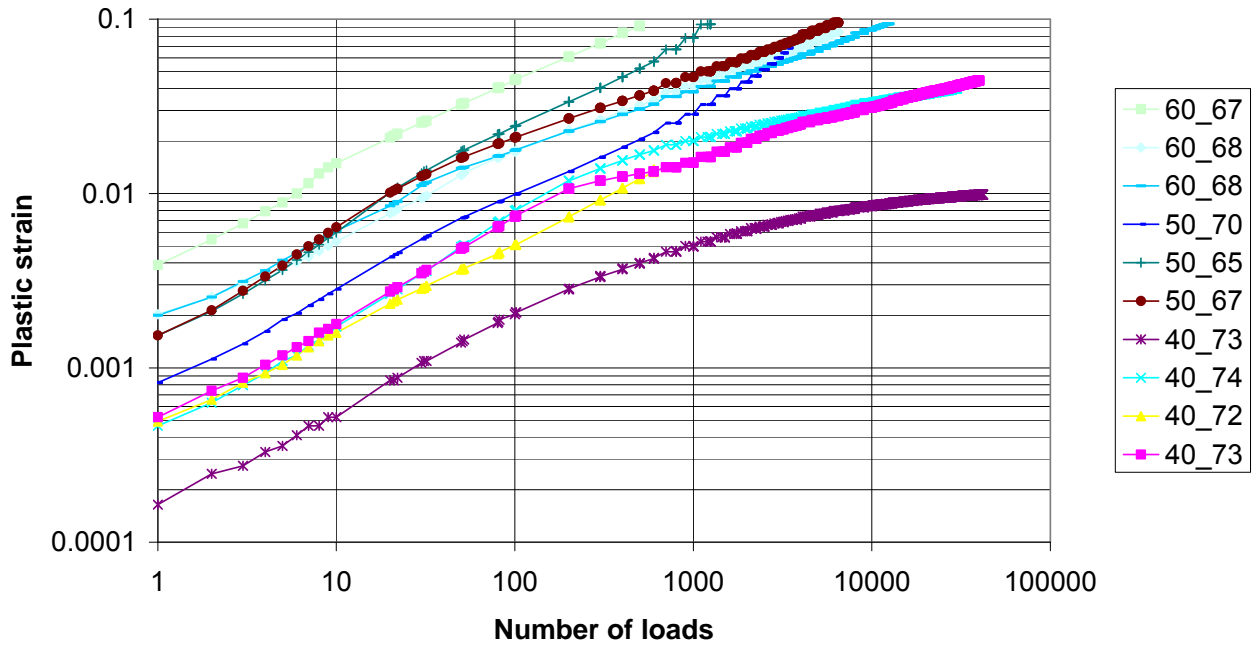


Figure 20. Results of RSST-CH tests. [Note: FMFC indicates field-mixed field compacted specimen taken by coring the pavement. AV5.5 indicates cores with approximately 5.5 percent air-voids. Each title in the legend indicates the RSST-CH test temperature (40, 50, or 60 °C) and average shear stress (MPa).]

Weibull function:

The Weibull function may be written as:

$$S = \exp(-A \times N^\alpha) \quad (21)$$

where S is the normalized plastic shear strains as defined by Equation 22 in terms of the elastic and permanent (inelastic) shear strains,
 N is the load repetitions,
 A and α are constants determined from the test.

To use a Weibull function S may be calculated from the plastic shear strain, “normalized” by inclusion of the term γ_{ref} , from:

$$S = 1 - \frac{\gamma^i}{\exp\left(\frac{\beta \times \tau}{\tau_{ref}}\right) \times \gamma^e \times \gamma_{ref}} \quad (22)$$

The value of the constant γ_{ref} must be selected so that S will never get below zero. A value of 1000 was used here.

Equation (21) may be rewritten as:

$$\ln(-\ln(S)) = \ln(A) + \alpha \times \ln(N) \quad (23)$$

The data from the Goal 3 tests in Figure 20 have been plotted on this format in Figure 21. Although there is a certain amount of scatter, the normalization seems to collapse the tests reasonably well.

Figure 22 shows the average values of the curves in Figure 21 as well as the best fitting straight line. Although the coefficient of correlation is quite high the fit is not very good and the slope of the line keeps changing with increasing number of loads. This is important as the maximum number of load applications during the RSST-CH tests is about 40,000, whereas the number of load applications during HVS testing (or on *in situ* roads) may be much larger.

Goal 3 DGAC FMFC AV5.5

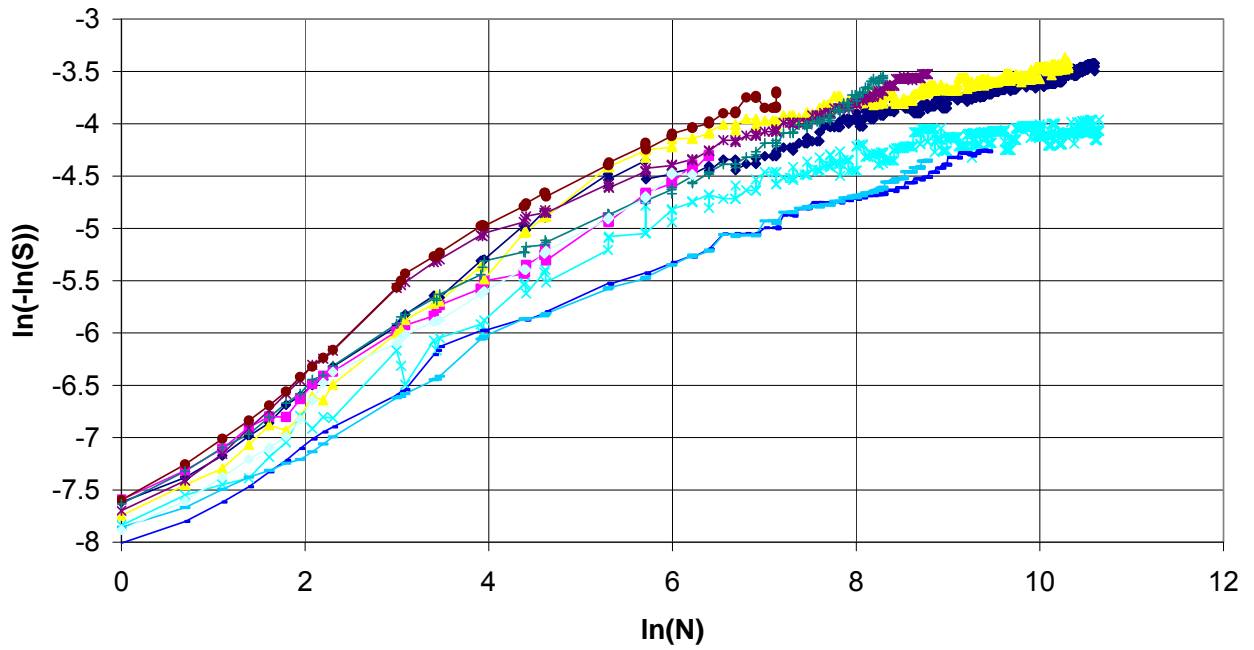


Figure 21. Normalized plastic strain versus number of load repetitions. (Note: legend is the same as in Figure 20).

Goal 3 DGAC FMFC AV5.5 Average

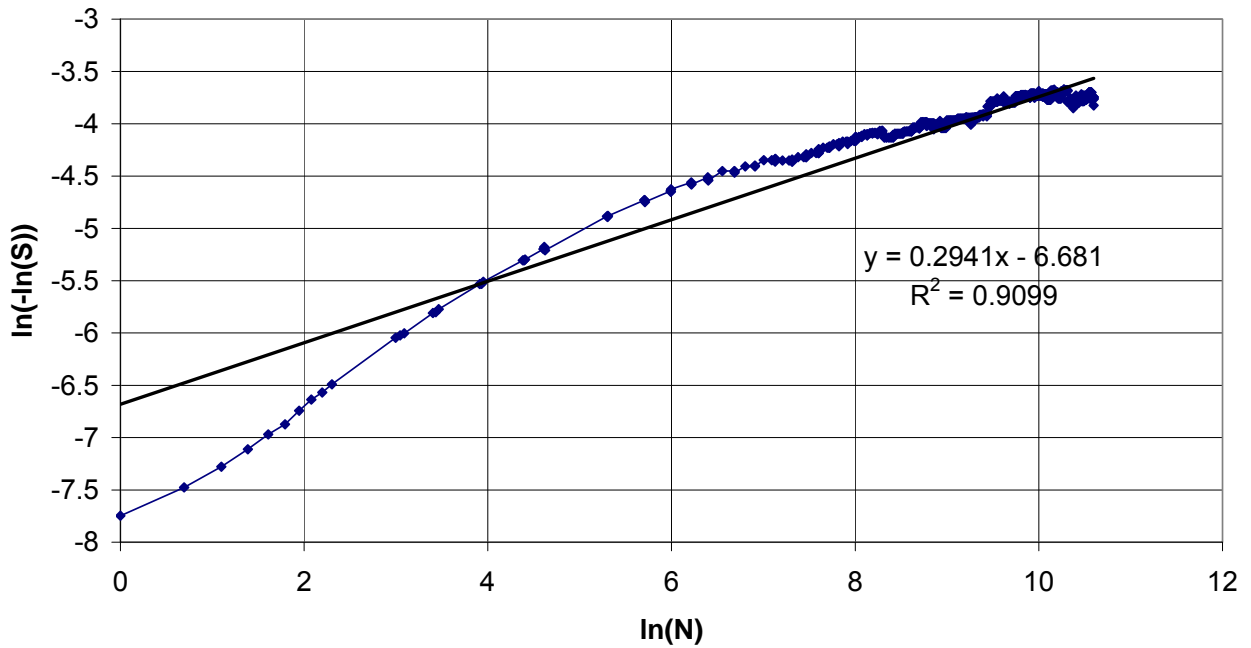


Figure 22. Average values for Figure 21 curves.

A relationship of the format:

$$\gamma^i = A \times \exp\left(-\left\{\left(\frac{\gamma}{N}\right)^\alpha\right\}\right) \times \exp\left(\frac{\beta \times \tau}{\tau_{ref}}\right) \times \gamma^e \quad (24)$$

was also attempted. This format is similar to the format used for unbound materials in the NCHRP 1-37A report. It did not improve the fit.

Gamma function:

An alternative to fit the data was a gamma function of the format:

$$y = A + \alpha \times \left[1 - \exp\left(-\frac{x}{\gamma}\right)\right] \times \left(1 + \frac{x}{\gamma}\right)$$

$$y = \ln\left(\frac{\gamma^i}{\exp\left(\frac{\beta \times \tau}{\tau_{ref}}\right) \times \gamma^e}\right), \text{ and } x = \ln(N) \quad (25)$$

The plastic strain may be calculated from:

$$\gamma^i = \exp\left(A + \alpha \times \left[1 - \exp\left(-\frac{\ln(N)}{\gamma}\right) \times \left(1 + \frac{\ln(N)}{\gamma}\right)\right]\right) \times \exp\left(\frac{\beta \times \tau}{\tau_{ref}}\right) \times \gamma^e \quad (26)$$

To use the time-hardening method in *CalME*, the apparent N must be calculated at the beginning of each time increment. The “apparent N” is the equivalent number of load repetitions at the temperature of the next time increment to reach the permanent shear strain calculated at the temperature of the current time increment. This cannot be done directly, but requires an iterative procedure, for example using the equation:

$$\frac{1 + \frac{\ln(N)}{\gamma}}{\exp\left(\frac{\ln(N)}{\gamma}\right)} = 1 - \frac{\ln\left(\frac{\gamma^i}{\exp\left(\frac{\beta \times \tau}{\tau_{ref}}\right) \times \gamma^e}\right) - A}{\alpha} \quad (27)$$

The following parameters were obtained:

- $A = -0.568$
- $\alpha = 4.208$
- $\gamma = 2.472$

The RMS value on the ln (Normalized strain) was 0.30.

Figure 23 shows that the Gamma function fits the measured data quite well. Therefore, it was selected for the rest of this study.

Goal 3 DGAC FMFC AV5.5

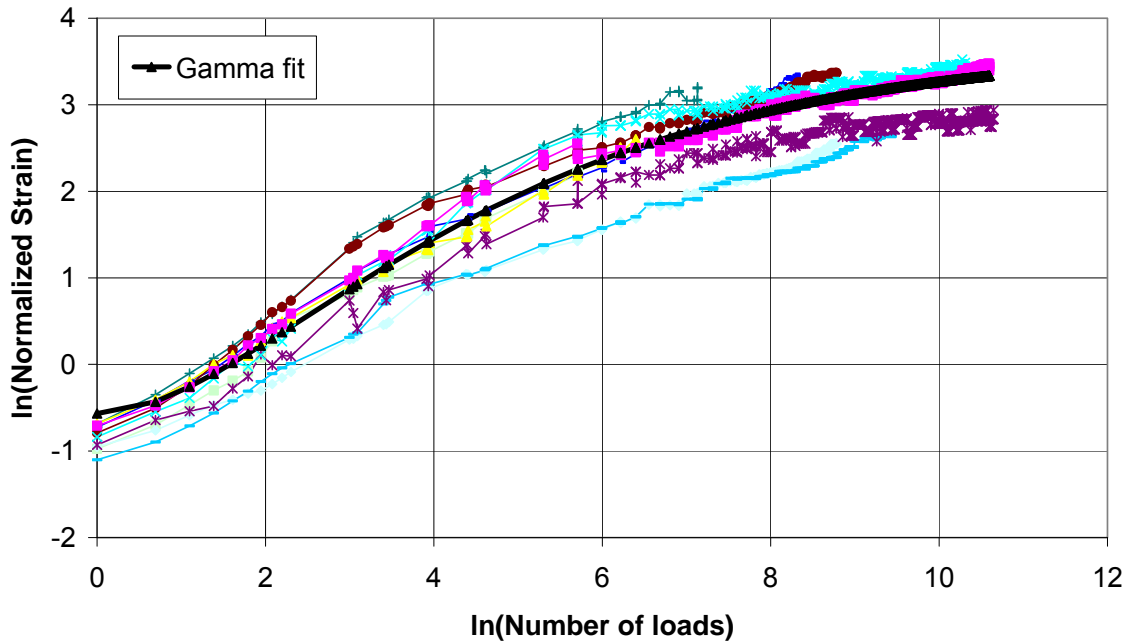


Figure 23. Best fitting Gamma function. (Note: legend is the same as in Figure 20 and Figure 21.)

For the Goal 1 DGAC mixes, all five tests (from the top layer and the bottom layer, which were not very different) were used to determine the parameters of the Gamma function:

- $A = -1.316$
- $\alpha = 5.218$
- $\gamma = 2.860$

The RMS was 0.16.

For the ARHM, with an air-void content of 10 percent, of Goal 3 the following parameters were obtained:

- $A = -0.506$
- $\alpha = 4.703$
- $\gamma = 2.572$

The RMS was 0.36.

The permanent deformation was still assumed to be a constant times the permanent shear strain, but in order to include permanent deformation in overlays less than 50 mm thick, the permanent deformations were prorated over the layers within a depth of 100 mm from the surface.

The shear stress, τ , was still calculated at a depth of 50 mm at the edge of a tire and by using the moduli of the pavement's individual layers. For each layer the elastic shear strain was then determined from:

$$\gamma^e = \frac{\tau}{E/(1+\nu)} \quad (28)$$

Where γ^e is the elastic shear strain,
 τ is the shear stress,
 ν is Poisson's ratio, and

E is the modulus of the layer considered, including any reduction in modulus caused by fatigue damage (also for the Goal 3 rutting tests).

The permanent shear strain in the layer was determined from Equation 26, and the permanent deformation was obtained by multiplying the permanent shear strain by the thickness of the layer (in mm) and by a constant, K .

A value of 0.25 was used for K for all materials, except the Goal 1 DGAC, which would either be tested at a relatively low temperature of about 20°C or would have been in place several years before being tested. Instead, a K value of 0.08 was used for the DGAC from Goal 1.

The permanent deformations shown in the simulations that appear later in this report for the individual HVS test sections were calculated by using the Gamma function and prorating the deformation, except for Goal 9 where the power function was used.

1.6.2 Unbound Materials

Permanent deformation, d_p , of the unbound materials is based on the vertical resilient strain at the top of the layer, $\mu\varepsilon$, and on the modulus of the material, E :

$$d_p, \text{ mm} = A \times MN^\alpha \times \left(\frac{\mu\varepsilon}{\mu\varepsilon_{ref}} \right)^\beta \times \left(\frac{E}{E_{ref}} \right)^\gamma \quad (29)$$

The input parameters used for the subgrade are given in the second column of Figure 24. The parameters are based on a series of full-scale tests in the Danish Road Testing Machine, with a subgrade of Danish "Moraine Clay," which is classified as a "clayey, silty sand" [AASHTO classification A-4(0)] (Ullidtz 2005).

	Fatigue, dE/Ei	Permanent deformation, mm	Crushing, dE/Ei	Roughness, IRI m/km
Response type	e	e	z	e
A	0	1.1	0	0.5
Sdf A	1.1	1.1	1.1	1.1
alfa	1	0.333	0.6	0.2
Respref	-1000	1000	1.53	1000
beta	5	1.333	7.69	1.333
Eref	10000	40	10000	40
gamma	2.5	0.333	-15.4	-1
delta	0.9			
Shift factor	9			

Figure 24. Input parameters for permanent deformation (rutting) of subgrade in second column.

The same parameters were used for the two granular layers, except that the value of A was reduced to 0.8.

The permanent compression of the unbound layers is rather small, and the scatter between different tests — and even between different MDDs within a single test — is quite large. Therefore, it is difficult to draw any definitive conclusions. However, the model and parameters given above appear to predict the permanent deformation of the unbound layers reasonably well.

1.7 Reflection Cracking

Reflection cracking damage was calculated using the method developed by Wu (2005). In this method the tensile strain at the bottom of the overlay is estimated using a regression equation. The calculated tensile strain at the bottom of the overlay is used with the fatigue equation described previously to calculate damage in the asphalt layers.

The regression equation for tensile strain at the bottom of the overlay is based on many two-dimensional (2D) Finite Element analyses of overlay structures from a parametric study shown in Table 14. Figure 25 compares the predicted 2D strain from the regression equation against the calculated strain.

Table 14. AC on AC, 2D Structural Parameter Combinations

Name	Description	Unit	Variations
Ea	Stiffness of Overlay	MPa	4000, 6000, 8000, 10000, 12000
Ha	Thickness of Overlay	mm	50, 75, 100, 150, 200, 250
Eu	Stiffness of the Underlayer	MPa	3000, 5000, 7000
Hu	Thickness of the Underlayer	mm	100, 200, 300
Eb	Stiffness of the Base/Sub-base	MPa	150, 300, 450
Es	Stiffness of the Subgrade	Ma	100, 200
L _S	Crack Spacing	mm	55, 110, 220, 440
<i>Total number of runs: 6,480</i>			

The variables in Table 14 are normalized for the parametric study so that they are close to 1.0 and dimensionless:

$$\hat{E}a = Ea / 10000 \text{ MPa}, \hat{L}_S = L_S / 200 \text{ mm}, \hat{H}a = Ha / 100 \text{ mm}, \hat{H}u = Hu / 200 \text{ mm},$$

$$\hat{E}u = Eu / 5000 \text{ MPa}, \hat{E}b = Eb / 300 \text{ MPa}, \hat{E}s = Es / 200 \text{ MPa}.$$

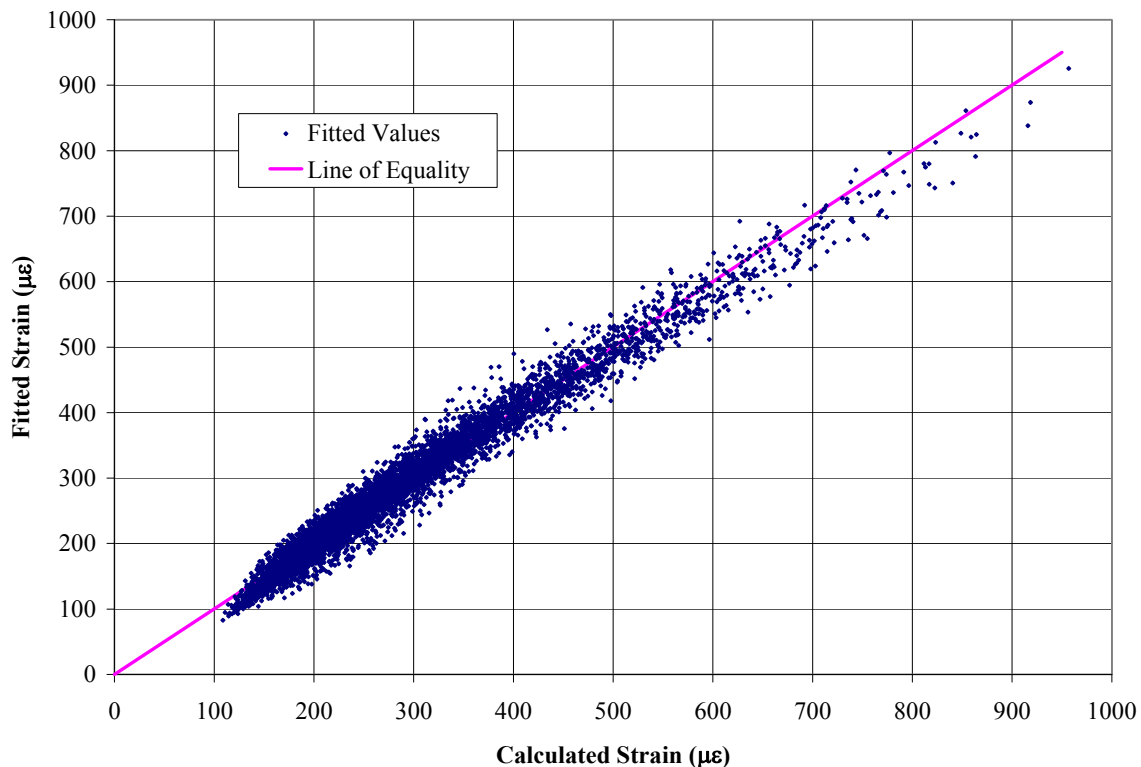


Figure 25. Comparison of fitted vs. calculated strain for AC-on-AC overlay, 2D.

The 2D strains are converted to three-dimensional (3D) strains using another regression equation based on hundreds of Finite Element analyses from the same factorial used for the 2D analysis.

The 2D strain function is:

$$\varepsilon_{2D} = \alpha \hat{E}_a^{-\beta_1} \hat{E}_b^{-\beta_2} \hat{E}_s^{-\beta_3} [1.0 + b_1 \ln(\hat{L}_s)] \exp(-b_2 \hat{H}_a)(1 + b_3 \hat{H}_u)(1 + b_4 \hat{E}_u) \quad (30)$$

with parameters $\alpha = 226.53$, $\beta_1 = 0.73722$, $\beta_2 = 0.26455$, $\beta_3 = 0.16295$,
 $b = 0.15272$, $b = 0.23069$, $b = -0.13011$, $b = 0.46881$.

Figure 25 shows a plot of the fitted versus the calculated 2D strains for AC-on-AC overlays.

For the 2D to 3D transformation $\varepsilon_{3D} = \gamma \cdot \varepsilon_{2D}$ and the coefficient γ can be expressed as:

$$\gamma = b_0 + b_1 \hat{E}_a + b_2 \hat{H}_a + b_3 \hat{E}_u + b_4 \hat{H}_u + b_5 \hat{E}_b + b_6 \hat{L}_s \quad (31)$$

with parameters $b_0 = 0.61594$, $b_1 = 0.32834$, $b_2 = 0.27215$, $b_3 = 0.070884$, $b_4 = 0.054061$,
 $b_5 = 0.13092$, $b_6 = 0.13633$.

A crack spacing of 200 mm was assumed in the Goal 3 simulations based on the crack spacings observed at the end of the Goal 1 tests.

2.0 GOAL 1 CRACKING TEST SIMULATIONS

2.1 Goal 1 Resilient Deformations

The pavement response was calculated for each hour of the HVS test, and it was assumed that each HVS loading sequence was evenly distributed over time (with an almost constant temperature this has little significance). The load was placed at five transverse positions across the width of the loaded area, which was 1,000 mm for all tests, the width of the wander pattern used for the HVS dual wheel. Damage to the asphalt for each wheel position was accumulated using the “time hardening” method, i.e., by first calculating the number of load applications required to cause the present damage, given the present pavement response and conditions, then by calculating the damage that would be caused by that number of load applications plus the number of loads applied at the wheel position during the hour under consideration.

Damage to the asphalt was based on the minor principal strain (compression as positive) at the bottom of the lowest asphalt layer (including the ATPB as an asphalt layer, as long as the damage of this layer was less than 0.9), when the layers were bonded. After debonding, the strain at the bottom of the top layer was used to calculate the damage of the top layer. Apparent damage to the unbound layers was calculated using the damage to the asphalt layers, the degree of bonding between asphalt layers, and the apparent damage to any unbound layer above the layer under consideration. Temperature variation in the asphalt layers also affects the apparent damage of the unbound layers.

The calculated damage (and apparent damage) were stored in the Performance table of the *DesignData.mdb* and for possible later use to calculate deflection at the MDD modules (or any other response value).

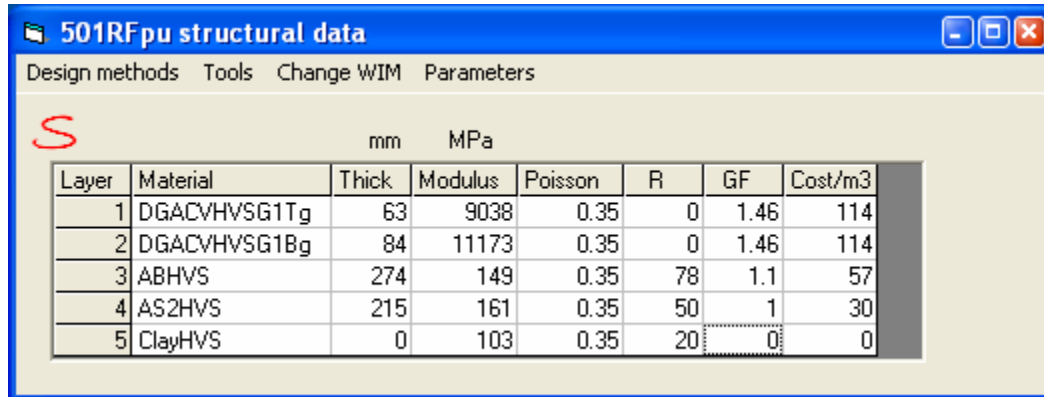
2.1.1 Section 501RF Resilient Deflections (Undrained)

The first calibration was done using Test Section 501RF. This section had no ATPB layer and the test was relatively short, lasting for a little more than three months. The MDDs also appeared to function correctly.

The following figures show the deflection of the top MDD modules, the resilient compression of the pavement layers (which is the difference in deflection between two MDD modules), and the deflection at the top of the subgrade. They are first shown for a wheel load of 40 kN, then for a wheel load of 100 kN. All

simulations were done with the stiffness parameters for the unbound materials given in Table 10. The shift factor for asphalt fatigue was 3 for all the asphalt layers, i.e., it took three HVS loads at a given strain, modulus, and temperature to produce the same damage as one load in the laboratory bending beam test. Slip was assumed to have been fully developed after 2 MESAL (million ESAL, calculated using the Caltrans 4.2 Exponent, which corresponds to approximately 200,000 load repetitions).

The first visible cracking was recorded at approximately 550,000 load repetitions.



Layer	Material	Thick	Modulus	Poisson	R	GF	Cost/m3
1	DGACVHVSG1Tg	63	9038	0.35	0	1.46	114
2	DGACVHVSG1Bg	84	11173	0.35	0	1.46	114
3	ABHVS	274	149	0.35	78	1.1	57
4	AS2HVS	215	161	0.35	50	1	30
5	ClayHVS	0	103	0.35	20	0	0

Figure 26. Section 501RF pavement structure.

In the figures below, measured deflections are indicated by an M, similarly followed by a number revealing MDD module depth, and calculated deflections are indicated by the letter C, again followed by a number denoting depth. For compression of a layer between two modules, the depths of the two modules are given, with M and C indicating measured and calculated values, respectively.

The following legend is used in Figure 28 and all subsequent figures of this type. Each item in the numbered list of explanations below appears boxed in Figure 28:

1. The wheel load under which the deflections were measured and calculated.
2. The MDDs that were used in the measurement. In the above case, the first measured value is from MDD stack number 1, module number 1, and the second measured value is from MDD stack number 2, module number 1 (the modules are counted from the top, so for both MDDs the top modules were used in the figure).
3. The legend for the first measured value (M for measured), which was at depth 0 mm (i.e., on the surface, for the second measured value, shown in the legend as M137, the depth was 137 mm). In figures where the measured difference in deflection or deformation between two modules is plotted, it will be shown as M0-640, which would indicate the measured deflection or deformation between the depths of 0 and 640 mm.
4. The legend for the first calculated value (C for calculated), which will be at the same depth as the first measured value (i.e., C0 is the calculated deflection on the surface; for the second calculated value, shown in the legend as C137, the depth was 137 mm). In figures where the calculated difference in deflection or deformation between two modules is plotted, it will be shown as C0-640, which would indicate the calculated deflection or deformation between the depths of 0 and 640 mm.

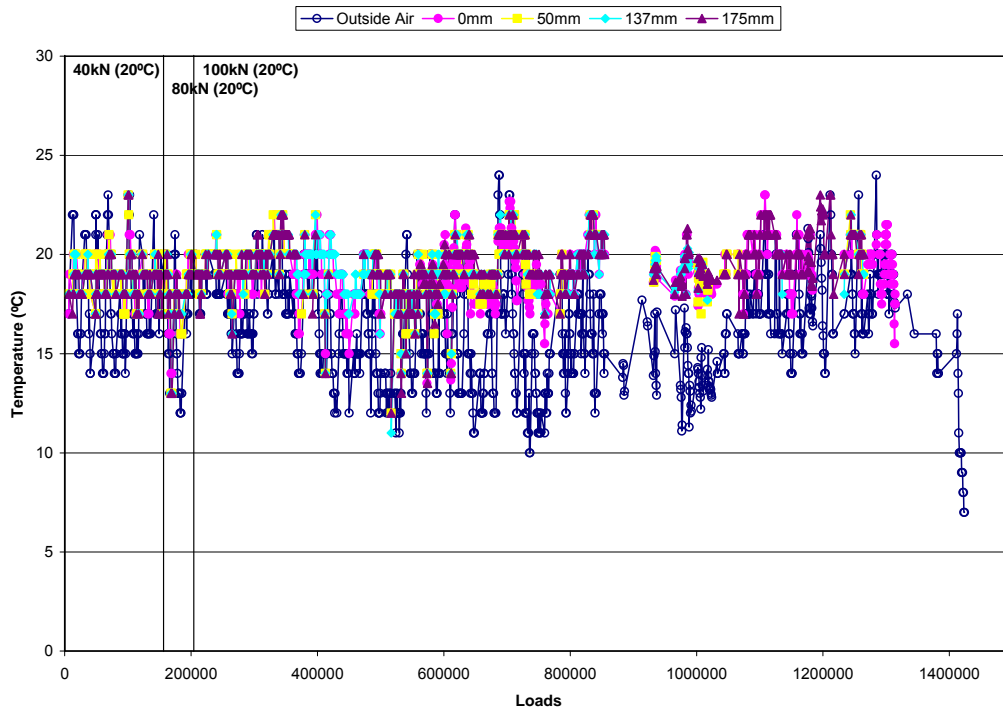


Figure 27. Section 501RF temperatures during testing.

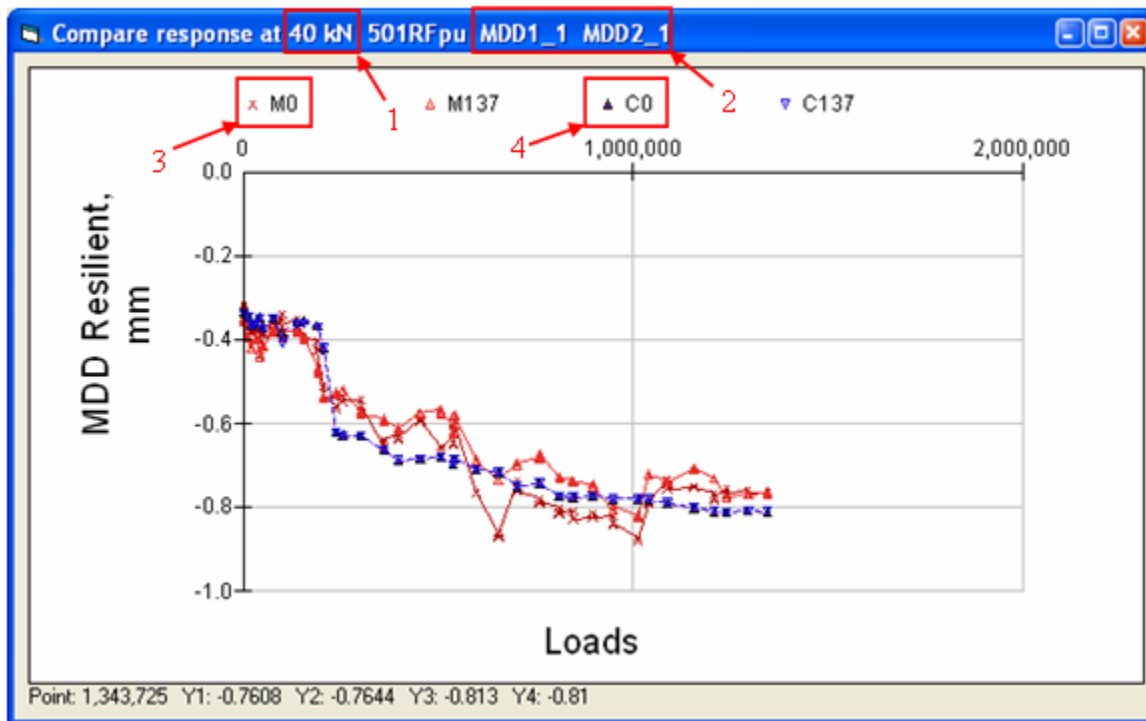


Figure 28. Section 501RF 40 kN top modules deflection.

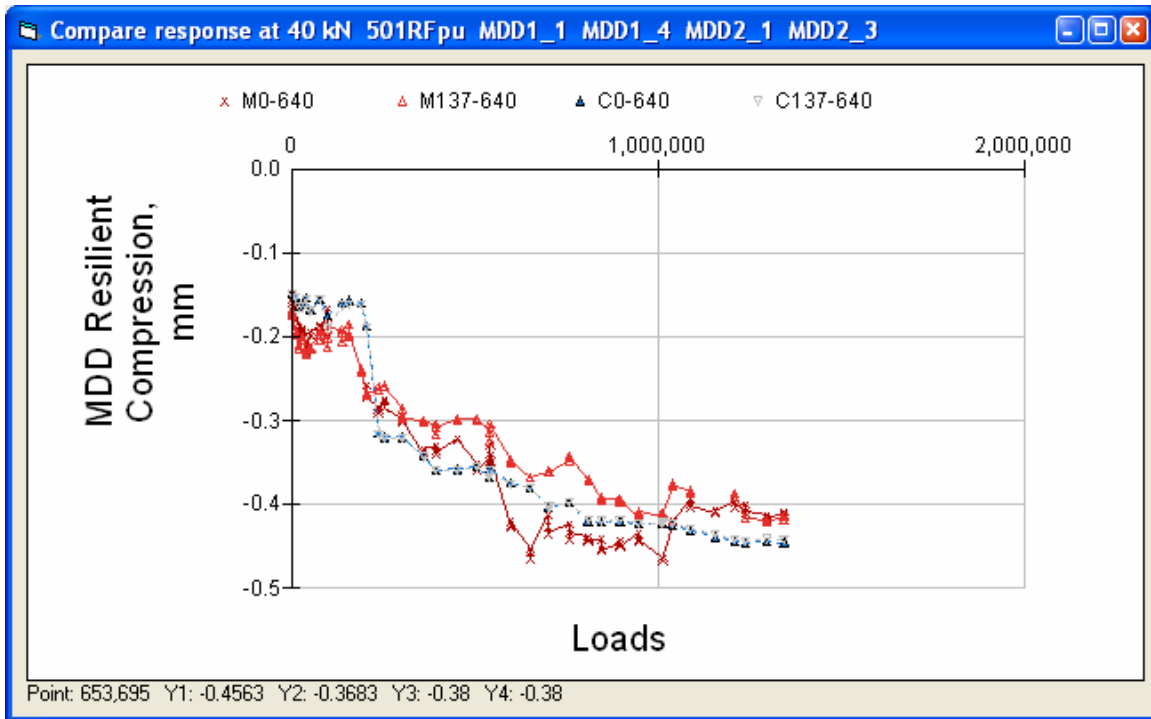


Figure 29. Section 501 RF 40 kN resilient compression of pavement layers.

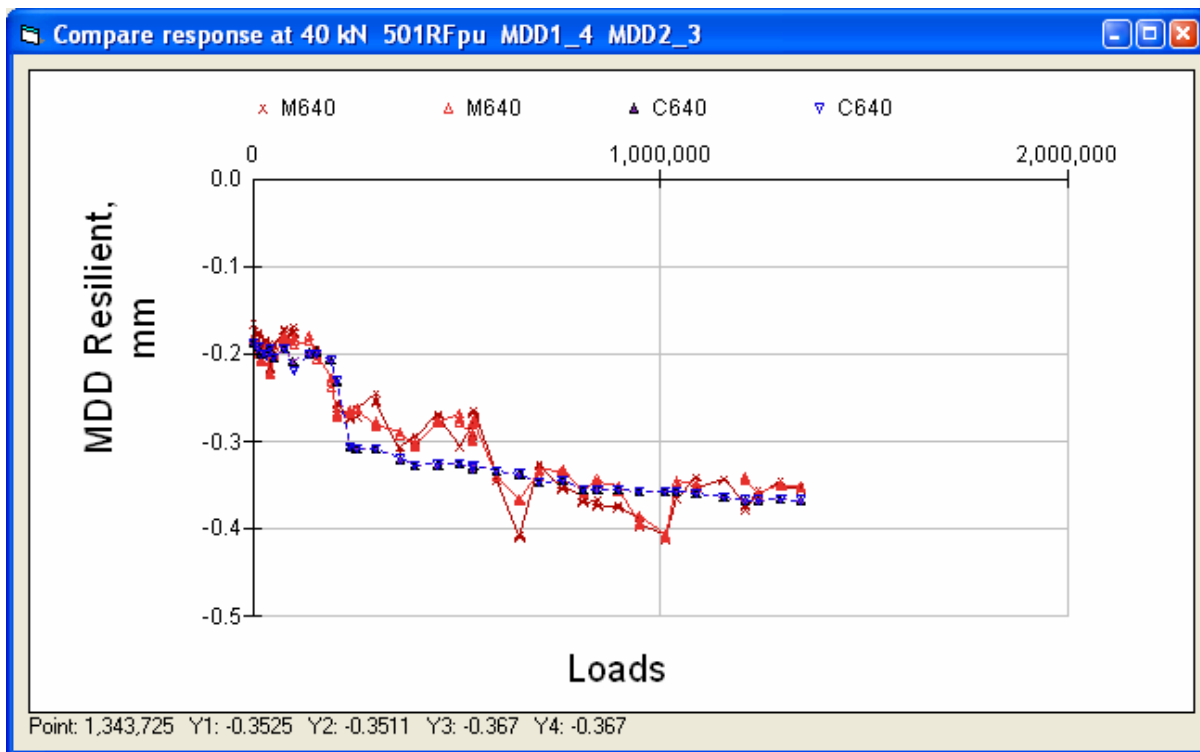


Figure 30. Section 501RF 40 kN deflection of subgrade.

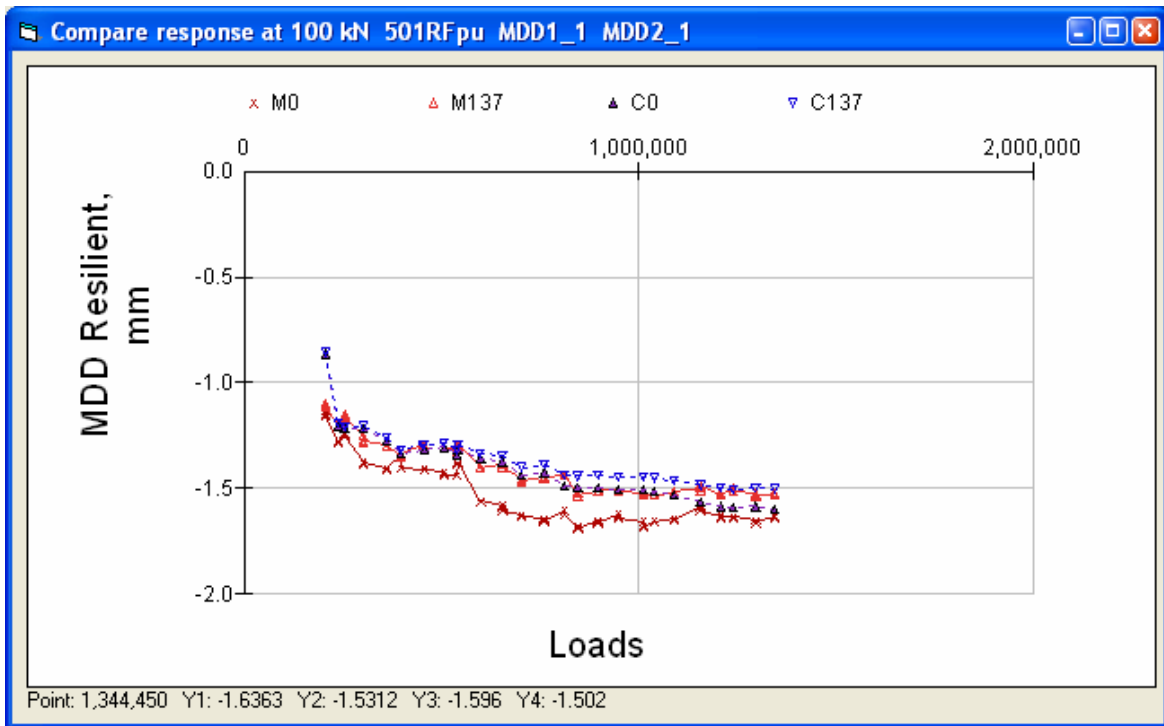


Figure 31. Section 501RF 100 kN deflection of top modules.

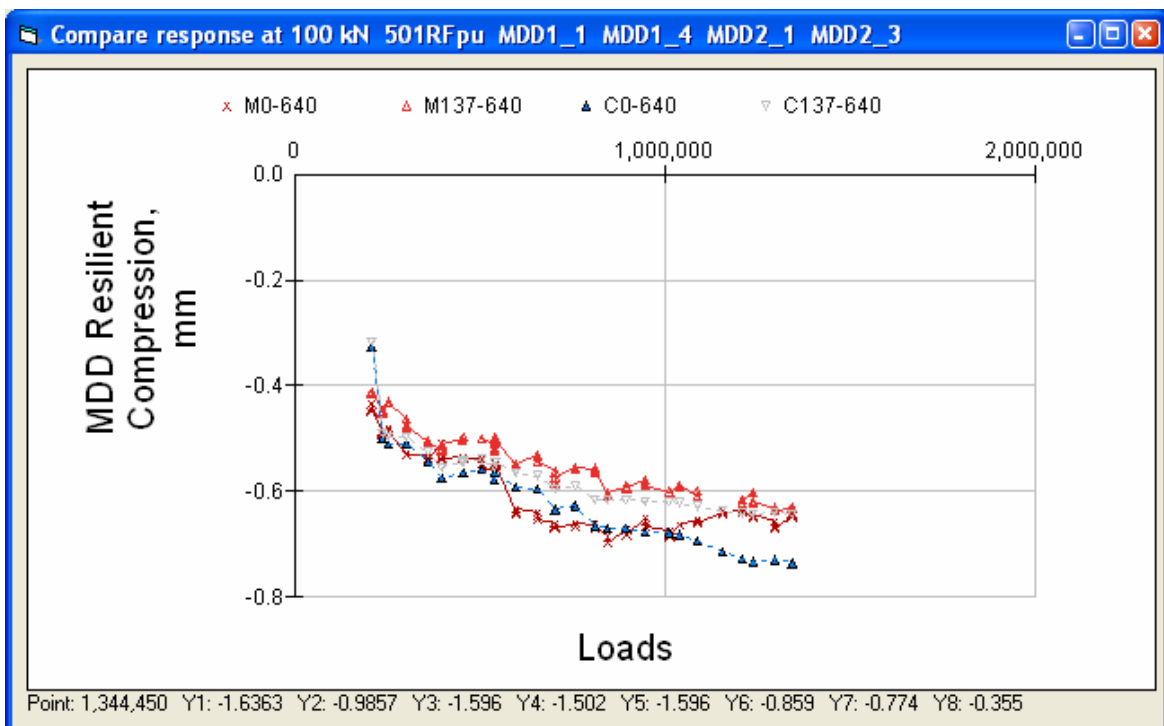


Figure 32. Section 501RF 100 kN resilient compression of pavement layers.

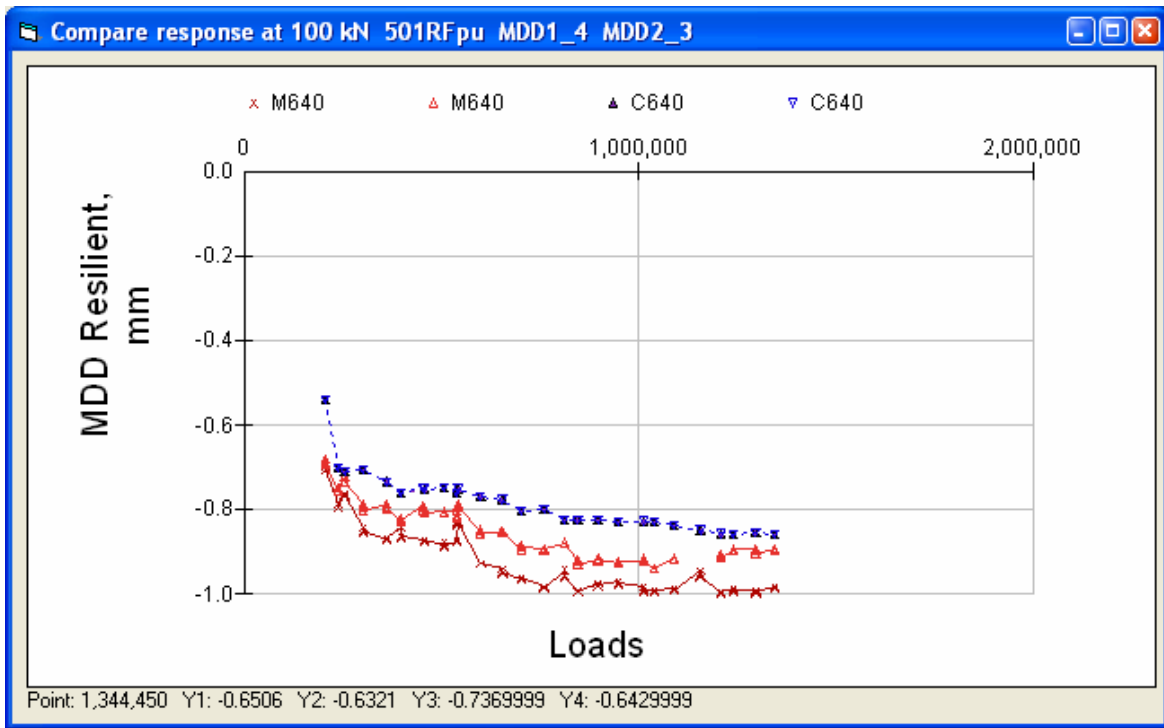


Figure 33. Section 501RF 100 kN deflection of subgrade.

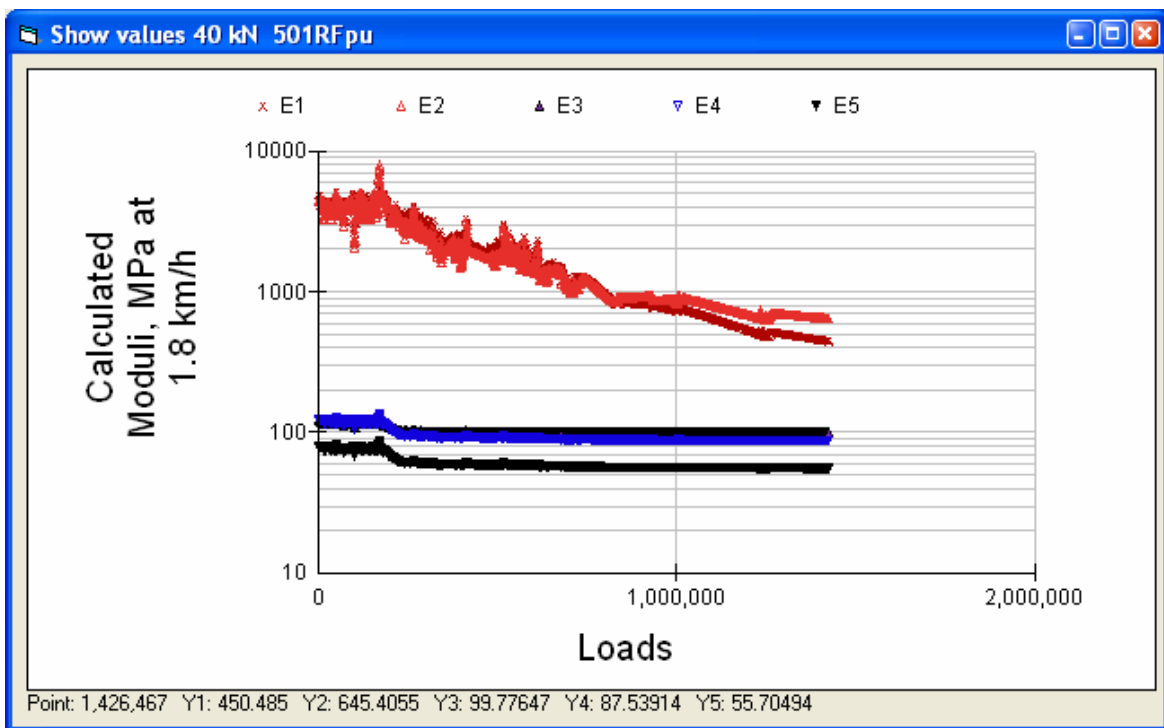


Figure 34. Section 501RF calculated moduli at 40 kN and actual temperature. (Note: in this and all other figures showing change in elastic moduli (E) under loading the lines are plotted for the modulus of each layer, i.e., E1 is the modulus of the first layer, E2 is the modulus of the second layer, etc.)

2.1.2 Section 503RF Resilient Deflections (Undrained)

The pavement structure for Section 503RF is shown in Figure 35. The first visible cracking was recorded at approximately 650,000 load repetitions.

Layer	Material	Thick	Modulus	Poisson	R	GF	Cost/m3
1	DGACVHVSG1Tg	74	9038	0.35	0	1.46	114
2	DGACVHVSG1Bg	88	11173	0.35	0	1.46	114
3	ABHVS	274	165	0.35	78	1.1	57
4	AS2HVS	305	182	0.35	50	1	30
5	ClayHVS	0	134	0.35	20	0	0

Figure 35. Section 503RF pavement structure.

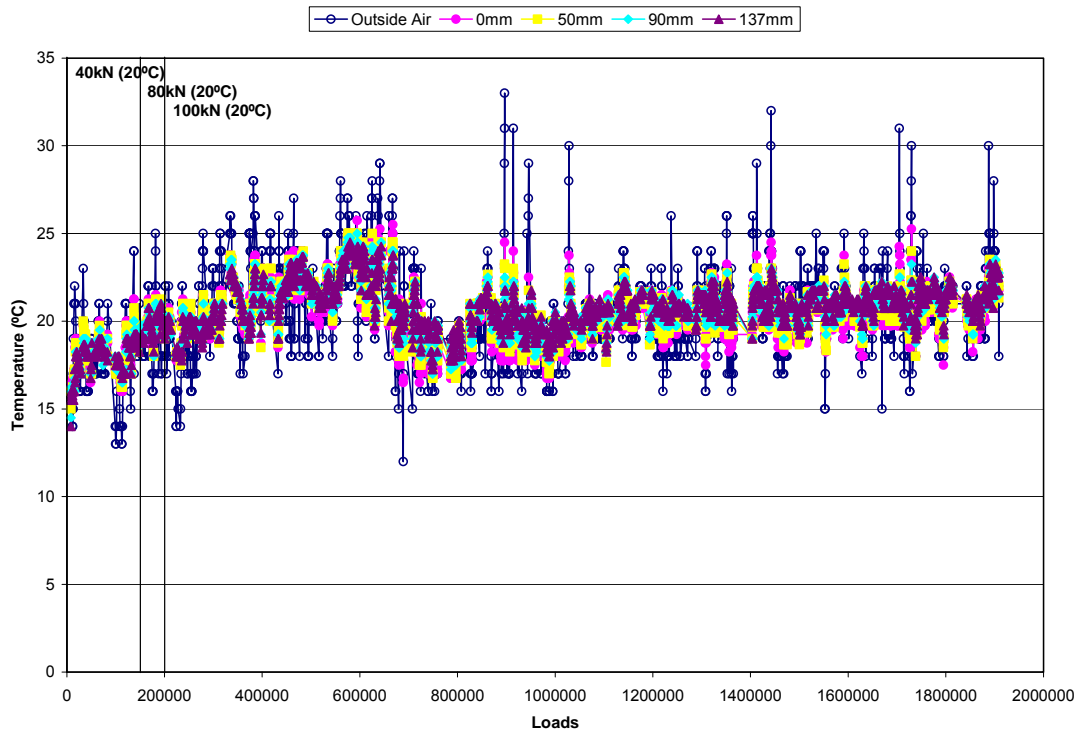


Figure 36. Section 503RF temperatures during testing.

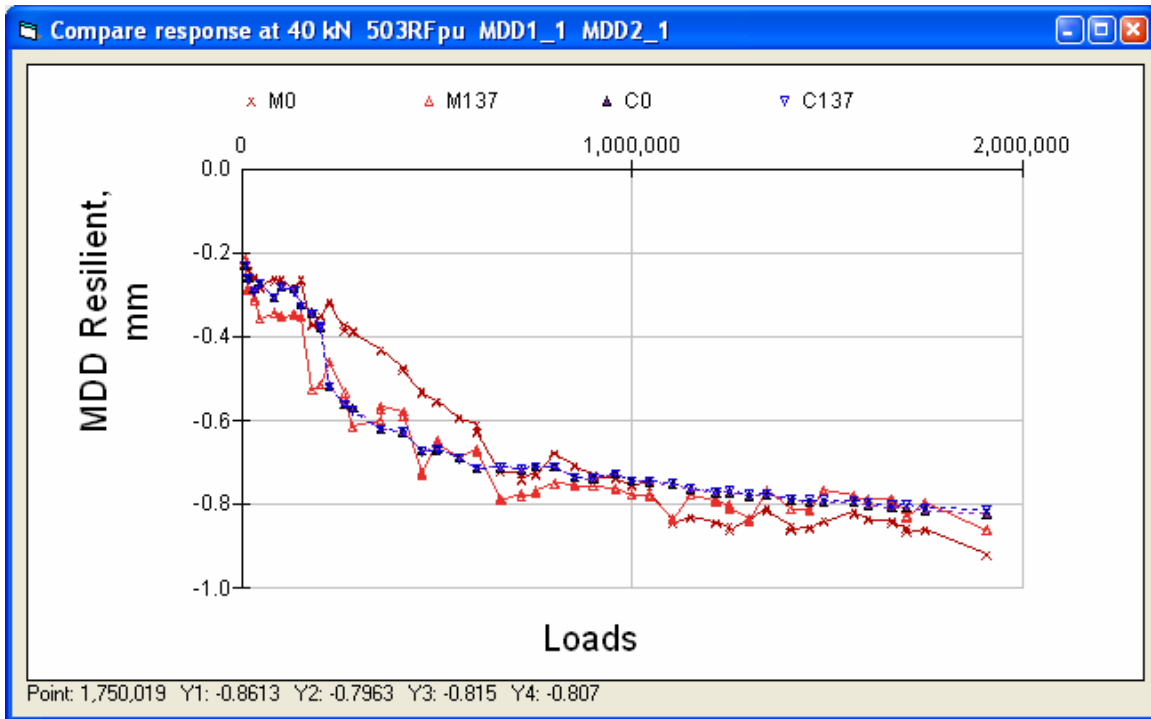


Figure 37. Section 503RF 40 kN deflection of top modules.

One of the MDDs on the subgrade only functioned for part of the test.

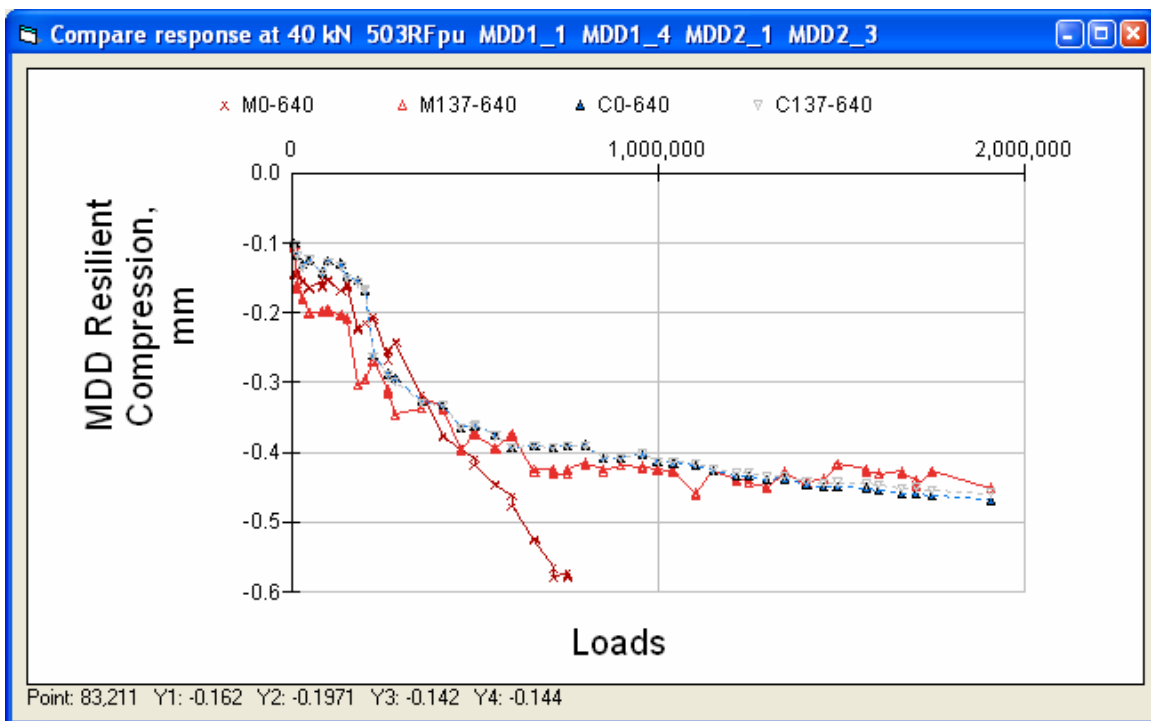


Figure 38. Section 503RF 40 kN compression of pavement layers.

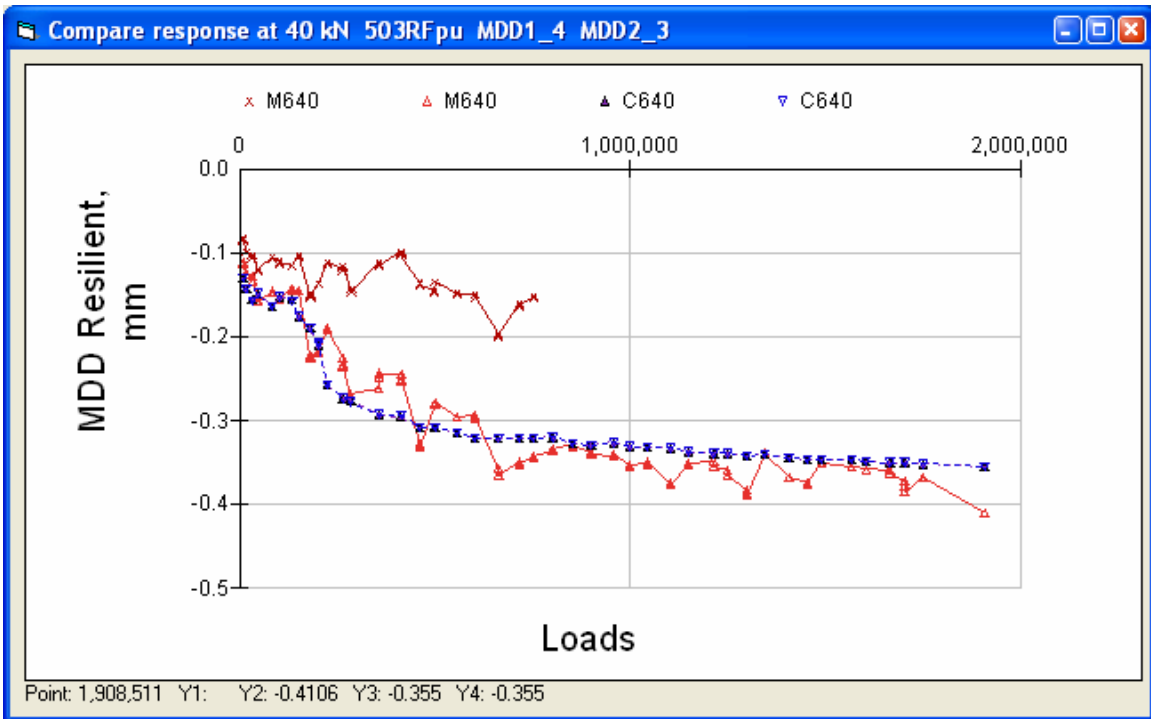


Figure 39. Section 503RF 40 kN deflection of subgrade.

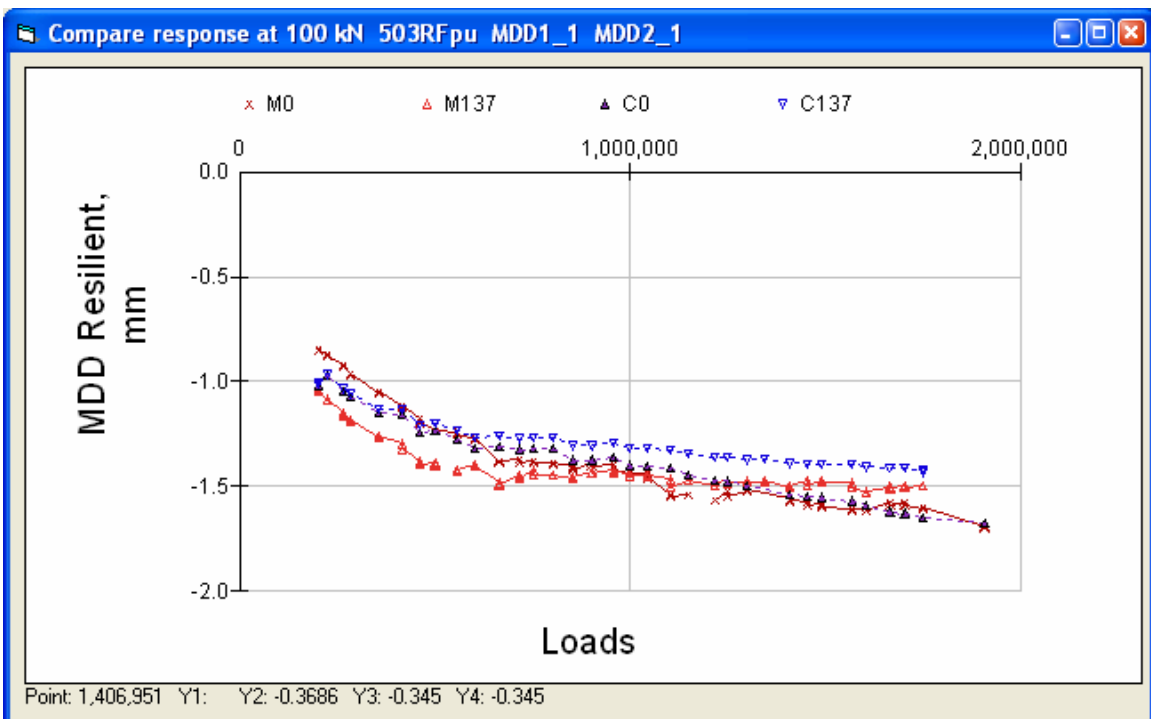


Figure 40. Section 503RF 100 kN deflection of top modules.

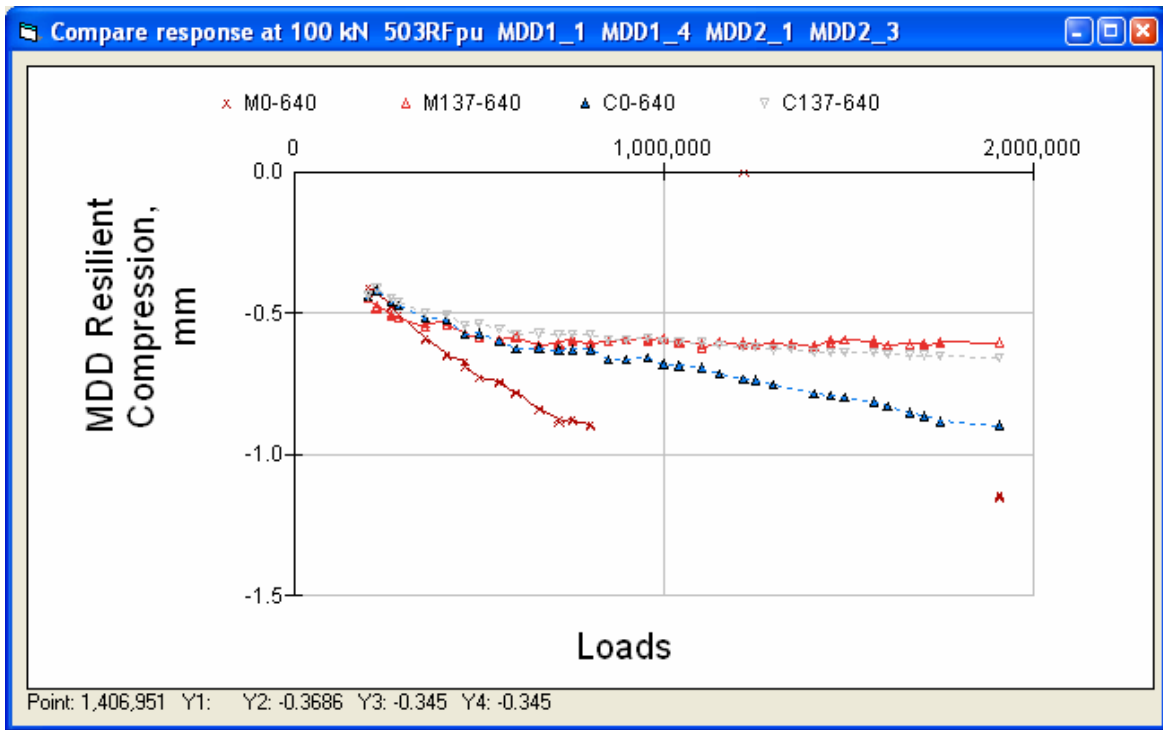


Figure 41. Section 503RF 100 kN resilient compression of pavement layers.

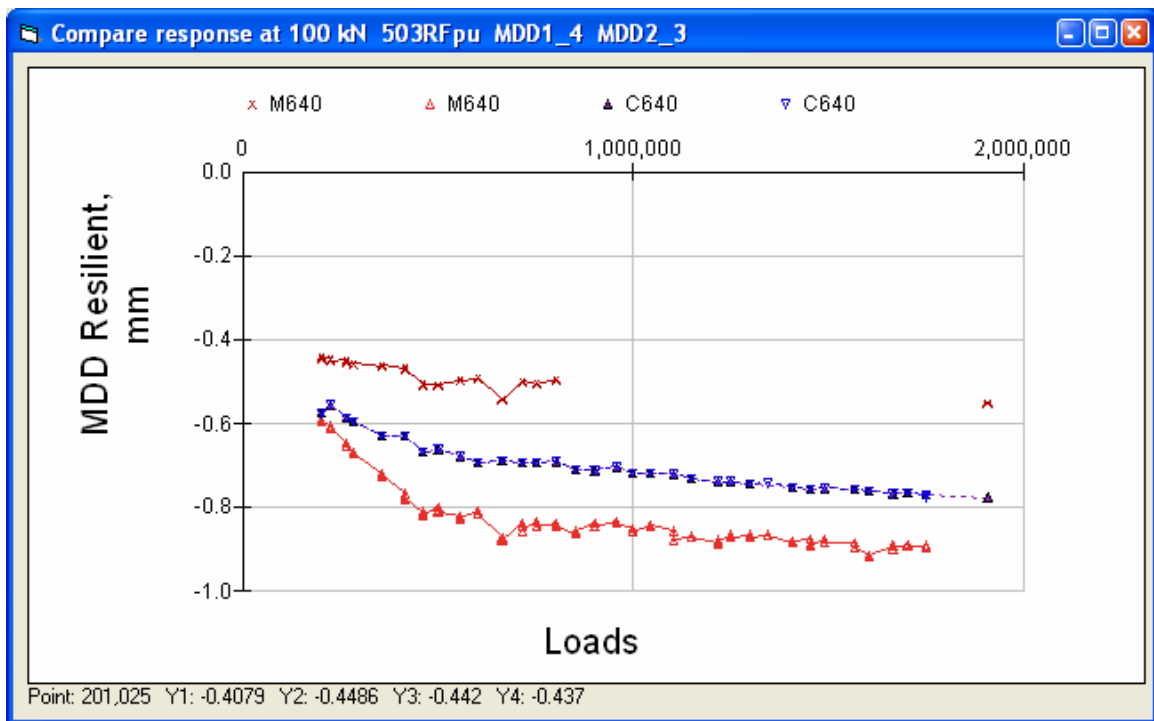


Figure 42. Section 503RF 100 kN deflection of subgrade.

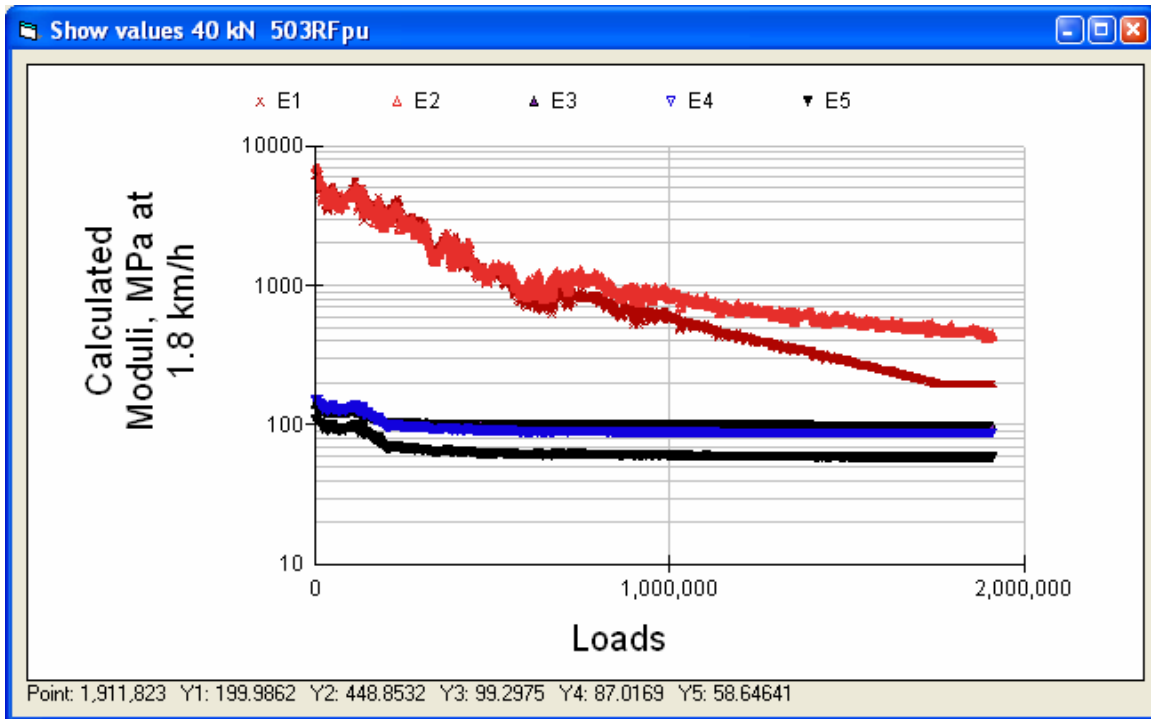


Figure 43. Section 503RF calculated layer moduli at 40 kN and actual temperature.

2.1.3 Section 500RF Resilient Deflections (Drained)

The pavement structure for Section 500RF is shown in Figure 44. The first visible cracking was recorded at approximately 650,000 load repetitions.

500RFpu structural data

Design methods Tools Change WIM Parameters

Layer	Material	Thick	Modulus	Poisson	R	GF	Cost/m3
1	DGACVHVSg1Tg	74	9038	0.35	0	1.46	114
2	DGACVHVSg1Bg	76	11173	0.35	0	1.46	114
3	ATPB-ACHVS	75	1143.5	0.35	0	1.4	82
4	ABHVS	182	206	0.35	78	1.1	57
5	AS2HVS	137	194	0.35	50	1	30
6	ClayHVS	0	107	0.35	20	0	0

Figure 44. Section 500RF pavement structure.

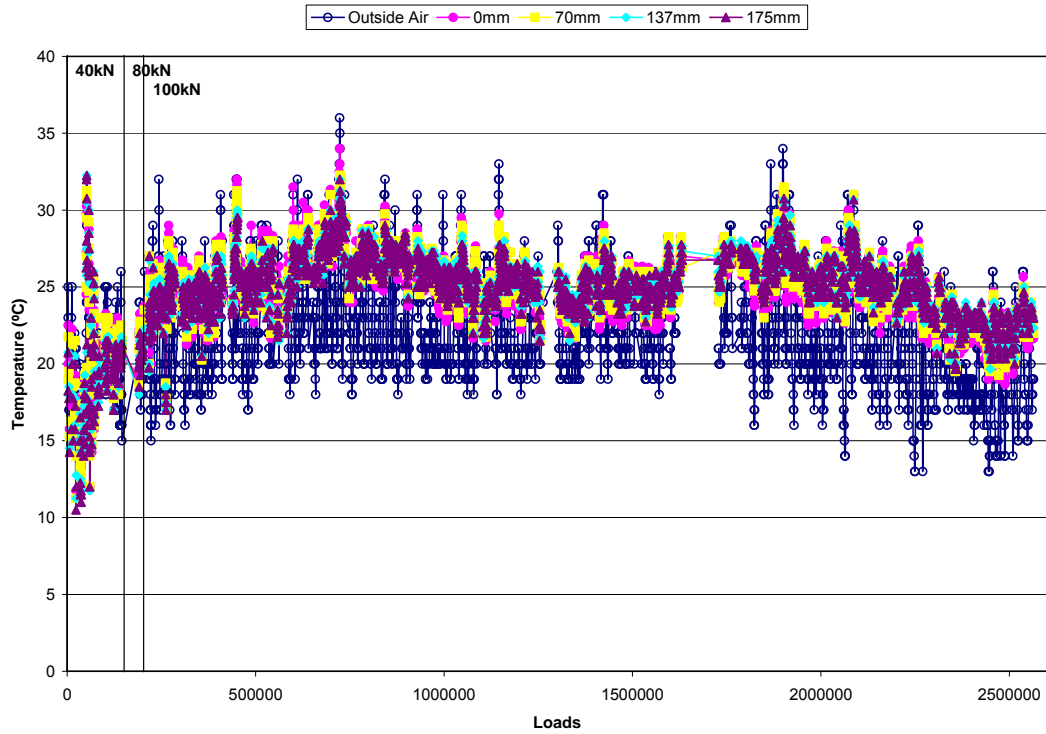


Figure 45. Section 500RF temperatures during testing.

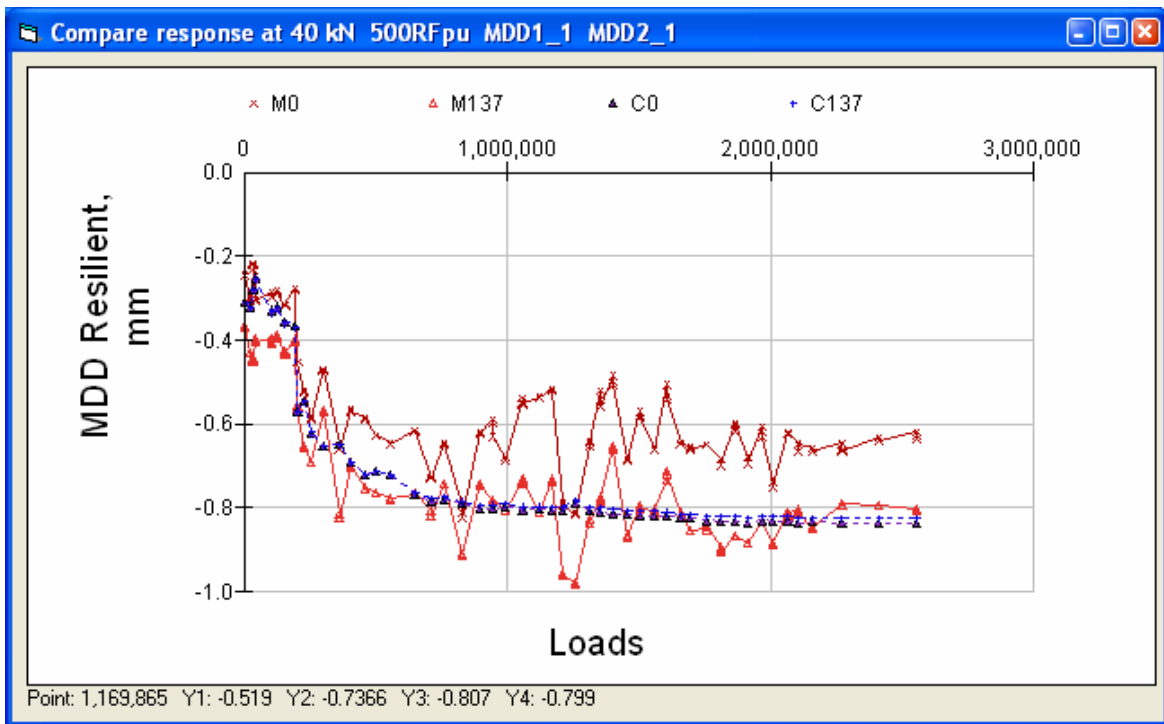


Figure 46. Section 500RF 40 kN deflection of top modules.

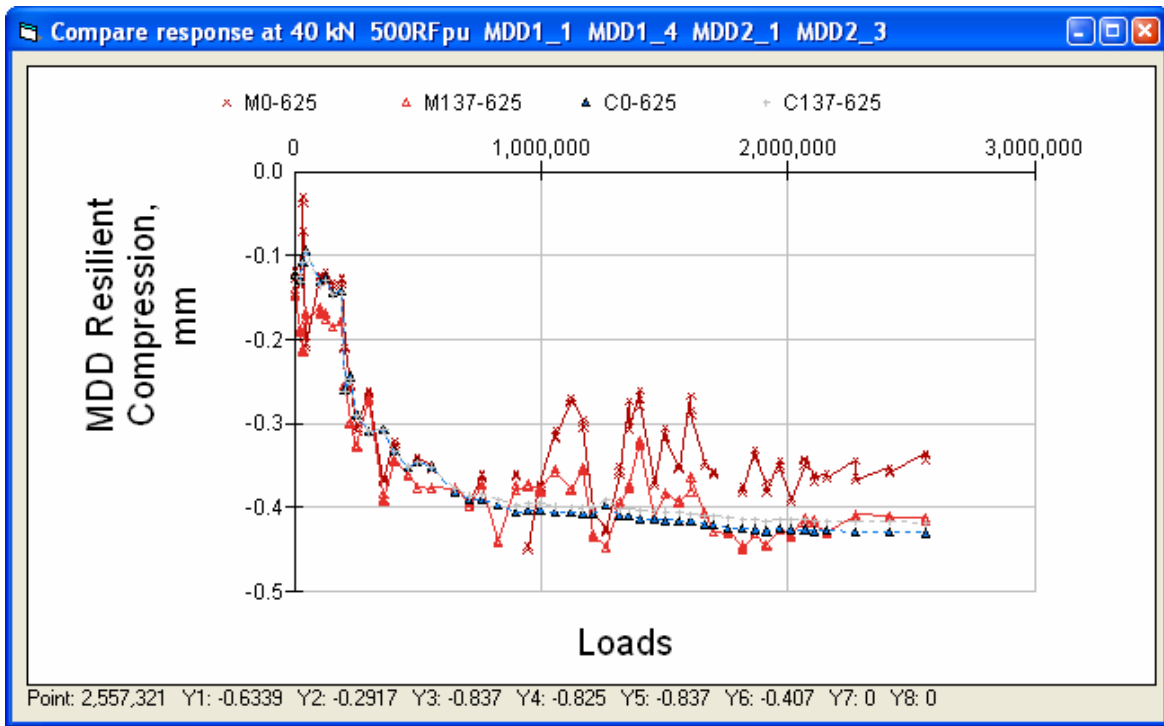


Figure 47. Section 500RF 40 kN resilient compression of pavement layers.

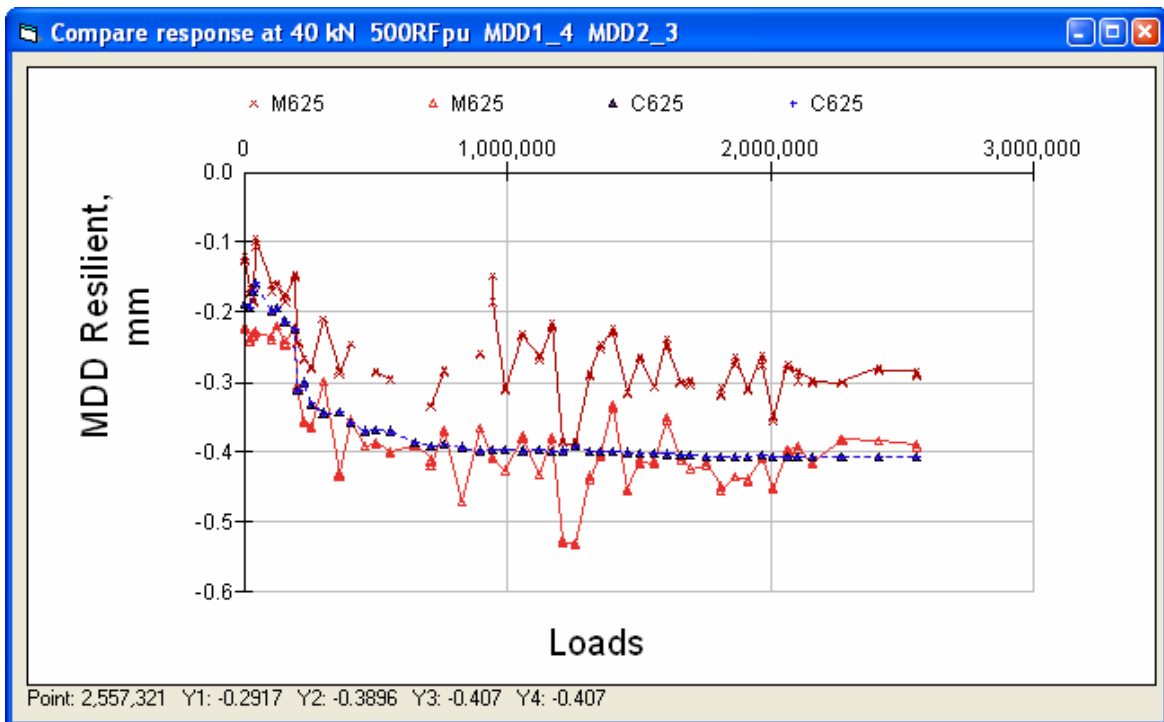


Figure 48. Section 500RF 40 kN deflection of subgrade.

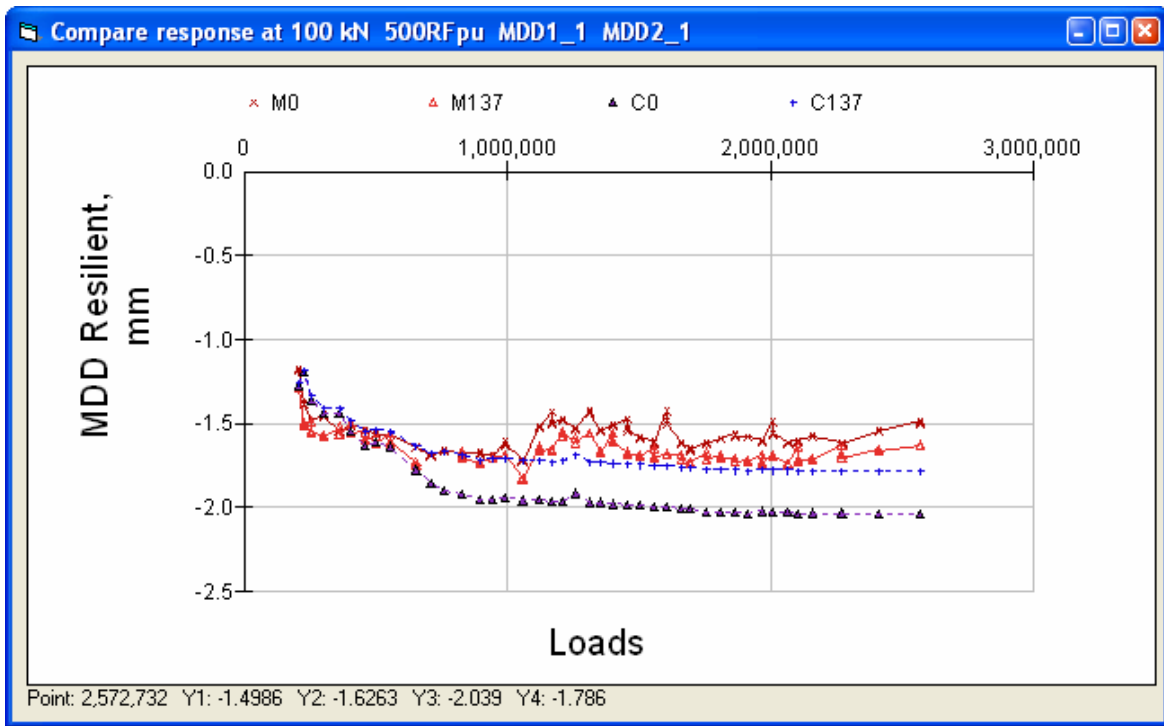


Figure 49. Section 500RF 100 kN deflection of top modules.

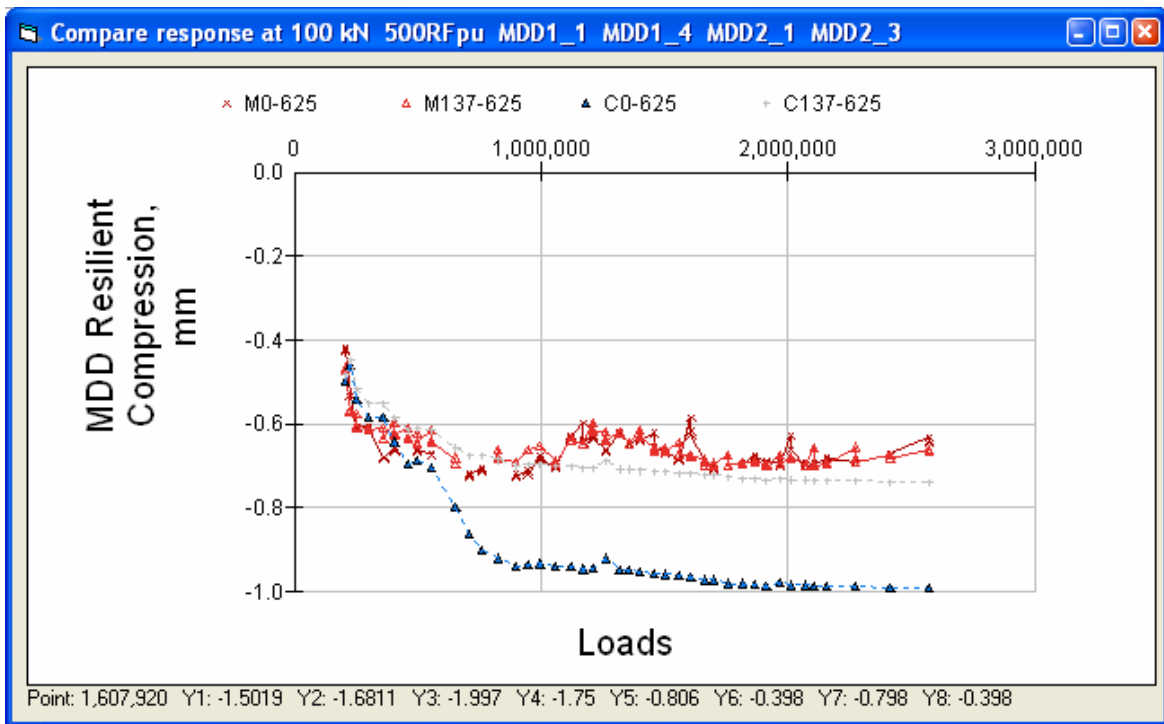


Figure 50. Section 500RF 100 kN compression of pavement layers.

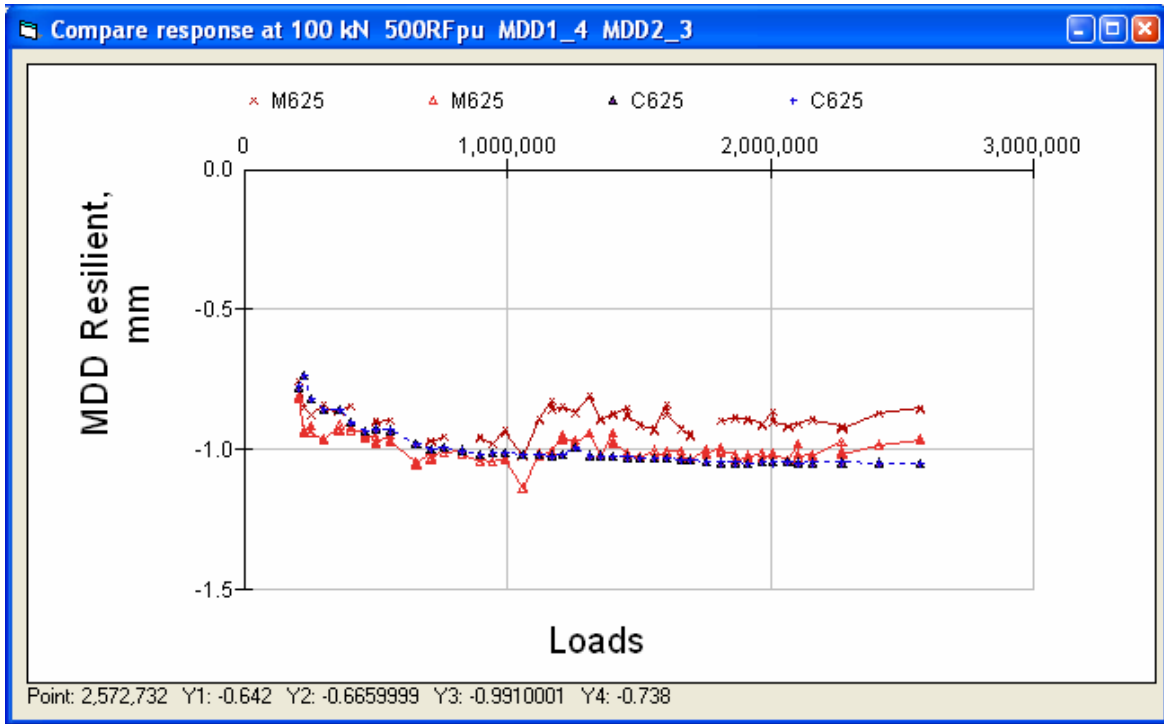


Figure 51. Section 500RF 100 kN deflection of subgrade.

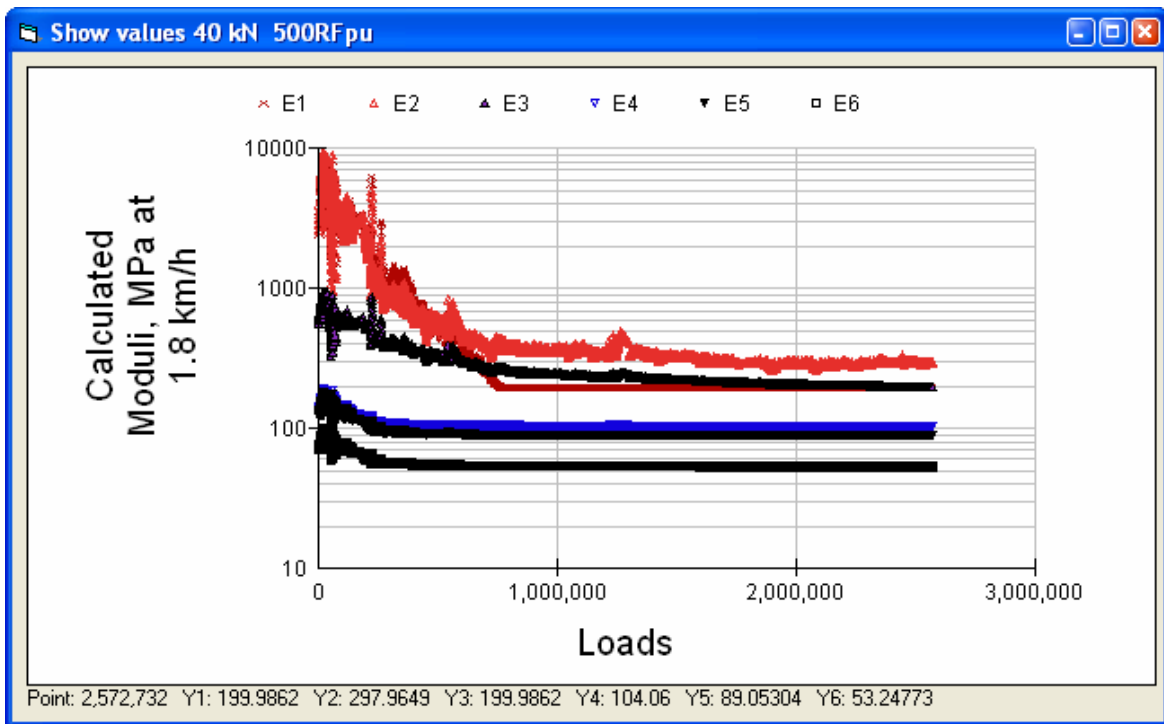


Figure 52. Section 500RF calculated moduli at 40 kN and actual temperature.

2.1.4 Section 502CT Resilient Deflections (Drained)

The pavement structure for Section 502CT is shown in Figure 53. Temperature data is missing from Section 502CT. For all layers throughout the test, 20°C was used. The first visible cracking was recorded at approximately 1,310,000 load repetitions.

Layer	Material	Thick	Modulus	Poisson	R	GF	Cost/m3
1	DGACVHMSG1Tg	68	9038	0.35	0	1.46	114
2	DGACVHMSG1Bg	80	11173	0.35	0	1.46	114
3	ATPB-ACHVS	75	1143.5	0.35	0	1.4	82
4	ABHVS	182	202	0.35	78	1.1	57
5	AS2HVS	215	191	0.35	50	1	30
6	ClayHVS	0	208	0.35	20	0	0

Figure 53. Section 502CT pavement structure.

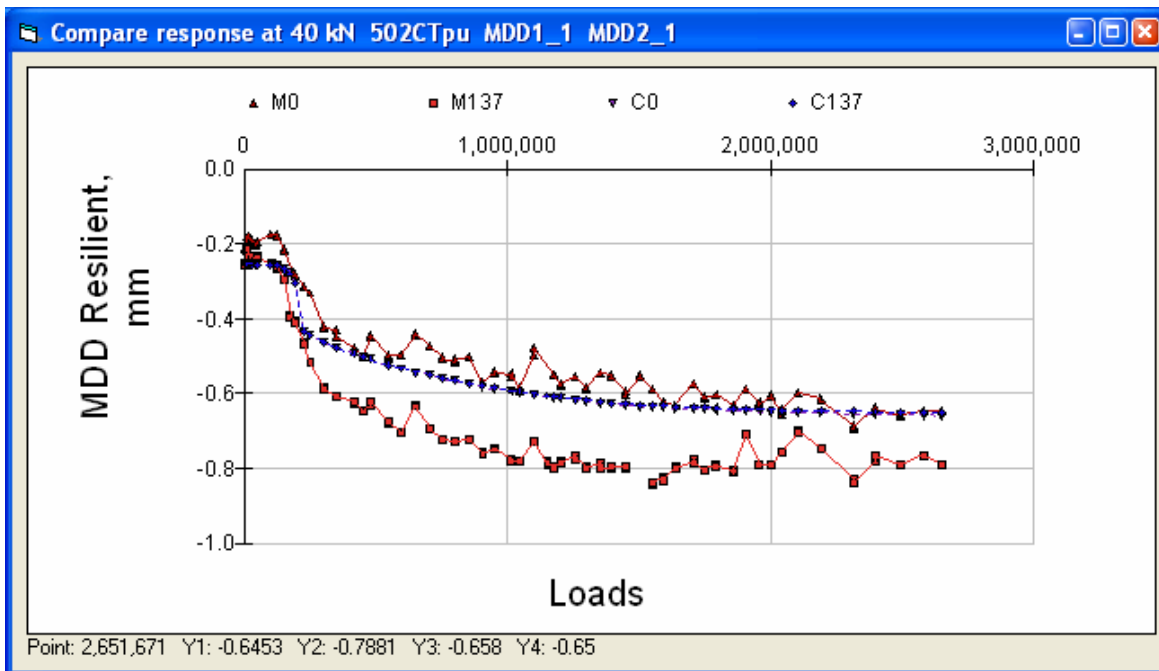


Figure 54. Section 502CT 40 kN deflection on top of AC.

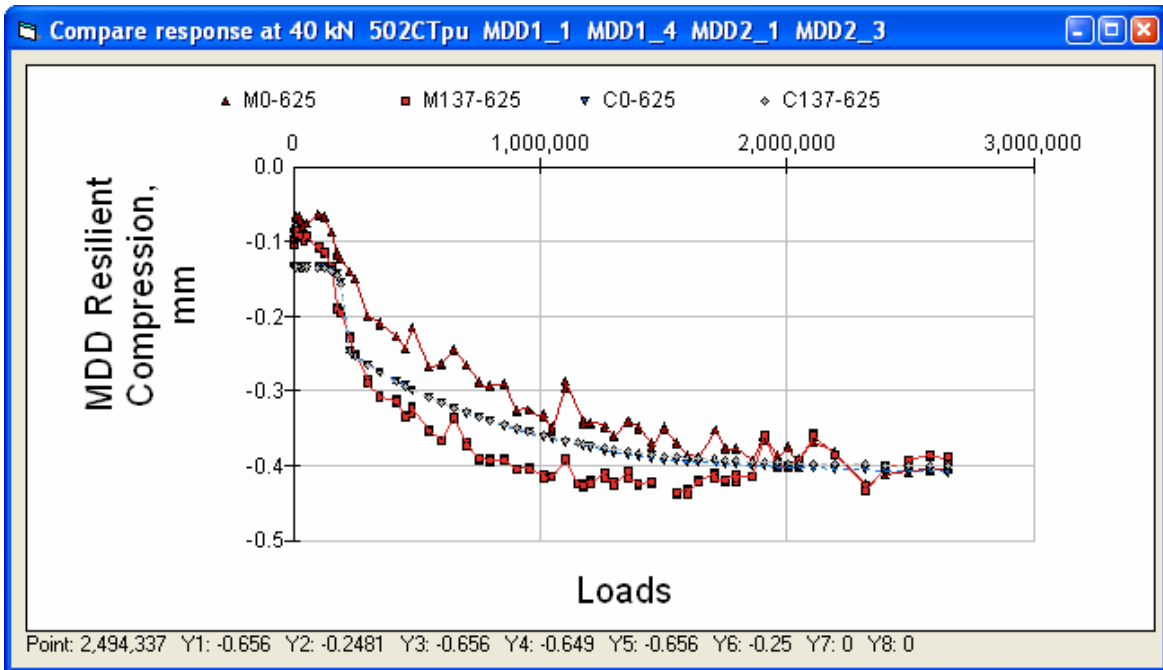


Figure 55. Section 502CT 40 kN compression of pavement layers.

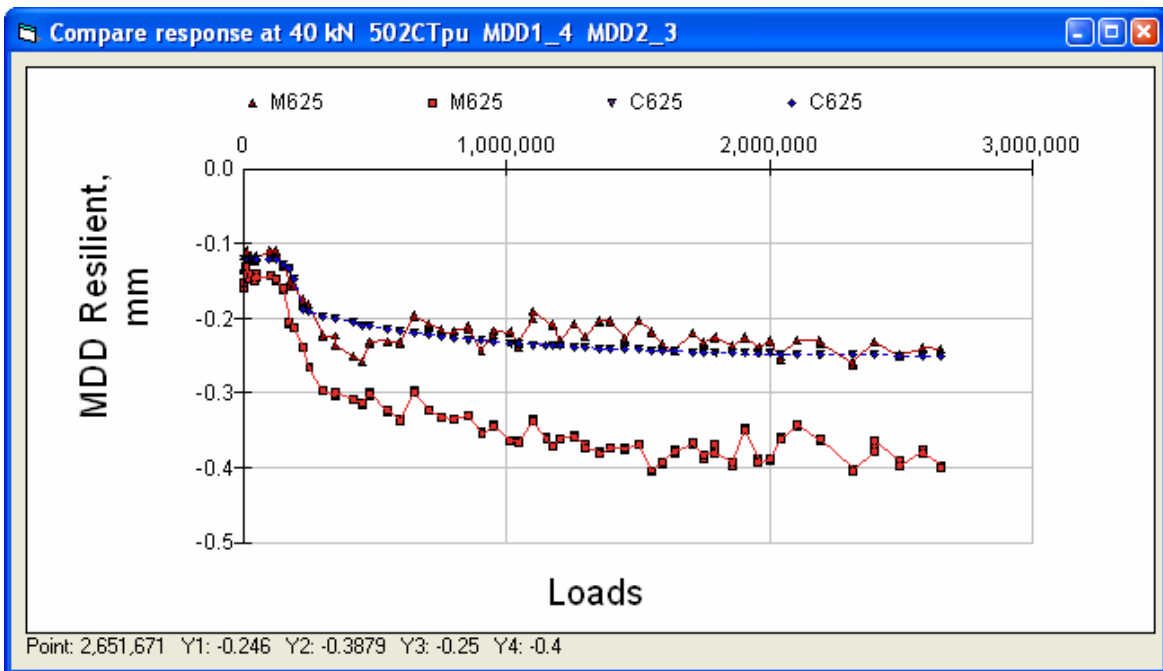


Figure 56. Section 502CT 40 kN deflection of subgrade.

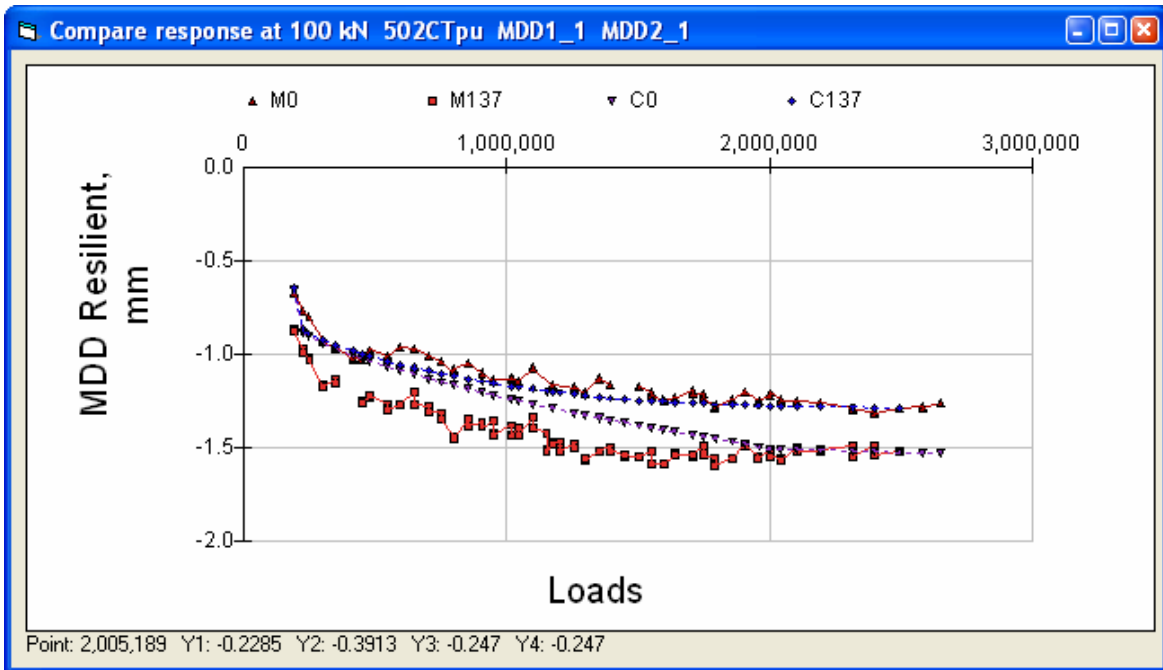


Figure 57. Section 502CT 100 kN deflection at top of AC.

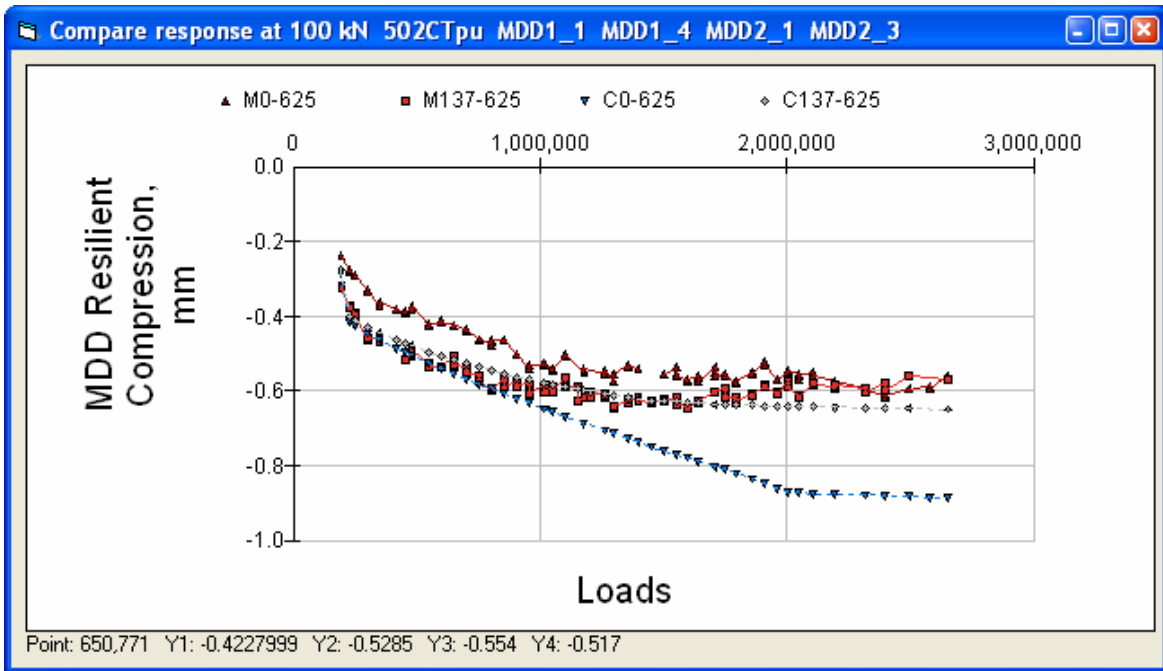


Figure 58. Section 502CT 100 kN resilient compression of pavement layers.

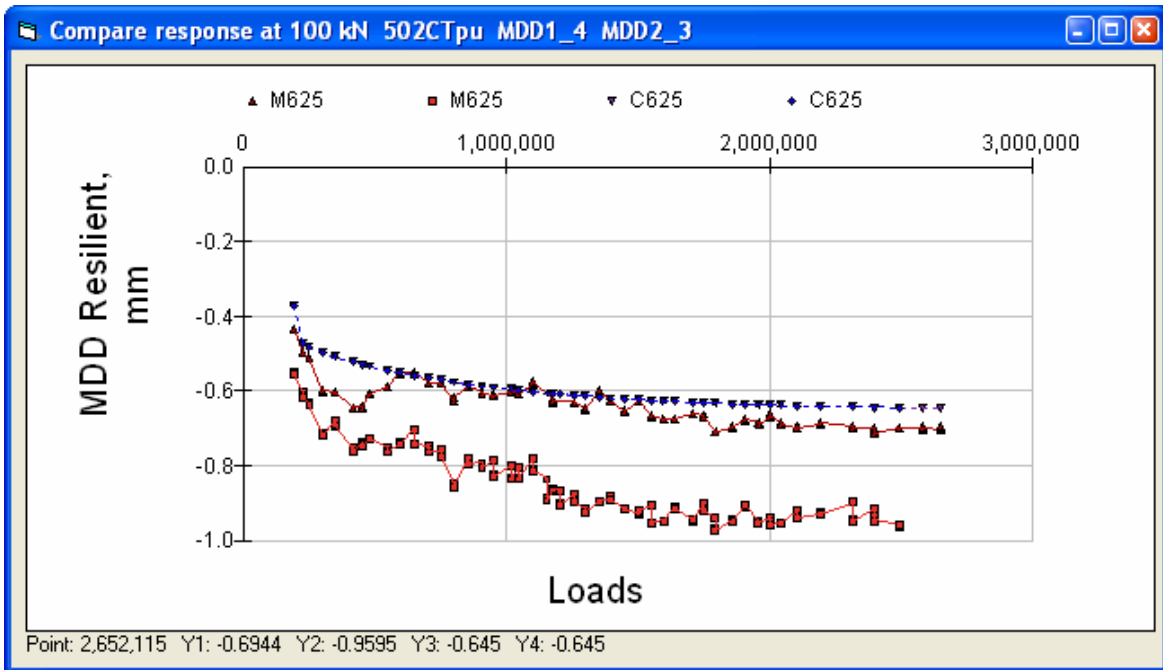


Figure 59. Section 502CT 100 kN deflection of subgrade.

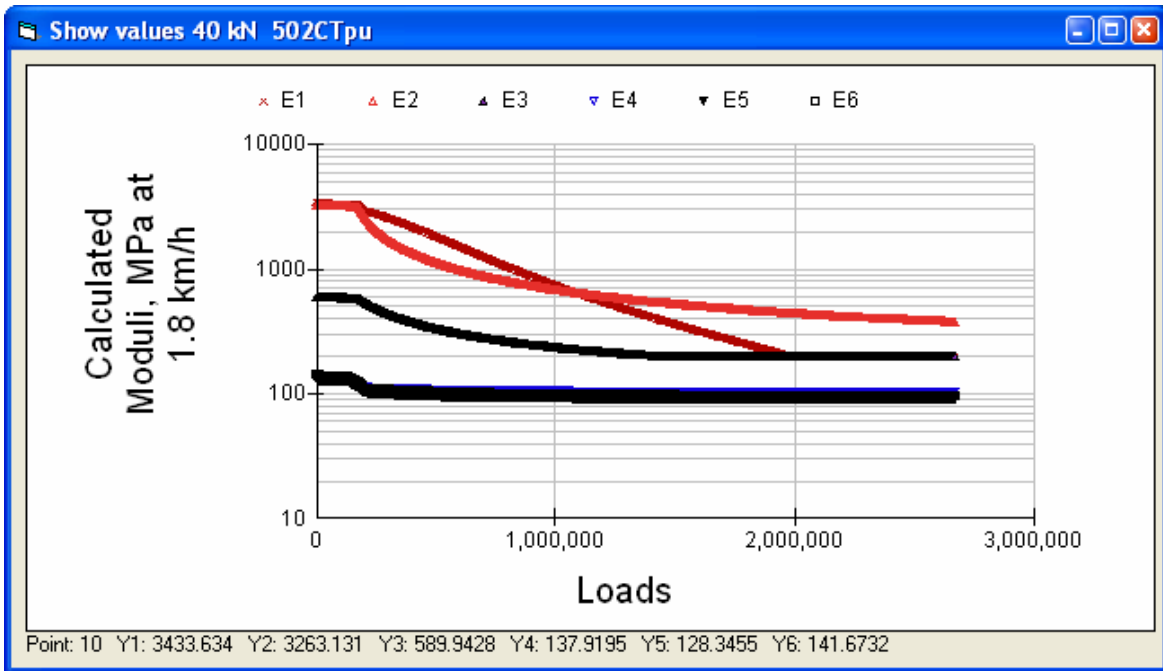


Figure 60. Section 502CT calculated moduli at 40 kN and 20°C.

Given the scatter in the measured data, the agreement between measured and calculated deflections and compressions could probably not have been much better. Although this does not guarantee that the strains calculated to determine the damage in the asphalt are correct (as was noted in the Introduction) or that the calculated moduli throughout the HVS test are in accordance with the actual moduli, it is a strong indication that this is the case.

It should be recalled, however, that a number of assumptions have been made, and it is possible that different assumptions could result in equally good or better agreement between measured and calculated deflections.

2.2 Visual Cracking Versus Damage of the Top Asphalt Layer, Goal 1

Cracking at the pavement surface was recorded in m/m^2 . In Figure 61, the observed cracking is shown versus the relative decrease in the modulus of the top asphalt layer, assuming an intact modulus of 5,669 MPa at a temperature of 20°C, a wheel speed of 7.6 km/h, and a minimum modulus of 200 MPa.

There is a clear difference between the drained and the undrained pavement sections. For the undrained sections (501RF and 503RF) the first visual cracking appears when the modulus has dropped by about 50–60 percent, whereas the corresponding drop in modulus for the drained sections is about 70–80 percent.

For all four test sections, the deflection under a 40-kN load — measured with the top MDD modules — had doubled before any surface cracking was observed. This also indicates that the pavement structures underwent considerable damage before any cracking was observed.

Visual cracking versus decrease in modulus

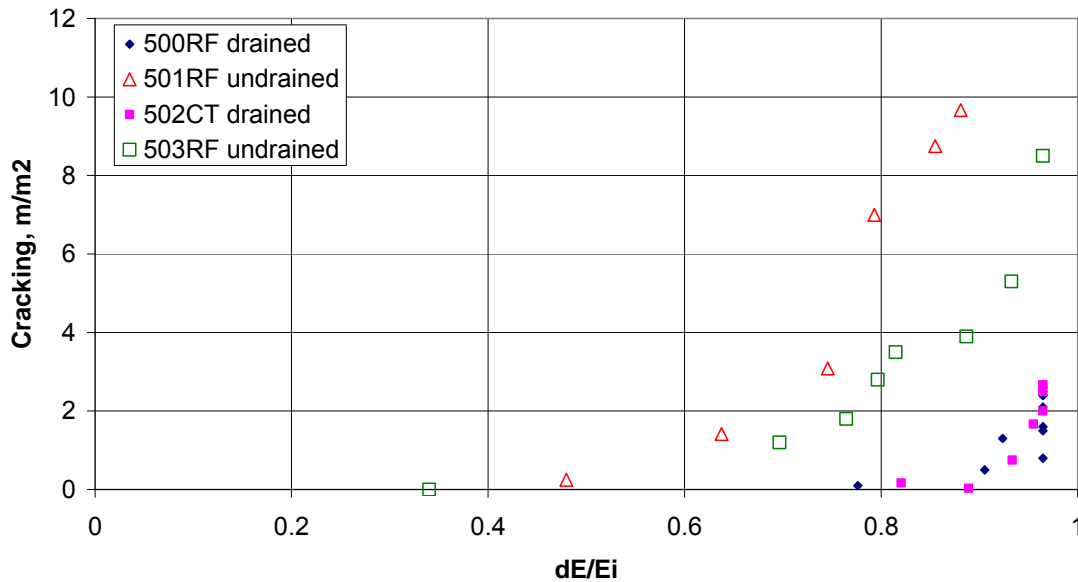


Figure 61. Cracking versus relative decrease in modulus of top AC layer for Goal 1.

Cracking versus relative deflection

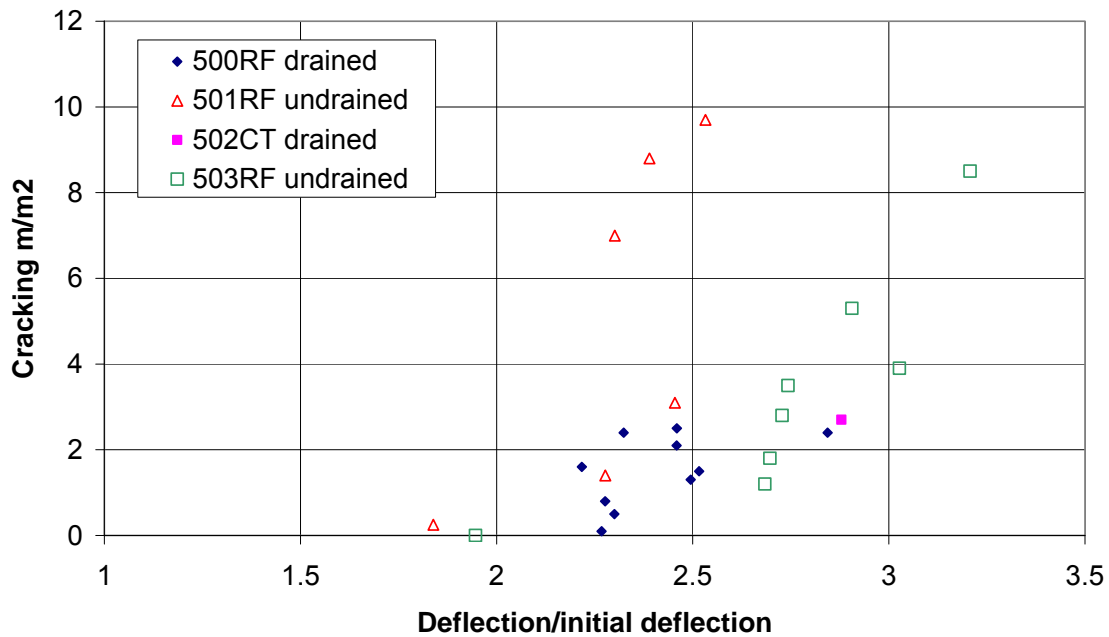


Figure 62. Goal 1, cracking versus increase in deflection.

For the two drained sections (500RF and 502CT), it was assumed that there was a full bond between the bottom AC layer and the ATPB layer, although there was evidence from Goal 5 that a slip could have developed.

The calculated layer moduli at a wheel speed of 1.8 km/h, a load of 40 kN, and the actual temperatures are shown in Table 15 for when testing began and in Table 16 for when the testing ended. The moduli are given in MPa.

Table 15. Initial Moduli MPa (1.8 km/h, 40 kN, Actual Temperature) for Each Section

Layer	501RF	503RF	500RF	502CT
AC top	4930	5695	5567	3433
AC bottom	4425	5681	6125	3263
ATPB			781	590
AB	122	136	159	135
ASB	125	145	148	124
Subgrade	81	106	86	136

Table 16. Final Moduli MPa (1.8 km/h, 40 kN, Actual Temperature) for Each Section

Layer	501RF	503RF	500RF	502CT
AC top	540	200	200	200
AC bottom	645	447	317	398
ATPB			200	200
AB	100	99	101	101
ASB	88	87	86	86
Subgrade	56	59	53	93

The percentage decrease in moduli is given in Table 17.

Table 17. Percentage Decrease in Layer Moduli for Each Section

Layer	501RF	503RF	500RF	502CT
AC top	89	96	96	94
AC bottom	85	92	95	88
ATPB			74	66
AB	18	27	36	25
ASB	30	40	42	31
Subgrade	31	44	38	32

The decrease in asphalt moduli is very large. However, to reach the increase in resilient deflection, either the decrease in asphalt moduli must be as large as shown in Table 17, or the decrease in the moduli of the unbound layers must have been even larger than shown in the table.

The damage parameter, ω , for the asphalt layers at the end of the test is given in Table 18.

Table 18. Damage Parameter for Asphalt Layers at End of Test for Each Section

Layer	501RF	503RF	500RF	502CT
AC top	0.64	1.0	1.0	1.0
AC bottom	0.49	0.59	.74	.67
ATPB			1.0	1.0

2.3 Goal 1 Permanent Deformation

Permanent deformation in the pavement layers was measured by the MDDs. Permanent deformation of the surface of the pavement was also measured using the laser profilometer, identified as “profile” in the permanent deformation figures in this report.

2.3.1 Section 501RF Permanent Deformations

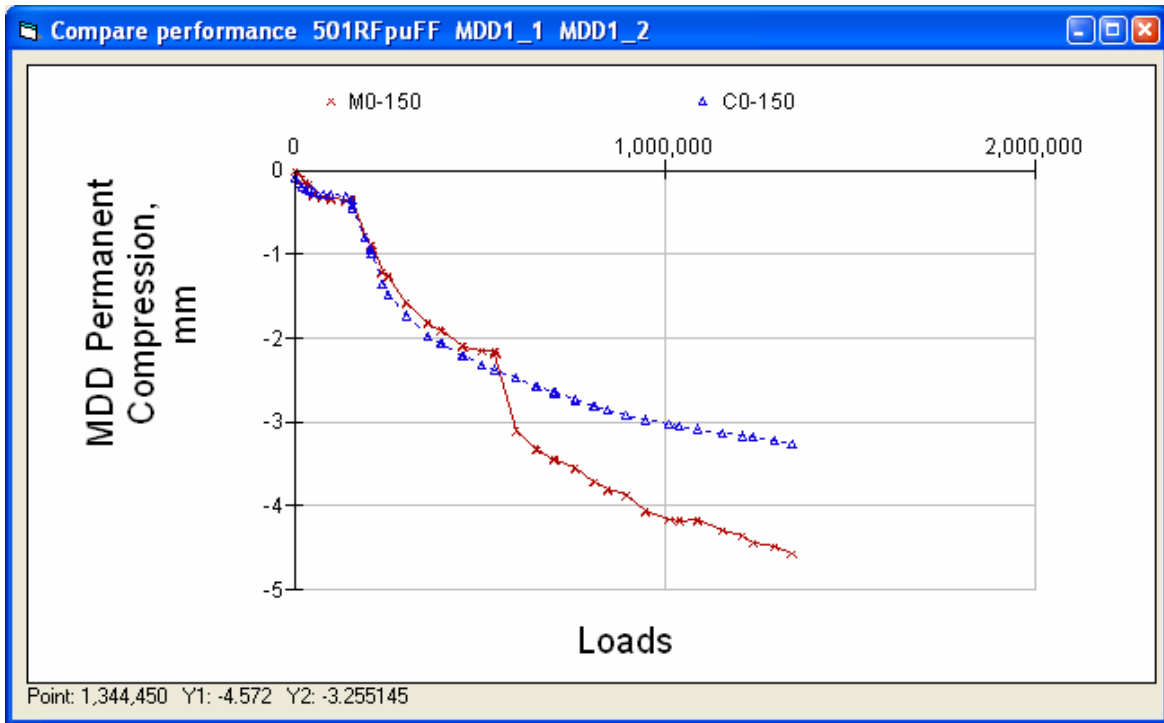


Figure 63. Permanent compression of AC layers.

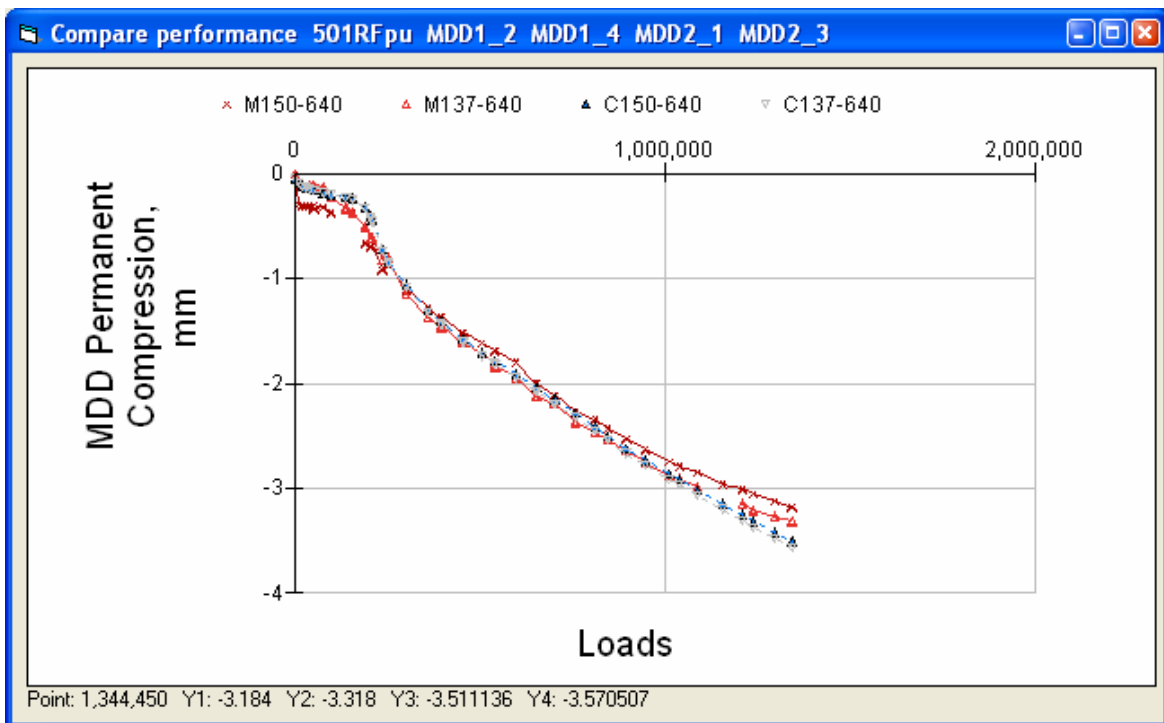


Figure 64. Permanent compression of granular layers.

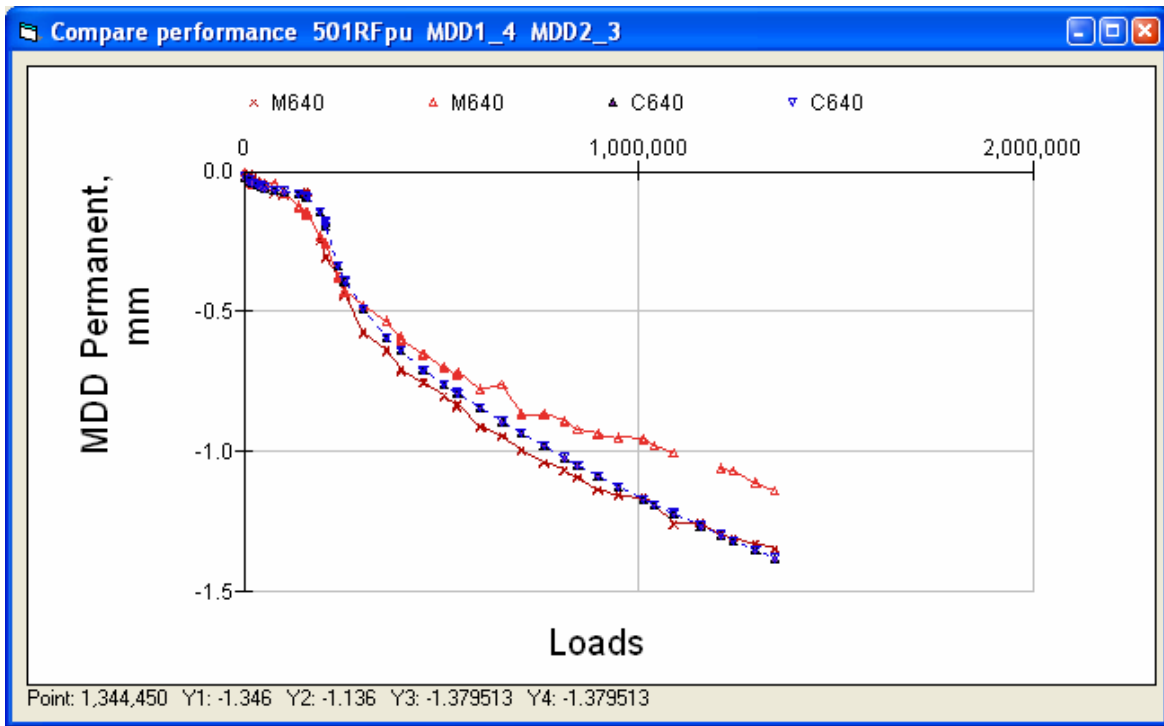


Figure 65. Permanent deformation of subgrade.

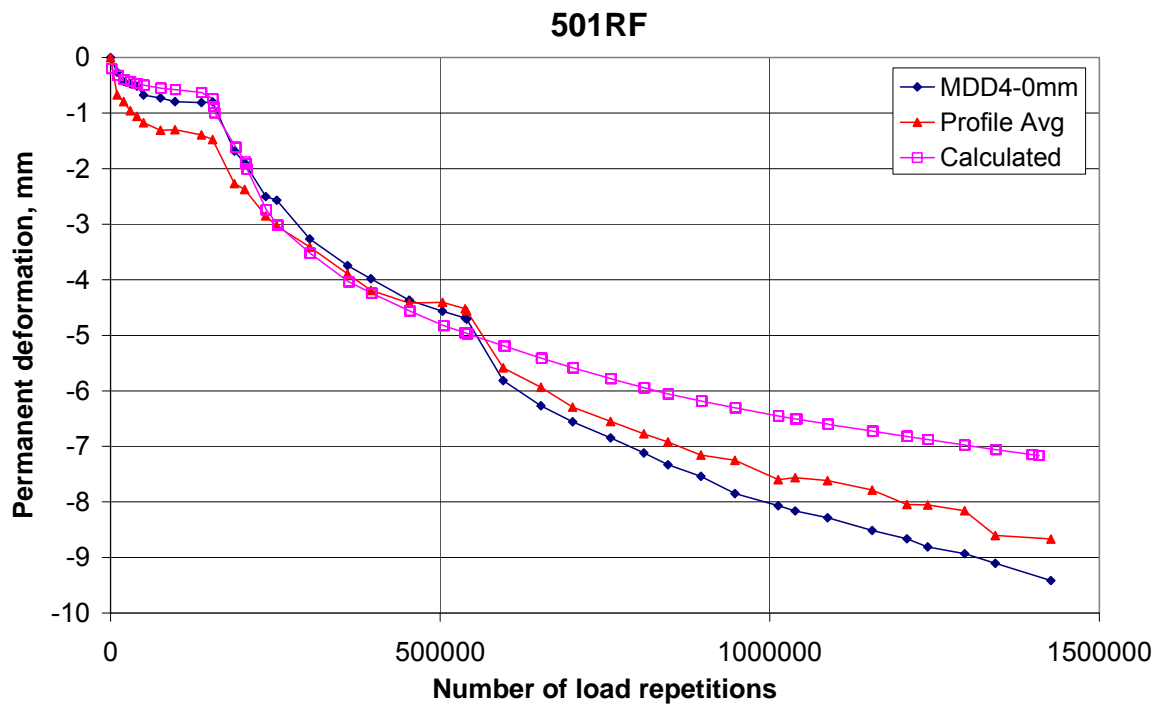


Figure 66. Permanent deformation at pavement surface.

2.3.2 Section 503RF Permanent Deformations

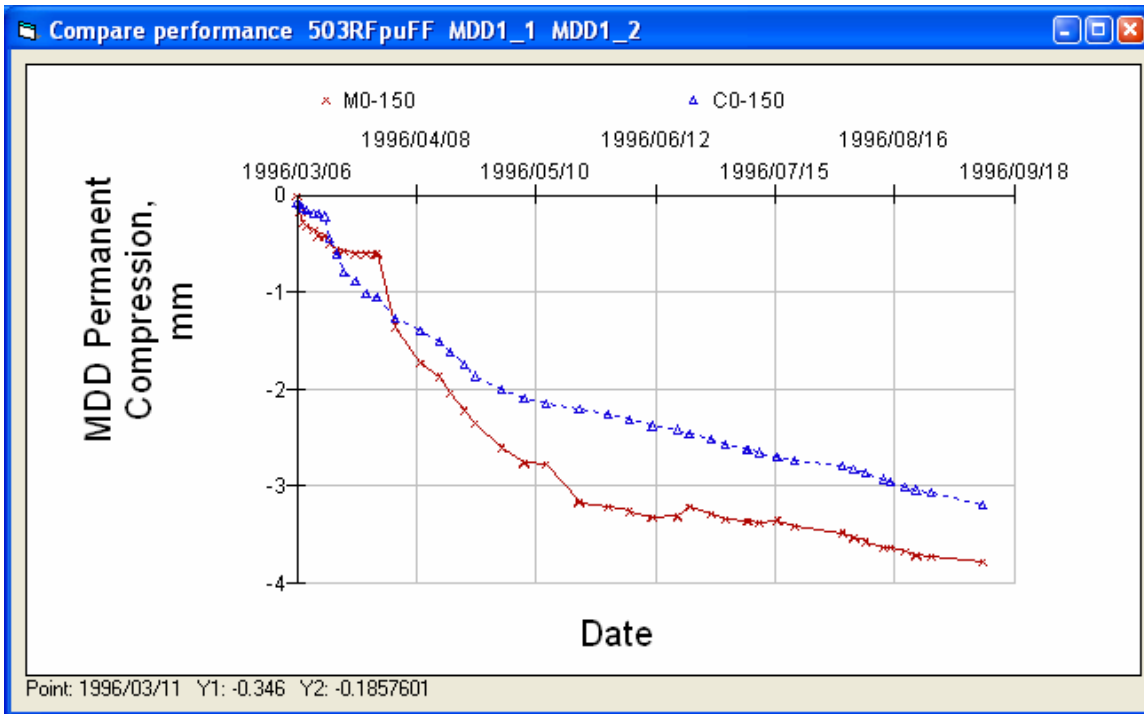


Figure 67. Permanent compression of AC layers.

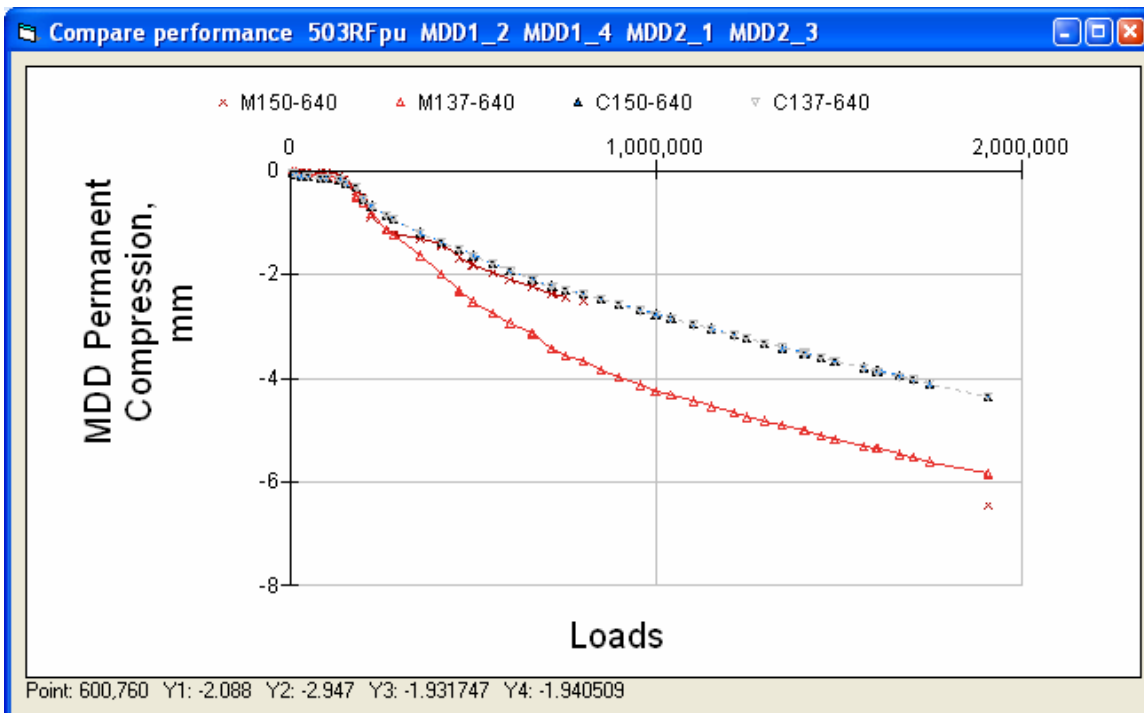


Figure 68. Permanent compression of granular layers.

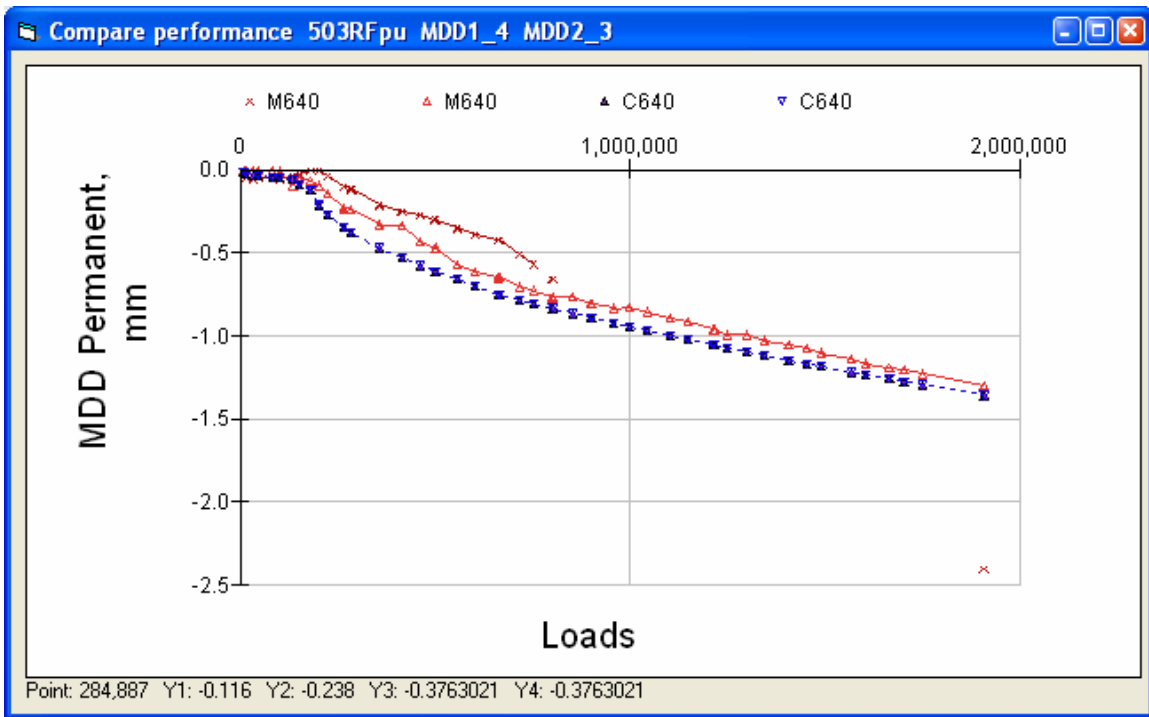


Figure 69. Permanent deformation of subgrade.

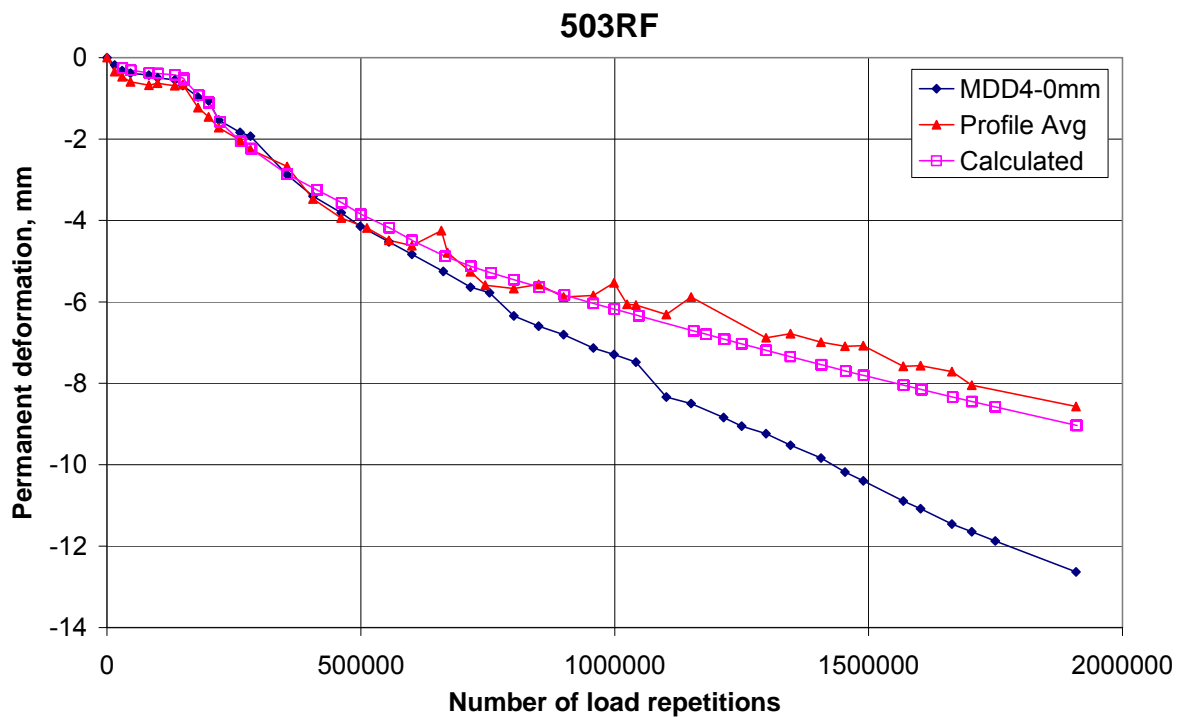


Figure 70. Permanent deformation at pavement surface.

2.3.3 Section 500RF Permanent Deformations

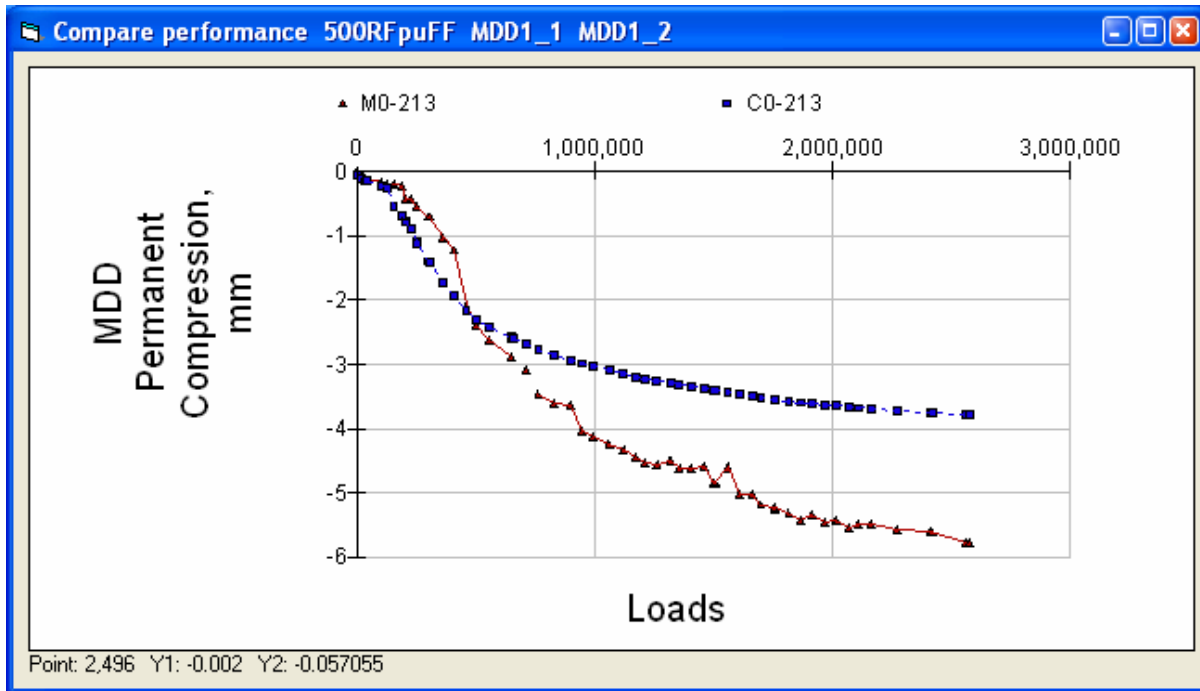


Figure 71. Permanent deformation of the AC layers.

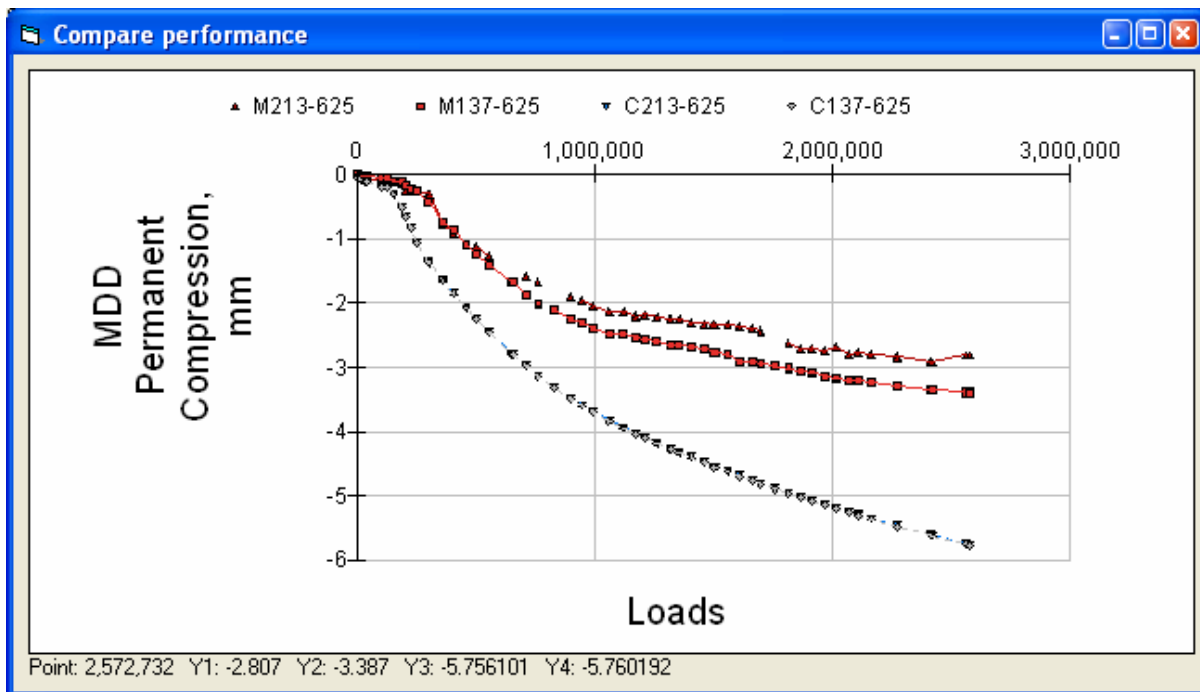


Figure 72. Permanent compression of the granular layers.

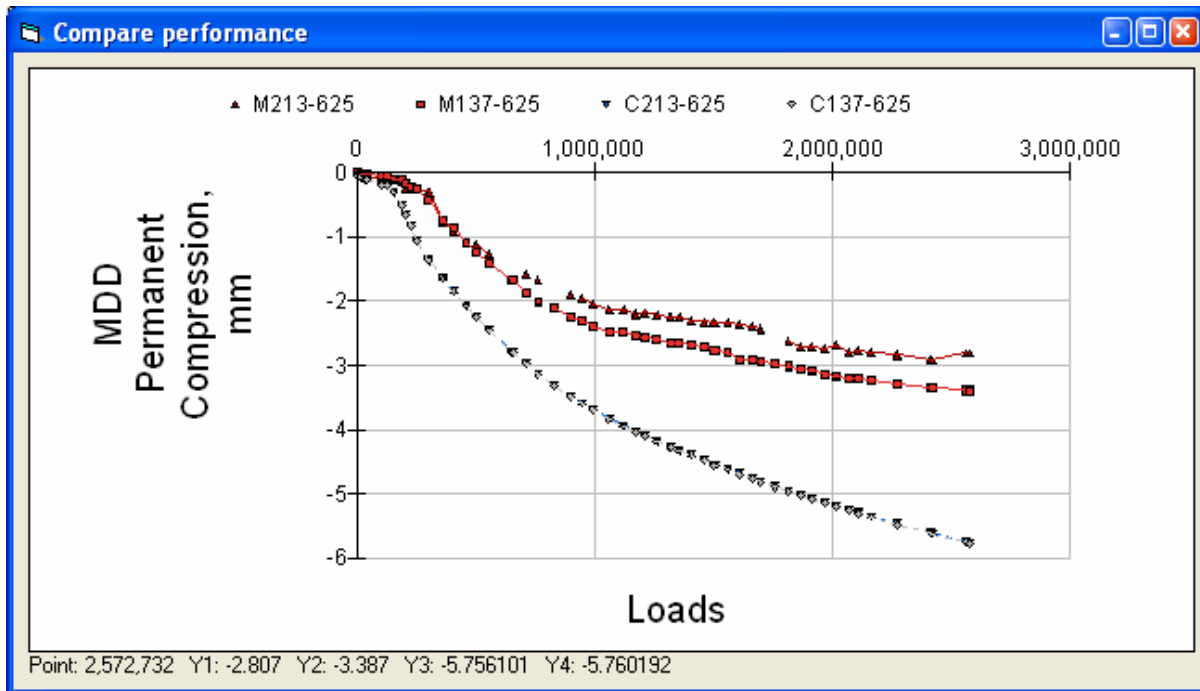


Figure 73. Permanent deformation of the subgrade.

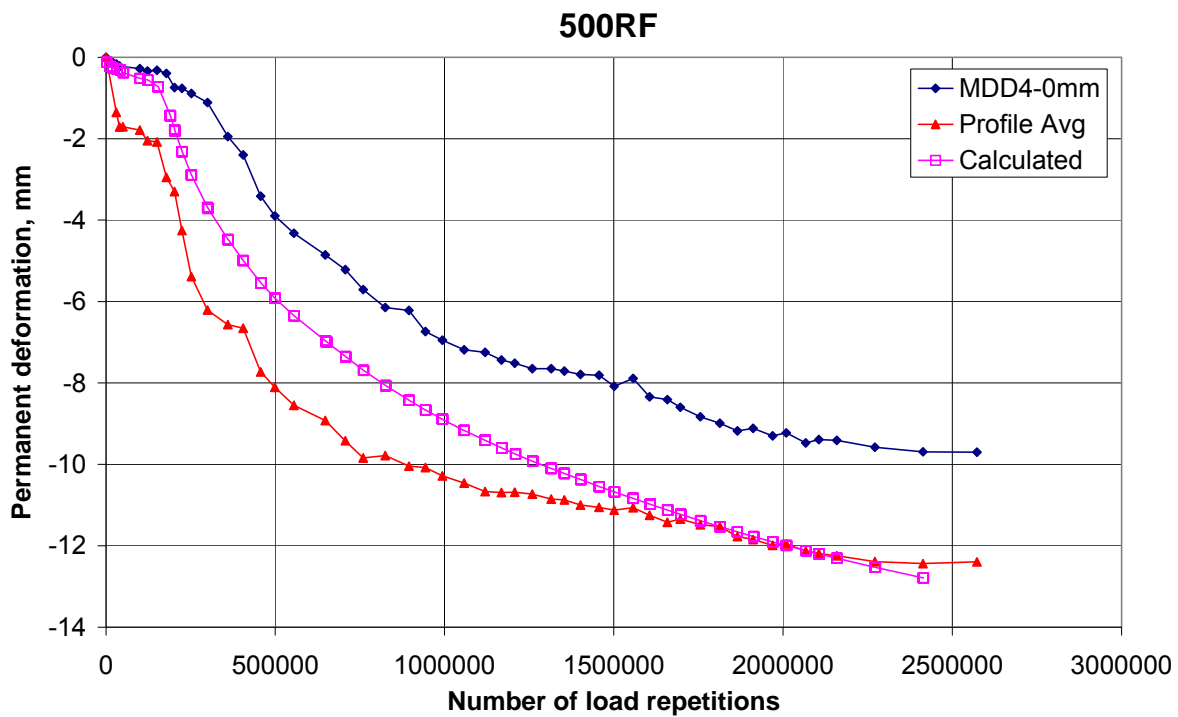


Figure 74. Permanent deformation at pavement surface.

2.3.4 Section 502CT Permanent Deformations

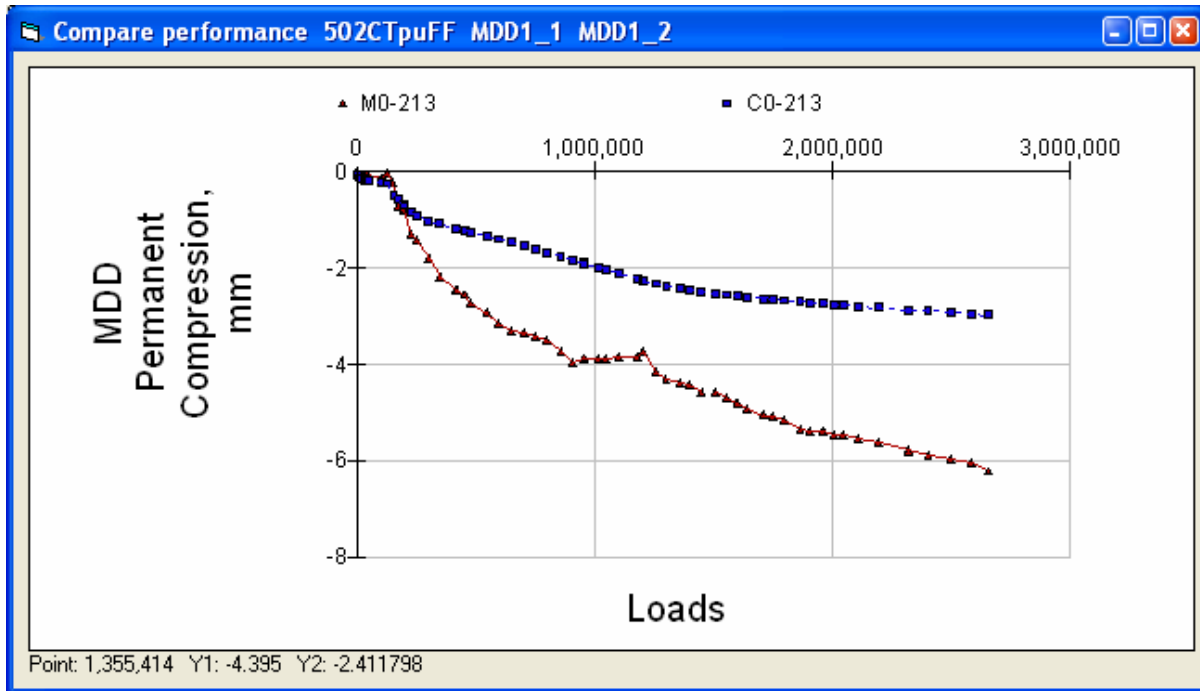


Figure 75. Permanent compression of the AC layers.

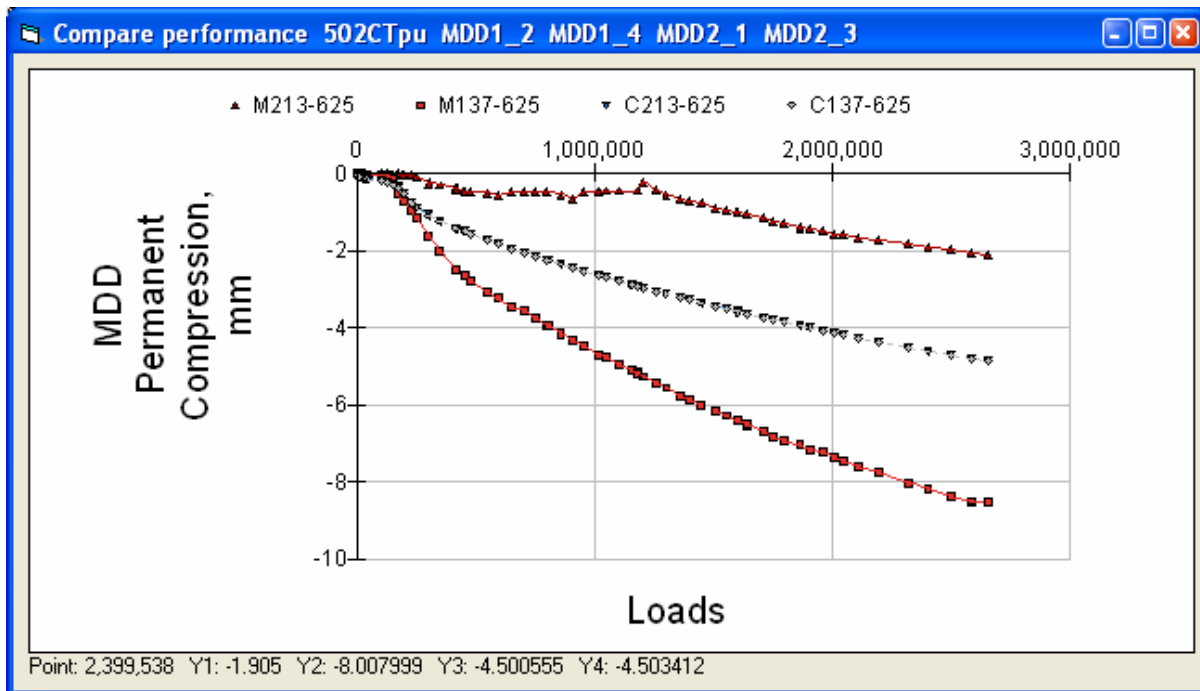


Figure 76. Permanent deformation of granular layers.

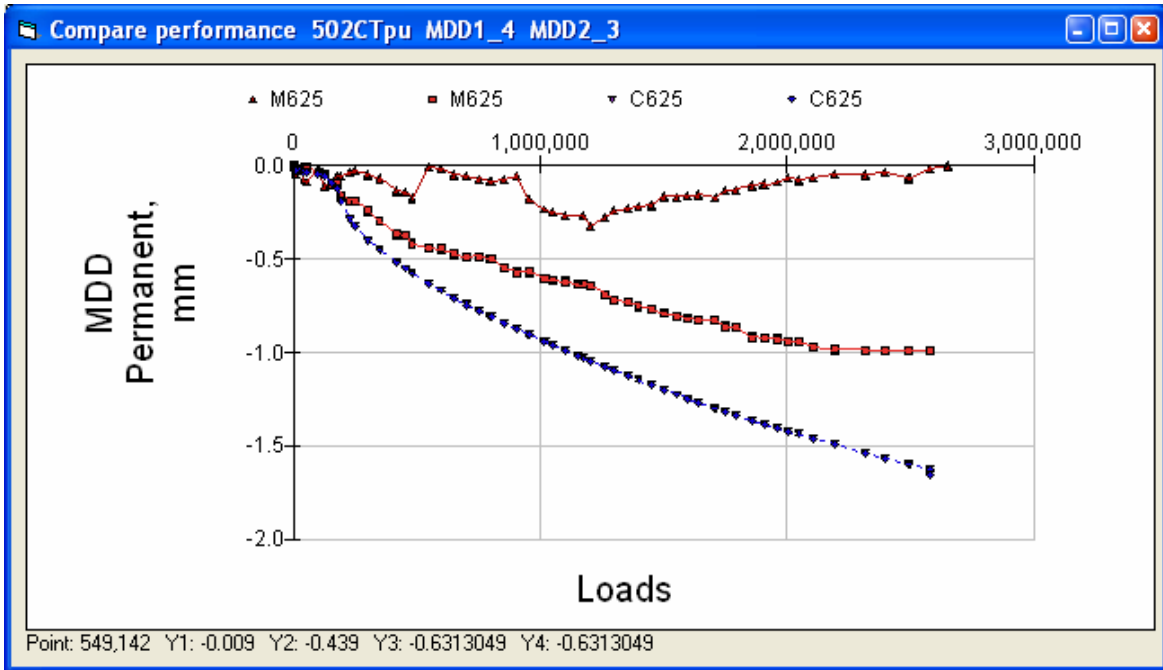


Figure 77. Permanent deformation of subgrade.

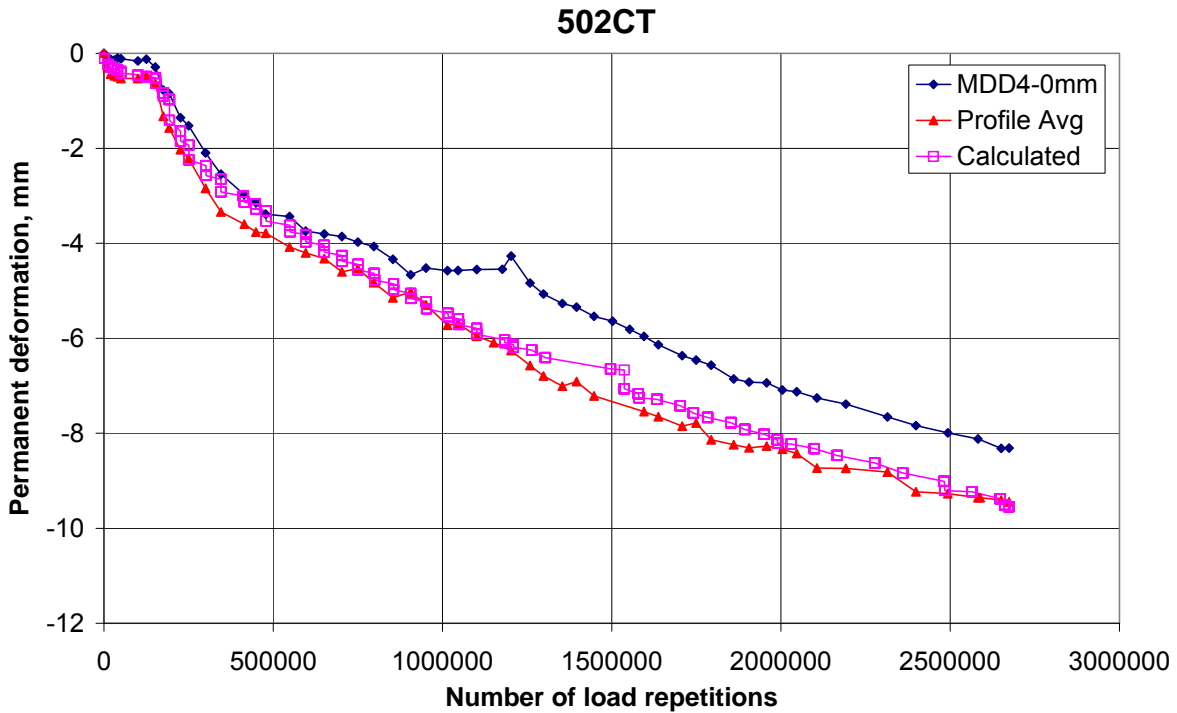


Figure 78. Permanent deformation at surface of pavement.

The permanent deformation from the MDD in Figure 78 is a combination of measurements from the two MDDs, as some of the modules did not function.

3.0 GOAL 3 REFLECTION CRACKING TESTS

The overlays of Goal 3, for the 20°C part of the tests, were placed on sections that had already been tested during Goal 1 (as indicated in Figure 1). At the end of Goal 1 the pavements had surface cracking from 2–10 m/m². The strains in the overlay (over the existing cracks in the top AC layer of Goal 1) were calculated using a method developed by Wu (2005); this was described in Section 1.

A period of time between several months to over a year elapsed between the completion of each of the Goal 1 tests and the start of the Goal 3 tests at the same location, which was now overlaid. In order to achieve reasonably correct initial deflections at the beginning of the Goal 3 tests some “healing” had to be assumed for the asphalt layers. The damage parameter, ω , of the “old” asphalt layers at the start of the loading is given in Table 19 and may be compared to the damage at the end of the initial tests, in Table 18.

Table 19. Initial Damage Parameters for “Old” Asphalt Overlay Sections

Damage	501RF	503RF	500RF	502CT
AC top	0.40	0.40	0.30	0.30
AC bottom	0.35	0.59	0.20	0.20
ATPB			0.20	0.20

The “old” asphalt layers deteriorated rather fast when loading was started. A shift factor of 0.6 was used, corresponding to a rate of deterioration five times higher than for the original materials. Slip between the old AC top and AC bottom was assumed to reappear after 100,000 ESALs (corresponding to 100,000 load repetitions).

For fatigue cracking of the ARHM and DGAC overlays, a shift factor of 3 was used. The same shift factor provided reasonable results for both materials, using their respective laboratory fatigue parameters.

3.1 Resilient Deflections

3.1.1 Section 517RF DGAC on Section 501RF Resilient Deflections

The pavement structure for section 517RF is shown in Figure 79. The first visible cracking was recorded at approximately 900,000 load repetitions.

517RFpu structural data

Design methods Tools Change WIM Parameters

S

mm MPa

Layer	Material	Thick	Modulus	Poisson	R	GF	Cost/m3
1	DGACVHVS3g	75	7653	0.35	0	1.46	114
2	DGACVHVS1T3g	63	1968	0.35	0	1.46	114
3	DGACVHVS1B3g	84	2733	0.35	0	1.46	114
4	ABHVS	274	162	0.35	78	1.1	57
5	AS2HVS	215	177	0.35	50	1	30
6	ClayHVS	0	113	0.35	20	0	0

Figure 79. Section 517RF pavement structure.

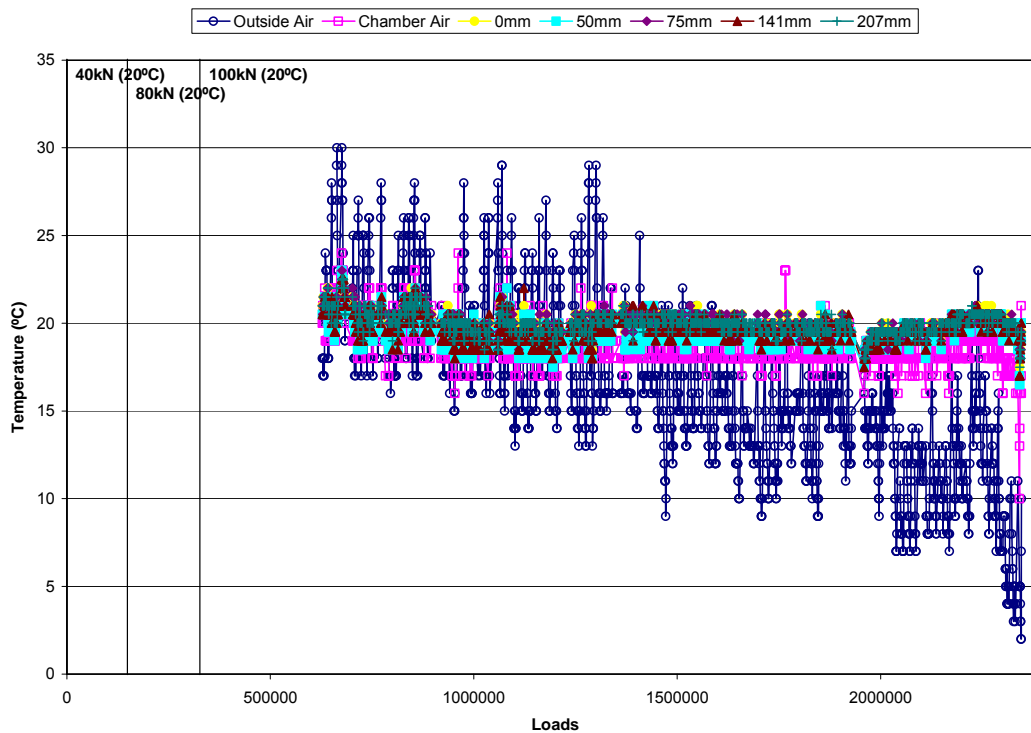


Figure 80. Section 517RF AC temperature during testing.



Figure 81. Section 517RF 40 kN deflection of top modules.



Figure 82. Section 517RF 40 kN compression of pavement layers.

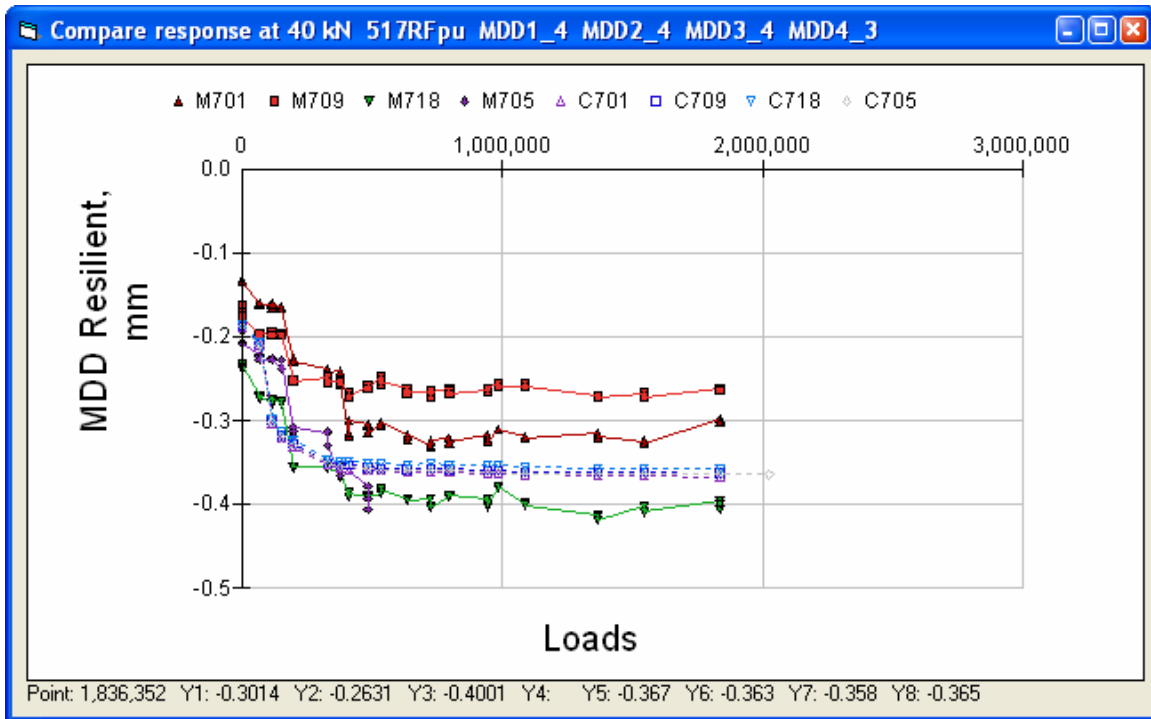


Figure 83. Section 517RF deflection of subgrade.

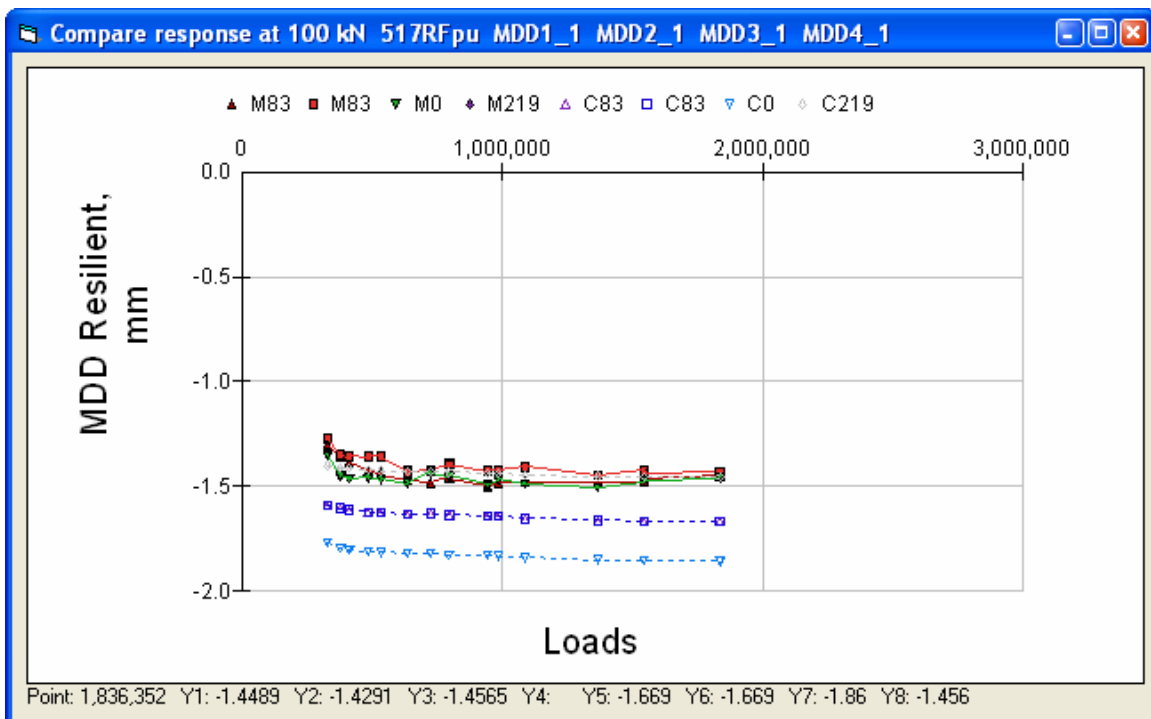


Figure 84. Section 517RF 100 kN top modules deflection.

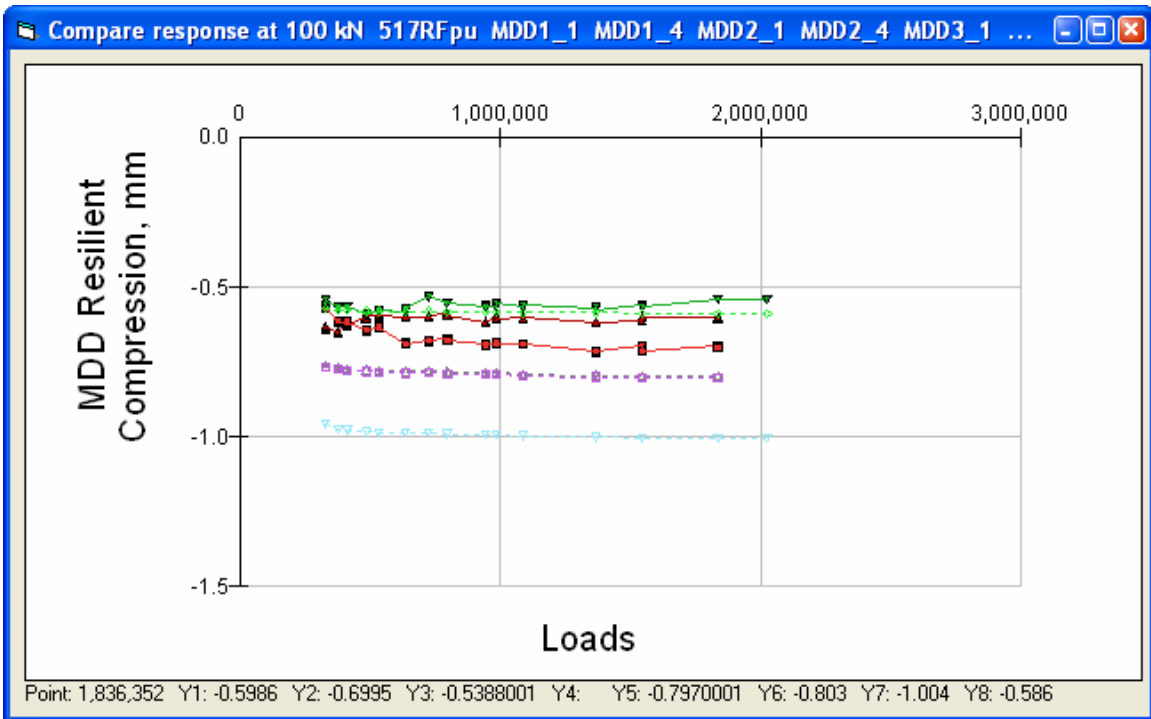


Figure 85. Section 517RF 100 kN compression of pavement layers.

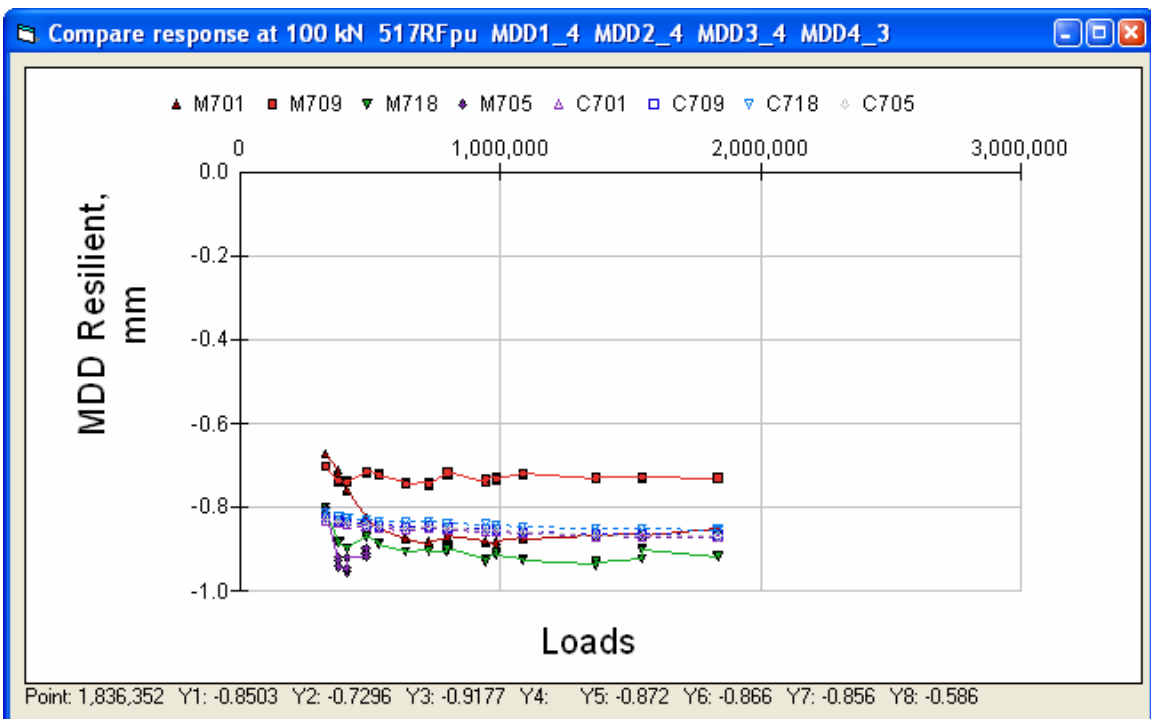


Figure 86. Section 517RF 100 kN deflection of subgrade.

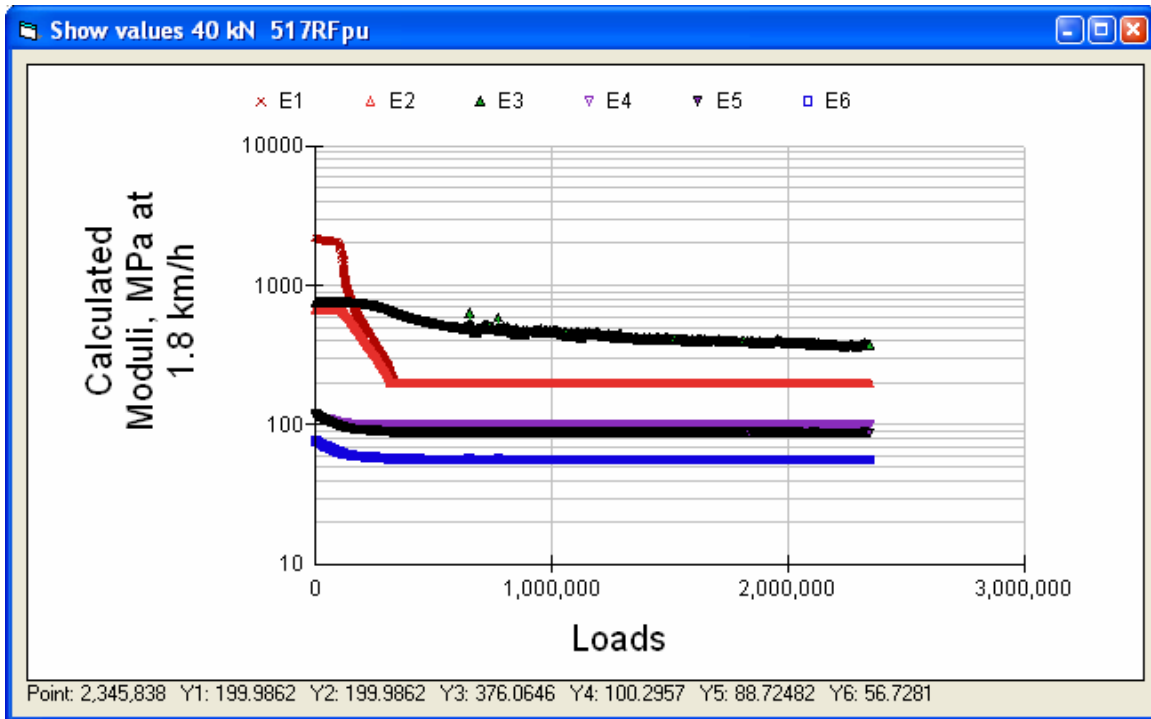


Figure 87. Section 517RF calculated moduli at 40 kN and actual temperature.

3.1.2 Section 518RF ARHM on Section 503RF Resilient Deflections

The pavement structure for Section 518RF is shown in Figure 88. The first visible cracking was recorded at approximately 650,000 load repetitions.

Layer	Material	Thick (mm)	Modulus (MPa)	Poisson	R	GF	Cost/m3
1	RAC-GHVSg	38	4755	0.35	0	1.46	134
2	DGACVHVSG1T3g	74	1968	0.35	0	1.46	114
3	DGACVHVSG1B3g	88	2733	0.35	0	1.46	114
4	ABHVS	274	133	0.35	78	1.1	57
5	AS2HVS	305	140	0.35	50	1	30
6	ClayHVS	0	102	0.35	20	0	0

Figure 88. Section 518RF pavement structure.

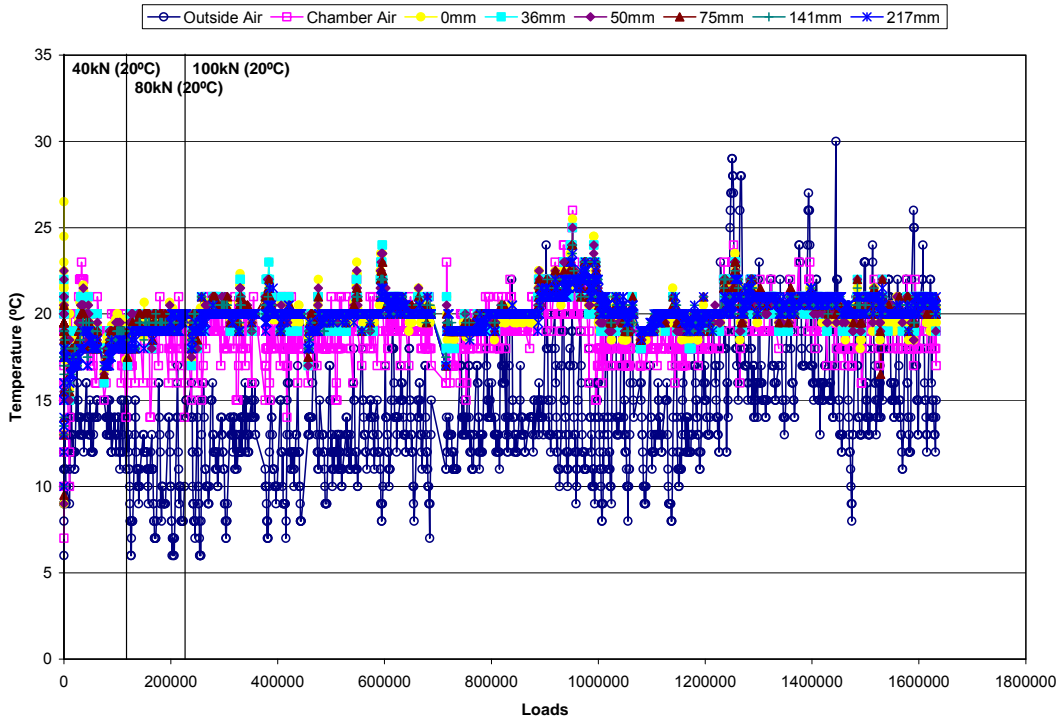


Figure 89. Section 518RF AC temperature during testing.

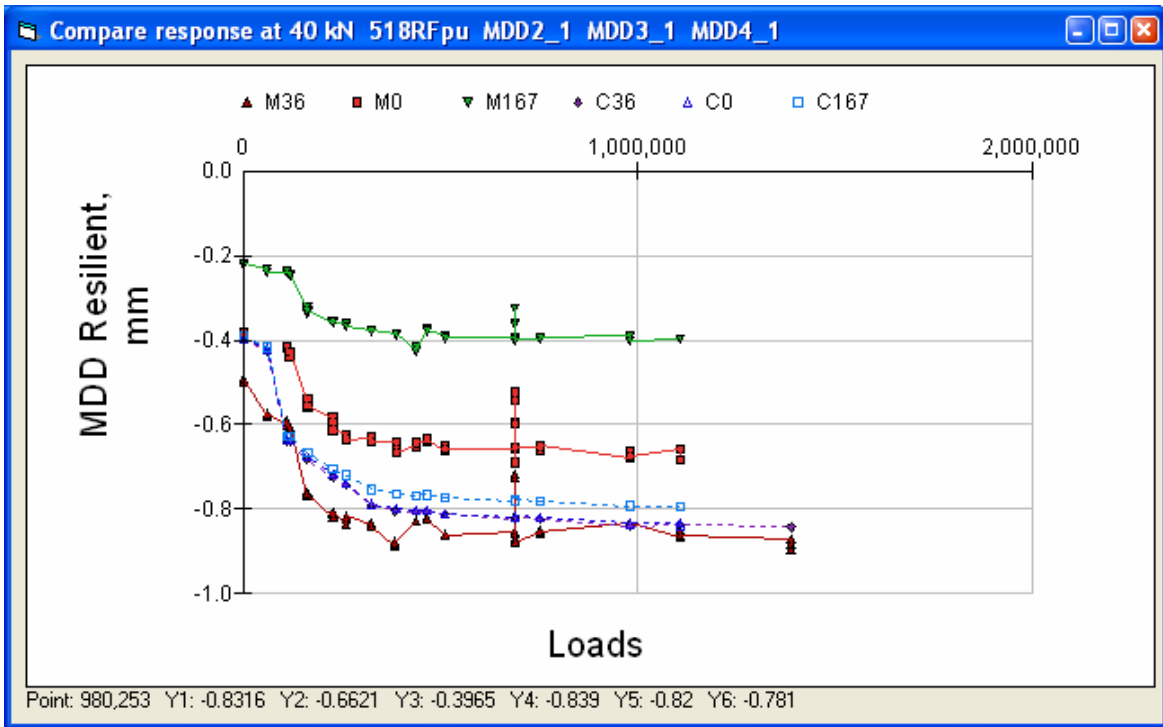


Figure 90. Section 518RF 40 kN top modules deflection.

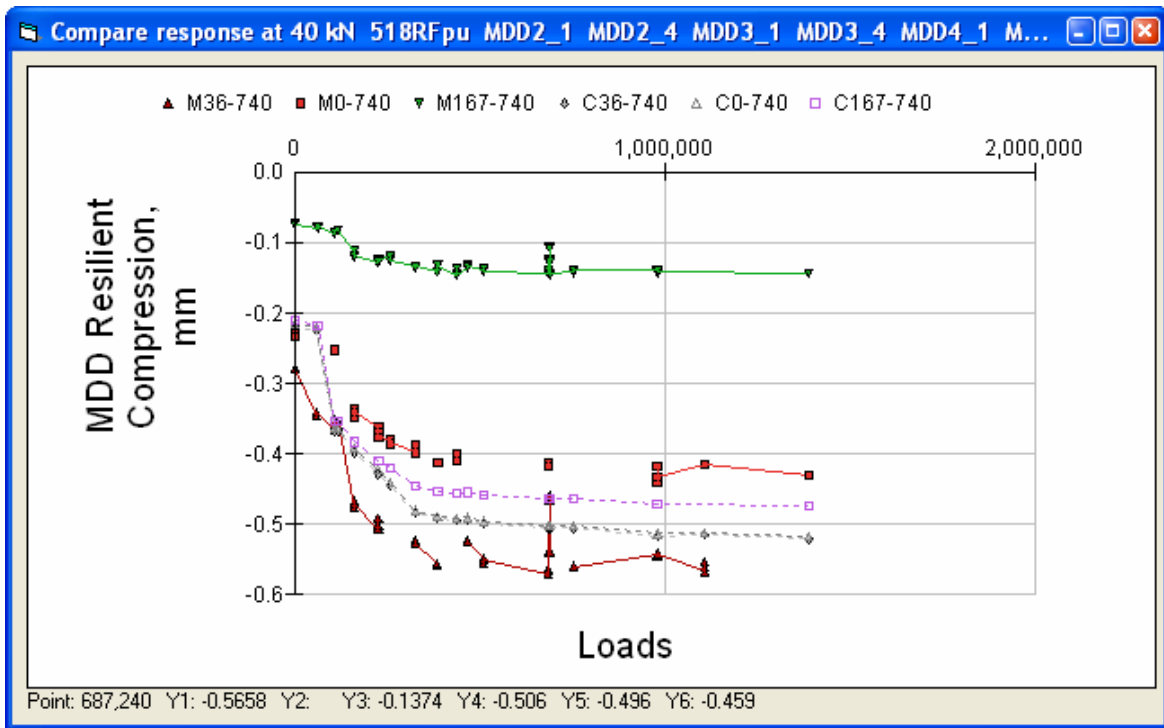


Figure 91. Section 518RF 40 kN resilient compression of pavement layers.

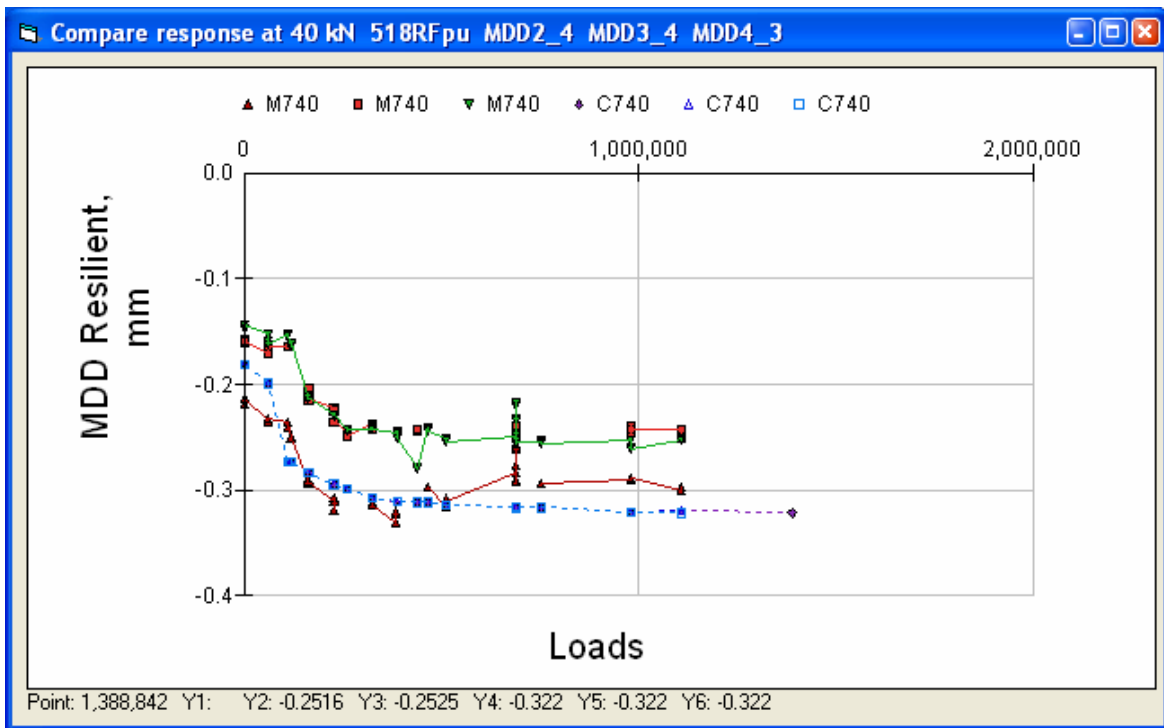


Figure 92. Section 518RF 40 kN deflection of subgrade.

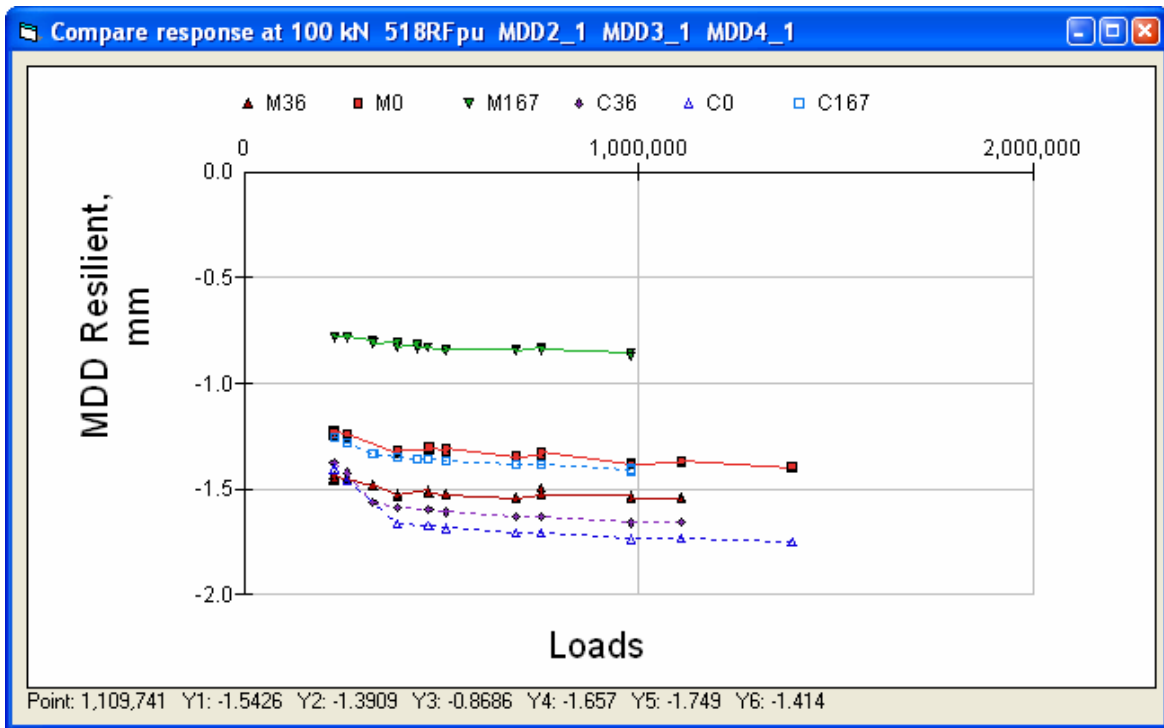


Figure 93. Section 518RF 100 kN top modules deflection.

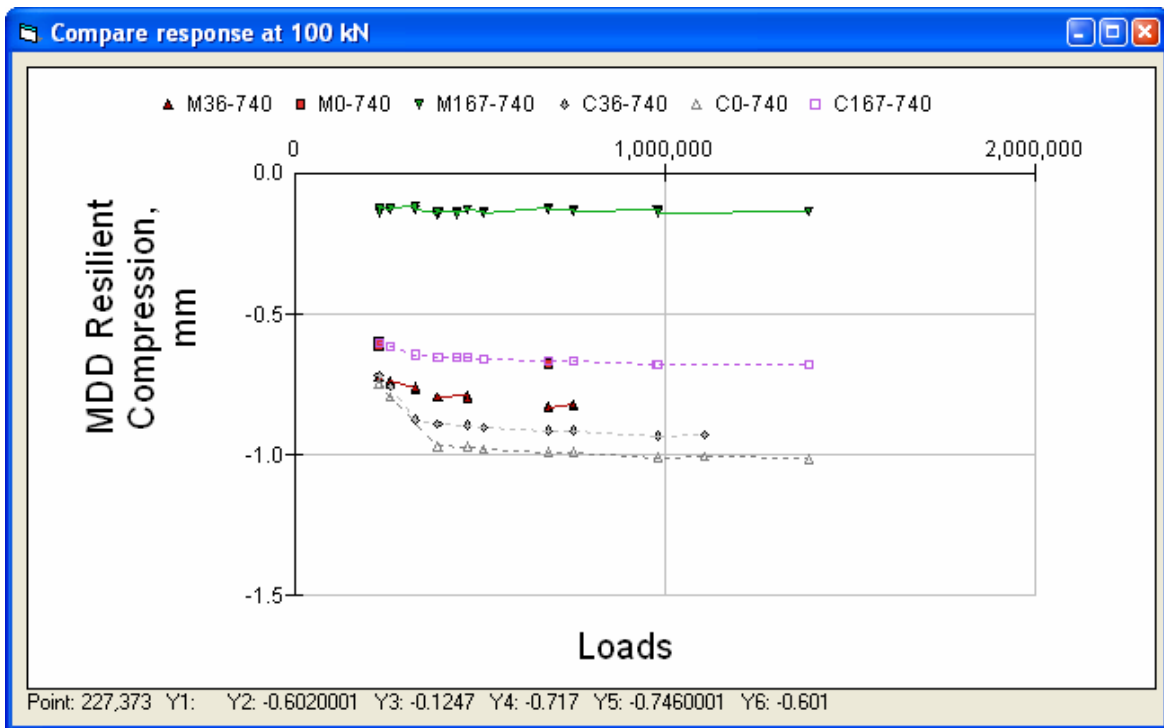


Figure 94. Section 518RF 100 kN compression of pavement layers.

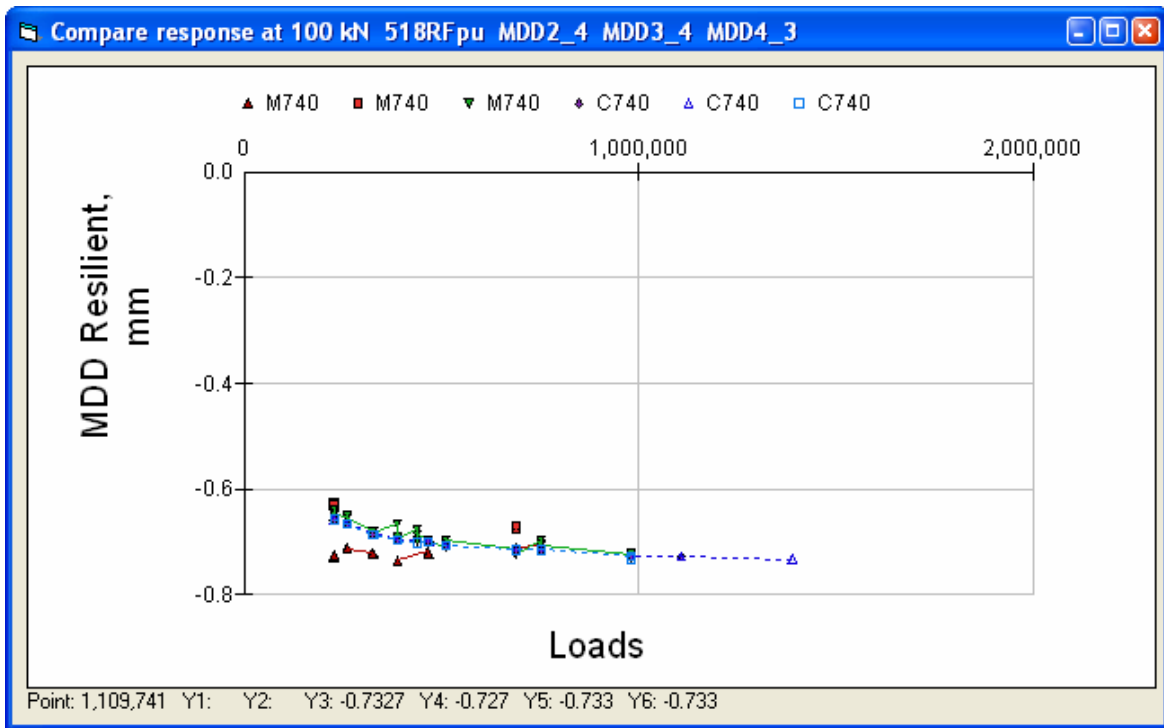


Figure 95. Section 518RF 100 kN deflection of subgrade.

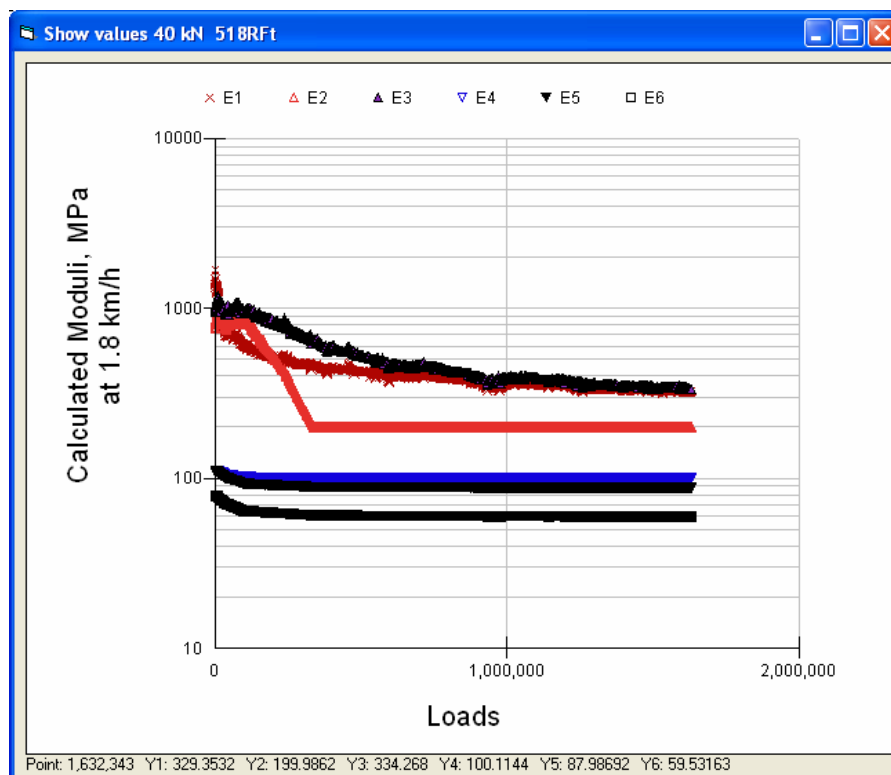


Figure 96. Section 518RF calculated moduli at 40 kN and actual temperature.

3.1.3 Section 514RF DGAC on Section 500RF Resilient Deflections

The pavement structure for Section 514RF is shown in Figure 97. The first visible cracking was recorded at approximately 800,000 load repetitions.

Layer	Material	Thick	Modulus	Poisson	R	GF	Cost/m3
1	DGACVHVSG3g	75	7653	0.35	0	1.46	114
2	DGACVHVSG1T3g	74	2881	0.35	0	1.46	114
3	DGACVHVSG1B3g	76	4997	0.35	0	1.46	114
4	ATPB-ACHVS3	75	807.0	0.35	0	1.4	82
5	ABHVS	182	242	0.35	78	1.1	57
6	AS2HVS	137	227	0.35	50	1	30
7	ClayHVS	0	125	0.35	20	0	0

Figure 97. Section 514RF pavement structure.

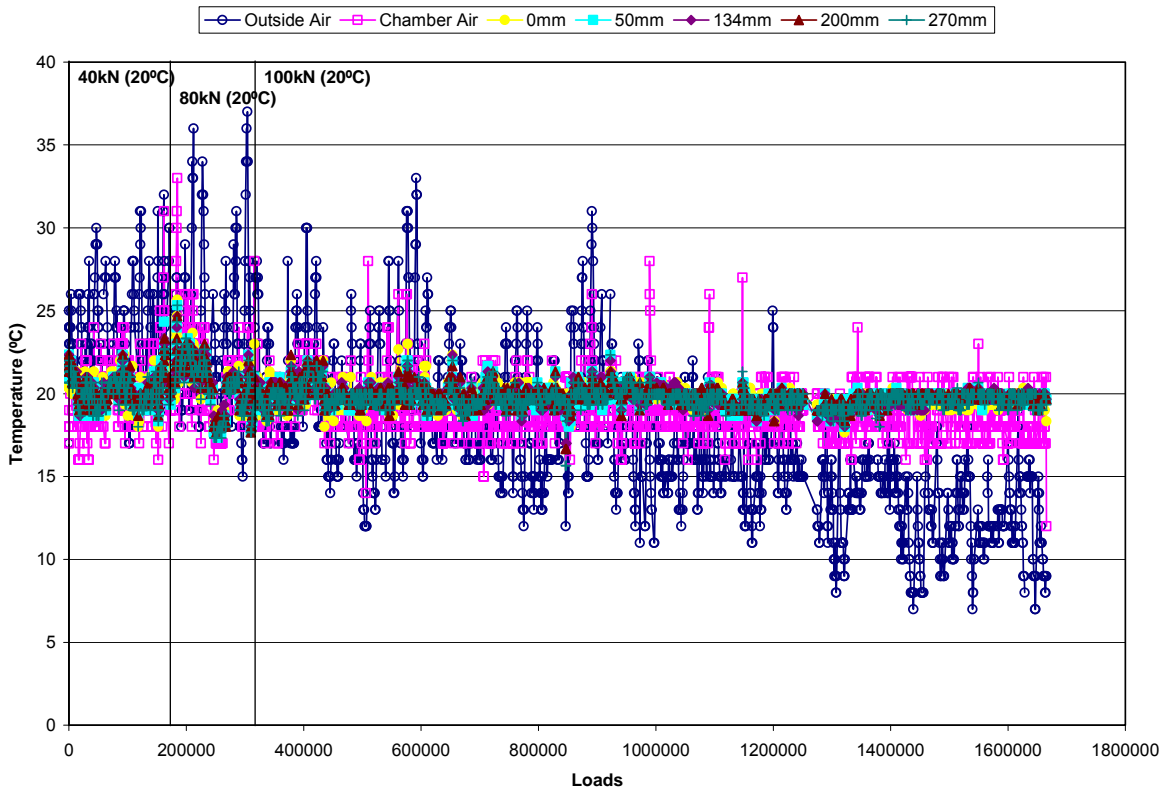


Figure 98. Section 514RF AC temperature during testing.

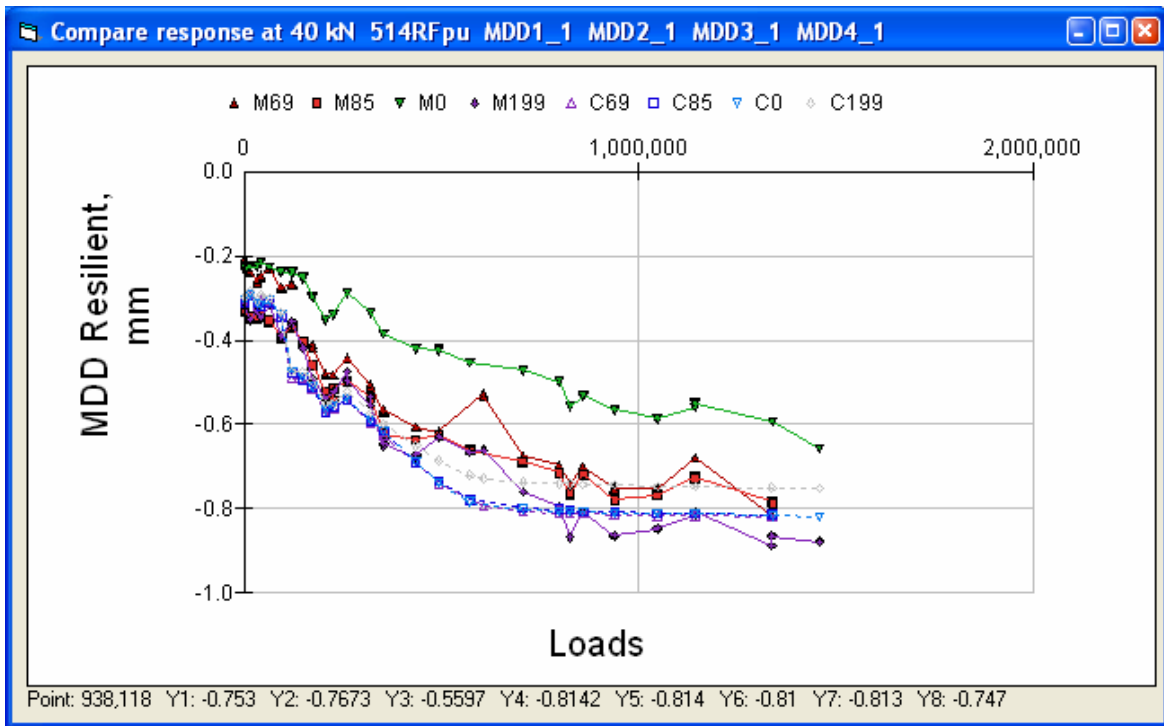


Figure 99. Section 514RF 40 kN top modules deflection.

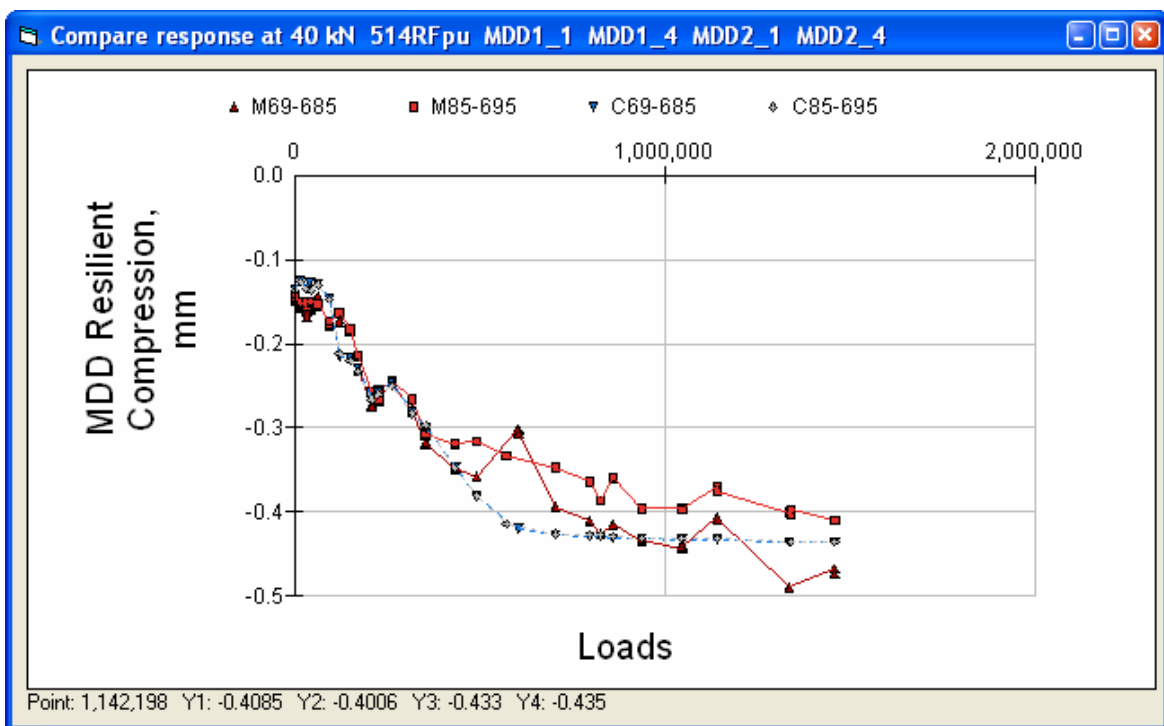


Figure 100. Section 514RF 40 kN compression of pavement layers, MDD1 and MDD2.

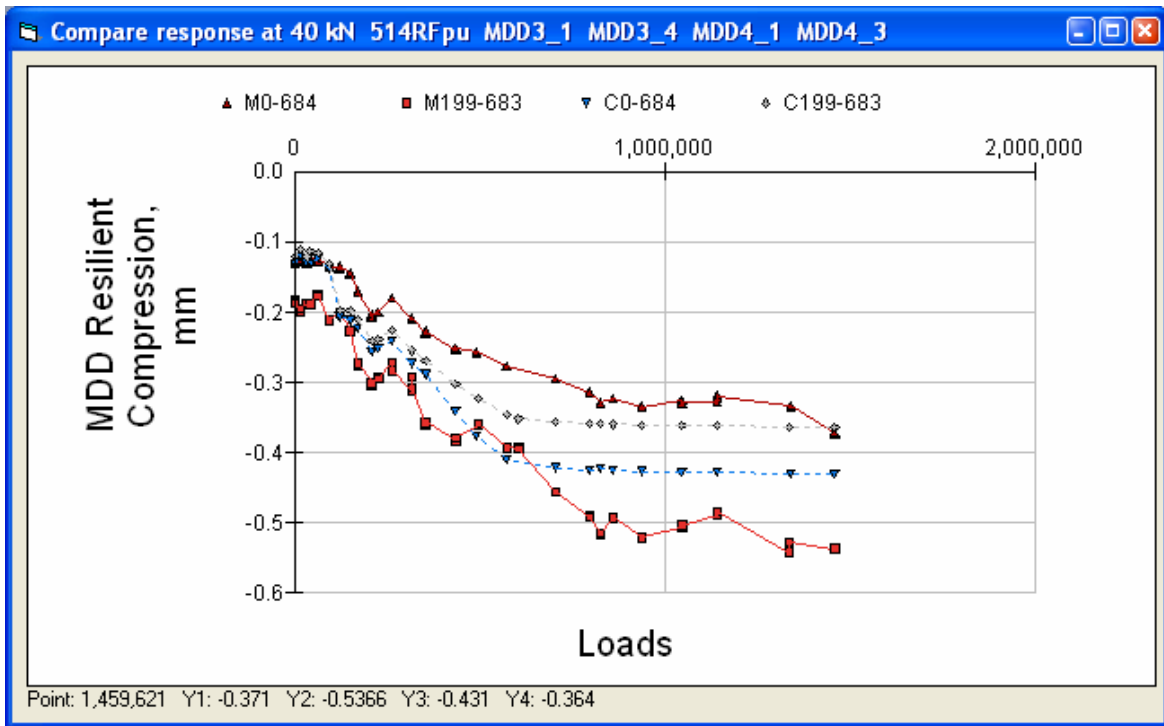


Figure 101. Section 514RF 40 kN compression of pavement layers, MDD3 and MDD4.

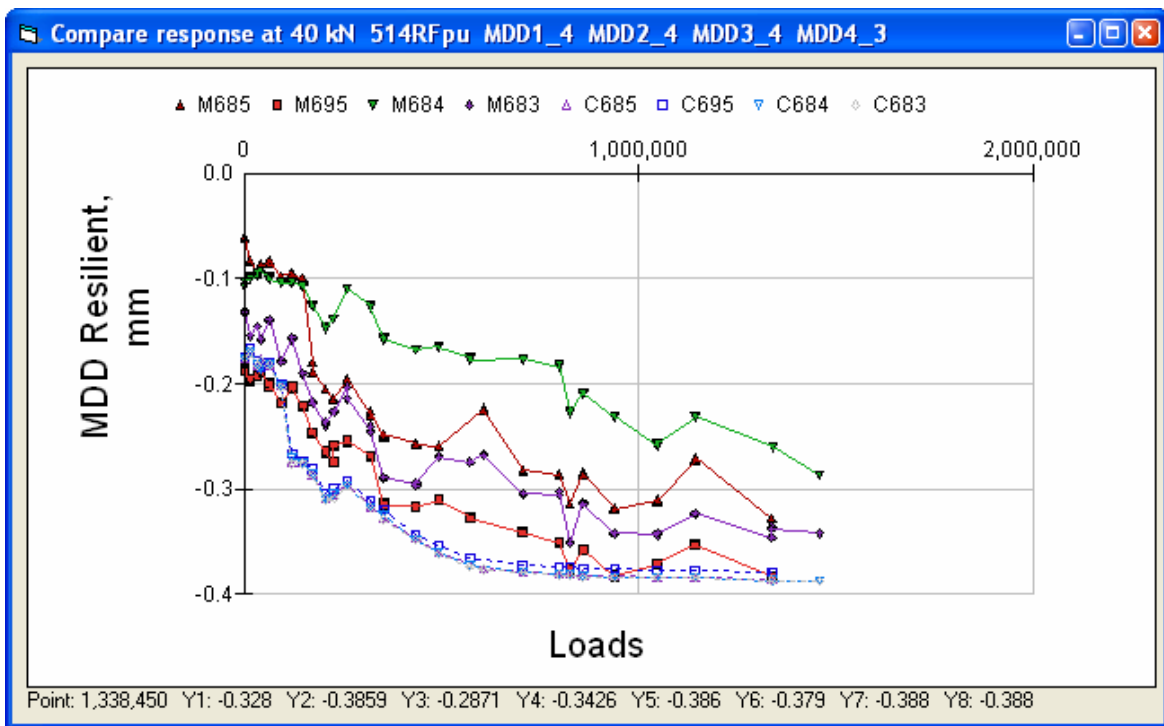


Figure 102. Section 514RF 40 kN deflection of subgrade.

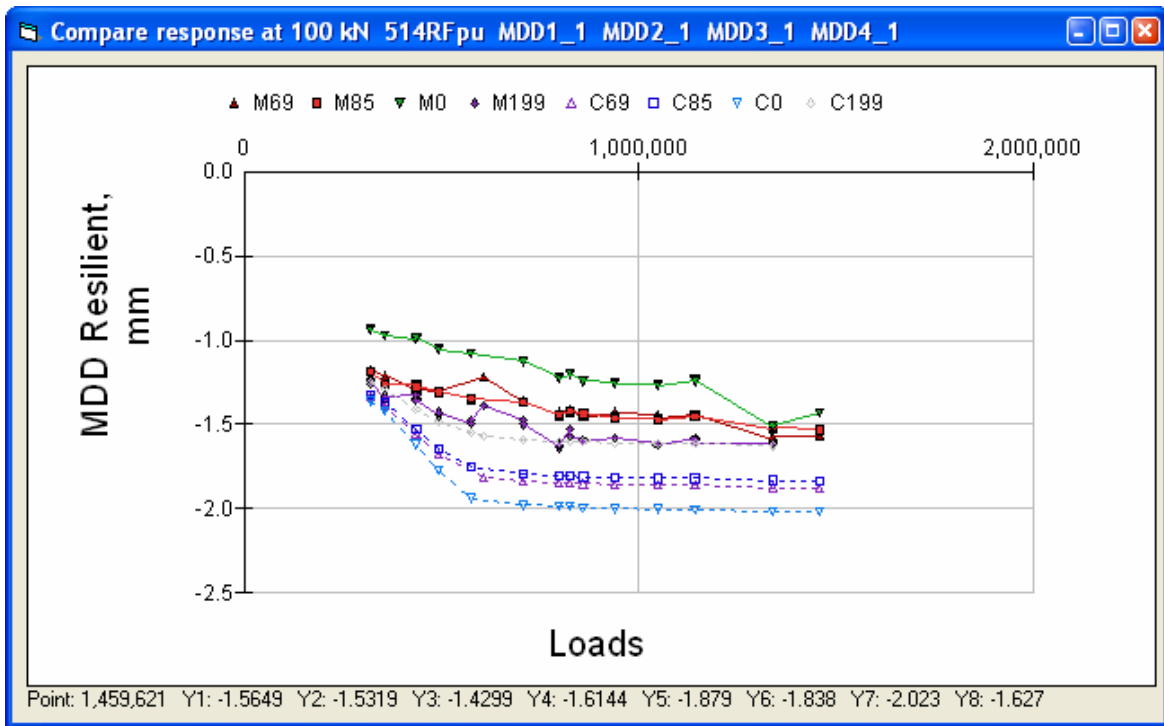


Figure 103. Section 514RF 100 kN top modules deflection.

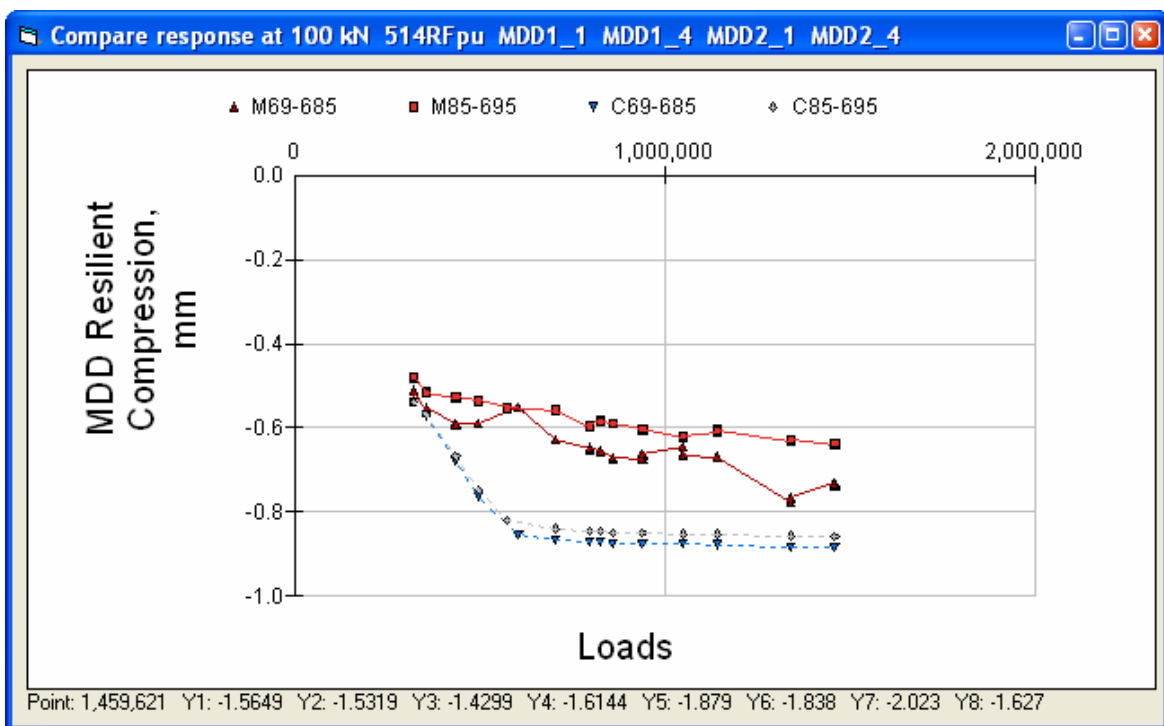


Figure 104. Section 514RF 100 kN compression of pavement layers, MDD1 and MDD2.

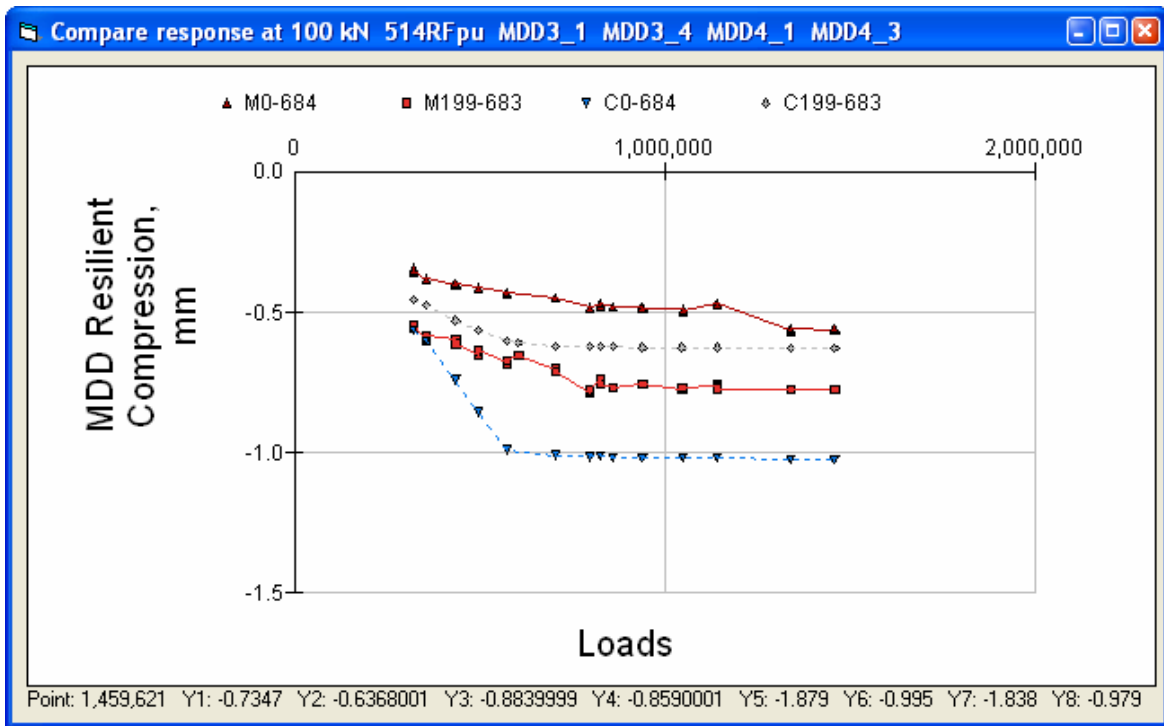


Figure 105. Section 514RF 100 kN compression of pavement layers, MDD3 and MDD4.

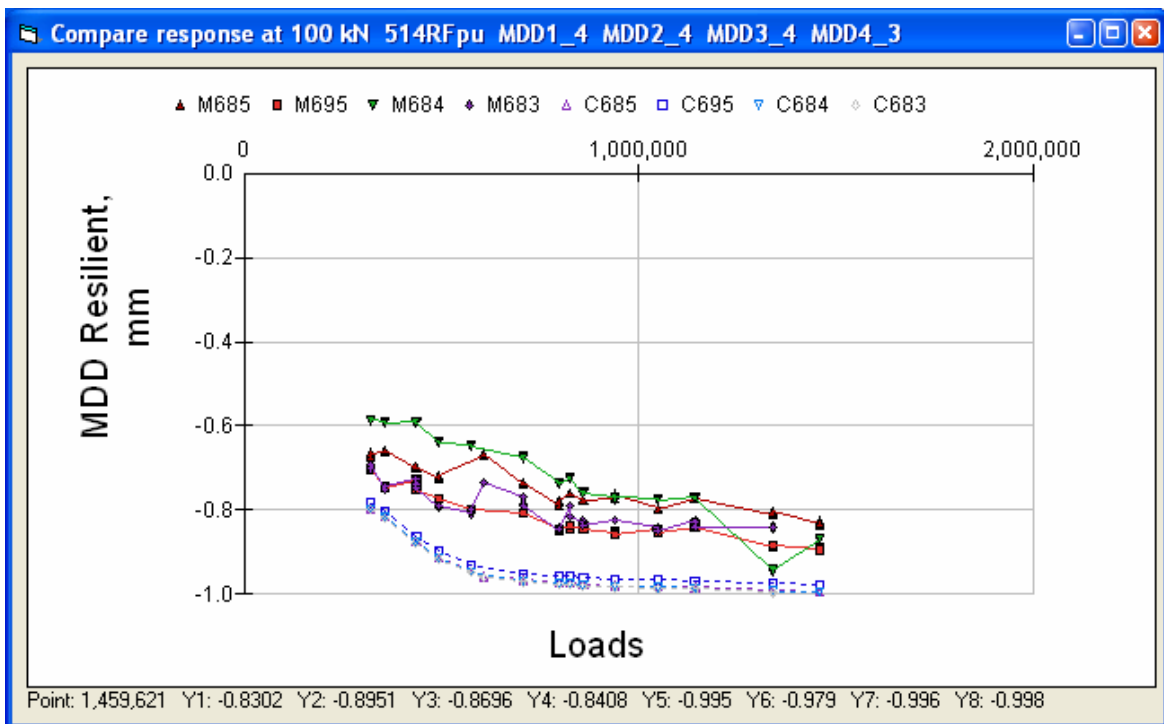


Figure 106. Section 514RF 100 kN deflection of subgrade.

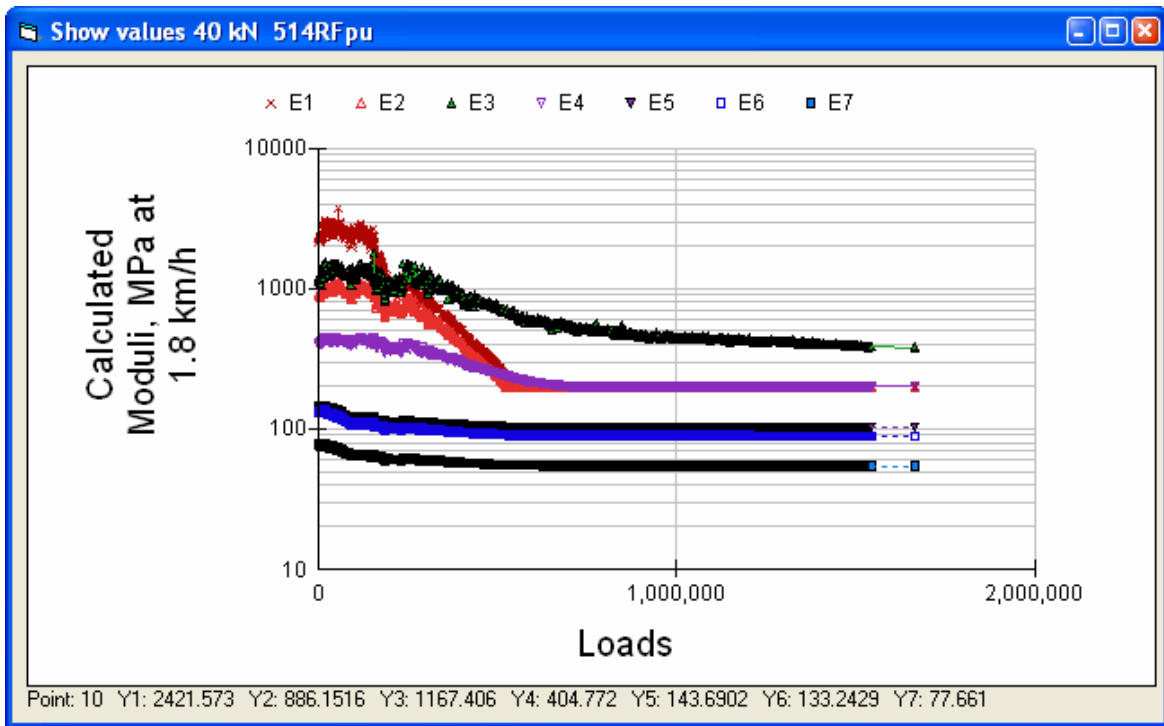


Figure 107. Section 514RF calculated moduli at 40 kN and actual temperature.

3.1.4 Section 515RF ARHM on Section 502CT Resilient Deflections

The pavement structure for Section 515RF is shown in Figure 108. The first visible cracking was recorded at approximately 510,000 load repetitions.

Layer	Material	Thick (mm)	Modulus (MPa)	Poisson	R	GF	Cost/m3
1	RAC-GHVSg	38	4755	0.35	0	1.46	134
2	DGACVHVSG1T3g	68	2881	0.35	0	1.46	114
3	DGACVHVSG1B3g	80	4997	0.35	0	1.46	114
4	ATPB-ACHVS3	75	807	0.35	0	1.4	82
5	ABHVS	182	175	0.35	78	1.1	57
6	AS2HVS	215	164	0.35	50	1	30
7	ClayHVS	0	178	0.35	20	0	0

Figure 108. Section 515RF pavement structure.

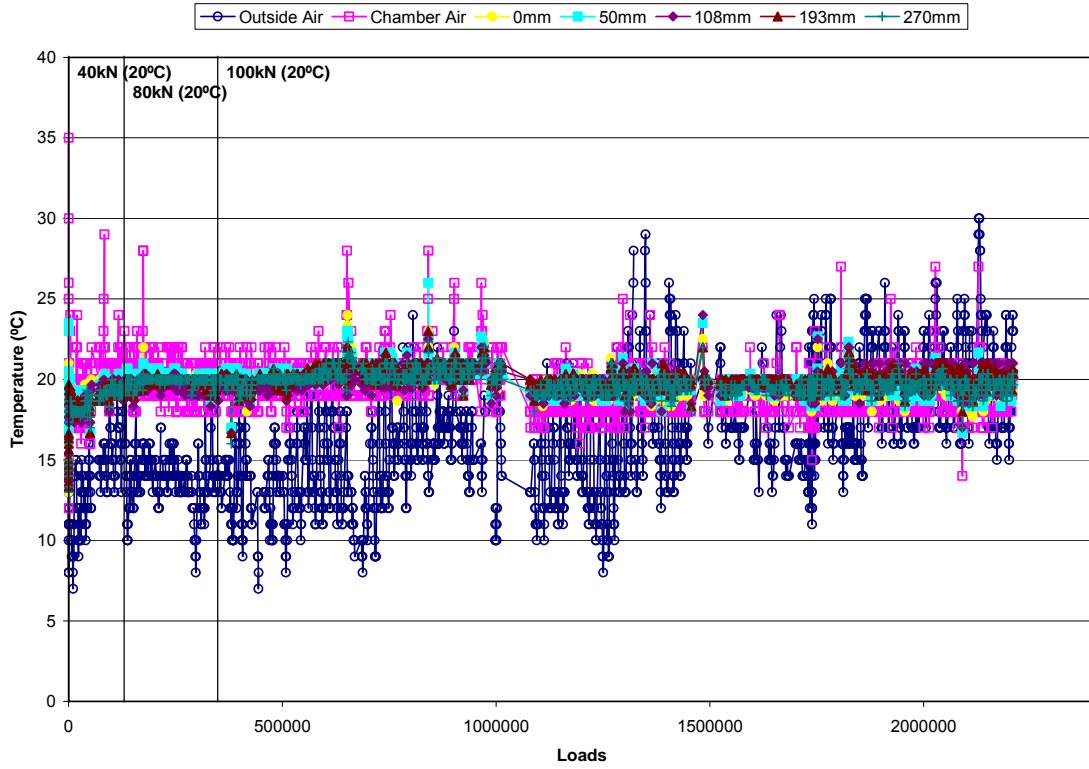


Figure 109. Section 515RF AC temperature during testing.

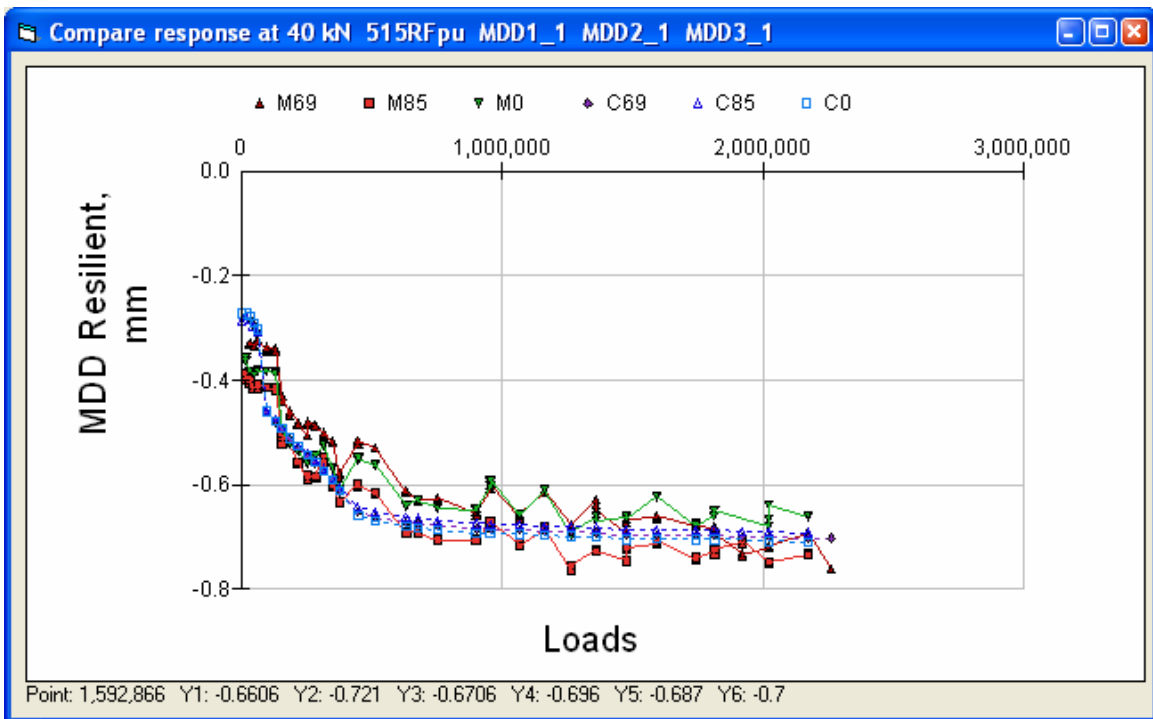


Figure 110. Section 515RF 40 kN top modules deflection.

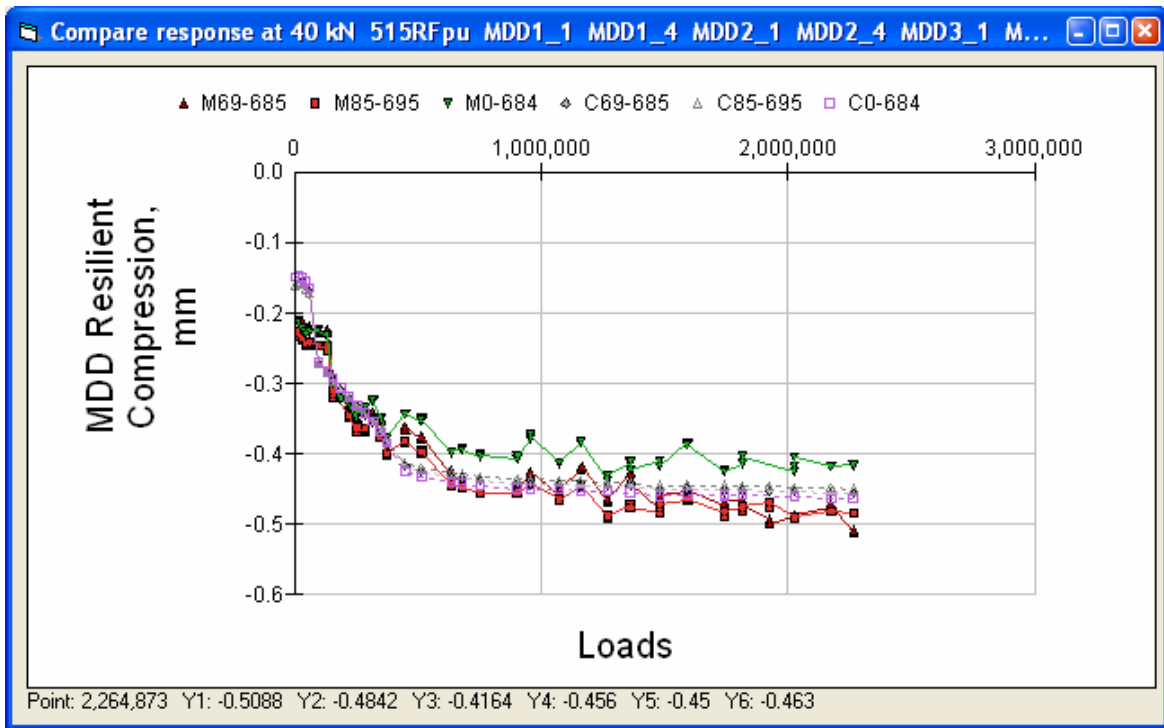


Figure 111. Section 515RF 40 kN resilient compression of pavement layers.

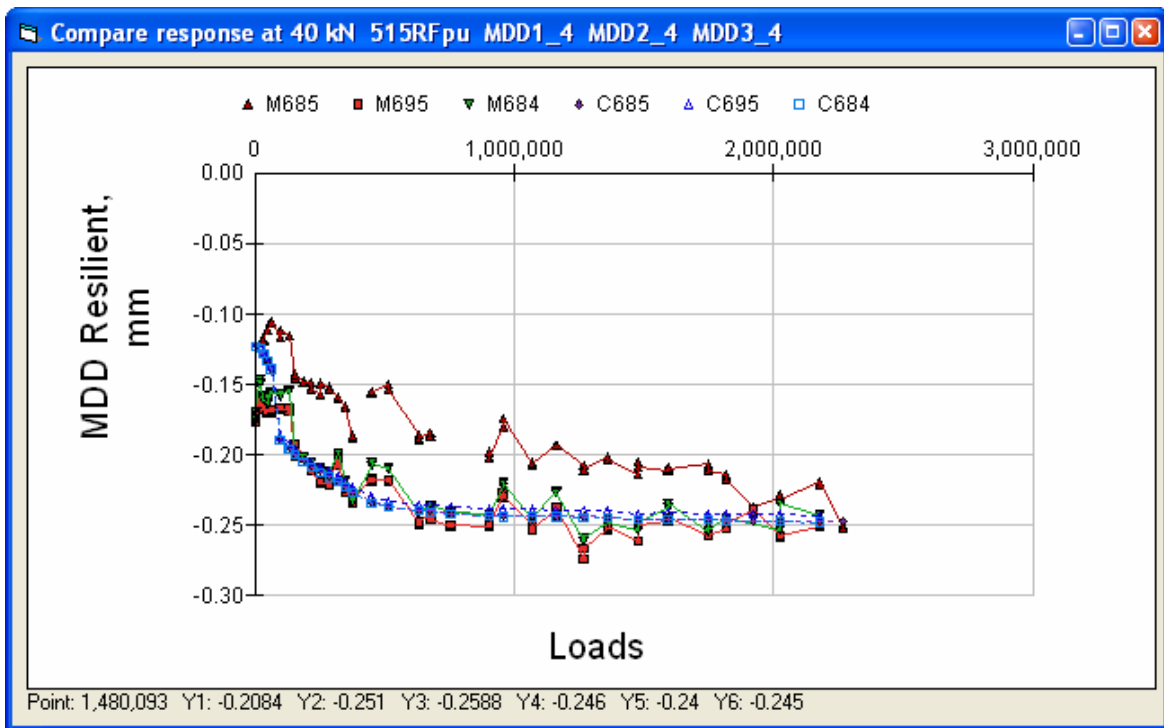


Figure 112. Section 515RF 40 kN deflection of subgrade.

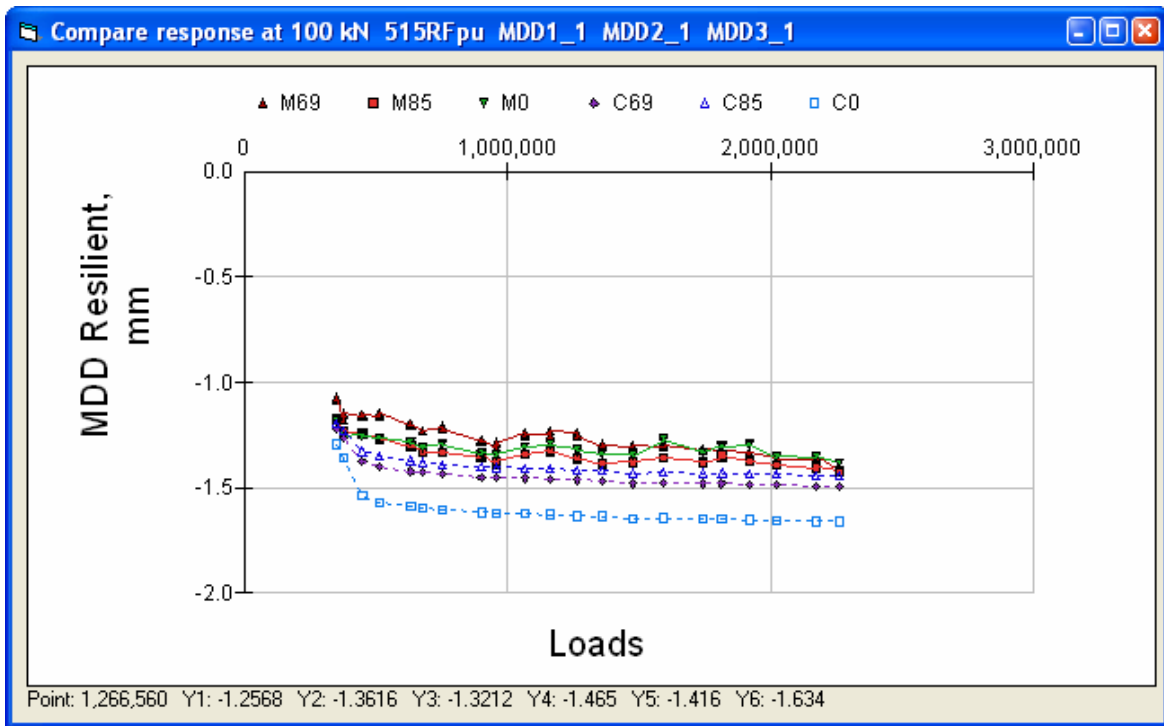


Figure 113. Section 515RF 100 kN top modules deflection.

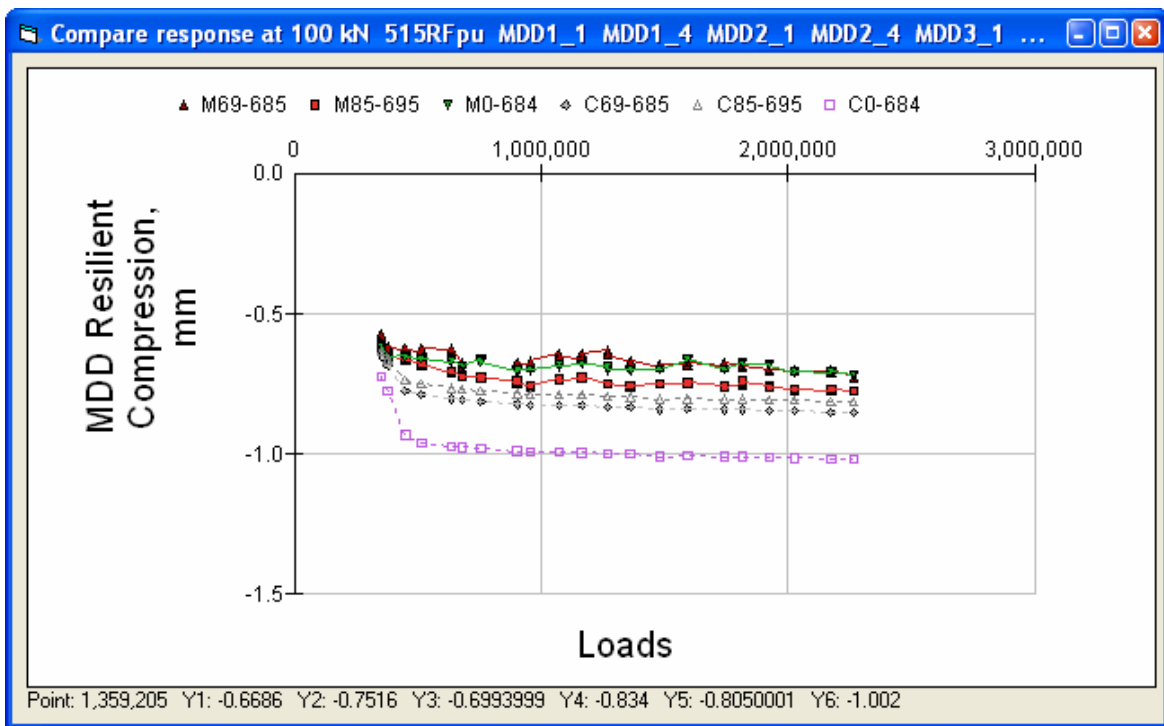


Figure 114. Section 515RF 100 kN compression of pavement layers.

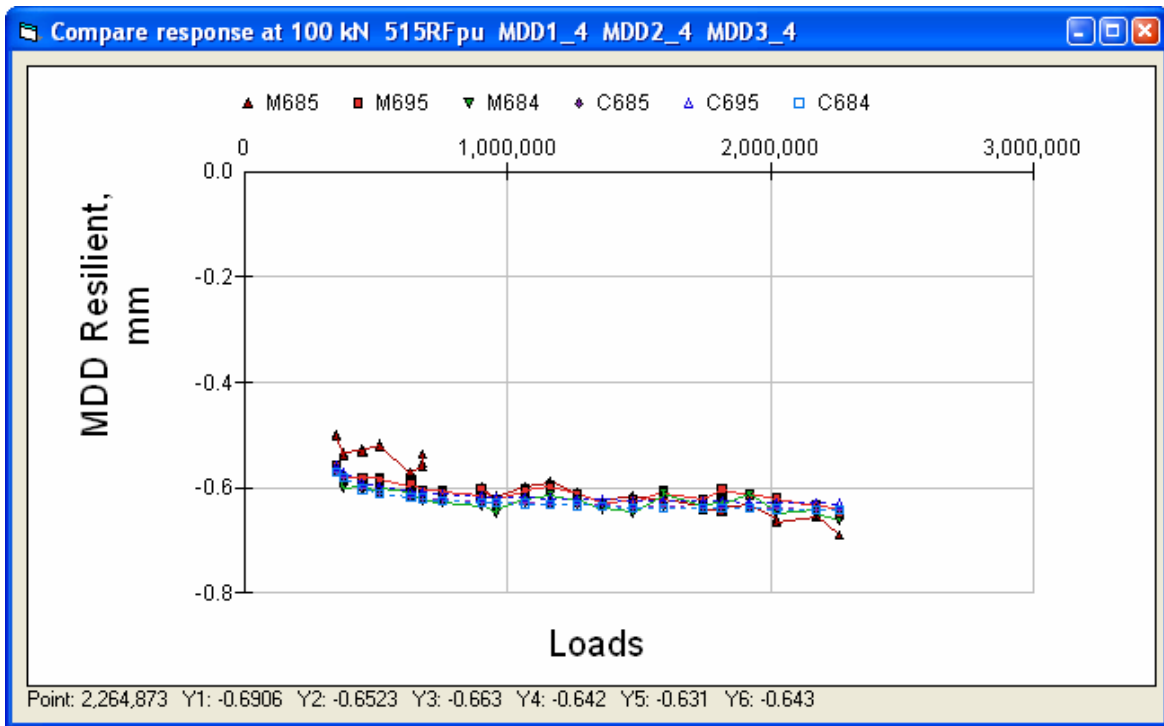


Figure 115. Section 515RF 100 kN deflection of subgrade.

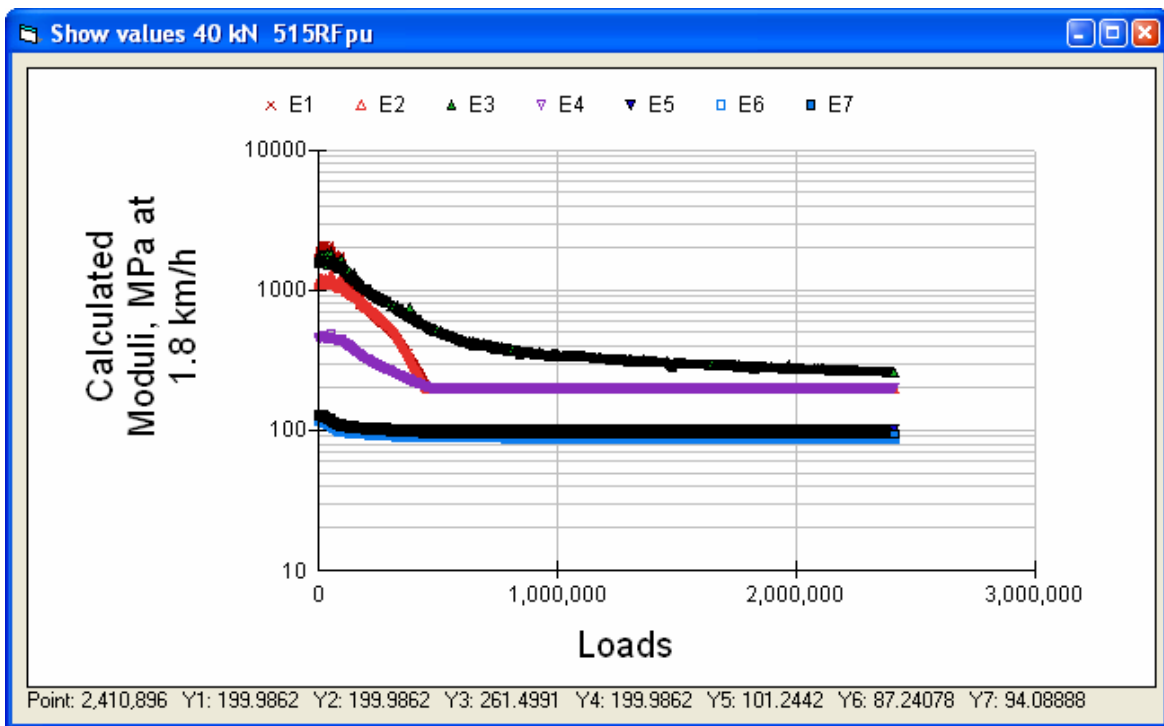


Figure 116. Section 515RF calculated moduli at 40 kN and actual temperatures.

3.2 Visual Cracking Versus Damage of the Overlay, Goal 3, 20°C

Figure 117 shows the visual cracking, in m/m^2 , as a function of the relative decrease in the overlay modulus. The first appearance of surface cracking occurs at a decrease in modulus similar to that observed for the original structures of Goal 1 (shown in Figure 61) but the growth in visual cracking with decrease in modulus is much faster than for the original structures.

There is no clear difference between the DGAC and the ARHM, or between the drained and the undrained sections.

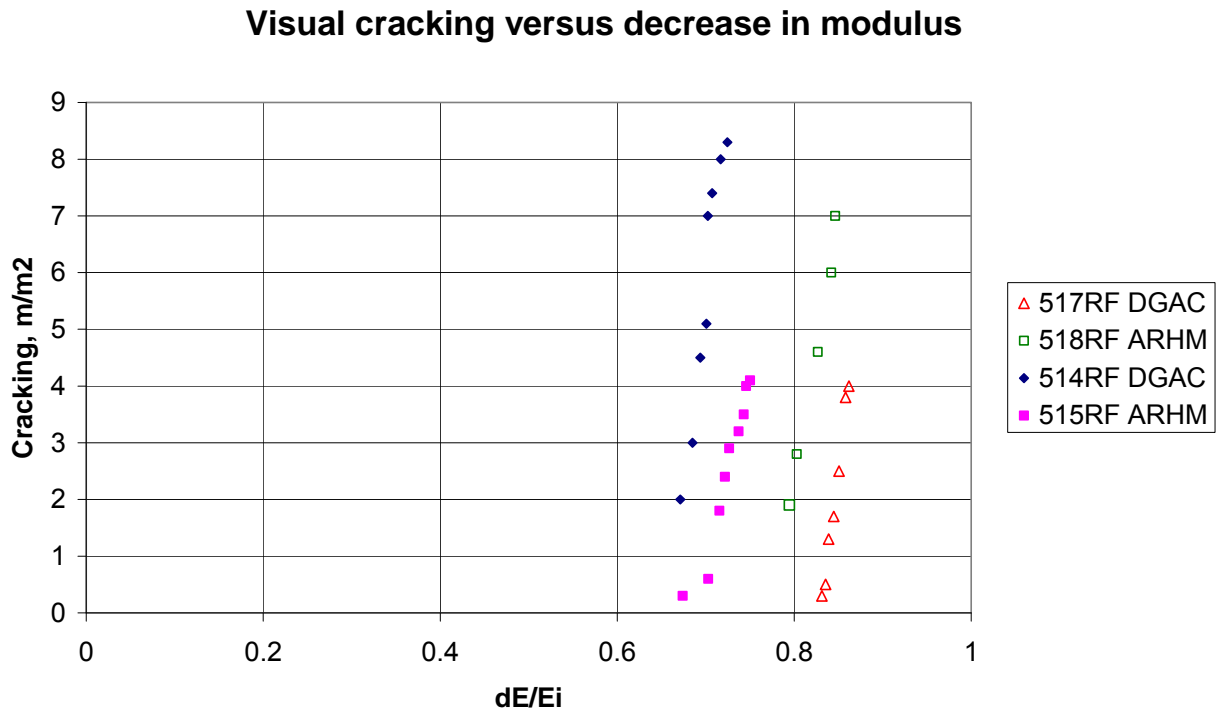


Figure 117. Cracking in overlay versus relative decrease in modulus of overlay, Goal 3.

There is very little increase in deflection with an increase in the amount of cracking observed at the surface, as can be seen in Figure 118. In some cases the deflection actually decreases with an increase in cracking, indicating that the increase in visual cracking is not directly related to a decrease in modulus. This confirms the tendency shown in Figure 117. This suggests that most of the damage, and the increase in deflections, has occurred prior to the appearance of visible cracks on the surface.

Cracking versus relative deflection

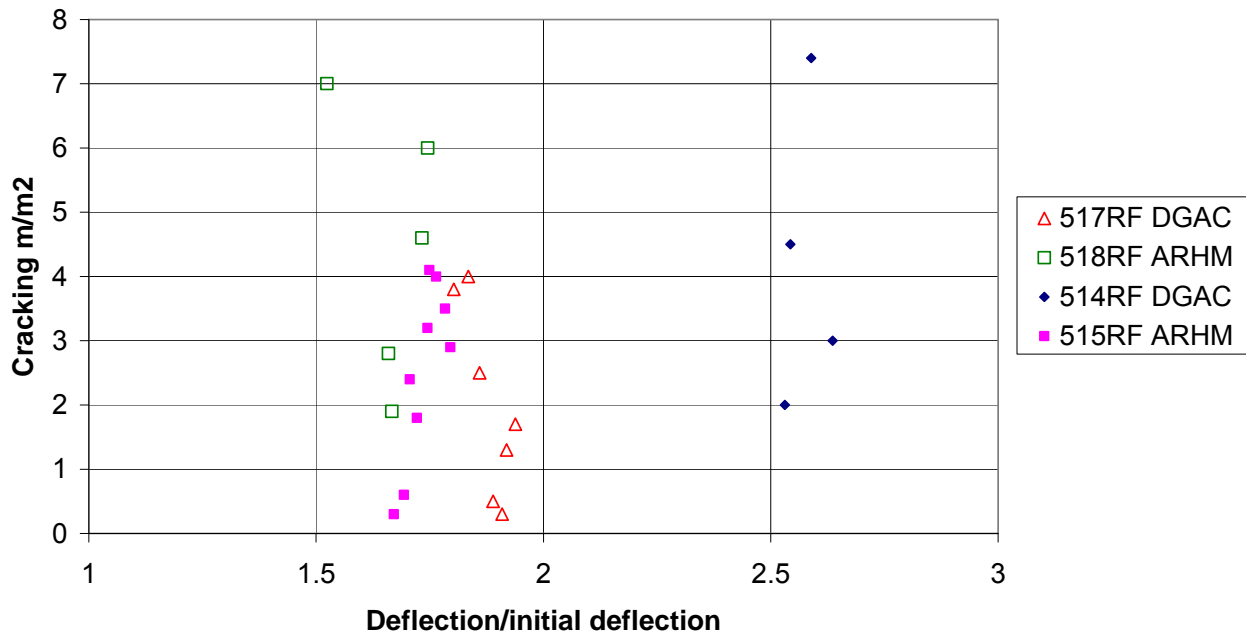


Figure 118. Goal 3, 20°C, cracking versus increase in deflection.

Table 20 shows the calculated layer moduli at a wheel speed of 1.8 km/h, a load of 40 kN, and the actual temperatures at the start of the test, and Table 21 shows the calculated moduli at the end of the test. Moduli are given in MPa.

Table 20. Layered Moduli at Start of Test, MPa

Start	Section 517RF	Section 518RF	Section 514RF	Section 515RF
(Original section)	(501RF)	(503RF)	(500RF)	(502CT)
Overlay type	DGAC	ARHM	DGAC	ARHM
Overlay	2204	1649	2313	1722
AC top	671	755	912	1078
AC bottom	762	950	1187	1645
ATPB			411	444
AB	118	111	143	128
ASB	119	110	135	118
Subgrade	77	78	78	129

Table 21. Layer Moduli at End of Test, MPa

Final	Section 517RF	Section 518RF	Section 514RF	Section 515RF
Overlay type	DGAC	ARHM	DGAC	ARHM
Overlay	427	329	727	442
AC top	200	200	200	200
AC bottom	439	329	589	343
ATPB			200	200
AB	101	100	105	102
ASB	90	88	93	88
Subgrade	58	59	56	95

The percentage decrease in moduli is given in Table 22. The trends are similar to those of the Goal 1 fatigue cracking.

Table 22. Percentage Decrease in Moduli

% Decrease	Section 517RF	Section 518RF	Section 514RF	Section 515RF
Overlay type	DGAC	ARHM	DGAC	ARHM
Overlay	81	80	69	74
AC top	70	74	78	81
AC bottom	42	65	50	79
ATPB			51	55
AB	14	10	27	20
ASB	24	20	31	25
Subgrade	25	24	28	26

3.3 Permanent Deformation Goal 3, 20°C

The permanent deformations, accumulated during the Goal 1 testing, were assumed to remain as initial permanent deformations in Goal 3, and it is assumed that there was no recovery of permanent deformation from Goal 1 to Goal 3. The deformations are given (in mm) in Table 23.

Table 23. Initial Permanent Deformations, Goal 3, in mm

Section	(517RF)	(518RF)	(514RF)	(515RF)
Overlay type	DGAC	ARHM	DGAC	ARHM
(Original) Test Section	501RF	503RF	500RF	502CT
AC top	3.6	3.4	4.0	3.2
AC bottom	0.0	0.0	0.0	0.0
ATPB			0.0	0.0
AB	2.7	3.3	3.5	3.2
ASB	1.0	1.2	1.8	1.6
Subgrade	1.4	1.2	3.2	1.7

3.3.1 Section 517RF 75-mm DGAC Permanent Deformations

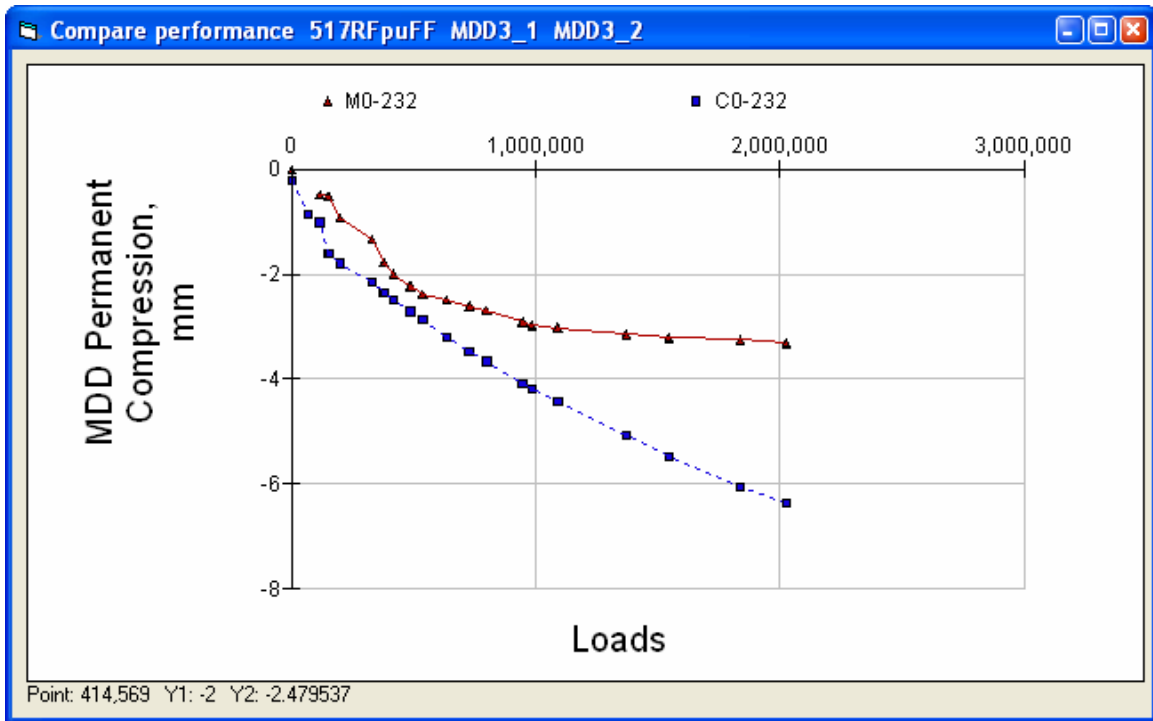


Figure 119. Section 517RF permanent deformation of AC layers.

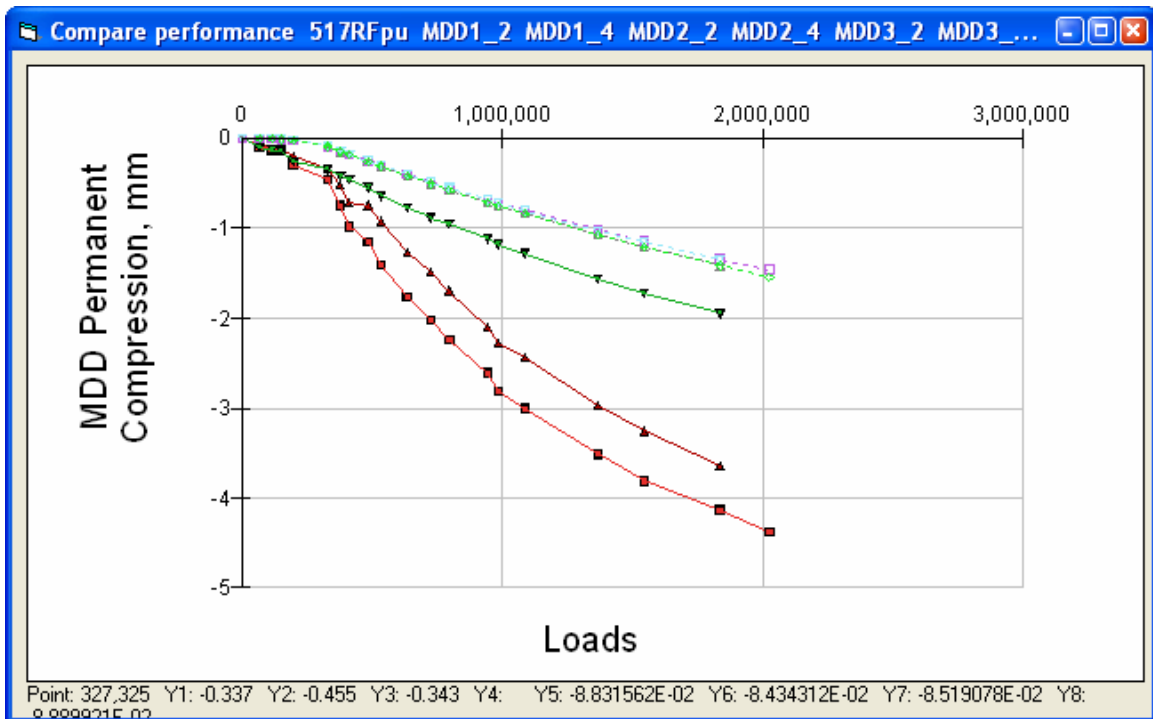


Figure 120. Section 517RF permanent deformation of granular layers.

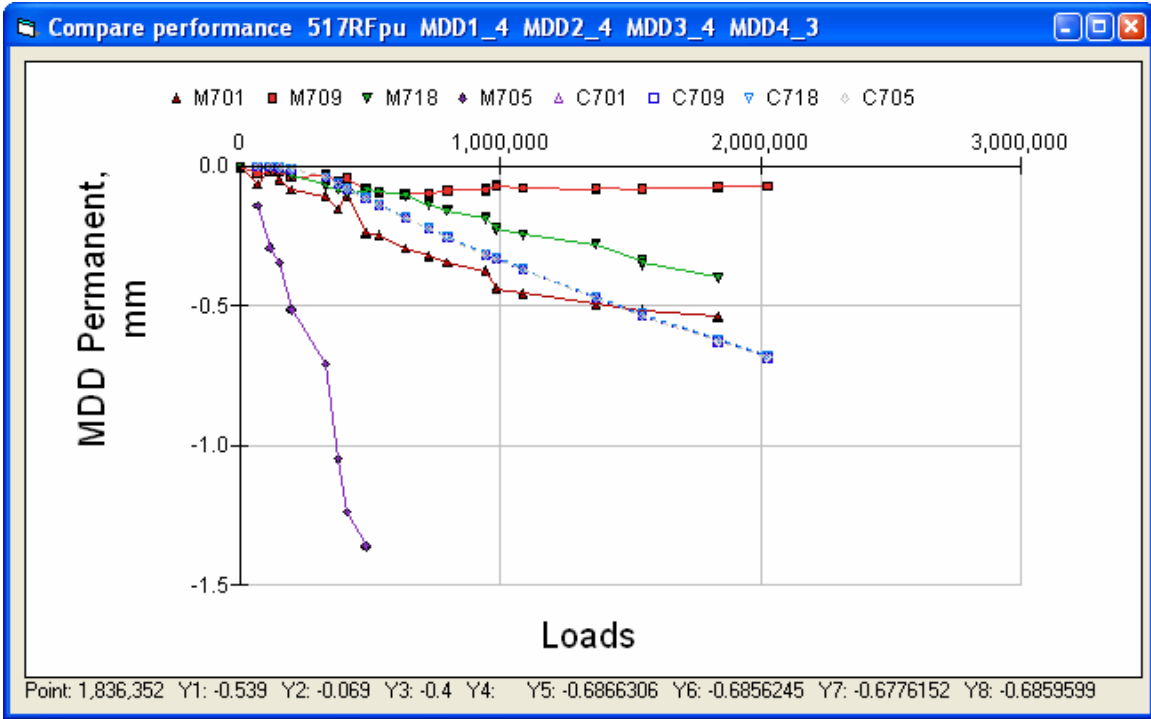


Figure 121. Section 517RF permanent deformation of subgrade.

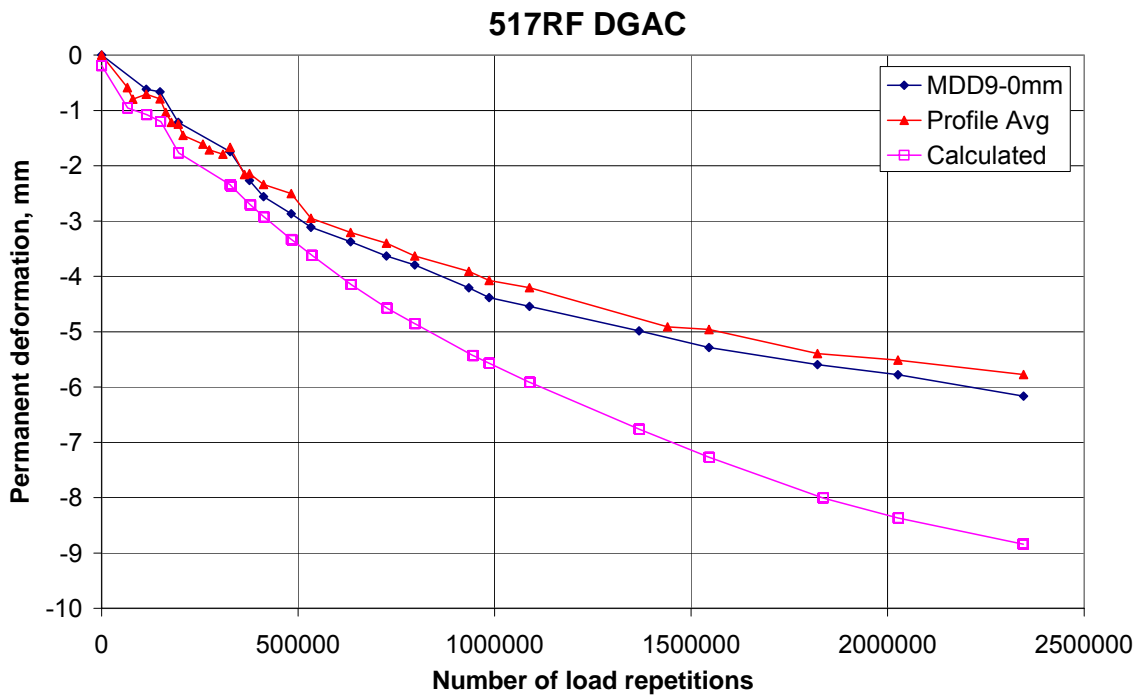


Figure 122. Section 517RF permanent deformation at pavement surface.

3.3.2 Section 518RF 38-mm ARHM Permanent Deformation

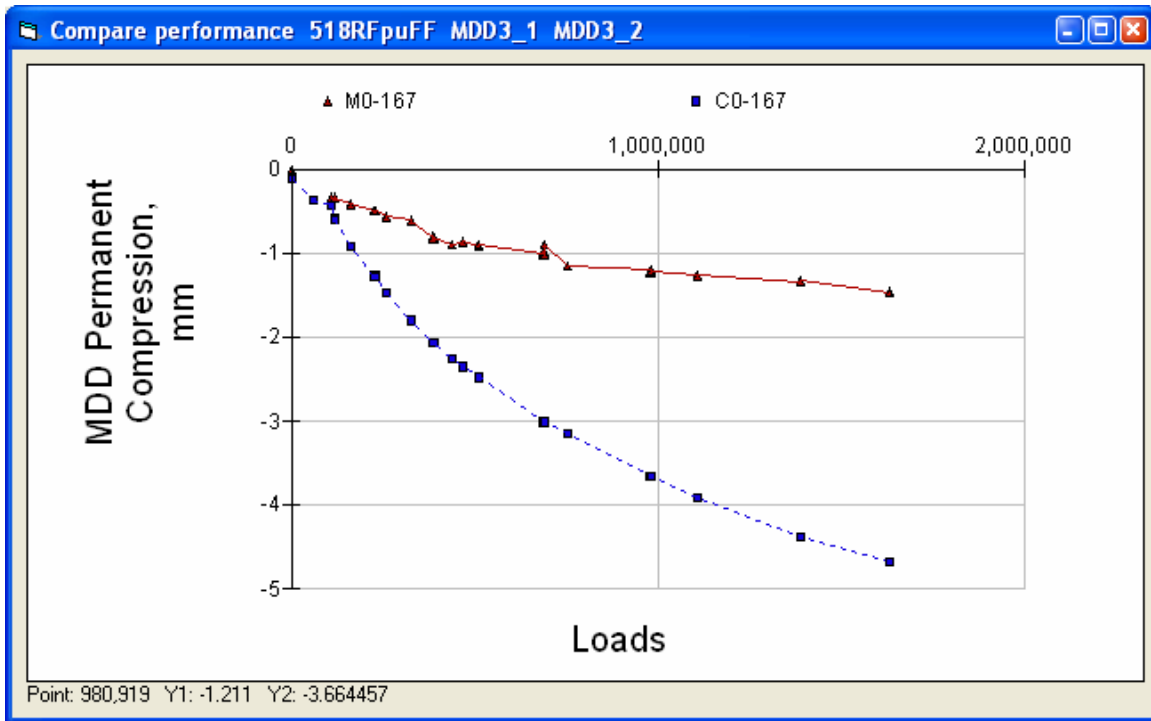


Figure 123. Section 518RF permanent deformation of AC layers.

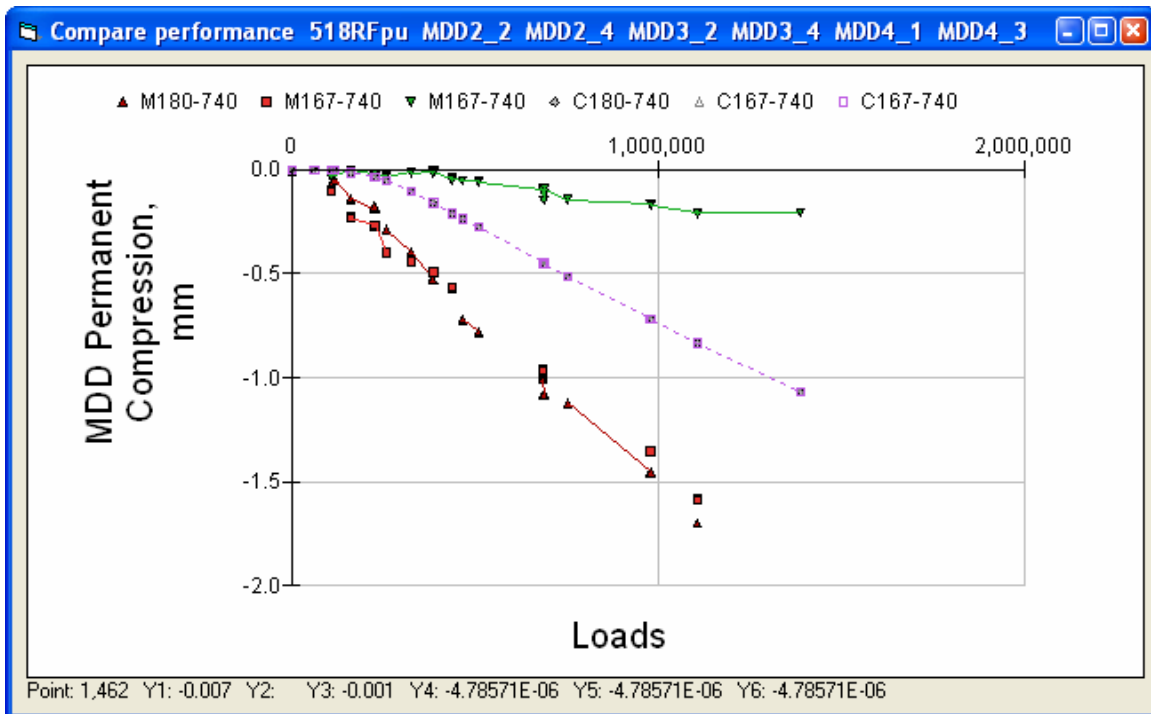


Figure 124. Section 518RF permanent deformation of granular layers.

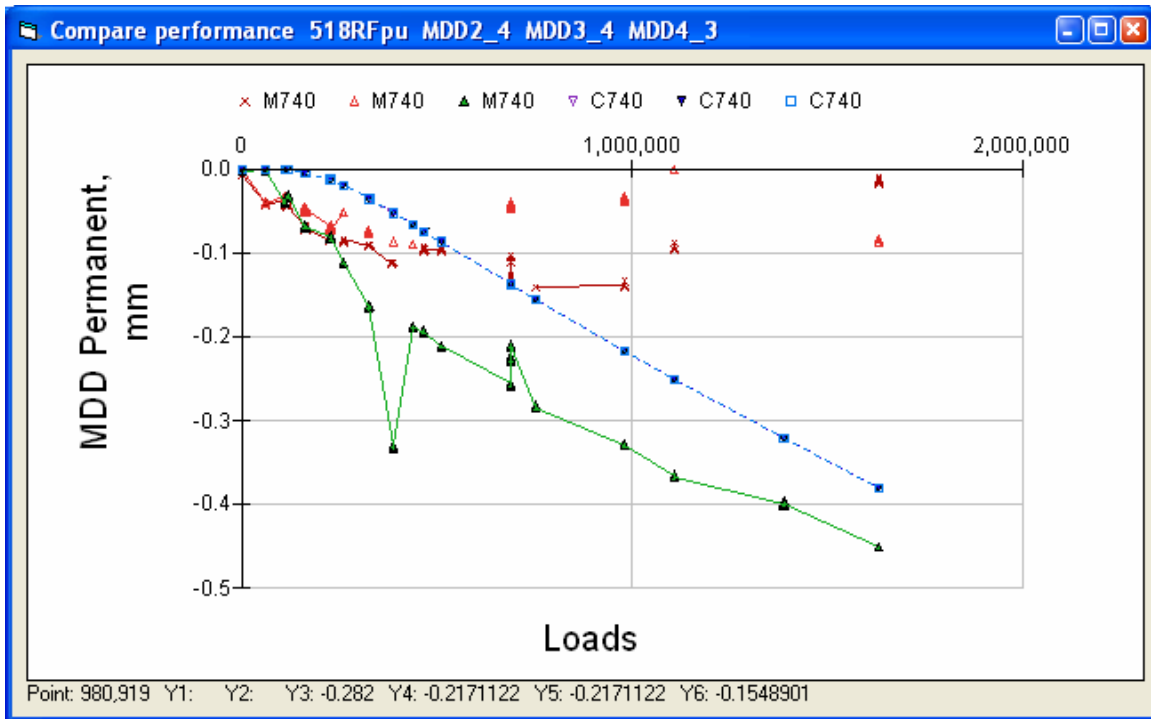


Figure 125. Section 518RF permanent deformation of subgrade.

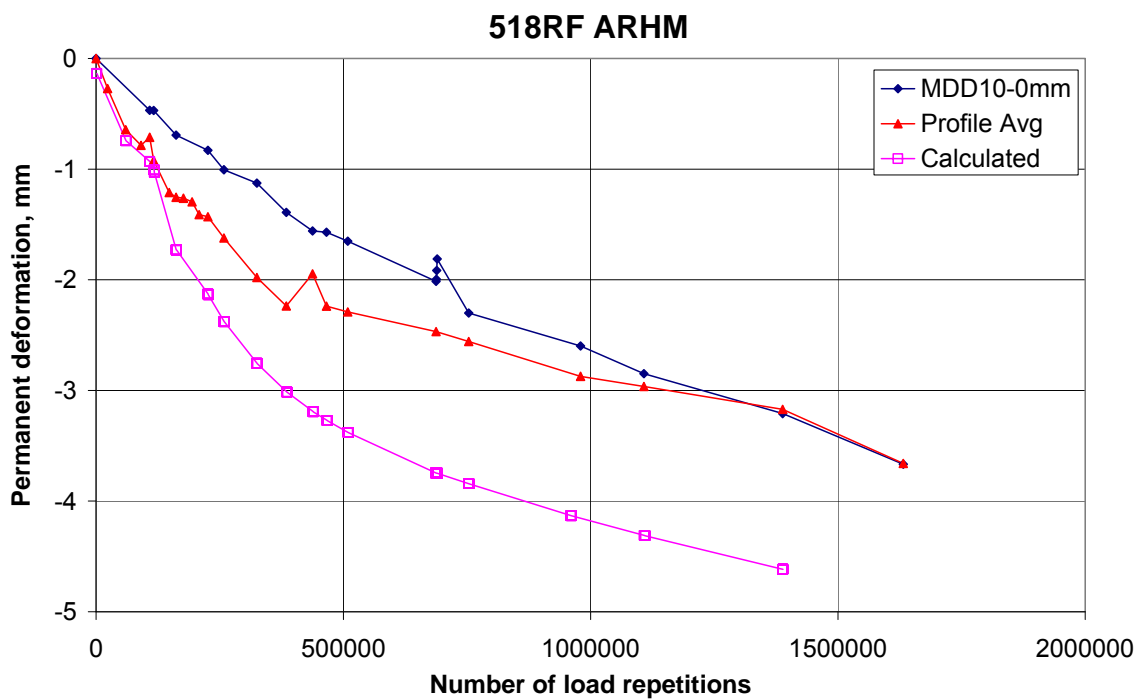


Figure 126. Section 518RF permanent deformation at pavement surface.

3.3.3 Section 514RF 75-mm DGAC Permanent Deformations

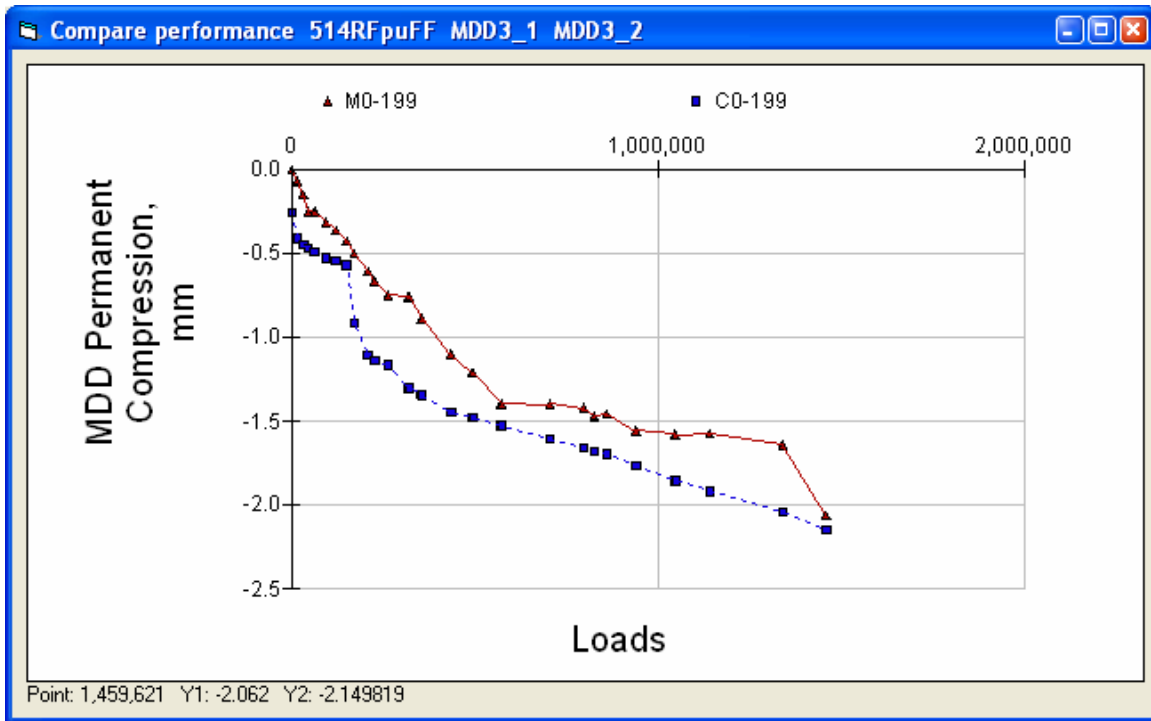


Figure 127. Section 514RF permanent deformation of AC layers.

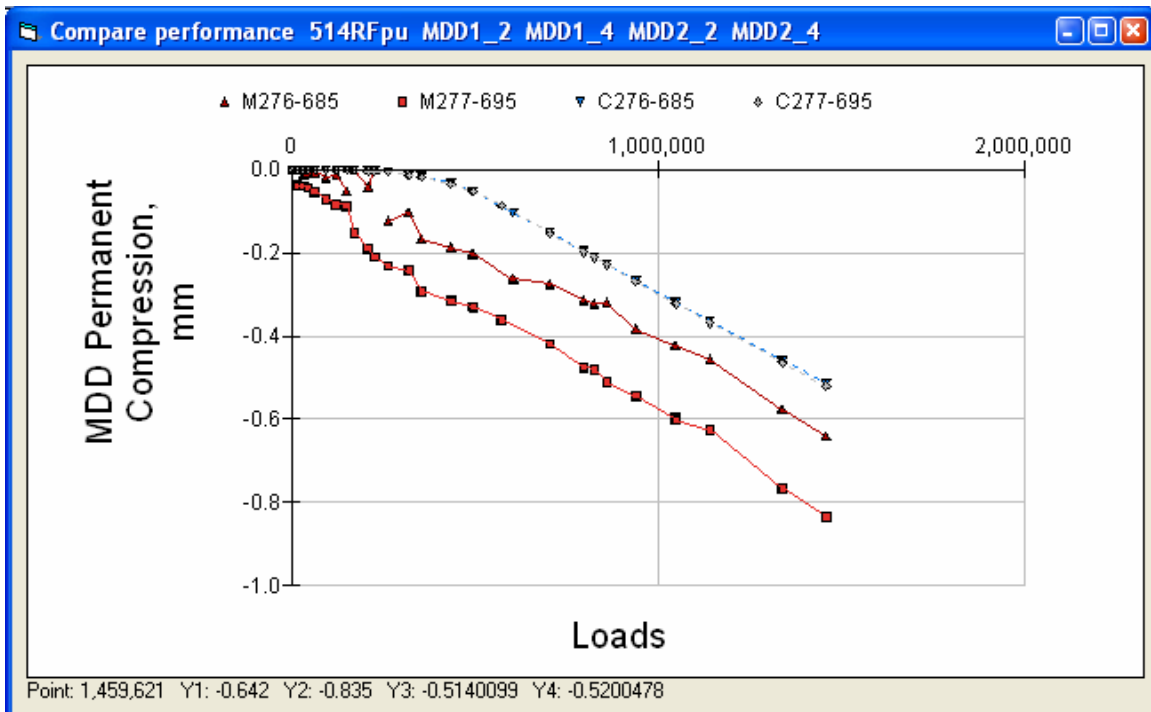


Figure 128. Section 514RF permanent deformation of granular layers, MDD1 and MDD2.

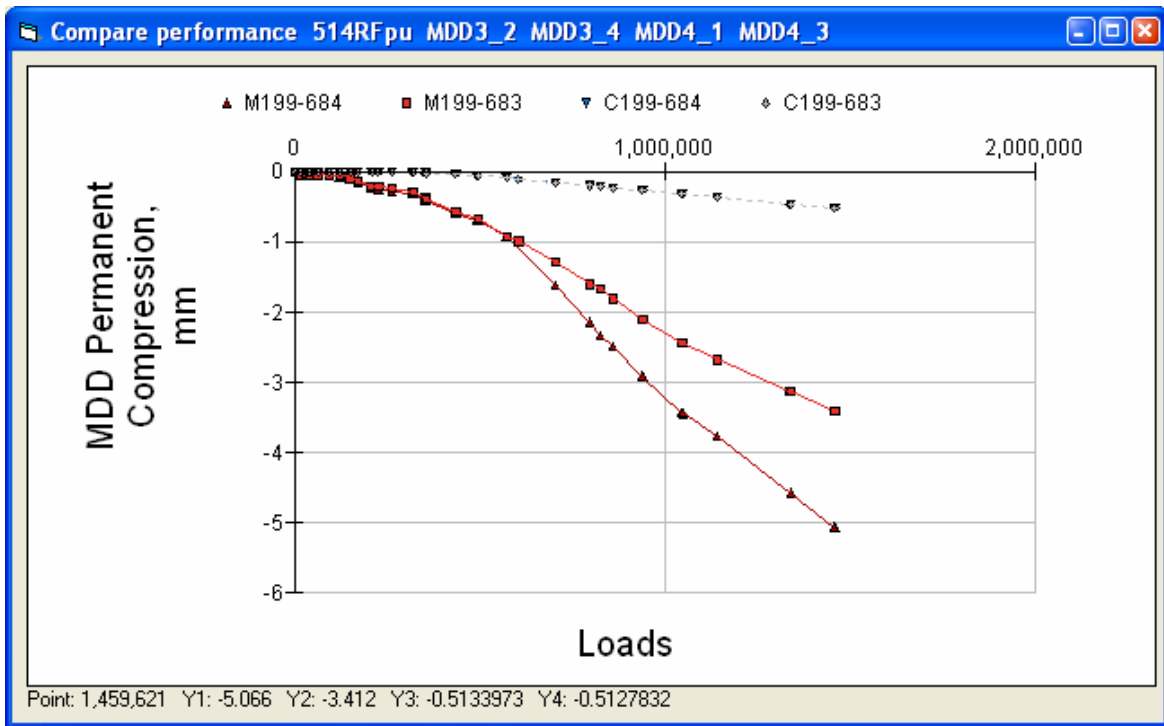


Figure 129. Section 514RF permanent deformation of granular layers, MDD3 and MDD4.

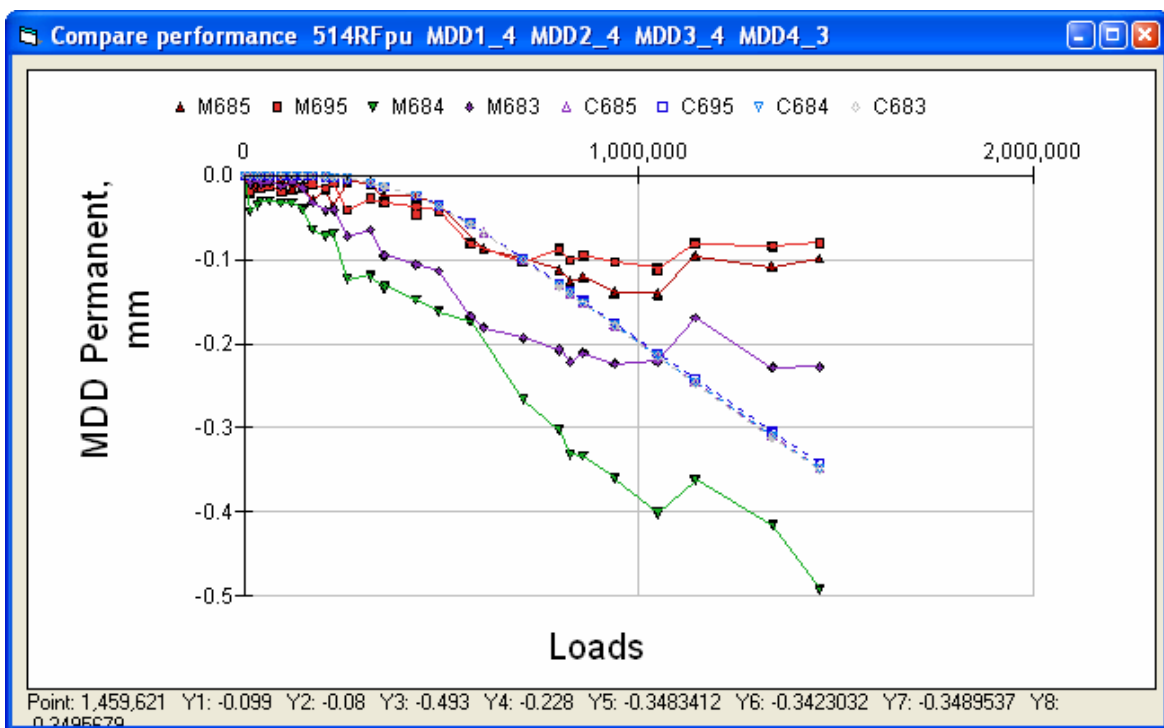


Figure 130. Section 514RF permanent deformation of subgrade.

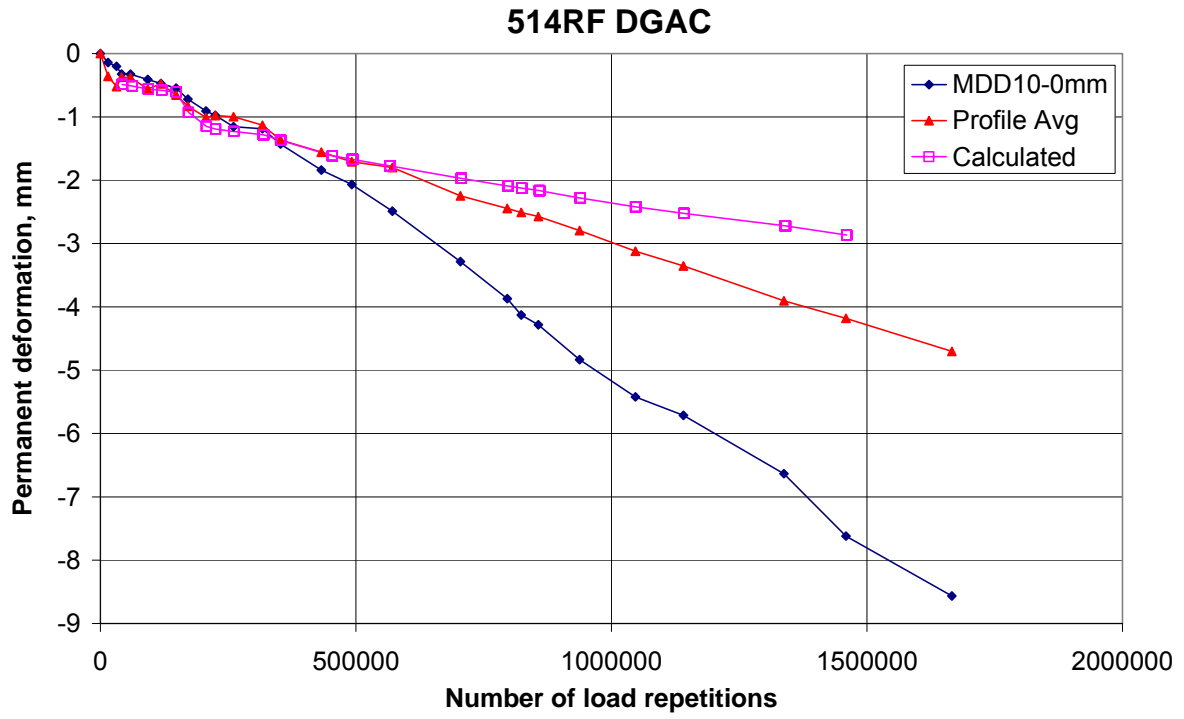


Figure 131. Section 514RF permanent deformation at pavement surface.

3.3.4 Section 515RF 38-mm ARHM Permanent Deformations

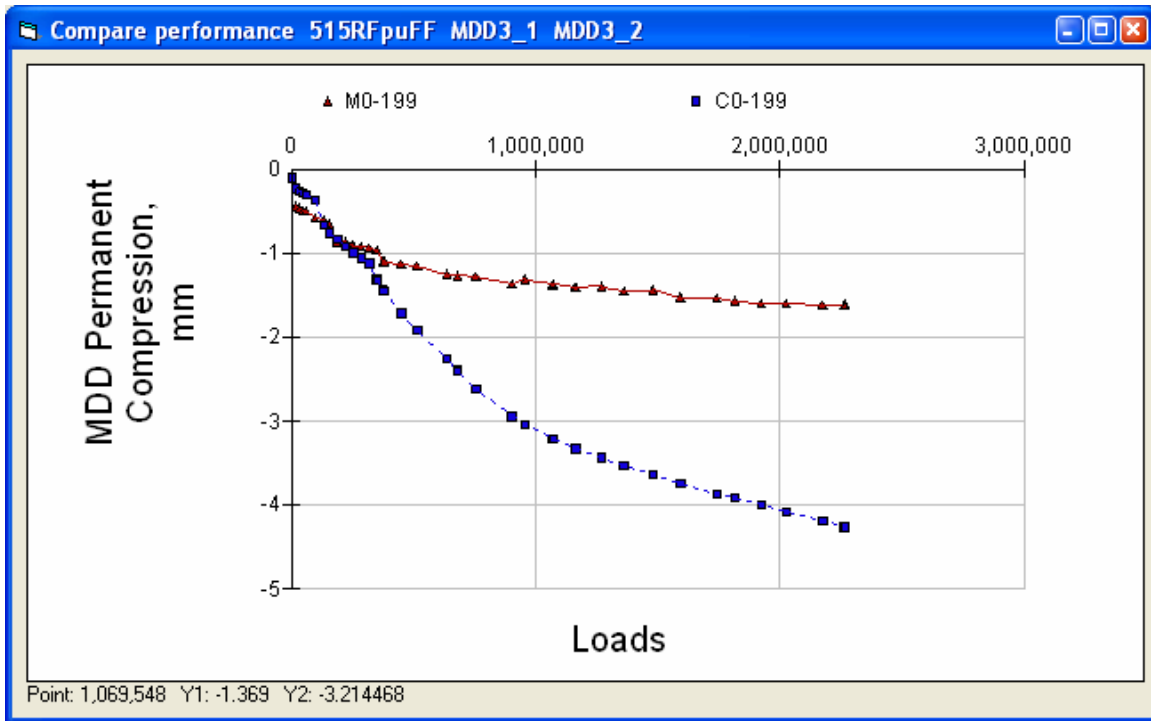


Figure 132. Section 515RF permanent deformation of AC layers.

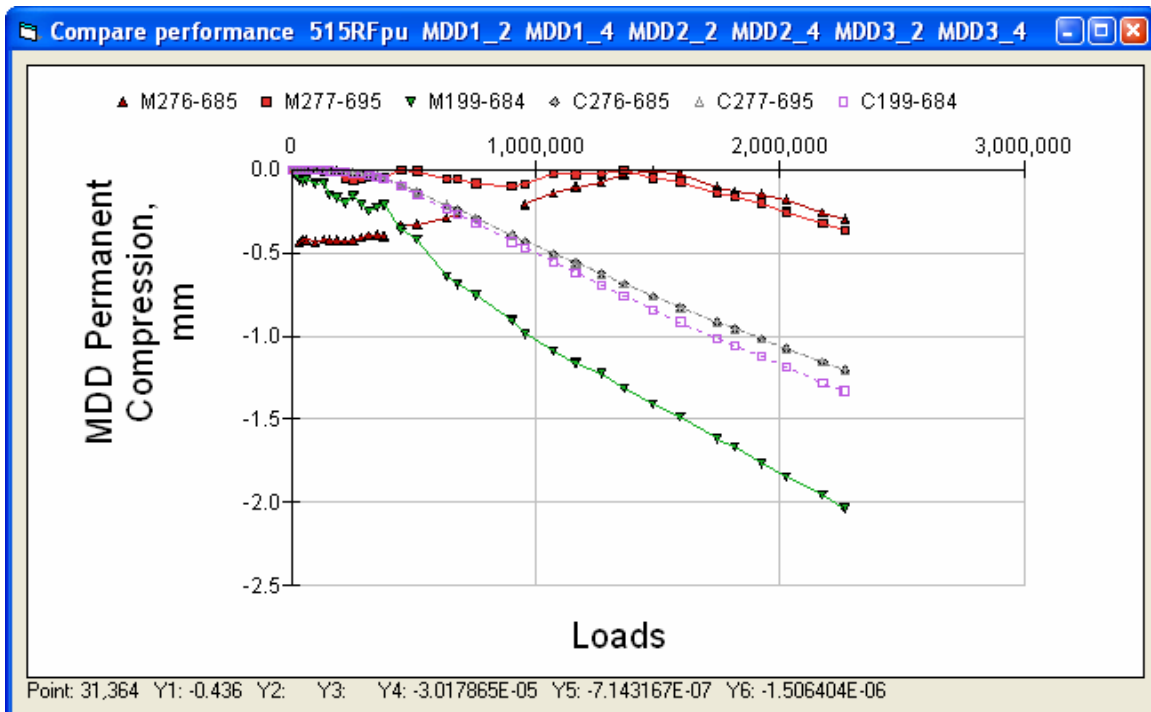


Figure 133. Section 515RF permanent deformation of granular layers.

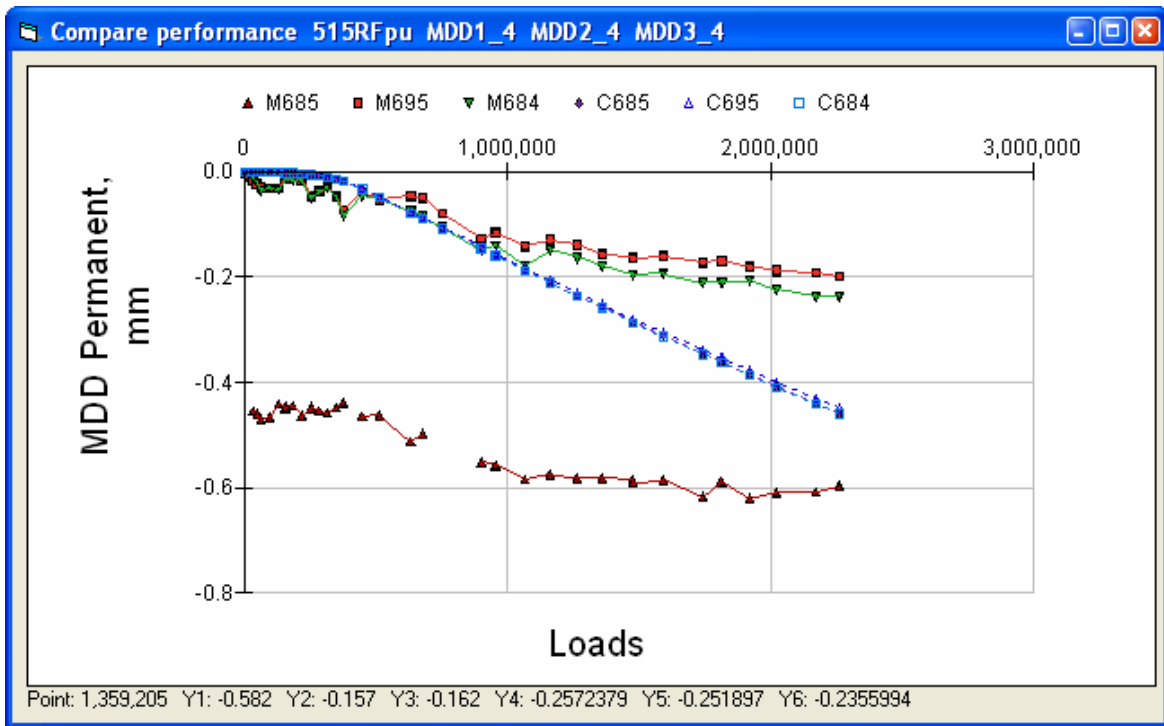


Figure 134. Section 515RF permanent deformation of subgrade.

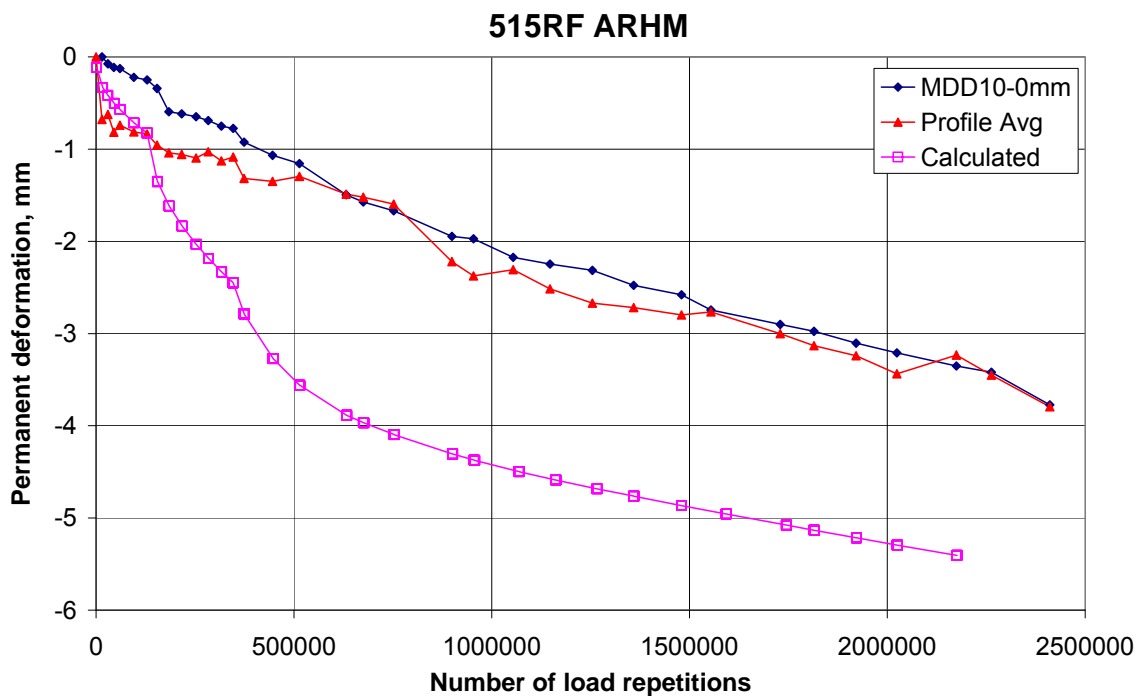


Figure 135. Section 515RF permanent deformation of the pavement surface.

4.0 GOAL 3 RUTTING EXPERIMENTS

The HVS Goal 3 rutting tests were performed on overlays placed on Goal 1 pavements that had not been previously loaded. The overlays were the same materials as in the Goal 3, 20°C experiments, but of varying thicknesses for the ARHM.

Several different wheels were used in these tests. The tire pressures are given in Table 24.

Table 24. Tire Types and Pressure, MPa

Tire-type	MPa
Bias-ply duals	0.620
Radial duals	0.723
Wide-Base single	0.758
Aircraft	1.034

All loading was unidirectional with a wheel load of 40 kN, except for Section 513RF. Loading on that section was done bidirectionally with the aircraft tire and a wheel load of 100 kN. Testing was done at elevated temperatures of 45–50°C.

Unidirectional loading has been found to result in larger rut depth than bidirectional loading. In Florida Tia et al. (28) found from HVS tests reported in 2002 that:

Although the bi-directional mode can apply almost twice the number of wheel passes per day as compared with the unidirectional mode, the unidirectional mode of loading still produced slightly higher rut depths for the same testing duration.

To compensate for this difference the value of K (the ratio between rut depth and permanent shear strain) was multiplied by a factor of 1.6 to give 0.13 for Goal 1 materials and 0.4 for all other materials.

The test sections were not instrumented with MDDs, but their surface profile was measured. No cracking was observed, but the same fatigue models used in the 20°C testing were used here too. They resulted in a considerable amount of predicted damage. The validity of the fatigue models at elevated temperatures is not known.

4.1 Section 504RF No Overlay, Wide-Base Single Tire

Temperature data was not available. A temperature profile with 48.5°C at the top and 35°C at a depth of 150 mm was estimated from data in Harvey et al. (2002), and used during the entire test.

504RFpu structural data

Design methods Tools Change WIM Parameters

S

mm MPa

Layer	Material	Thick	Modulus	Poisson	R	GF	Cost/m3
1	DGACVHVSG1TRg	74	9055	0.35	0	1.46	114
2	DGACVHVSG1BRg	88	11189	0.35	0	1.46	114
3	ABHVS	274	166	0.35	78	1.1	57
4	AS2HVS	305	182	0.35	50	1	30
5	ClayHVS	0	115	0.35	20	0	0

Figure 136. Section 504RF pavement structure.

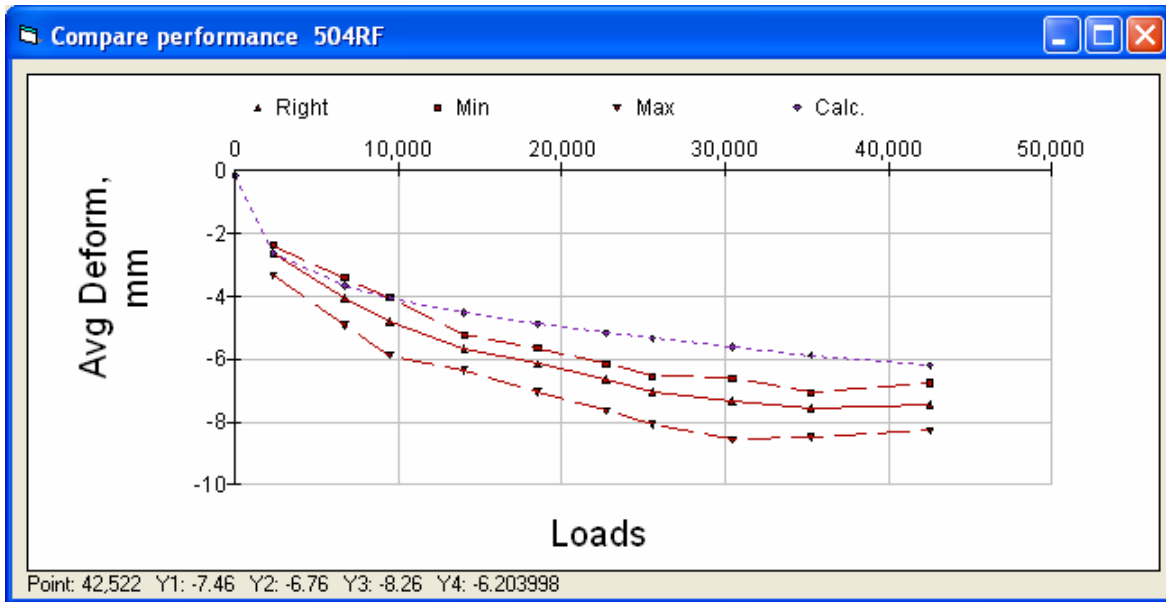


Figure 137. Section 504RF permanent deformation at pavement surface from profilometer.

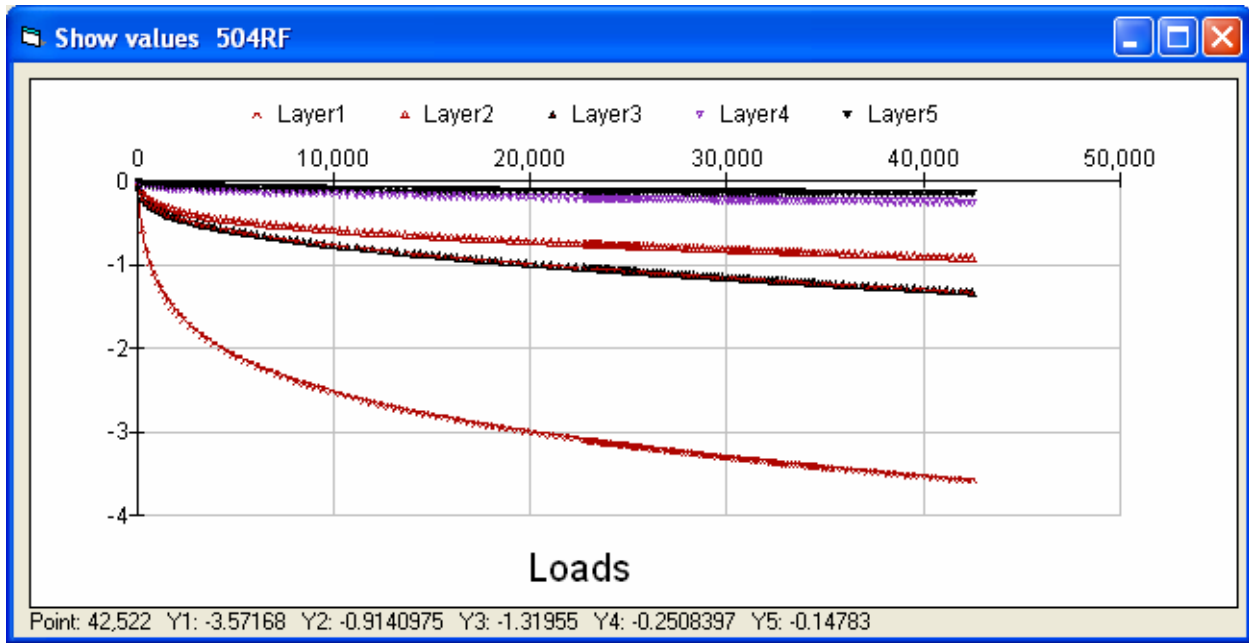


Figure 138. Section 504RF calculated permanent deformation of pavement layers.

4.2 Section 505RF DAGC Overlay, Bias-Ply Dual Tire

505RFpu structural data

Design methods Tools Change WIM Parameters

S

mm MPa

Layer	Material	Thick	Modulus	Poisson	R	GF	Cost/m3
1	DGACVHMSG3Rg	62	7653	0.35	0	1.46	114
2	DGACVHMSG1TRg	74	9055	0.35	0	1.46	114
3	DGACVHMSG1BRg	76	11189	0.35	0	1.46	114
4	ATPB-ACHVSR	75	1143.5	0.35	0	1.4	82
5	ABHVS	183	321	0.35	78	1.1	57
6	AS2HVS	135	309	0.35	50	1	30
7	ClayHVS	0	141	0.35	20	0	0

Figure 139. Section 505RF pavement structure.

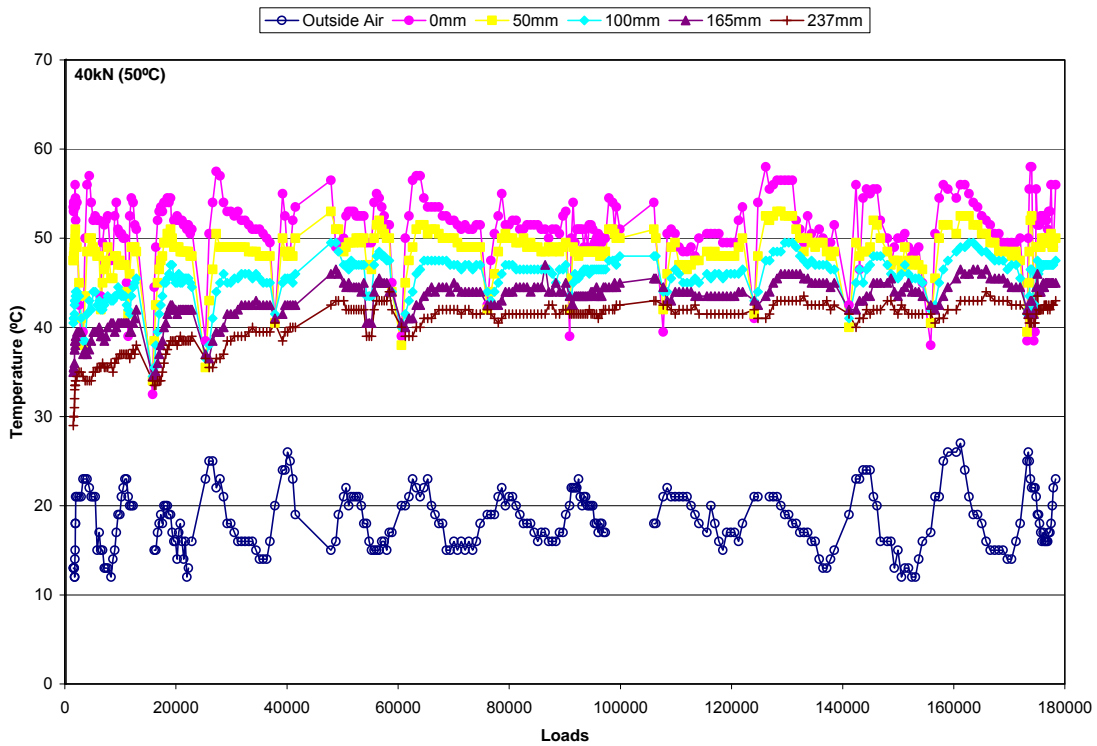


Figure 140. Section 505RF temperatures during testing.

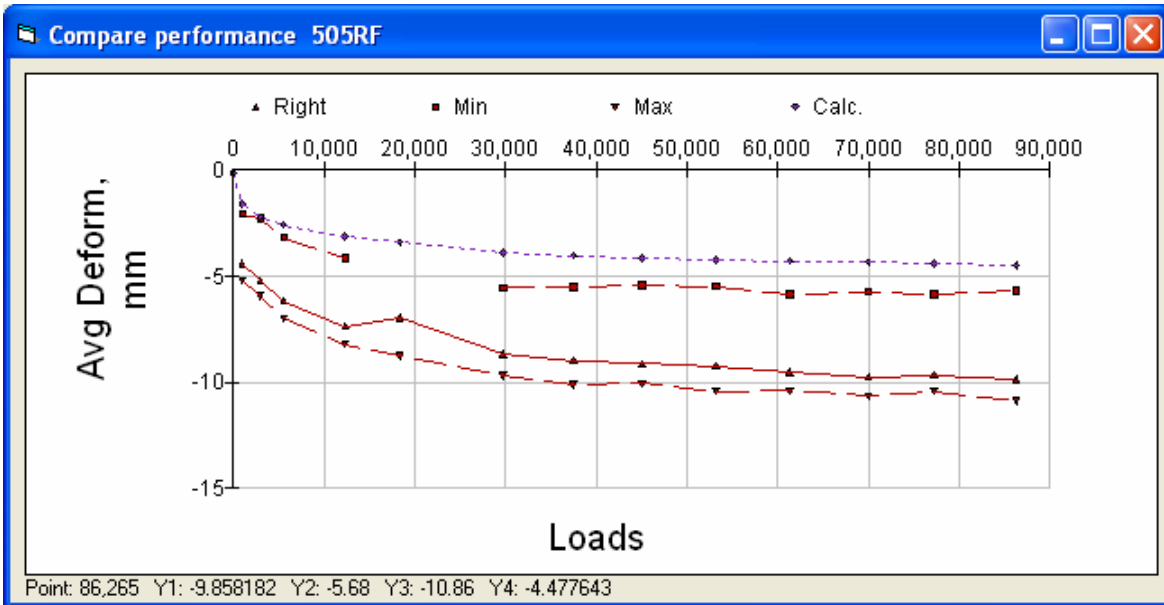


Figure 141. Section 505RF permanent deformation at pavement surface from profilometer.

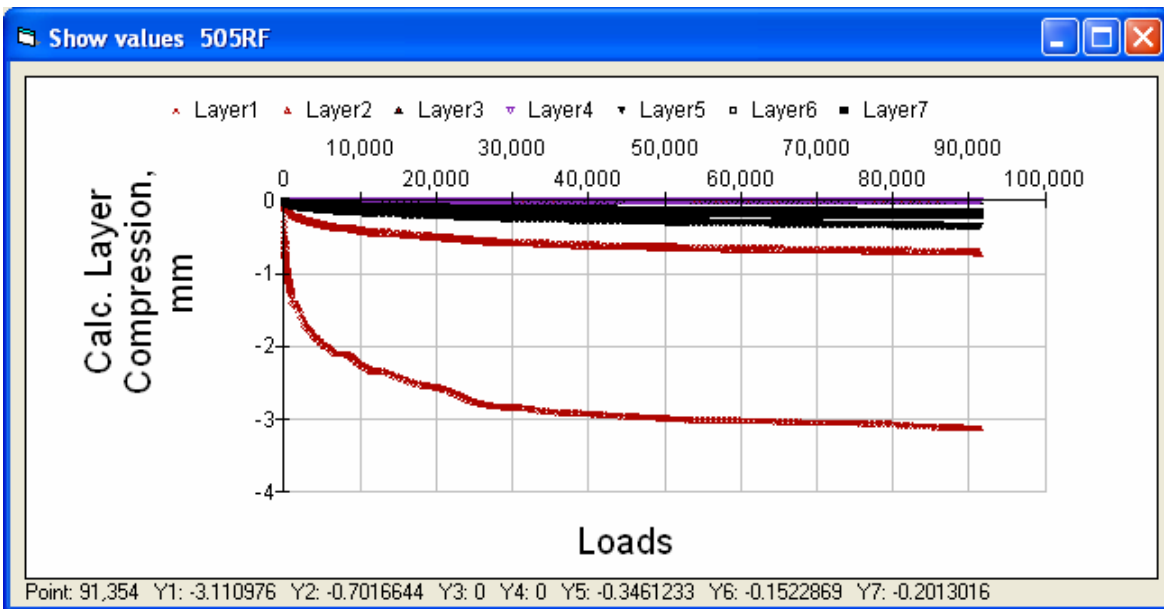


Figure 142. Section 505RF calculated permanent deformation of pavement layers.

4.3 Section 506RF DGAC Overlay, Radial Dual Tire

506RFpu structural data

Design methods Tools Change WIM Parameters

S

		mm	MPa				
Layer	Material	Thick	Modulus	Poisson	R	GF	Cost/m3
1	DGACVHVSG3Rg	62	7653	0.35	0	1.46	114
2	DGACVHVSG1TRg	63	9055	0.35	0	1.46	114
3	DGACVHVSG1BRg	84	11189	0.35	0	1.46	114
4	ABHVS	274	231	0.35	78	1.1	57
5	AS2HVS	177	268	0.35	50	1	30
6	ClayHVS	0	134	0.35	20	0	0

Figure 143. Section 506RF pavement structure.

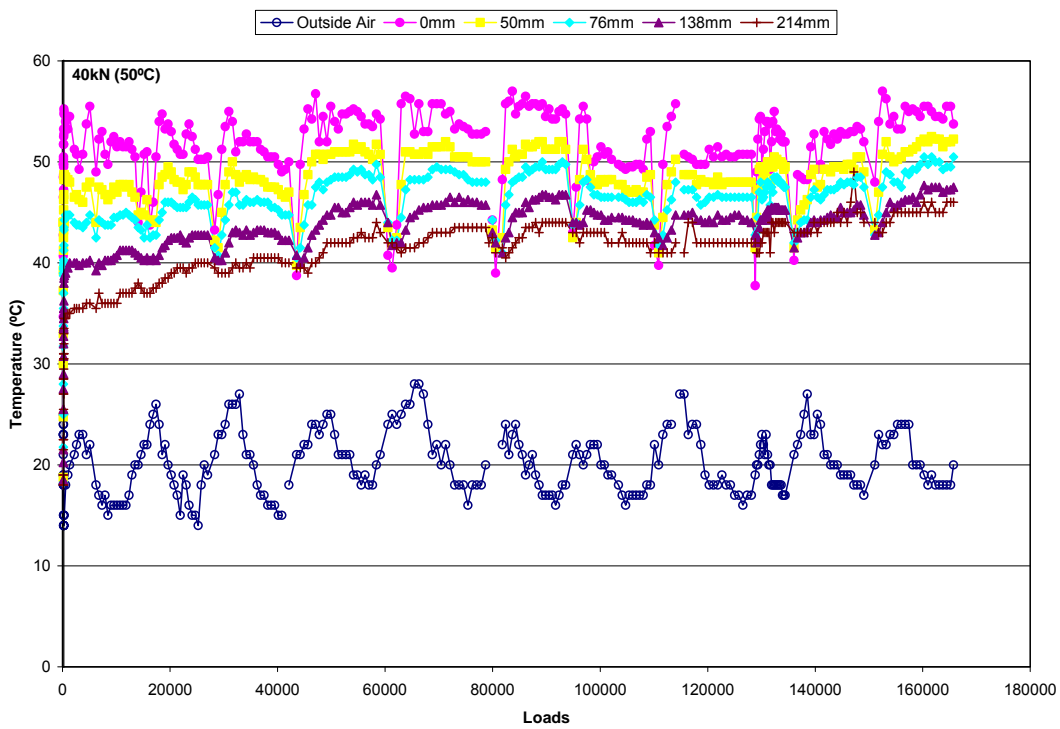


Figure 144. Section 506RF temperatures during testing.

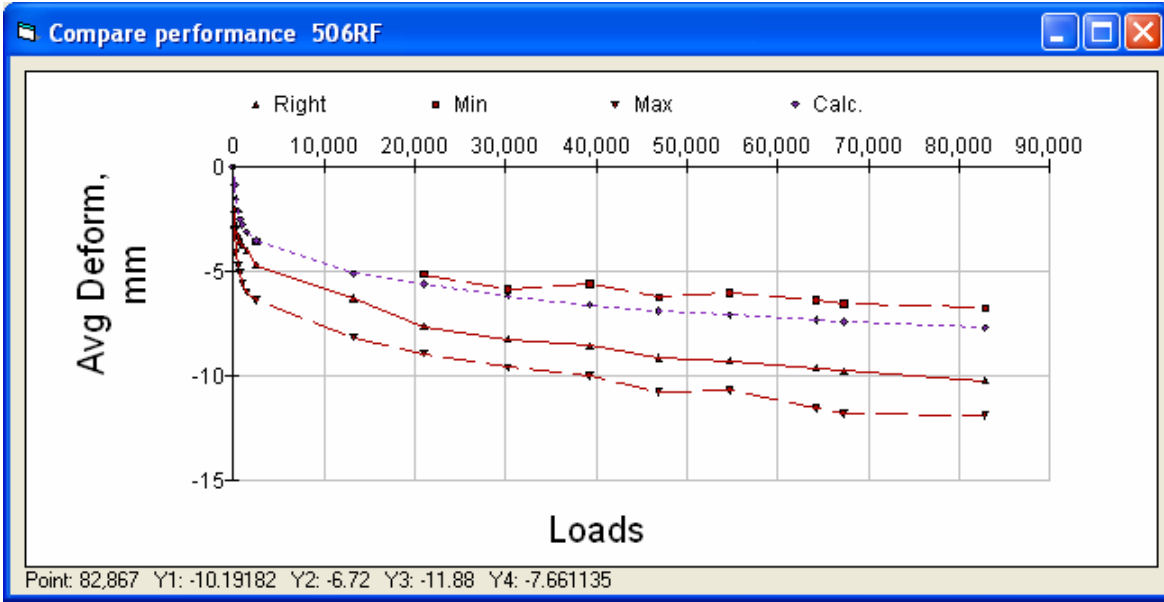


Figure 145. Section 506RF permanent deformation at pavement surface from profilometer.

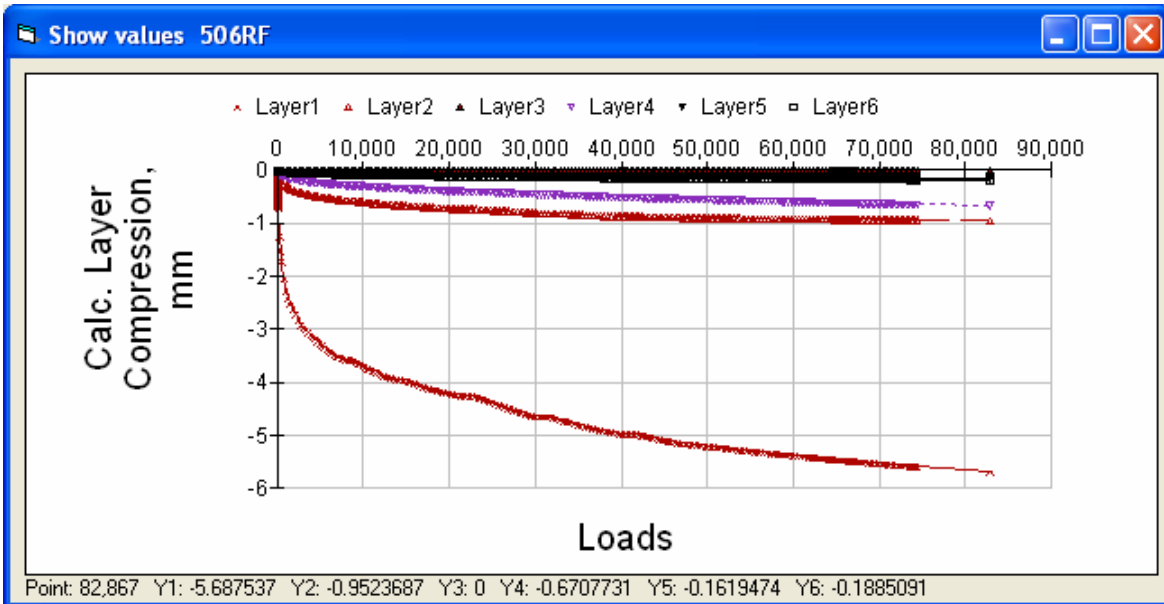


Figure 146. Section 506RF calculated permanent deformation of pavement layers.

4.4 Section 507RF DGAC Overlay, Wide-Base Single Tire

507RFpu structural data

Design methods Tools Change WIM Parameters

S

mm MPa

Layer	Material	Thick	Modulus	Poisson	R	GF	Cost/m3
1	DGACVHVSG3Rg	62	7653	0.35	0	1.46	114
2	DGACVHVSG1TRg	63	9055	0.35	0	1.46	114
3	DGACVHVSG1BRg	84	11189	0.35	0	1.46	114
4	ABHVS	274	231	0.35	78	1.1	57
5	AS2HVS	233	268	0.35	50	1	30
6	ClayHVS	0	150	0.35	20	0	0

Figure 147. Section 507RF pavement structure.

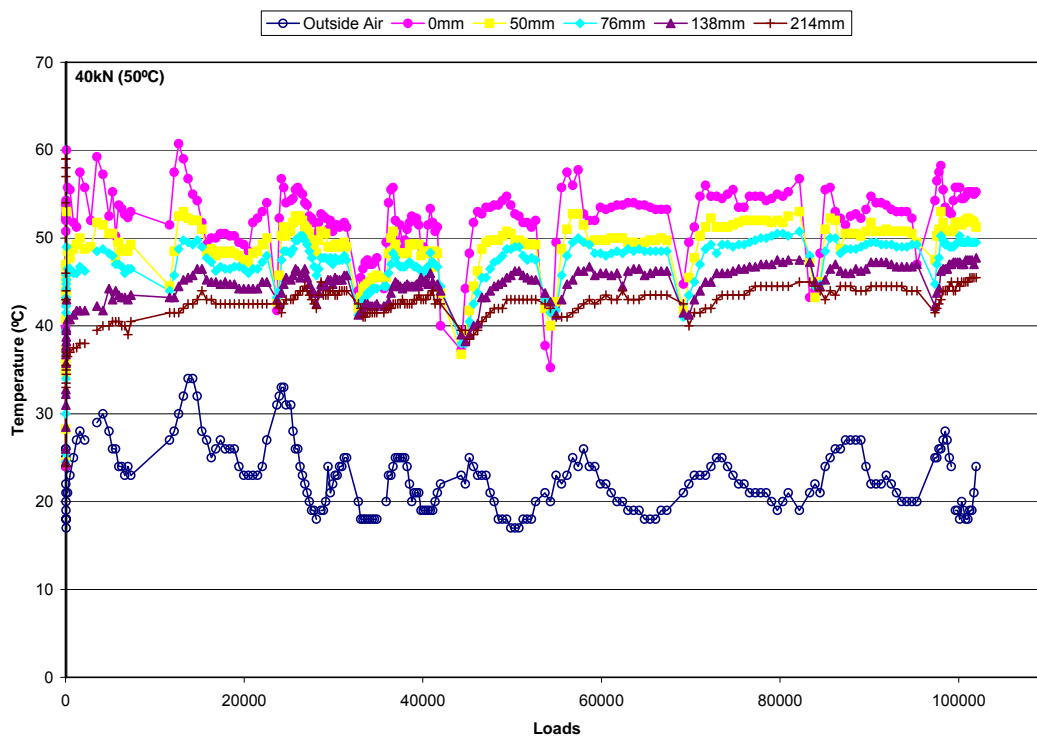


Figure 148. Section 507RF temperatures during testing.

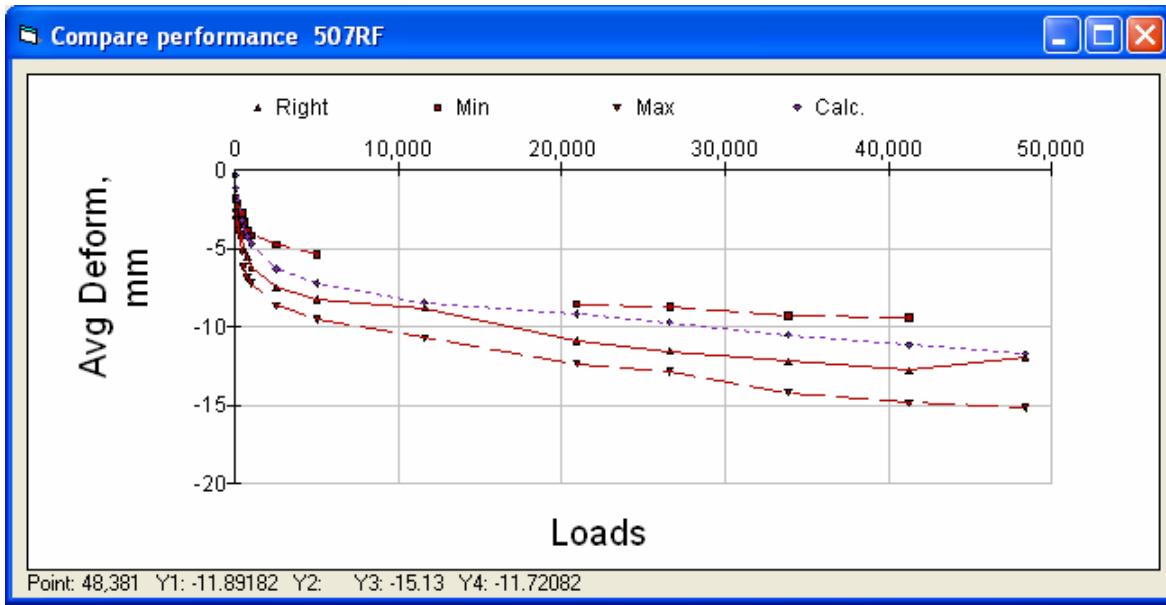


Figure 149. Section 507RF permanent deformation at pavement surface from profilometer.

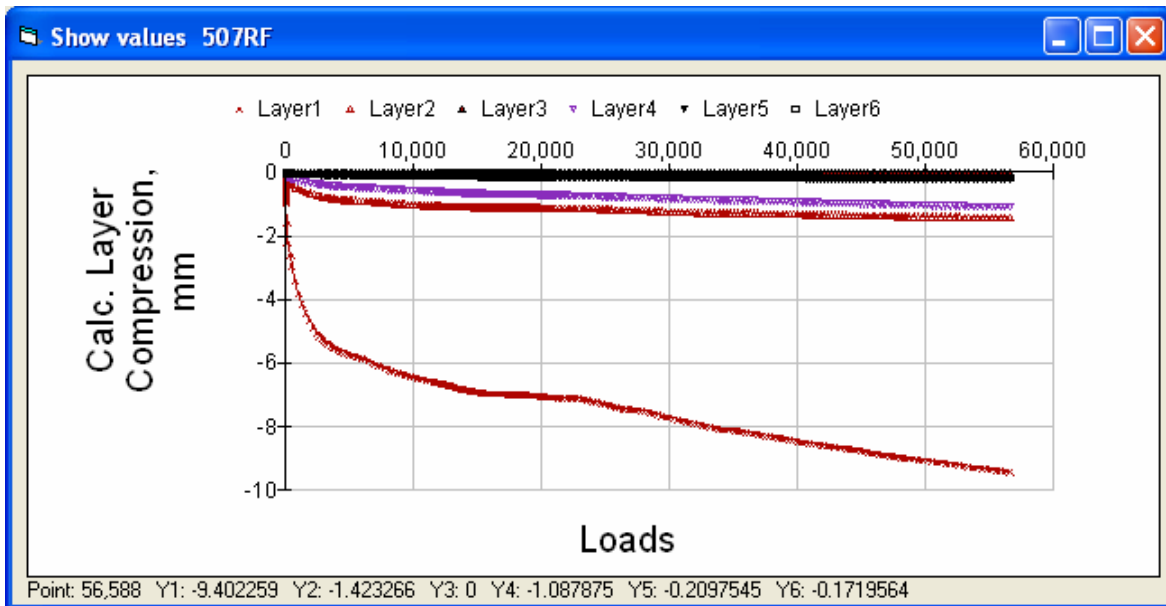


Figure 150. Section 507RF calculated permanent deformation of pavement layers.

4.5 Section 508RF ARHM Overlay, Wide-Base Single Tire

508RFpu structural data

Design methods Tools Change WIM Parameters

S

mm MPa

Layer	Material	Thick	Modulus	Poisson	R	GF	Cost/m3
1	RAC-GHVSRg	60	4755.0	0.35	0	1.46	134
2	DGACVHVSG1TRg	74	9055.0	0.35	0	1.46	114
3	DGACVHVSG1BRg	88	11189.0	0.35	0	1.46	114
4	ABHVS	274	244	0.35	78	1.1	57
5	AS2HVS	306	285	0.35	50	1	30
6	ClayHVS	0	185	0.35	20	0	0

Figure 151. Section 508RF pavement structure.

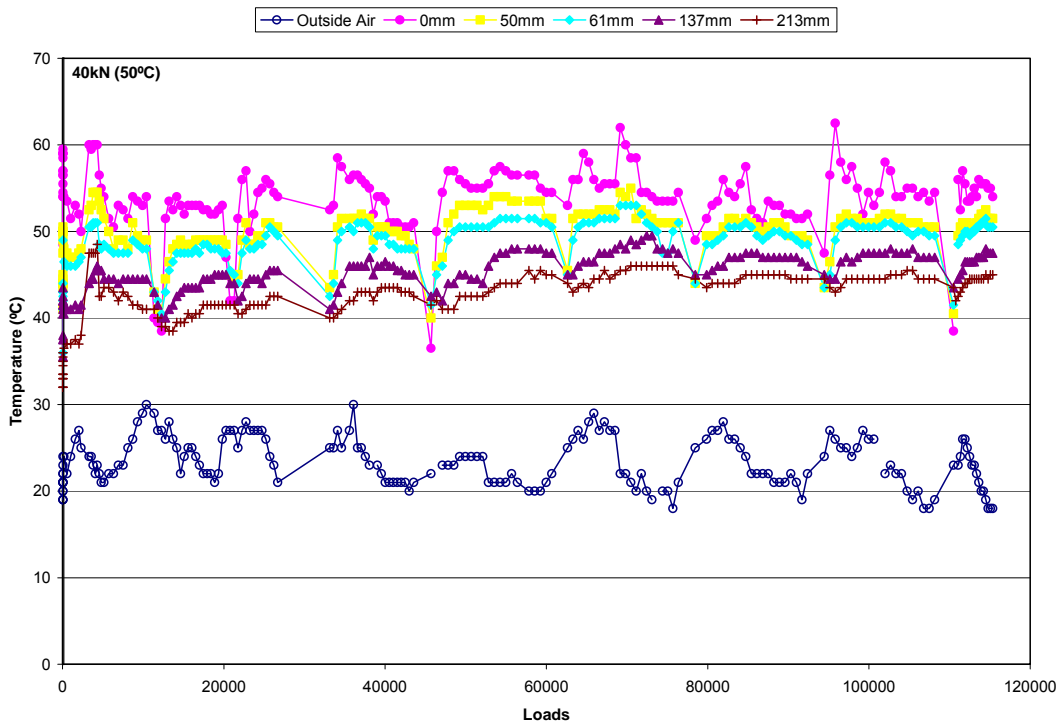


Figure 152. Section 508RF temperatures during testing.

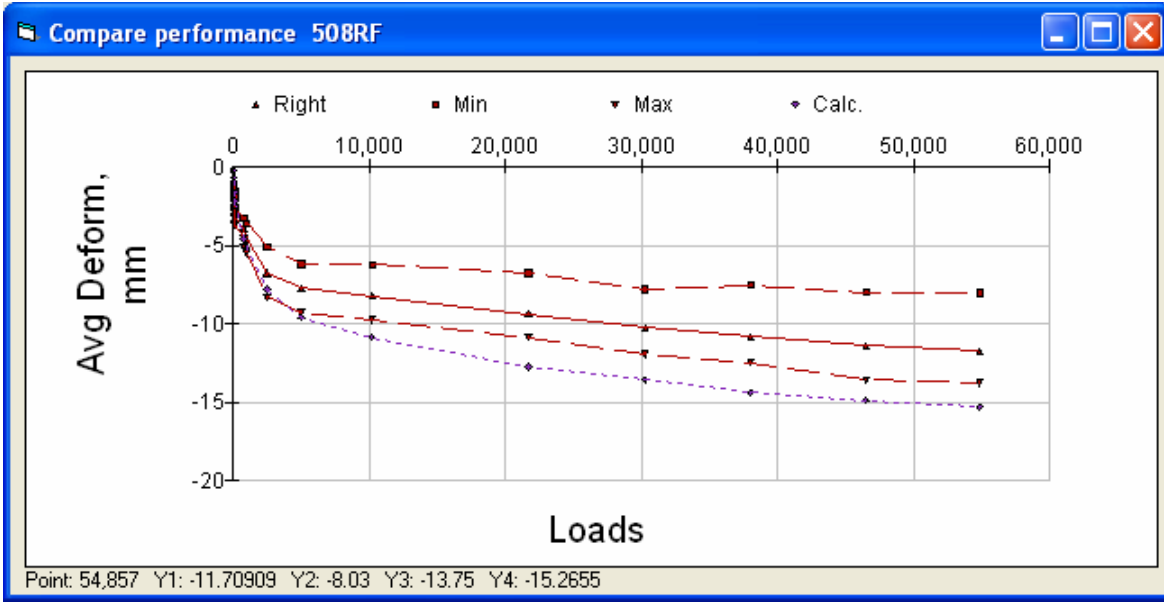


Figure 153. Section 508RF permanent deformation at pavement surface from profilometer.

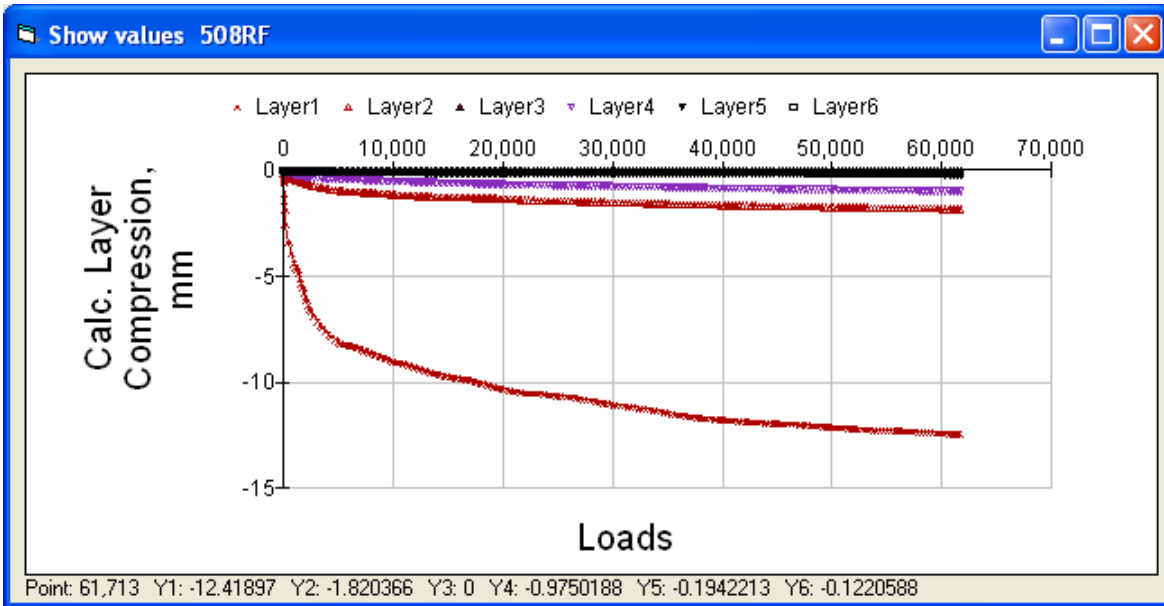


Figure 154. Section 508RF calculated permanent deformation of pavement layers.

4.6 Section 509RF ARHM Overlay, Radial Dual Tire

509RFpu structural data

Design methods Tools Change WIM Parameters

S

mm MPa

Layer	Material	Thick	Modulus	Poisson	R	GF	Cost/m3
1	RAC-GHVSrg	60	4755.0	0.35	0	1.46	134
2	DGACVHVSG1TRg	74	9055.0	0.35	0	1.46	114
3	DGACVHVSG1BRg	88	11189.0	0.35	0	1.46	114
4	ABHVS	274	252	0.35	78	1.1	57
5	AS2HVS	289	295	0.35	50	1	30
6	ClayHVS	0	185	0.35	20	0	0

Figure 155. Section 509RF pavement structure.

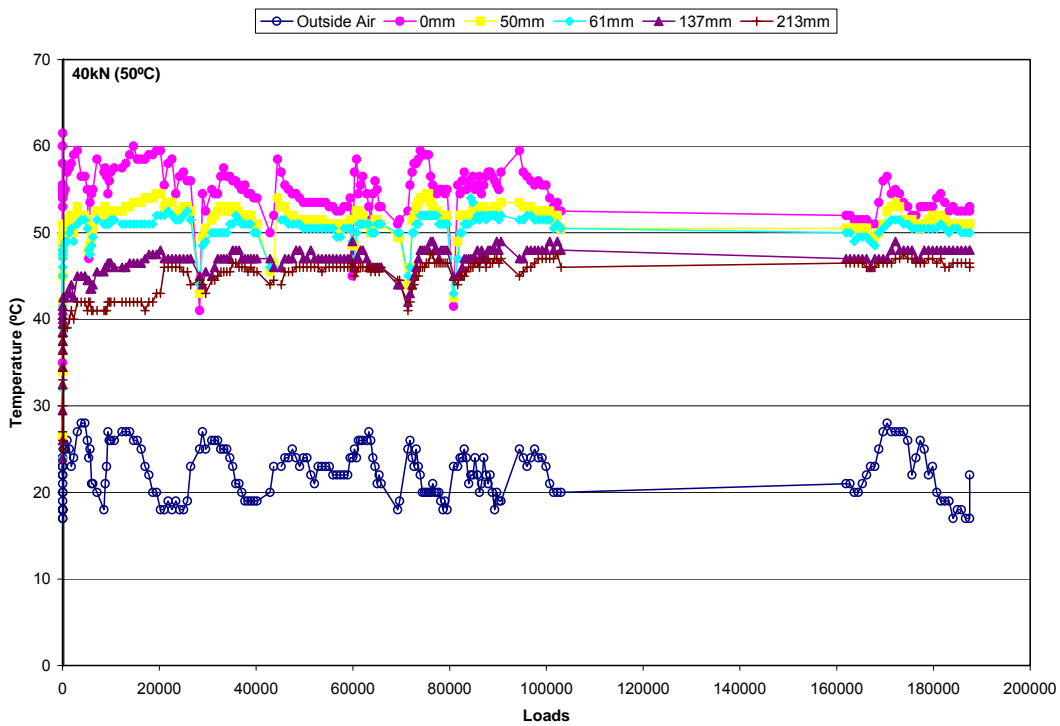


Figure 156. Section 509RF temperatures during testing.

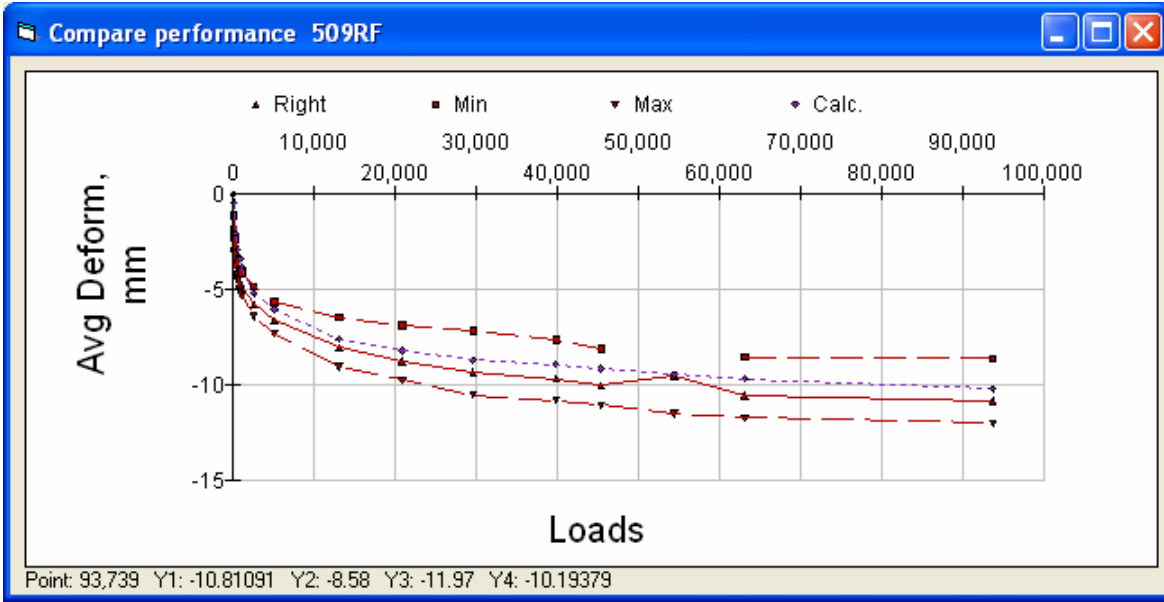


Figure 157. Section 509RF permanent deformation at pavement surface from profilometer.

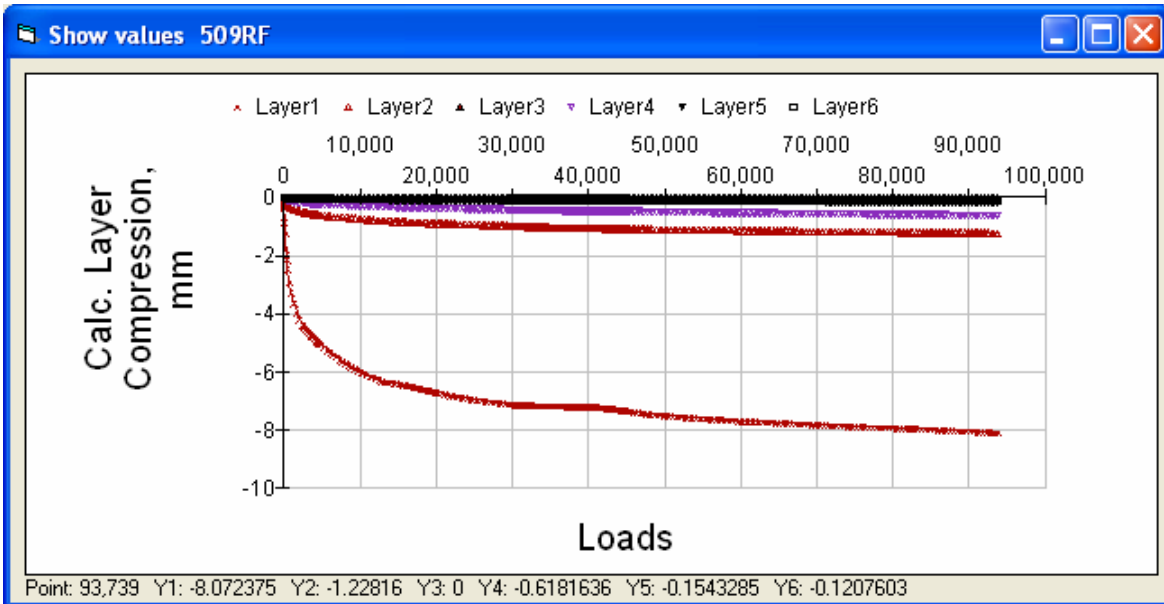


Figure 158. Section 509RF calculated permanent deformation of pavement layers.

4.7 Section 510RF ARHM Overlay, Radial Dual Tire

510RFpu structural data

Design methods Tools Change WIM Parameters

S

mm MPa

Layer	Material	Thick	Modulus	Poisson	R	GF	Cost/m3
1	RAC-GHVSRg	38	4755.0	0.35	0	1.46	134
2	DGACVHVSG1TRg	68	9055.0	0.35	0	1.46	114
3	DGACVHVSG1BRg	80	11189.0	0.35	0	1.46	114
4	ATPB-ACHVSR	75	1143.5	0.35	0	1.4	82
5	ABHVS	183	252	0.35	78	1.1	57
6	AS2HVS	253	240	0.35	50	1	30
7	ClayHVS	0	140	0.35	20	0	0

Figure 159. Section 510RF pavement structure.

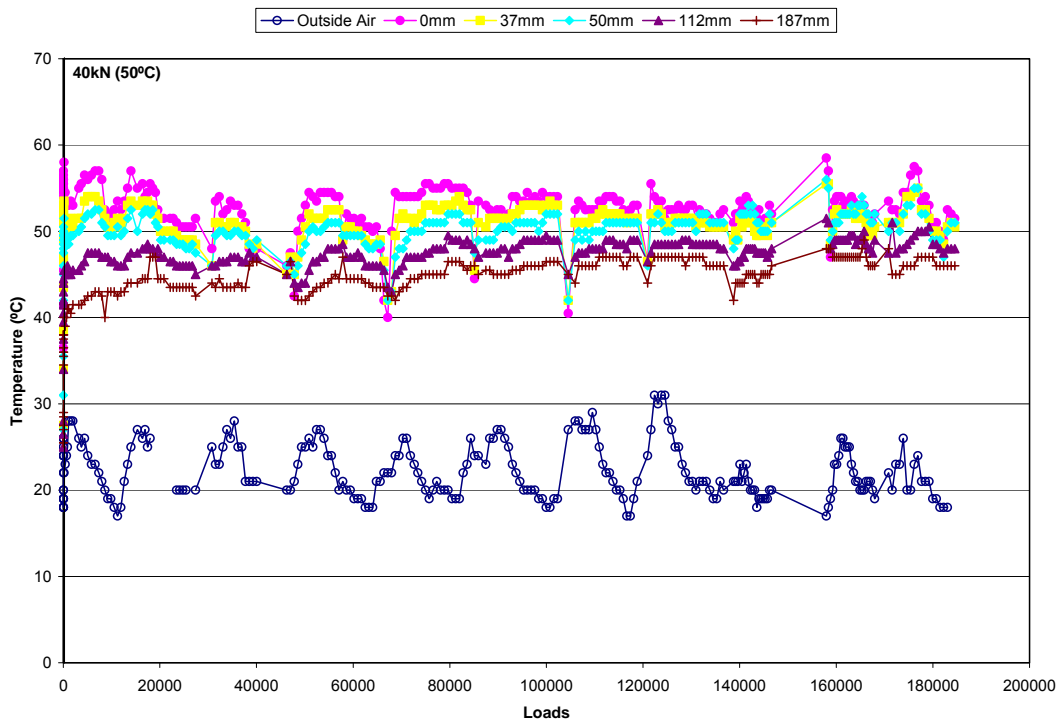


Figure 160. Section 510RF temperatures during testing.

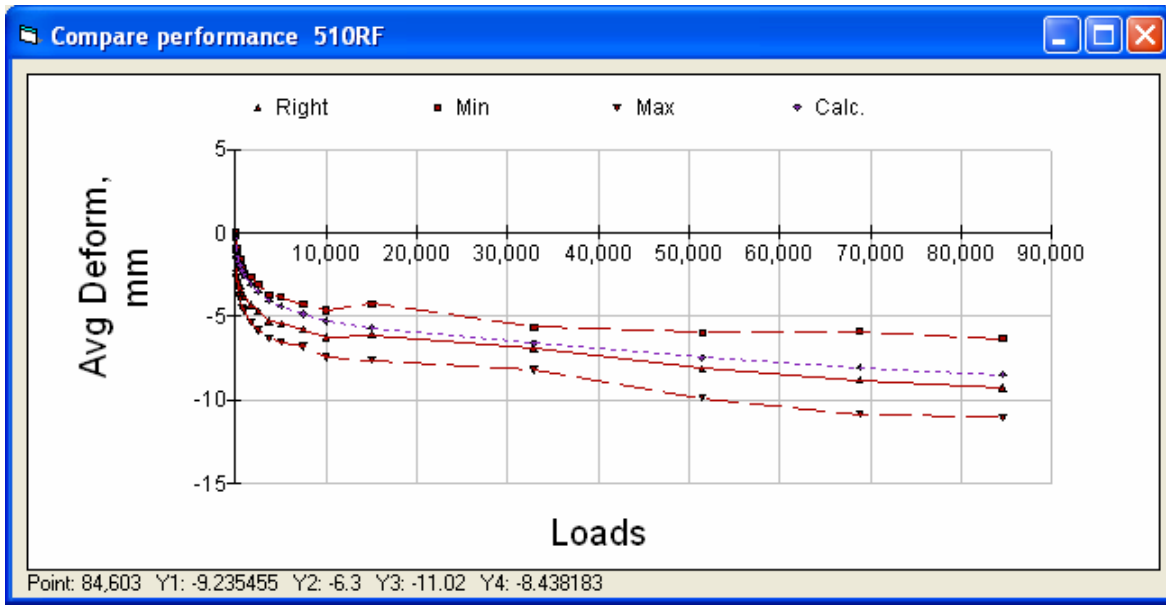


Figure 161. Section 510RF permanent deformation at pavement surface from profilometer.

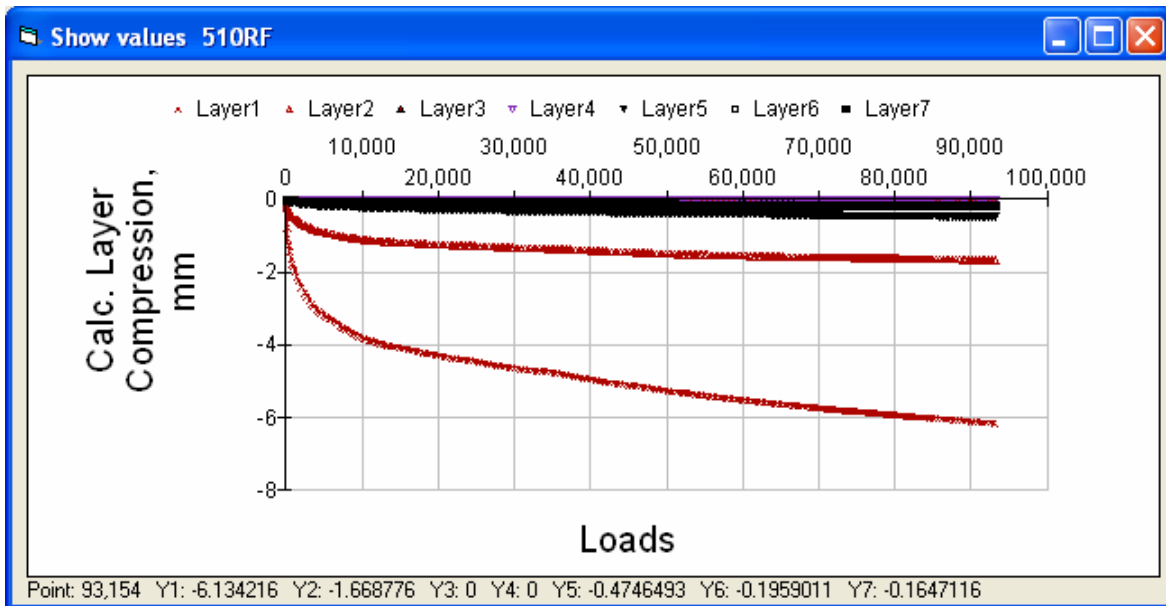


Figure 162. Section 510RF calculated permanent deformation of pavement layers.

4.8 Section 511RF ARHM Overlay, Wide-Base Single Tire

511RFpu structural data

Design methods Tools Change WIM Parameters

S

mm MPa

Layer	Material	Thick	Modulus	Poisson	R	GF	Cost/m3
1	RAC-GHVSRg	40	4755	0.35	0	1.46	134
2	DGACVHVSG1TRg	68	9055	0.35	0	1.46	114
3	DGACVHVSG1BRg	80	11189	0.35	0	1.46	114
4	ATPB-ACHVSR	75	1143.5	0.35	0	1.4	82
5	ABHVS	183	255	0.35	78	1.1	57
6	AS2HVS	276	243	0.35	50	1	30
7	ClayHVS	0	148	0.35	20	0	0

Figure 163. Section 511RF pavement structure.

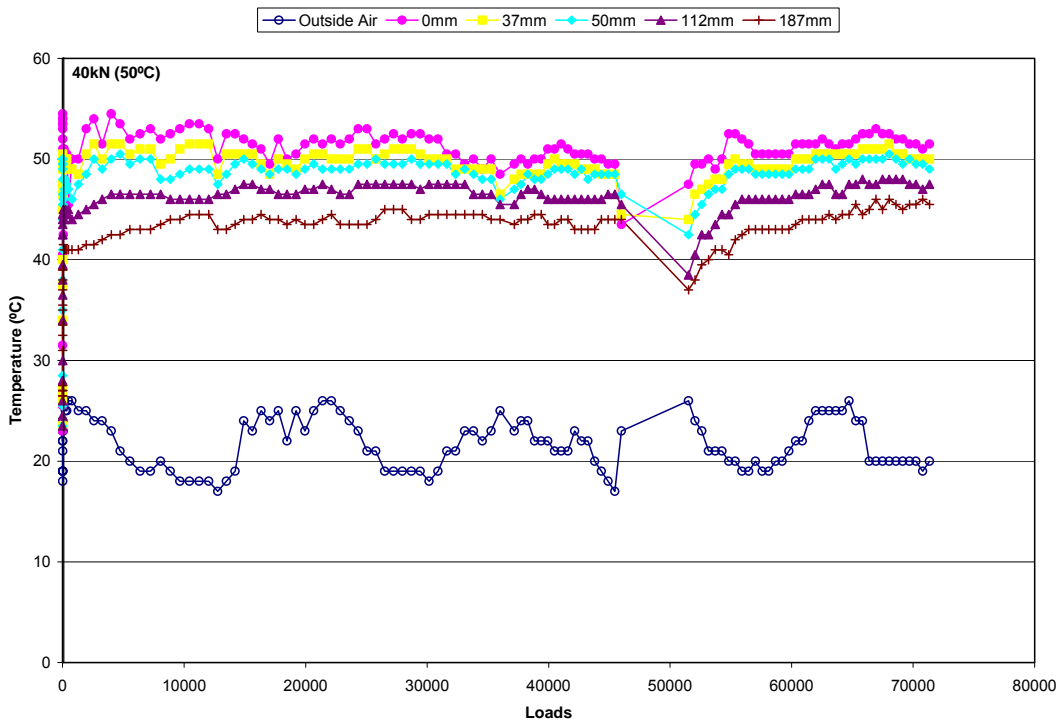


Figure 164. Section 511RF temperatures during testing.

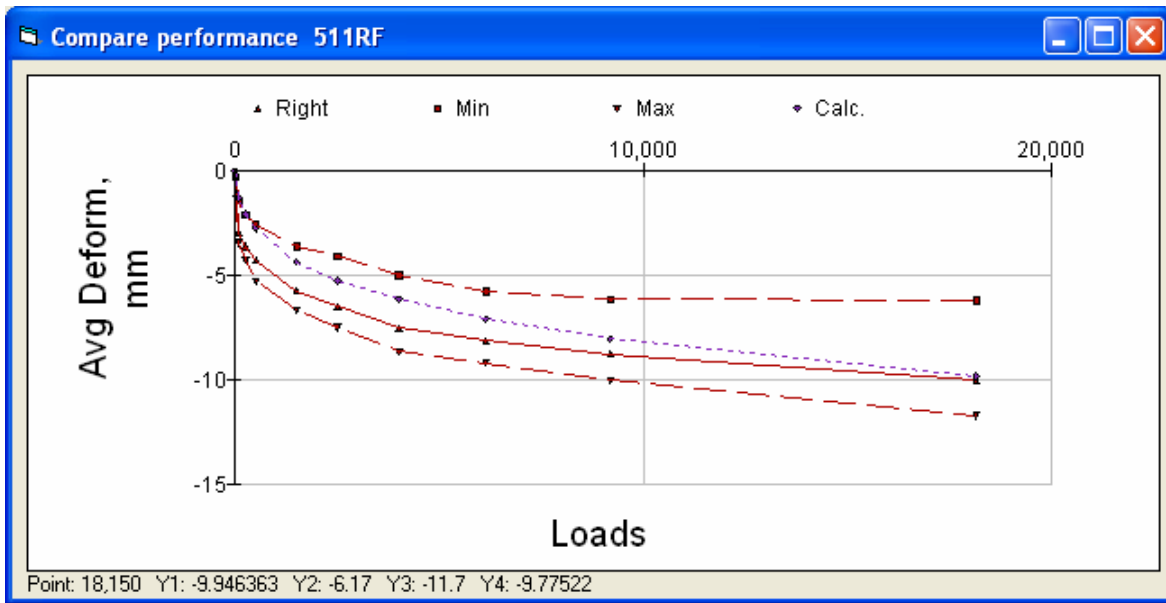


Figure 165. Section 511RF permanent deformation at the pavement surface.

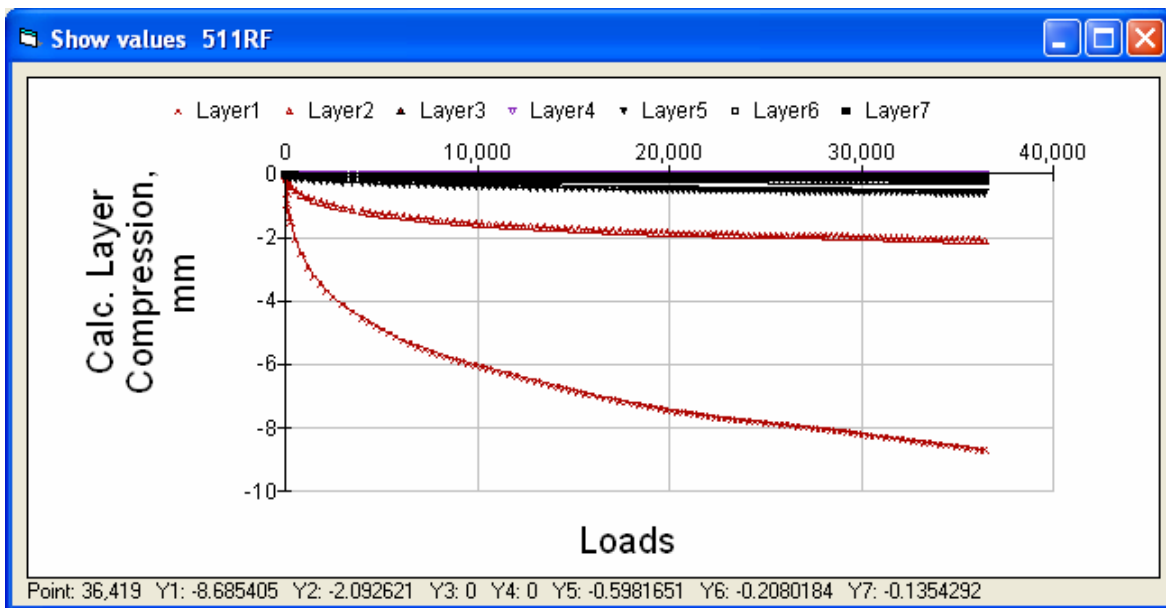


Figure 166. Section 511RF calculated permanent deformation of the pavement layers.

4.9 Section 512RF DGAC Overlay, Wide-Base Single Tire

512RFpu structural data

Design methods Tools Change WIM Parameters

S

mm MPa

Layer	Material	Thick	Modulus	Poisson	R	GF	Cost/m3
1	DGACVHVSG3Rg	60	7653	0.35	0	1.46	114
2	DGACVHVSG1TRg	74	9055	0.35	0	1.46	114
3	DGACVHVSG1BRg	76	11189	0.35	0	1.46	114
4	ATPB-ACHVSR	75	1143.5	0.35	0	1.4	82
5	ABHVS	183	316	0.35	78	1.1	57
6	AS2HVS	230	304	0.35	50	1	30
7	ClayHVS	0	169	0.35	20	0	0

Figure 167. Section 512RF pavement structure.

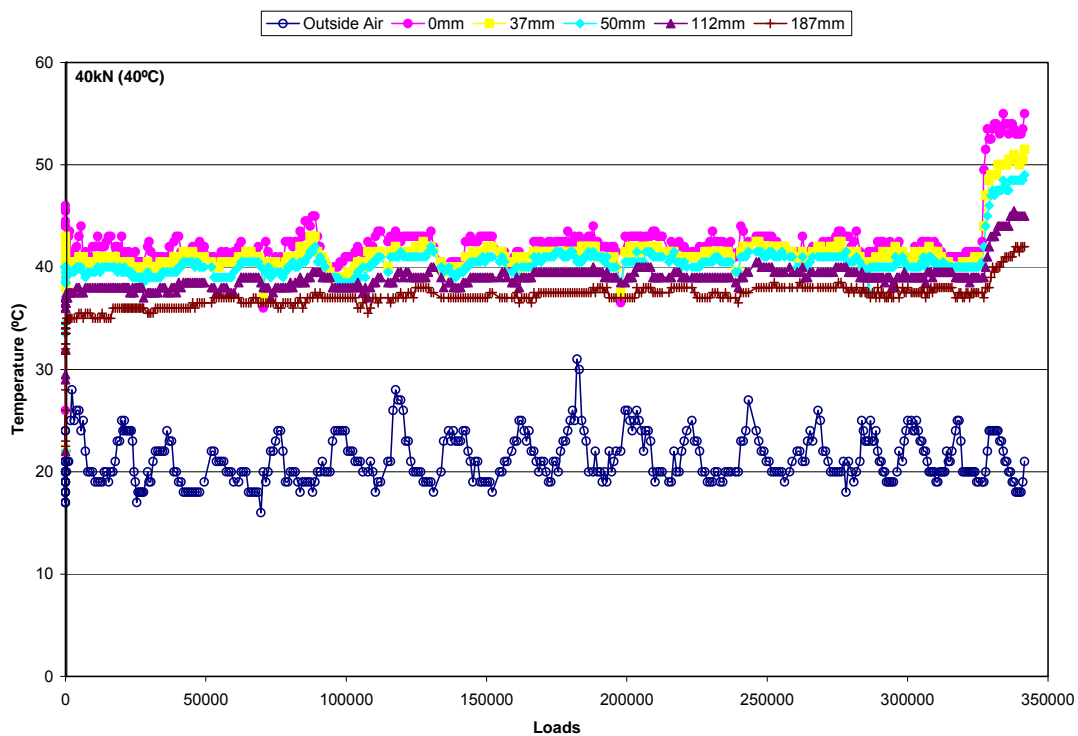


Figure 168. Section 512RF temperatures during testing.

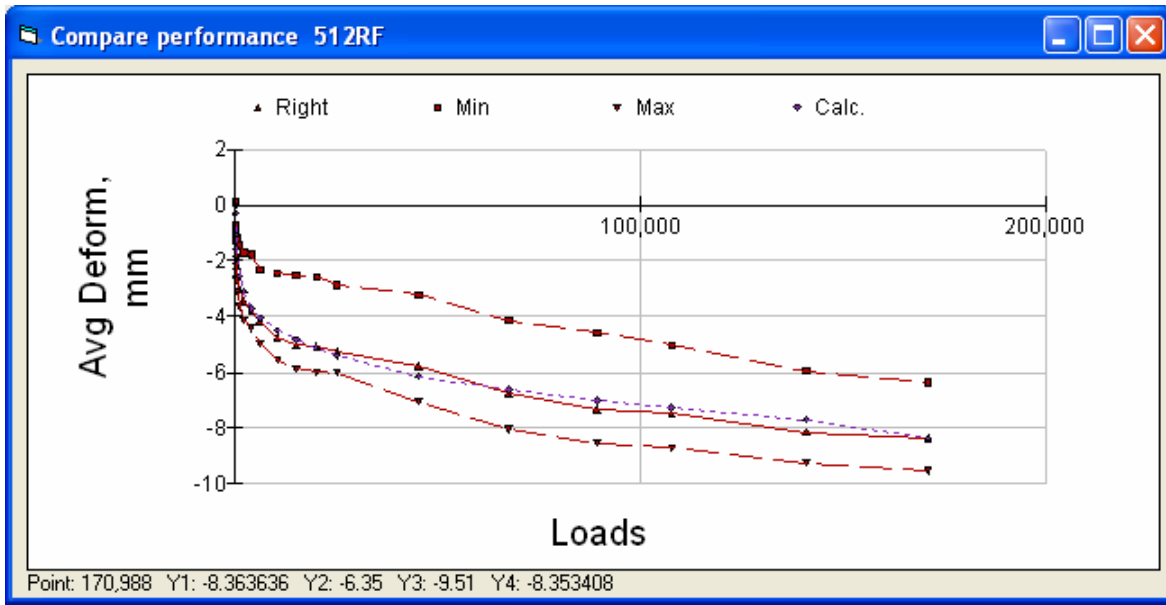


Figure 169. Section 512RF permanent deformation at pavement surface from profilometer.

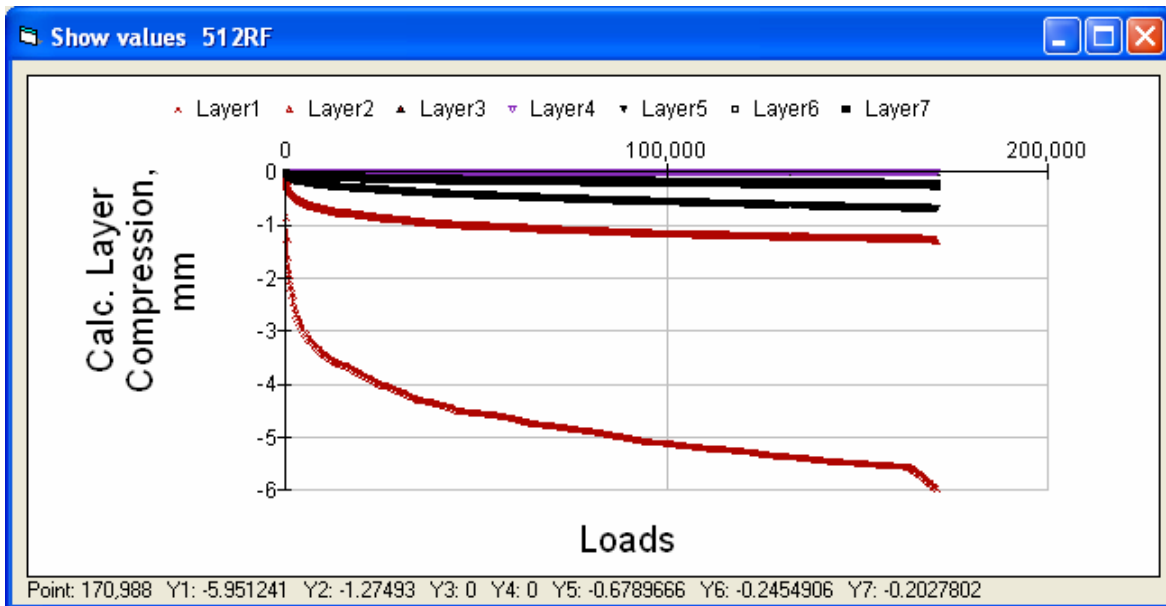


Figure 170. Section 512RF calculated permanent deformation of the pavement layers.

4.10 Section 513RF DGAC Overlay, Aircraft Tire

Layer	Material	Thick	Modulus	Poisson	R	GF	Cost/m3
1	DGACVHVSG3Rg	62	7653	0.35	0	1.46	114
2	DGACVHVSG1TRg	63	9055	0.35	0	1.46	114
3	DGACVHVSG1BRg	84	11189	0.35	0	1.46	114
4	ABHVS	274	231	0.35	78	1.1	57
5	AS2HVS	243	268	0.35	50	1	30
6	ClayHVS	0	153	0.35	20	0	0

Figure 171. Section 513RF pavement structure.

Temperature data was not available in the database. The following temperatures were estimated from data in Harvey et al. (2000).

Table 25. Estimated Temperatures for Section 513RF

Depth, mm	0	25	50	75	100	125	150	175	200	225
Temperature, °C	51	49.5	48	44.5	43	41.5	40	39	37.5	37

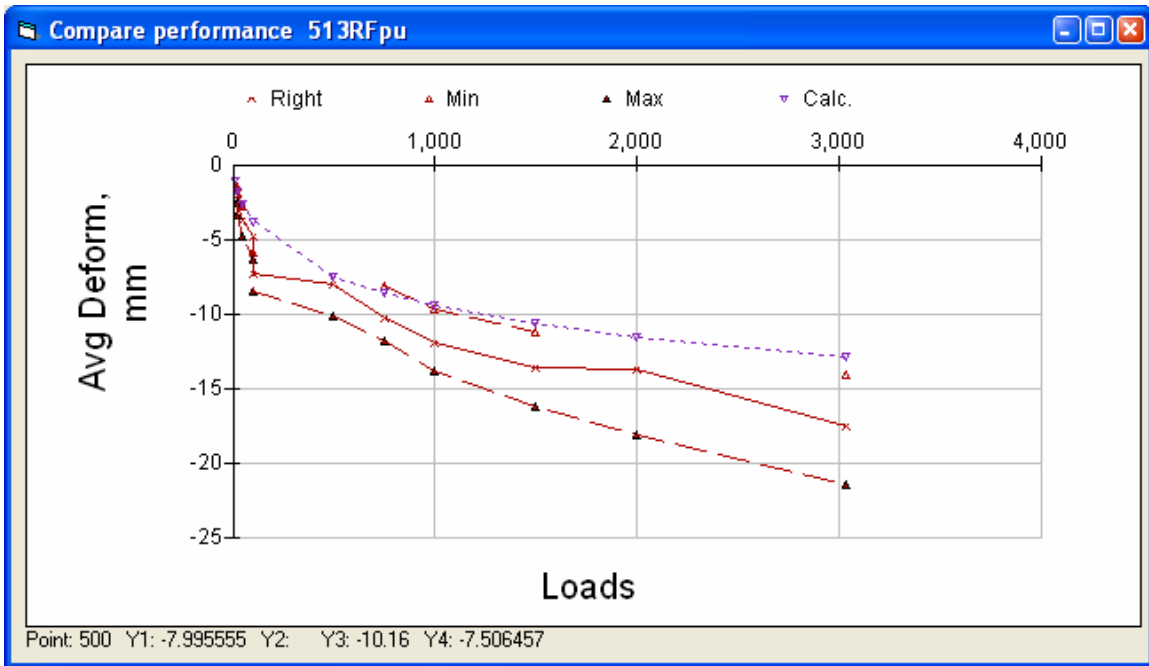


Figure 172. Section 513RF permanent deformation at pavement surface from profilometer.

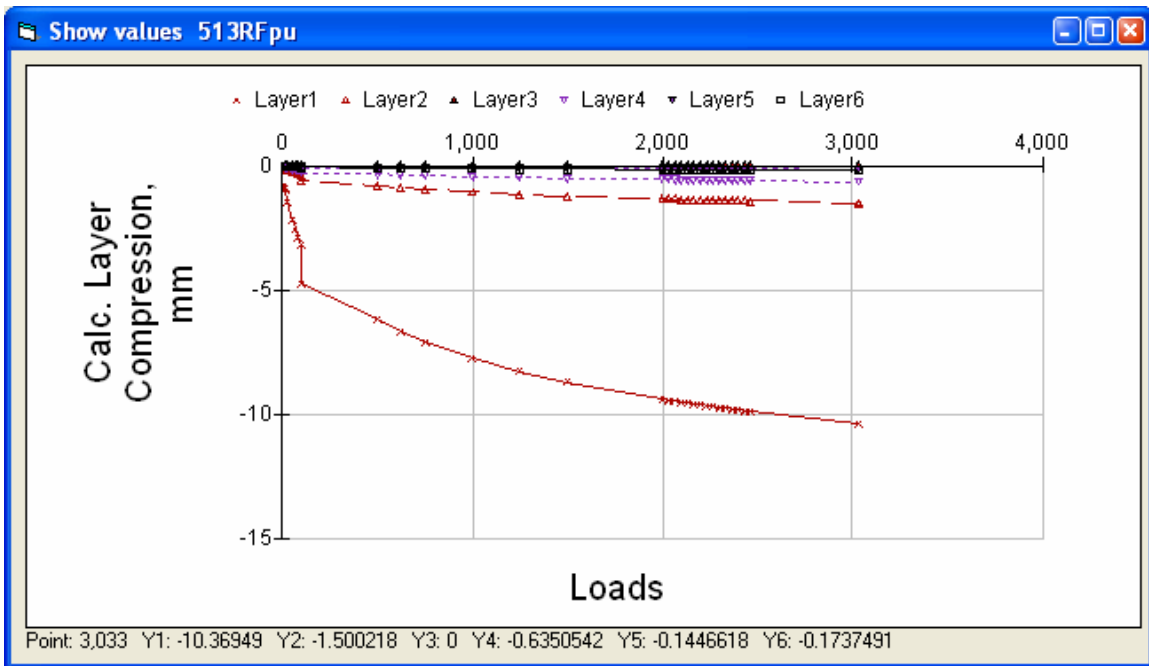


Figure 173. Section 513RF calculated permanent deformation of pavement layers.

5.0 GOAL 5 WET CONDITIONS

As Section 1 notes, in each of the Goal 5 tests water from a drip system was introduced into the HVS test section pavements. The water entered the pavements at the top of their base layers (either ATPB or aggregate) through holes drilled on the sections' upstream side.

In the simulations a slip was assumed to develop between the two AC layers of Goal 1 (as in the simulations of Goal 1 and Goal 3). There was clear evidence that slip also developed between the overlay and the AC top layer of Goal 1 at some locations, and that the ATPB of Section 543RF disintegrated (as shown Figure 174).

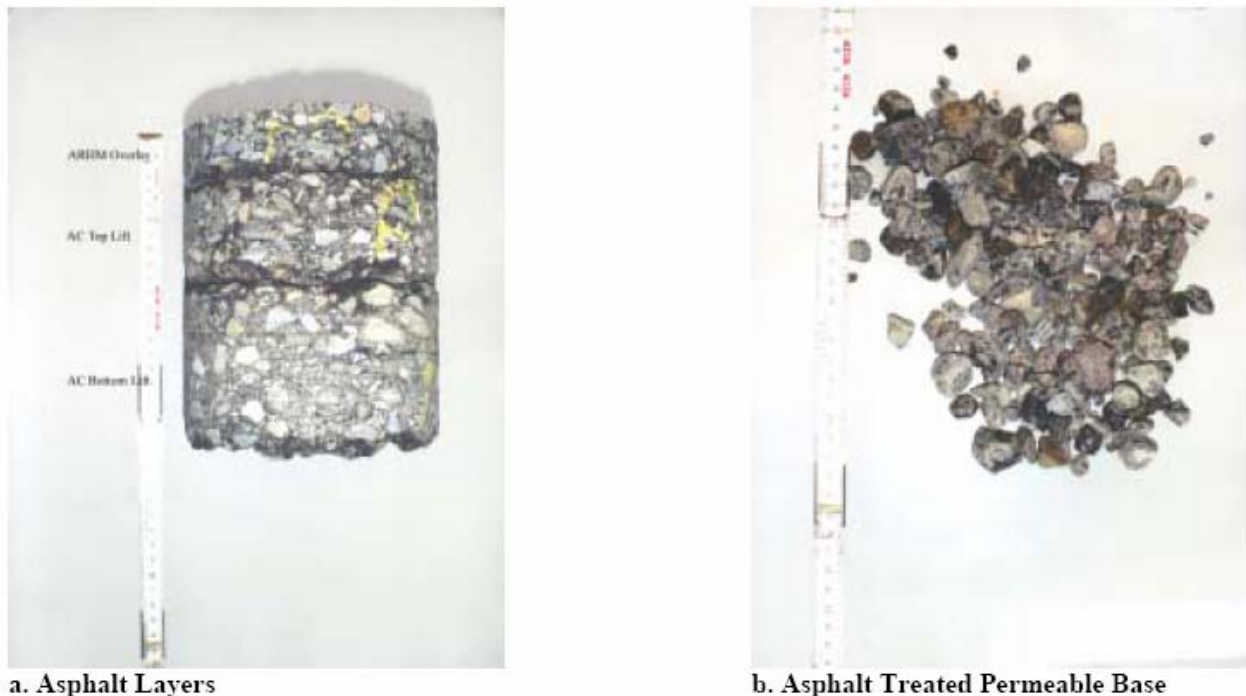


Figure 174. Cores from trafficked area of Section 543RF after HVS loading show stripping and disintegration of ATPB, as well as signs of moisture damage between the the three lifts of asphalt concrete (Bejarano et al. 2003).

To get reasonably good agreement between calculated and measured deflections, the stiffness factors of the unbound materials, previously discussed in Section 1.5.2 of this report (see Equations 17 and 18) were assumed to be 0.55, 0.45, and 0.3 for AB, ASB, and subgrade, respectively. These are the same values used during Goal 1 and Goal 3 for simulations with full bond. It would have been more consistent for the research team to use the same stiffness factor values that it did when simulating slip conditions in Goal 1 and Goal 3 (although the wet conditions could have resulted in different values than the dry condition). However, several attempts to combine those values with different slips at different interfaces failed to produce reasonably good agreement between the measured and calculated responses. This could be due to the difficulty of simulating the correct slip conditions. The above values were used instead because of the importance of having the correct response for calibrating fatigue and permanent deformation parameters.

Only a few Multi-depth Deflectometer (MDD) modules functioned correctly during the wet testing. The moduli of the unbound layers were chosen to give a reasonably good agreement with the initial deflections measured with these MDDs and with the Road Surface Deflectometer (RSD). For the asphalt layers the same moduli were used as in the previous simulations, i.e., from frequency sweep data. The asphalt fatigue models and the permanent deformation models were also the same as in the previous simulations.

5.1 Section 543RF ARHM Overlay, Drained

Figure 175 shows the pavement structure for Section 543RF. It was assumed that a slip developed between layer 2 and layer 3 at 8 million ESALs (corresponding to approximately 600,000 load repetitions using the Caltrans 4.2 exponent). The models did not do well calculating the permanent deformation of the ATPB and the granular base after the stripping and collapse of the ATPB at about 600,000 repetitions. The modeled pavement appears to have simulated response and performance prior to the collapse fairly well.

Layer	Material	Thick	Modulus	Poisson	R	GF	Cost/m3
1	RAC-GHVSg	37	4755	0.35	0	1.46	134
2	DGACVHVSG1Tg	70	9038	0.35	0	1.46	114
3	DGACVHVSG1Bg	71	11173	0.35	0	1.46	114
4	ATPB-ACHVS	75	1143.8	0.35	0	1.4	82
5	ABHVS5	181	230	0.35	78	1.1	57
6	AS2HVS5	187	218	0.35	50	1	30
7	ClayHVS5	0	205	0.35	20	0	0

Figure 175. Section 543RF pavement structure.

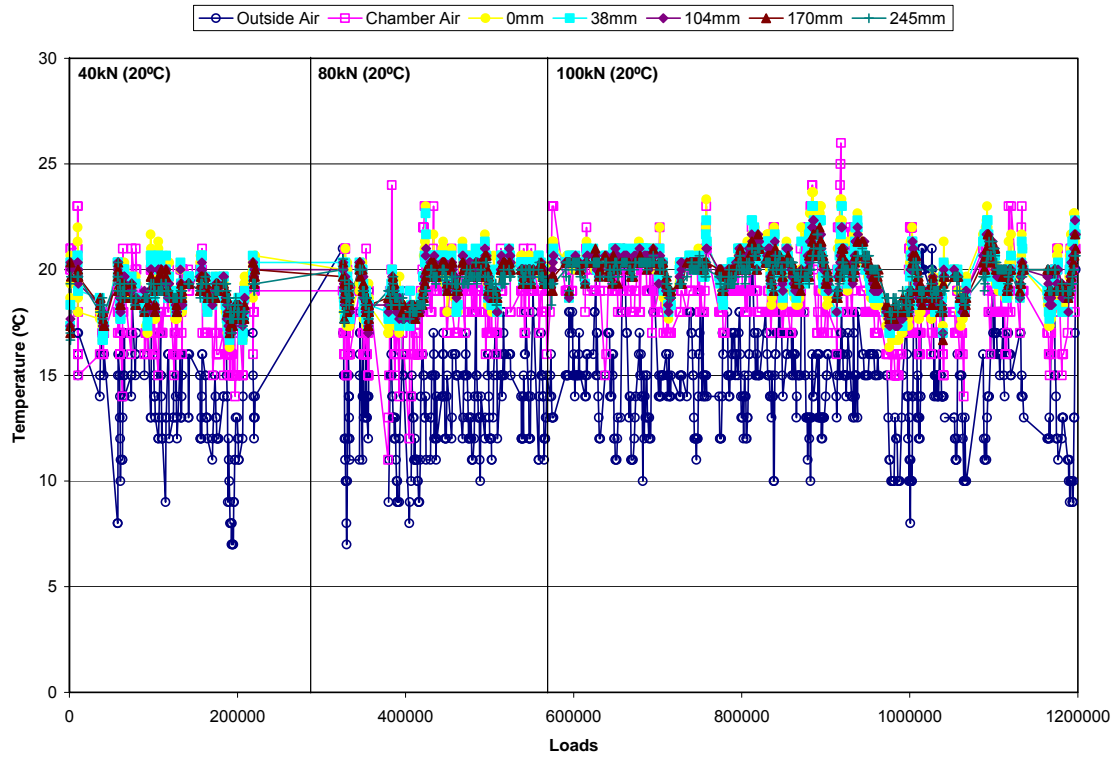


Figure 176. Section 543RF temperatures during testing.



Figure 177. Section 543RF Road Surface Deflectometer, at 40 kN.

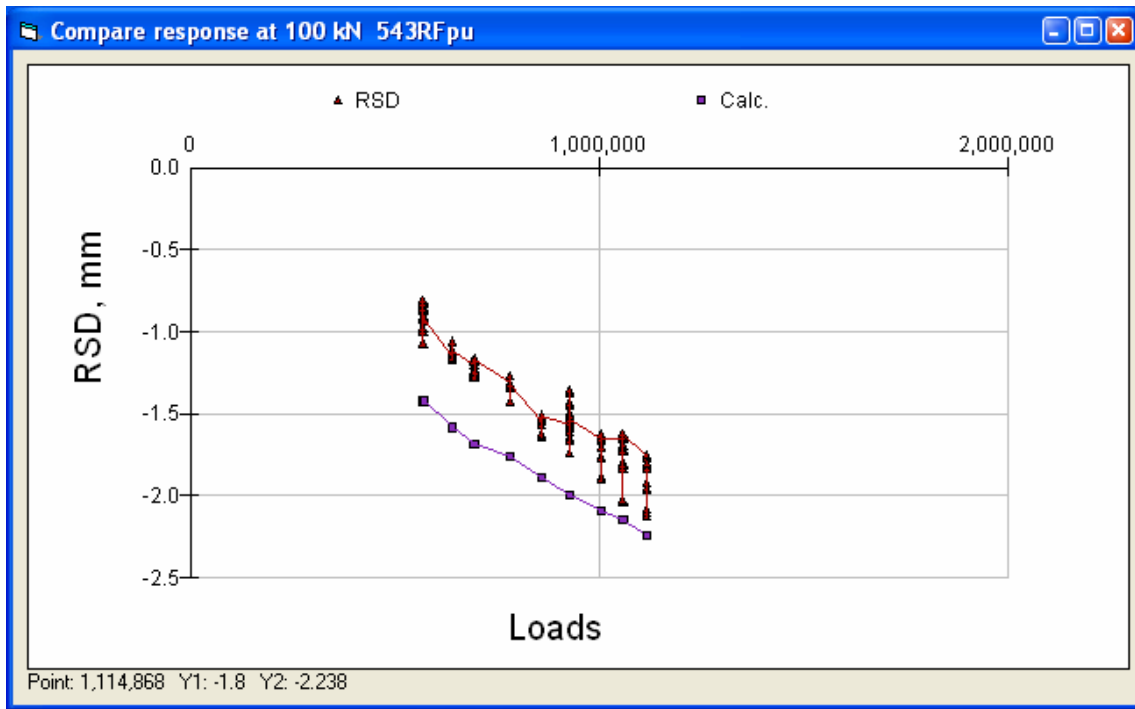


Figure 178. Section 543RF Road Surface Deflectometer, at 100 kN.

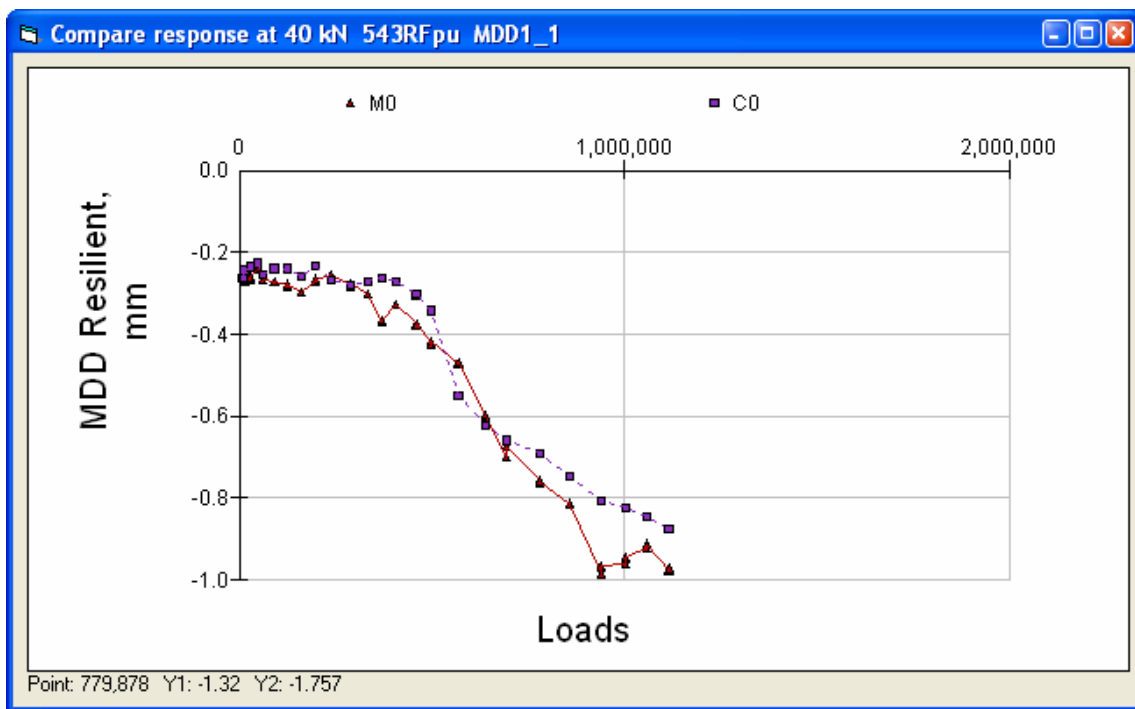


Figure 179. Section 543RF 40 kN top module.

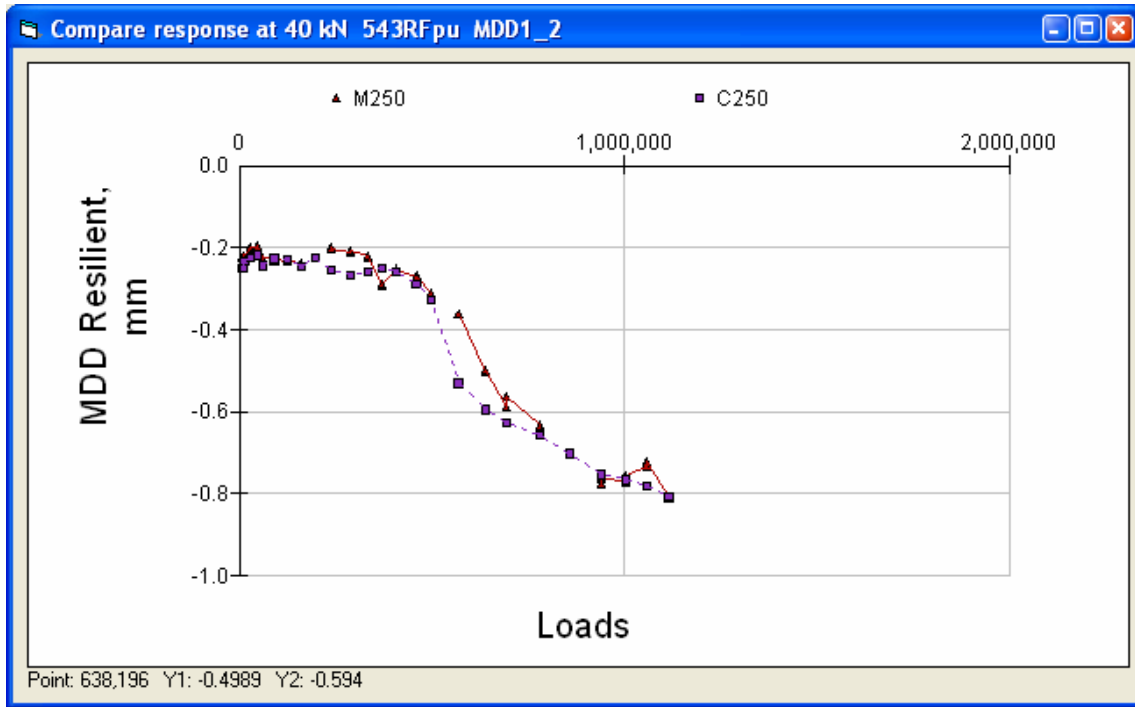


Figure 180. Section 543RF 40 kN top of aggregate base.

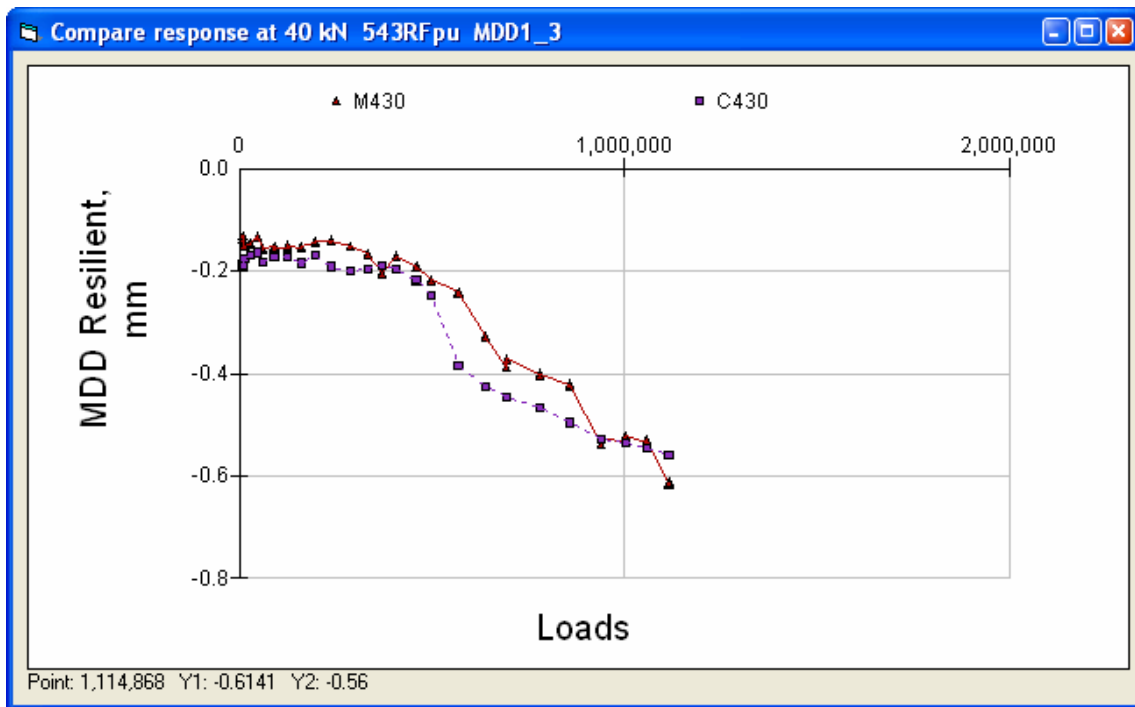


Figure 181. Section 543RF 40 kN top of aggregate subbase.

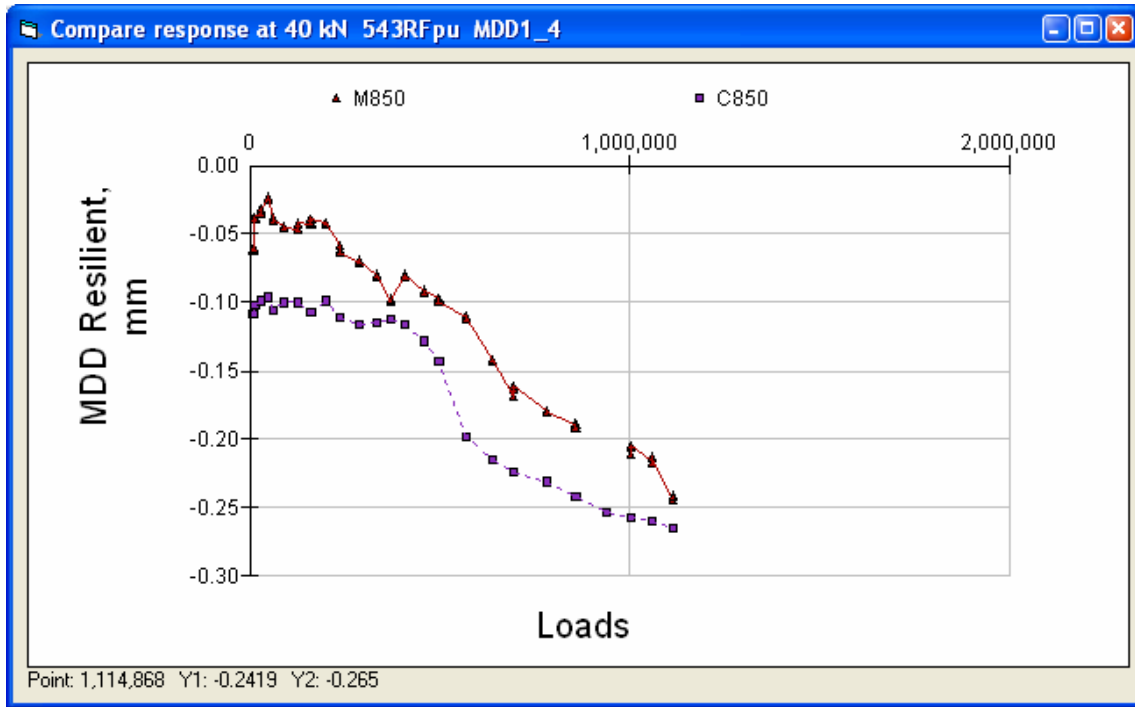


Figure 182. Section 543RF 40 kN deflection of subgrade (850 mm depth).

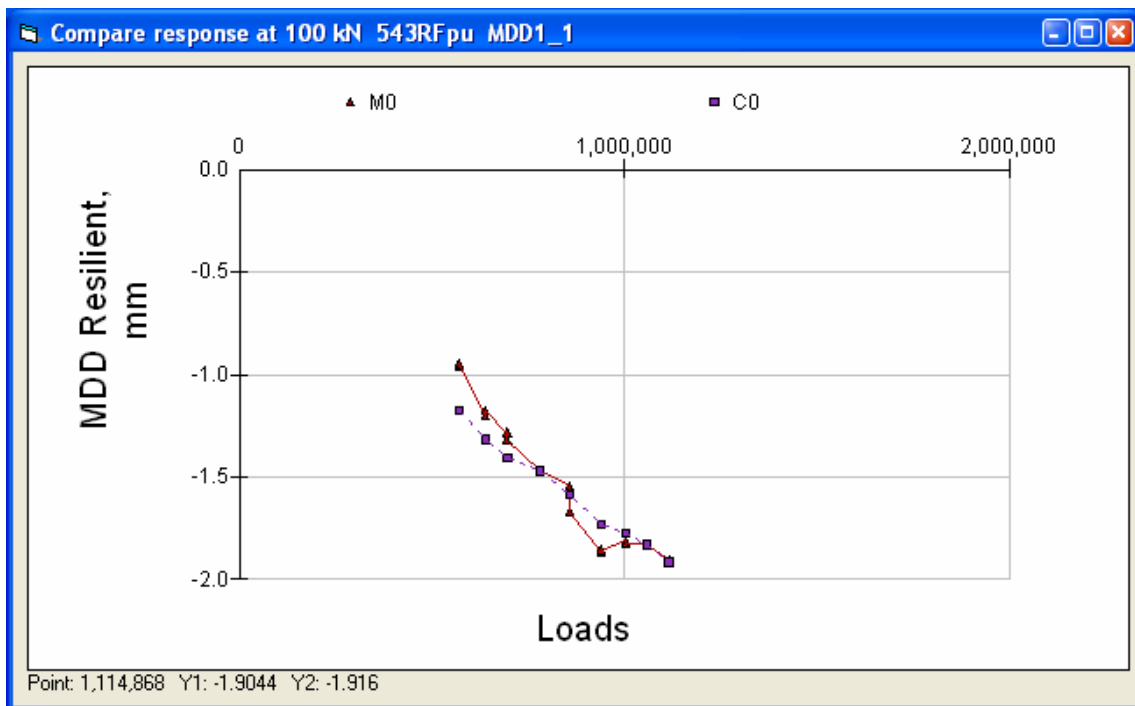


Figure 183. Section 543RF 100 kN top module.

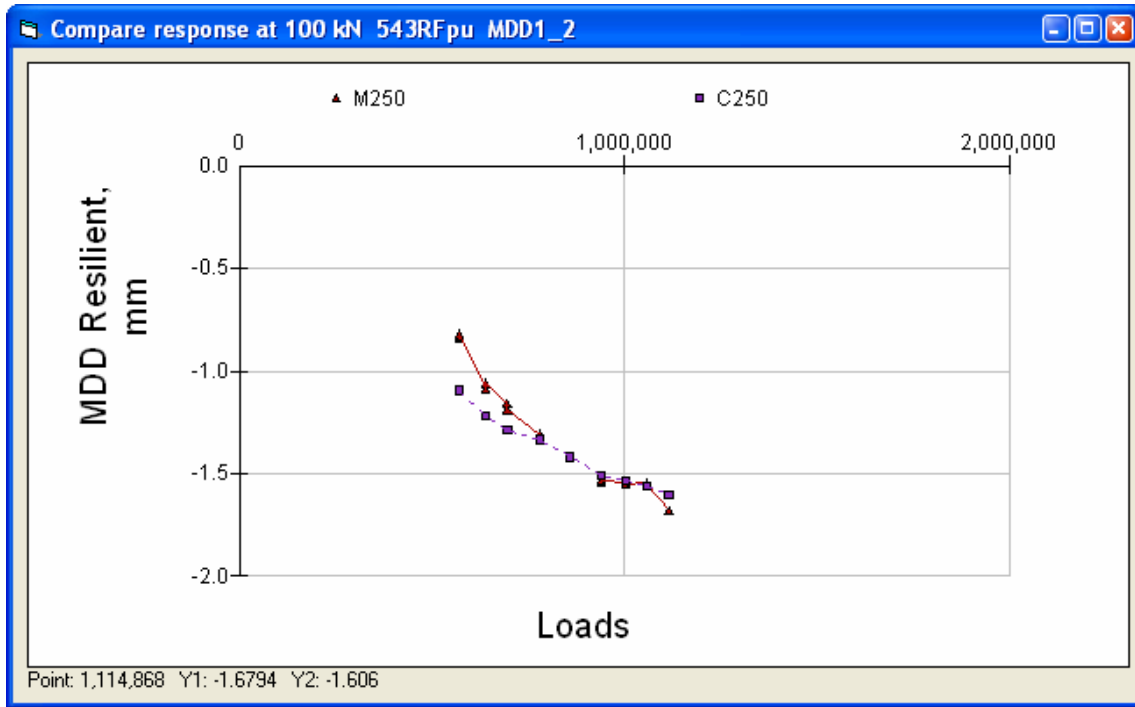


Figure 184. Section 543RF 100 kN top of aggregate base.

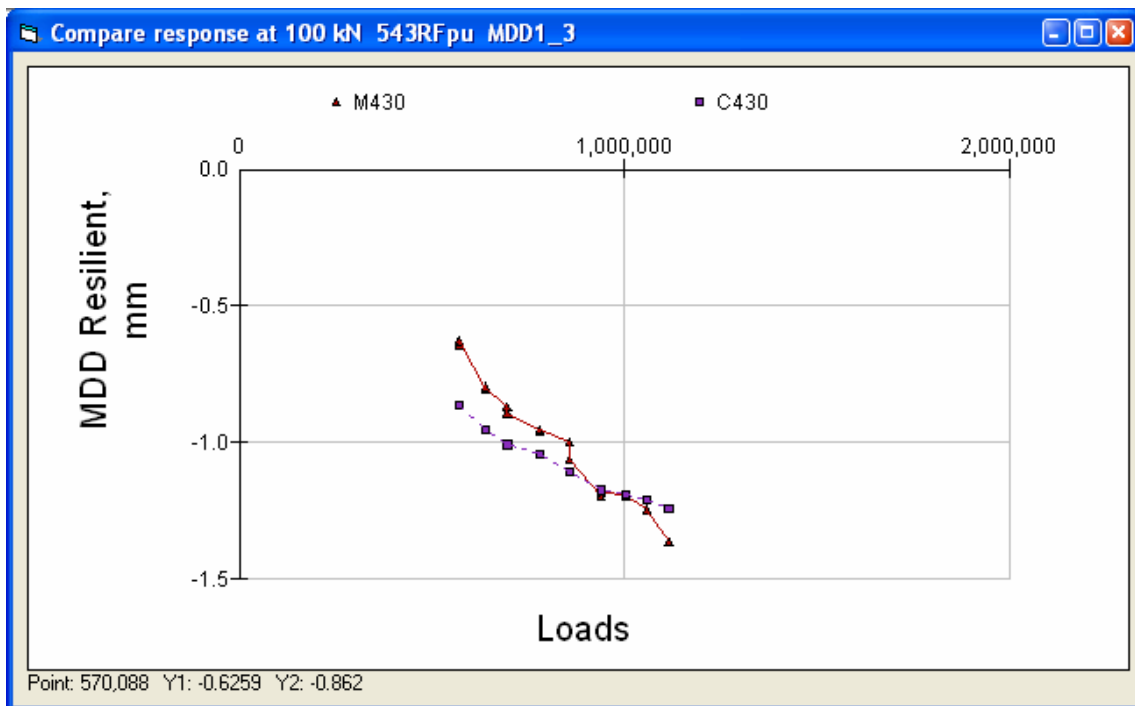


Figure 185. Section 543RF 100 kN top of aggregate subbase.

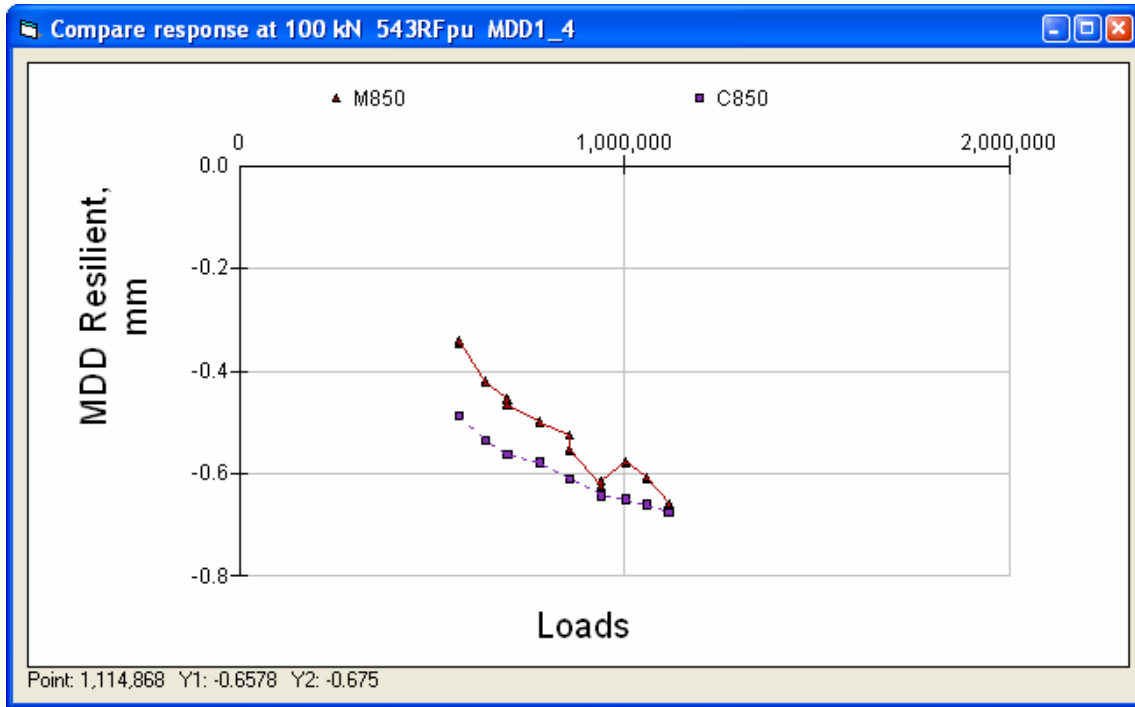


Figure 186. Section 543RF 100 kN deflection of subgrade (850 mm depth).

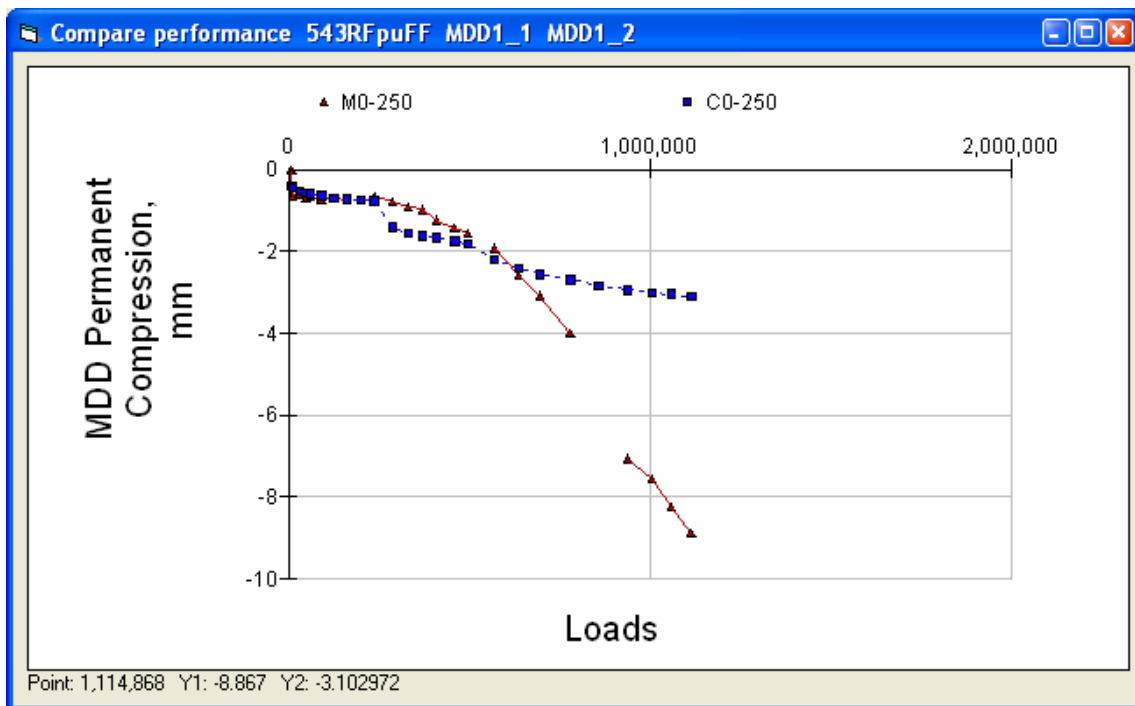


Figure 187. Section 543RF Permanent deformation of asphalt layers.

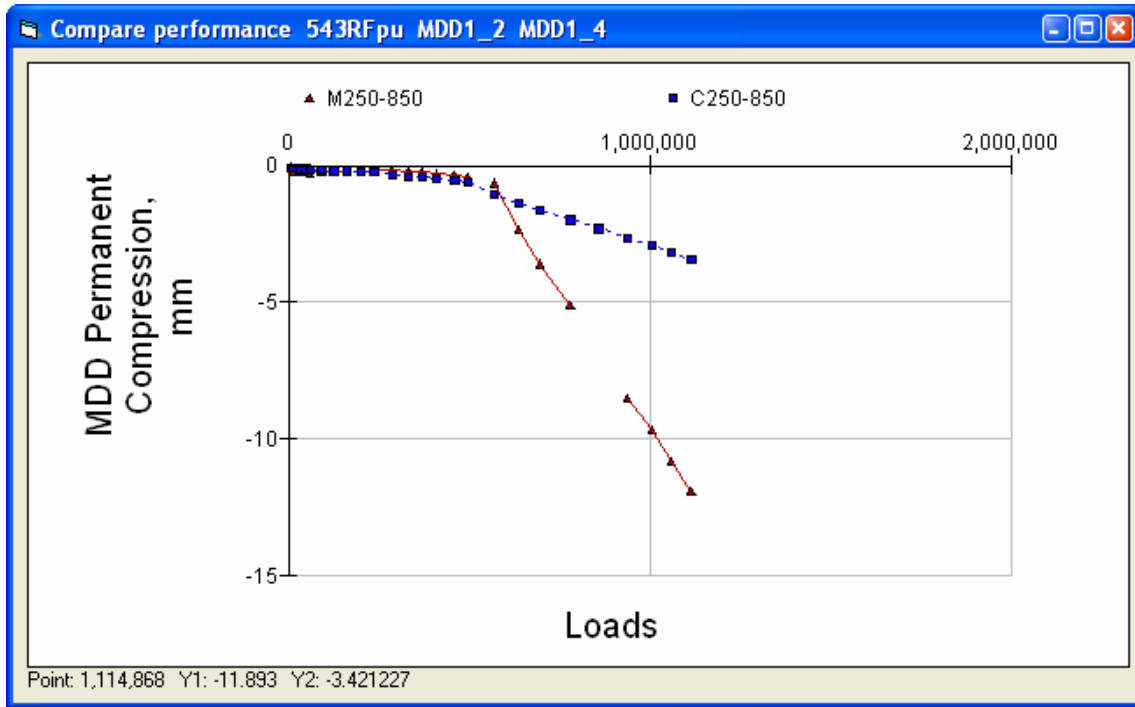


Figure 188. Section 543RF permanent deformation of granular layers plus top of subgrade.

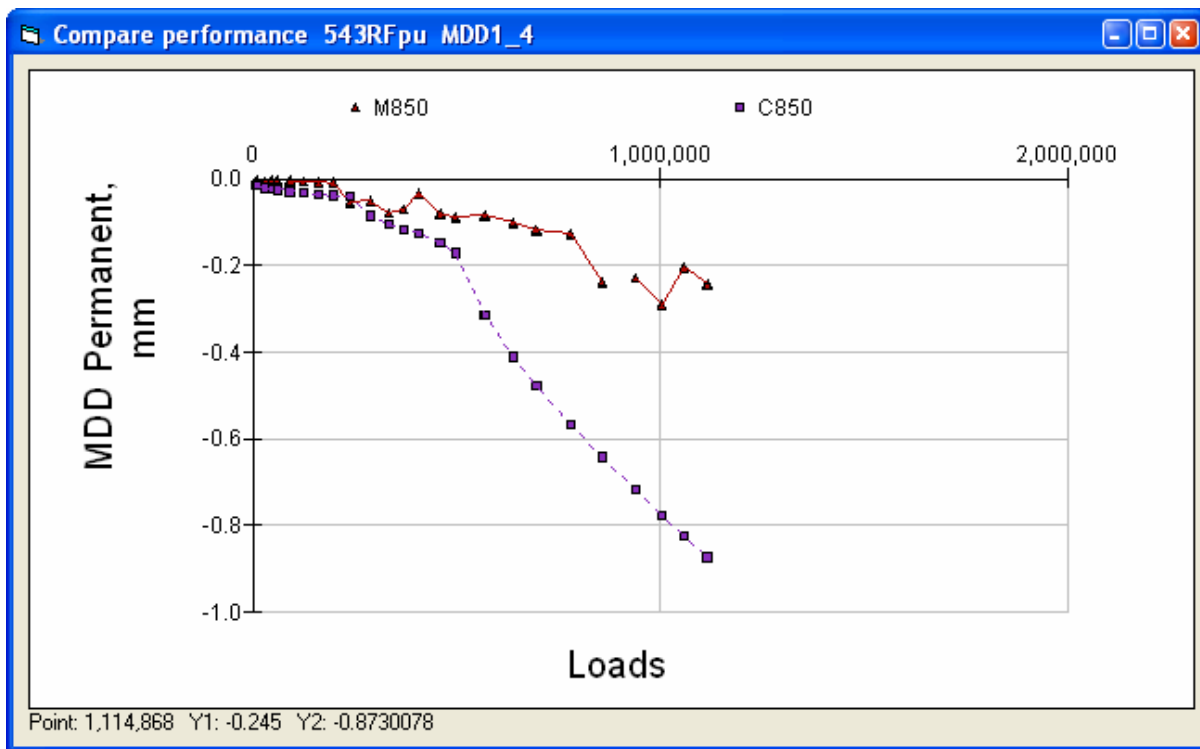


Figure 189. Section 543RF permanent deformation in subgrade (850 mm depth).

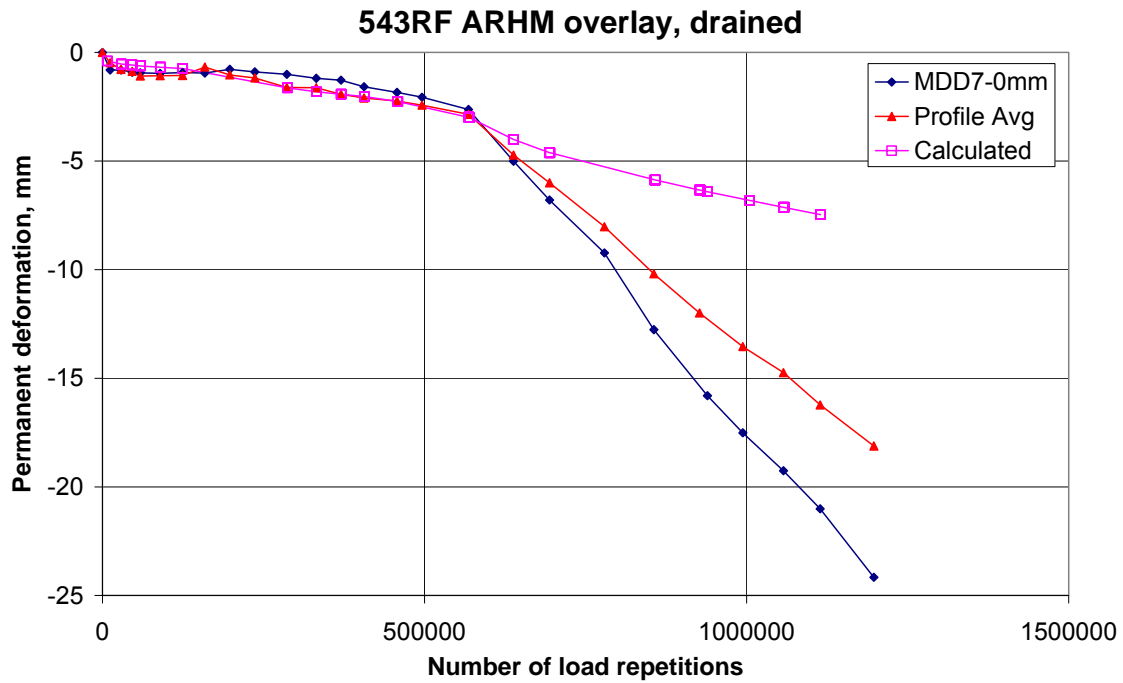


Figure 190. Section 543RF permanent deformation at pavement surface.

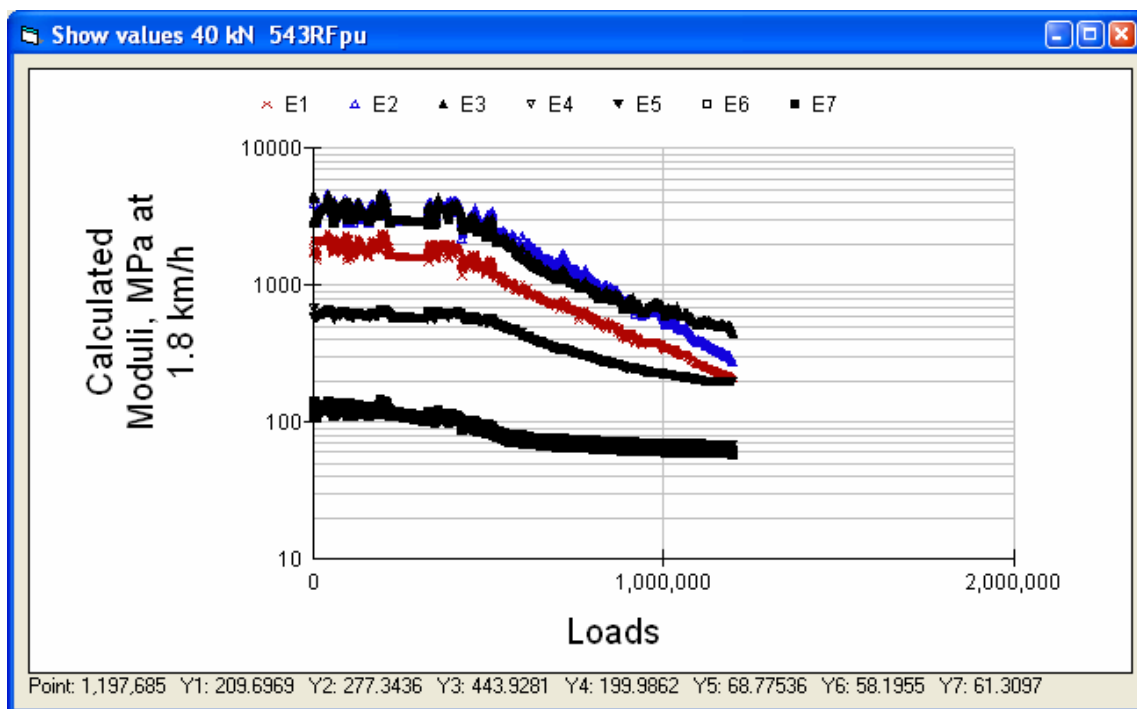


Figure 191. Section 543RF calculated layer moduli, at 40 kN and actual temperatures.

5.2 Section 544RF ARHM Overlay, Undrained

The pavement structure for Section 544RF is shown in Figure 192. Slip was assumed to develop between layer 2 and layer 3 at 2 million ESALs (corresponding to approximately 300,000 load repetitions).

Layer	Material	Thick	Modulus	Poisson	R	GF	Cost/m3
1	RAC-GHVSrg	51	4755	0.35	0	1.46	134
2	DGACVHVSG1TRg	74	9055	0.35	0	1.46	114
3	DGACVHVSG1BRg	75	11189	0.35	0	1.46	114
4	ABHVS5	272	198	0.35	78	1.1	57
5	AS2HVS5	258	233	0.35	50	1	30
6	ClayHVS5	0	168	0.35	20	0	0

Figure 192. Section 544RF pavement structure.

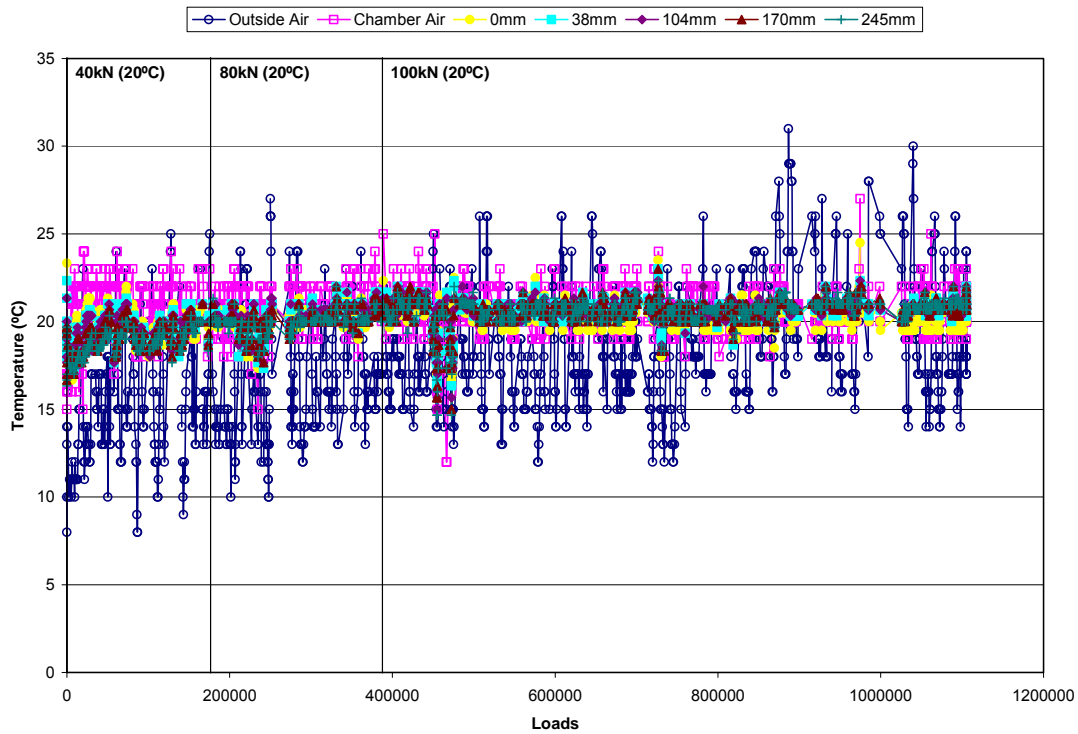


Figure 193. Section 544RF temperatures during testing.

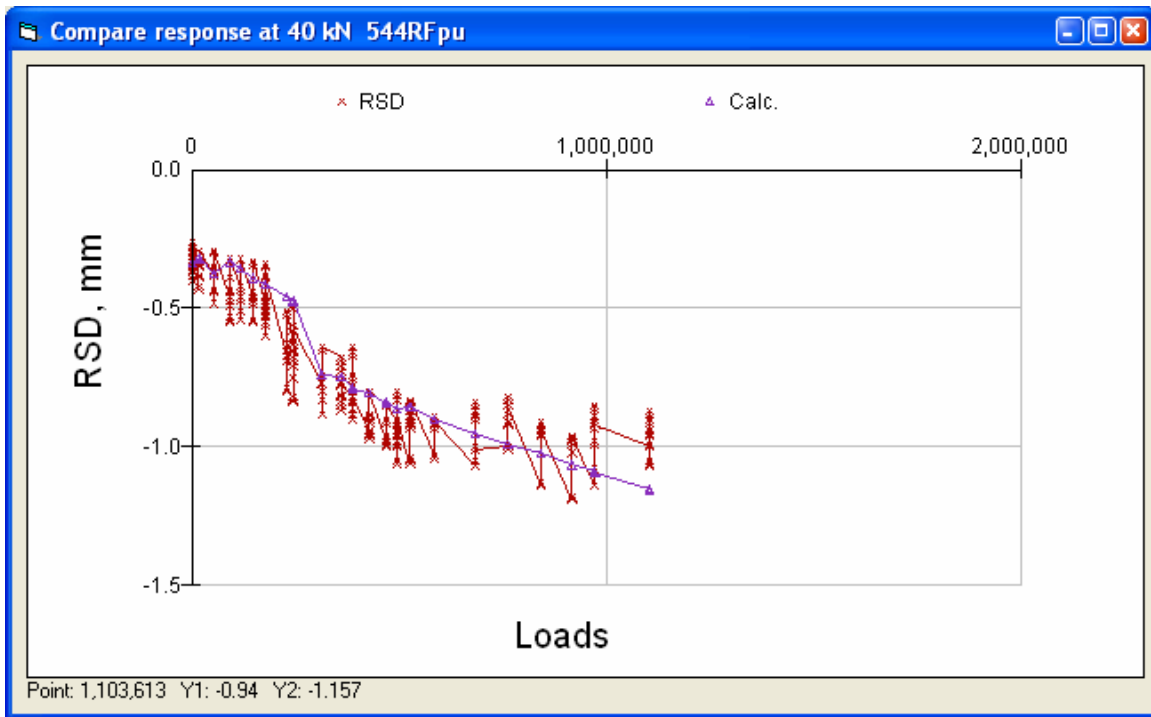


Figure 194. Section 544RF Road Surface Deflectometer, at 40 kN.

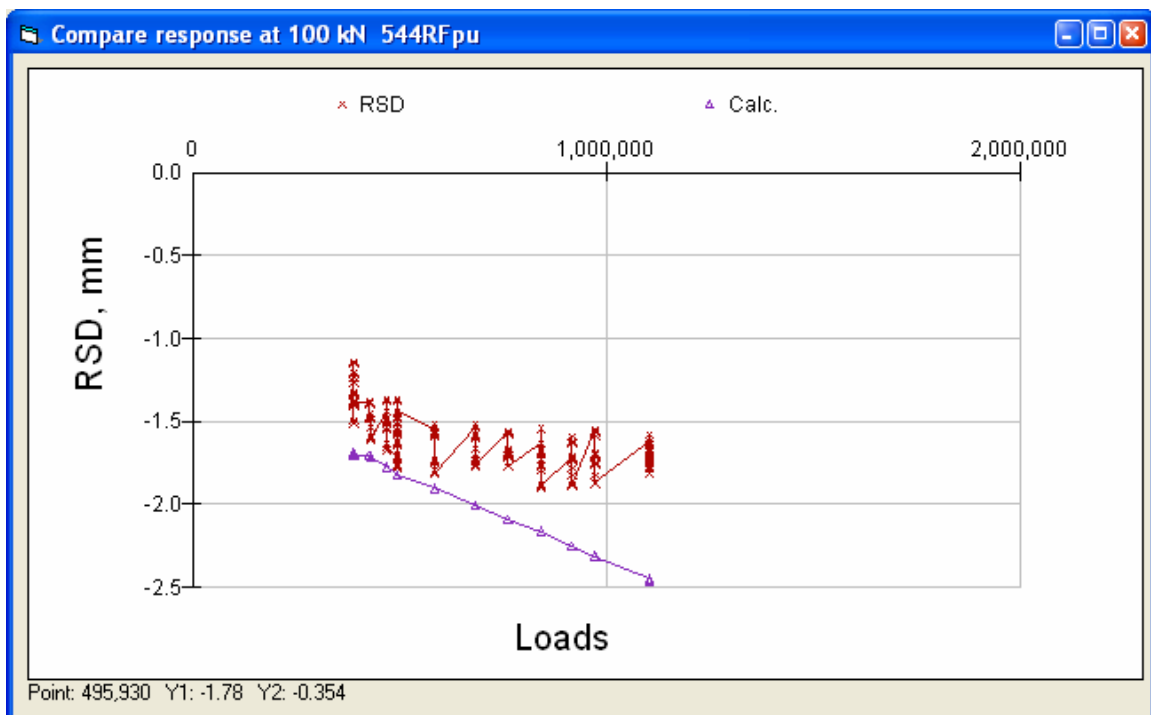


Figure 195. Section 544RF Road Surface Deflectometer, at 100 kN.

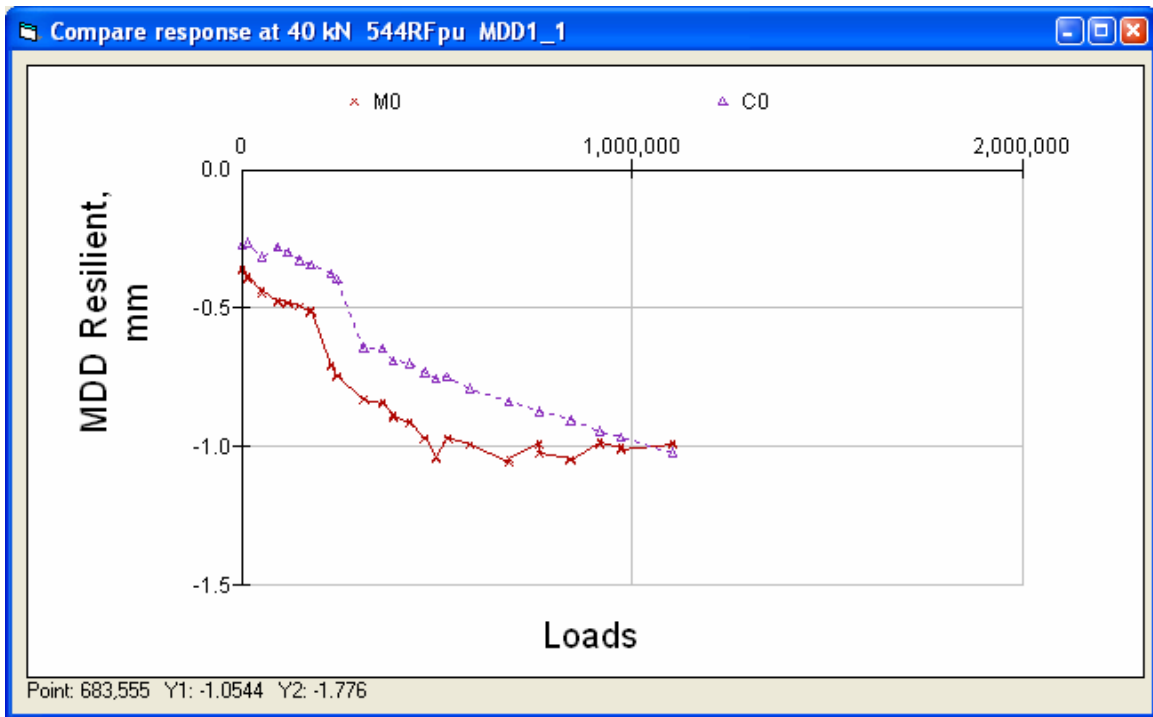


Figure 196. Section 544RF 40 kN top module.

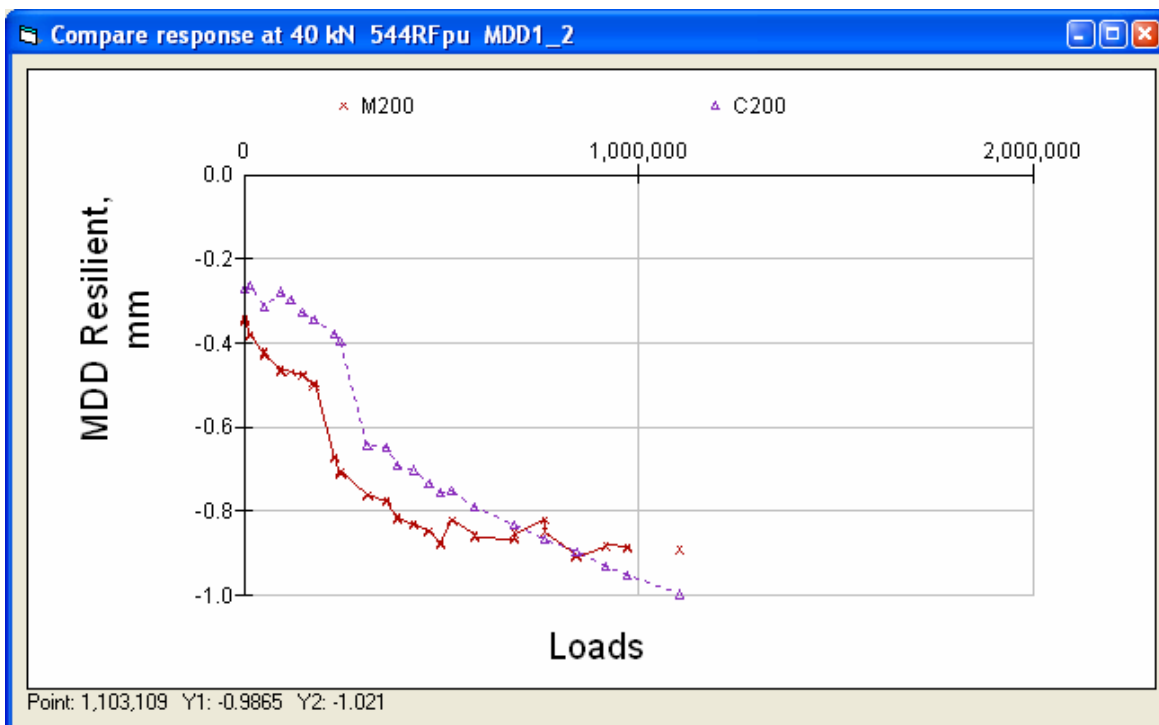


Figure 197. Section 544RF 40 kN top of aggregate base.

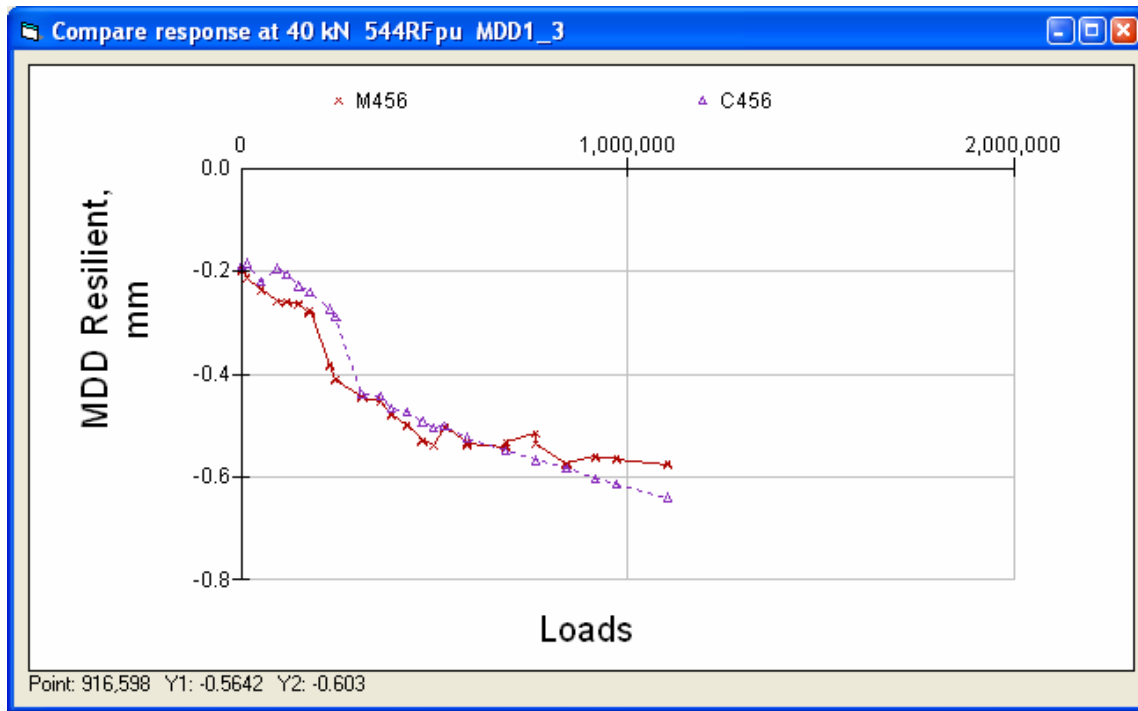


Figure 198. Section 544RF 40 kN top of aggregate subbase.

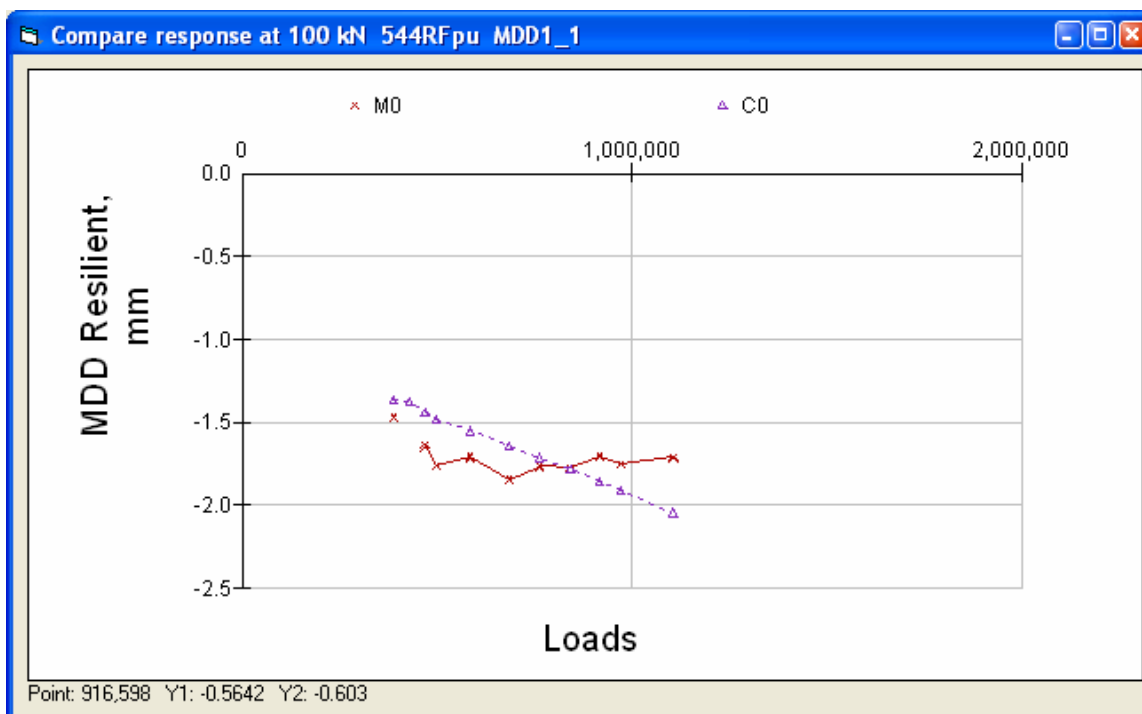


Figure 199. Section 544RF 100 kN top module.

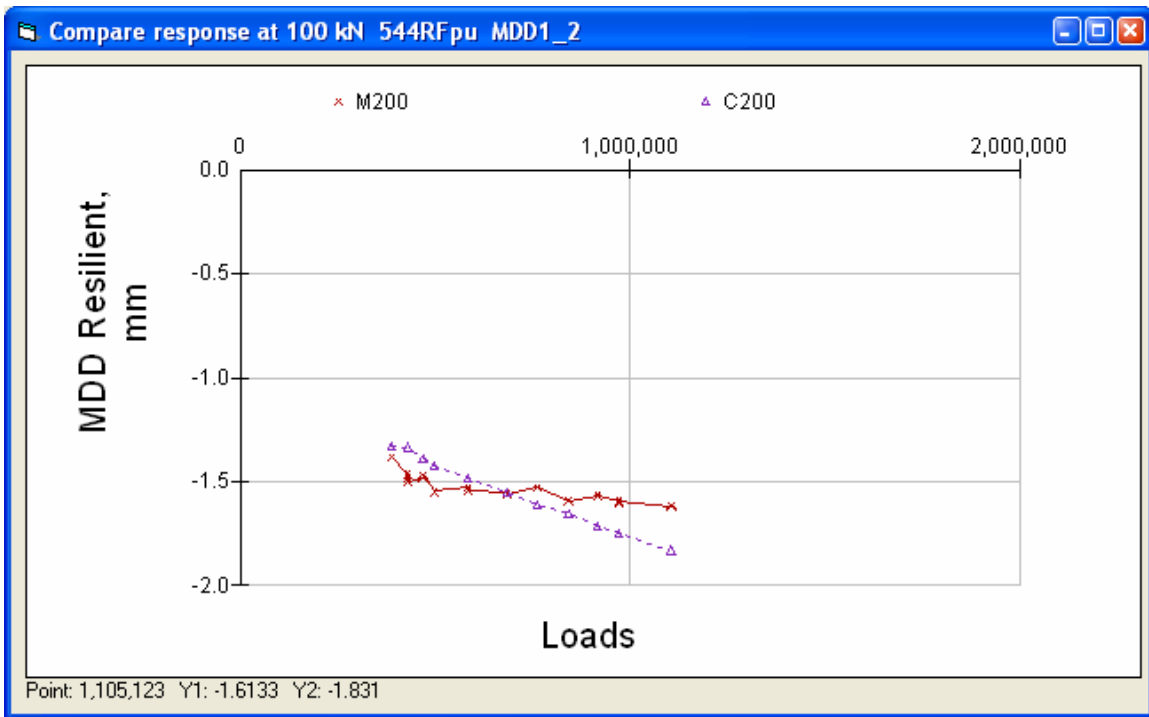


Figure 200. Section 544RF 100 kN top of aggregate base.

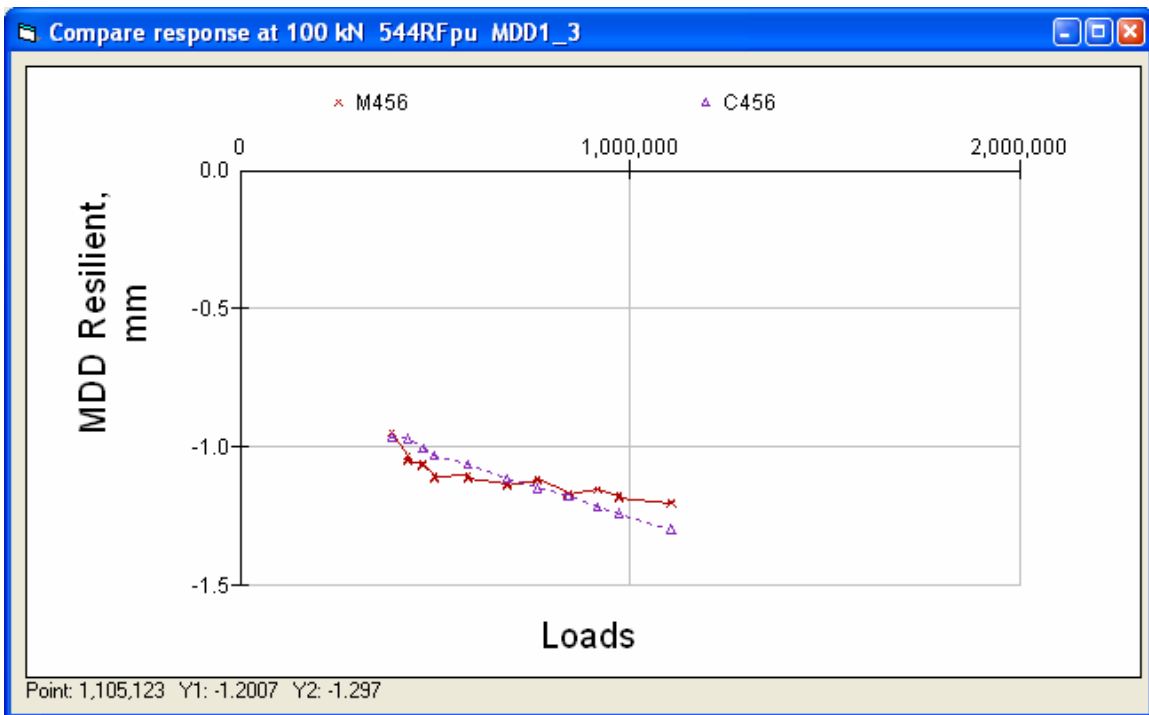


Figure 201. Section 544RF 100 kN top of aggregate subbase.

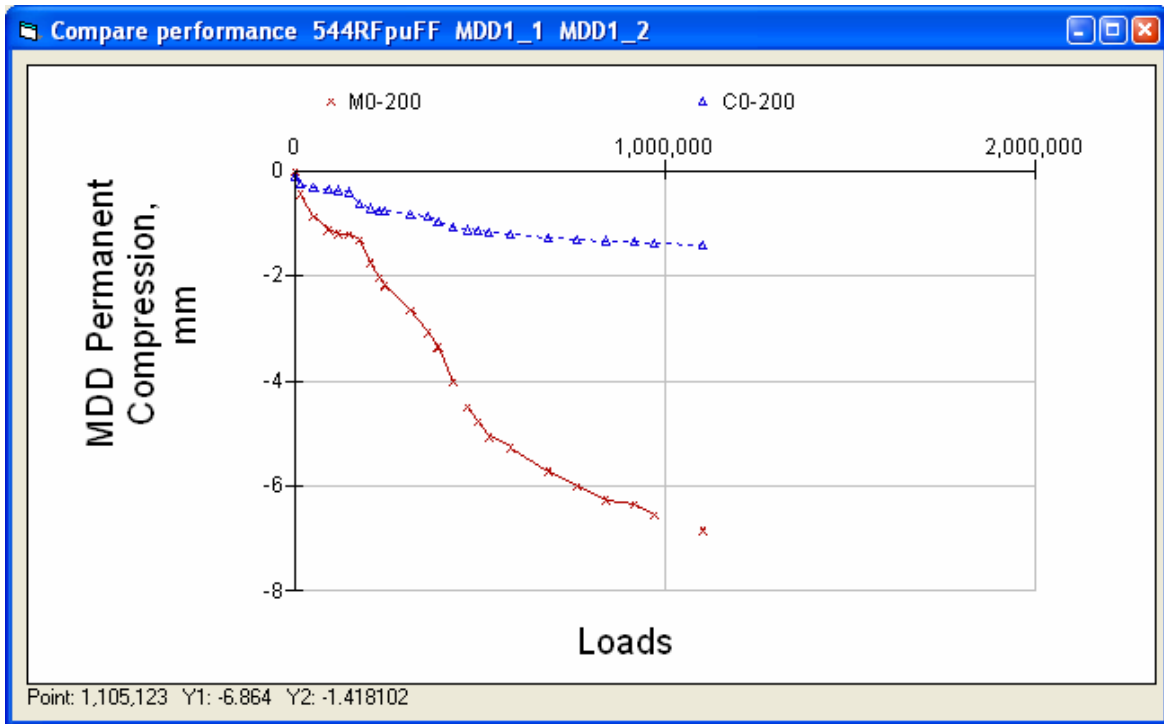


Figure 202. Section 544RF Permanent deformation of asphalt layers.

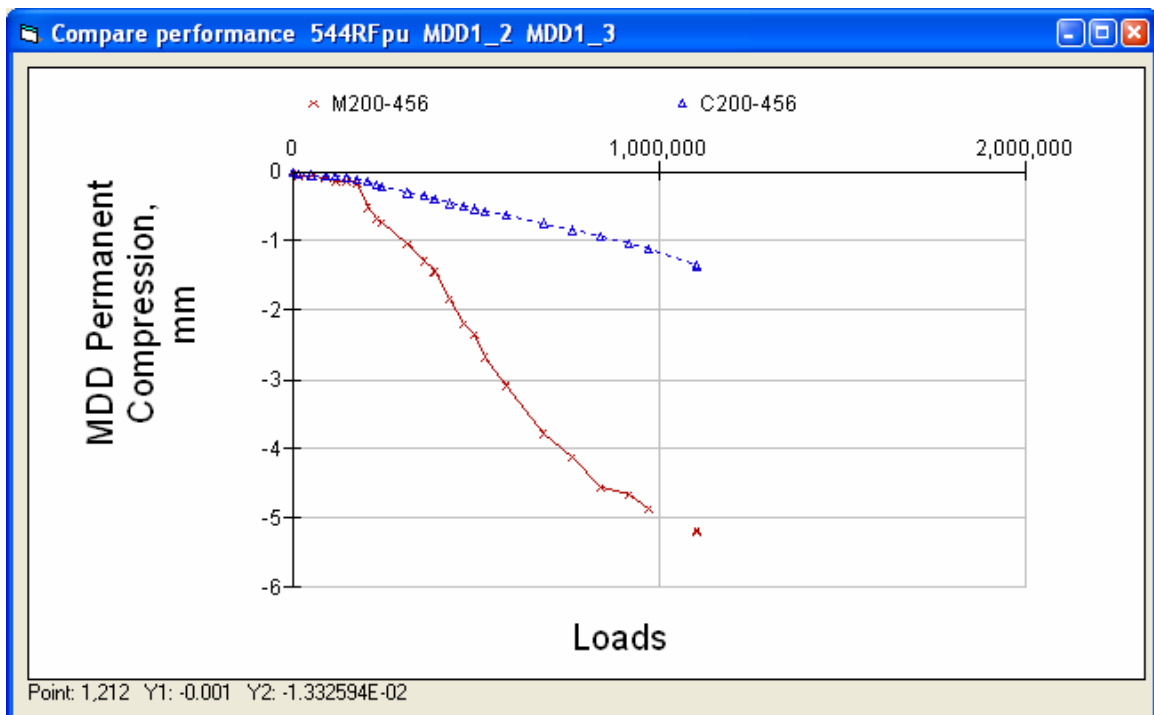


Figure 203. Section 544RF permanent deformation of aggregate base.

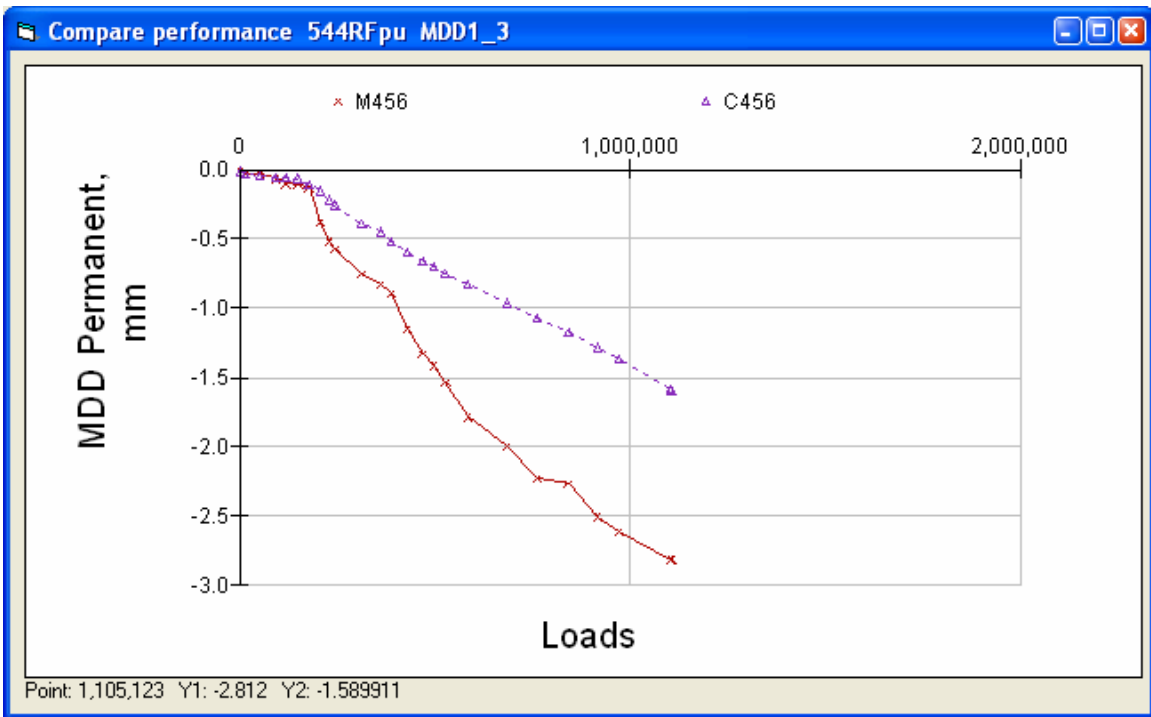


Figure 204. Section 544RF permanent deformation on top of basecourse.

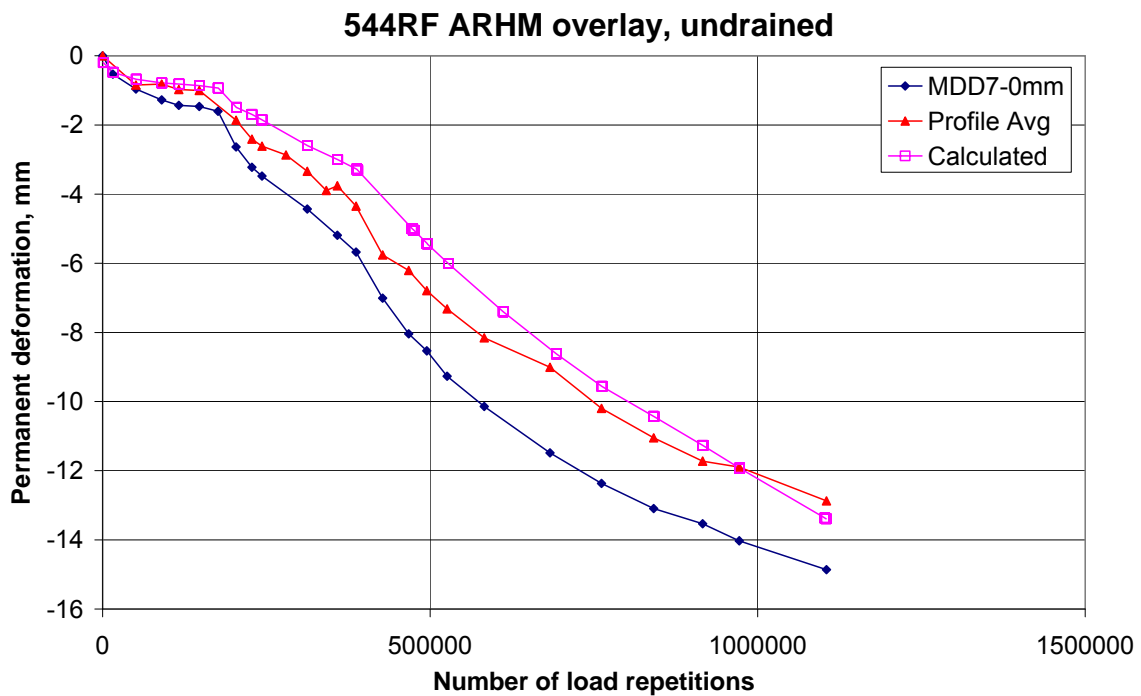


Figure 205. Section 544RF permanent deformation at pavement surface.

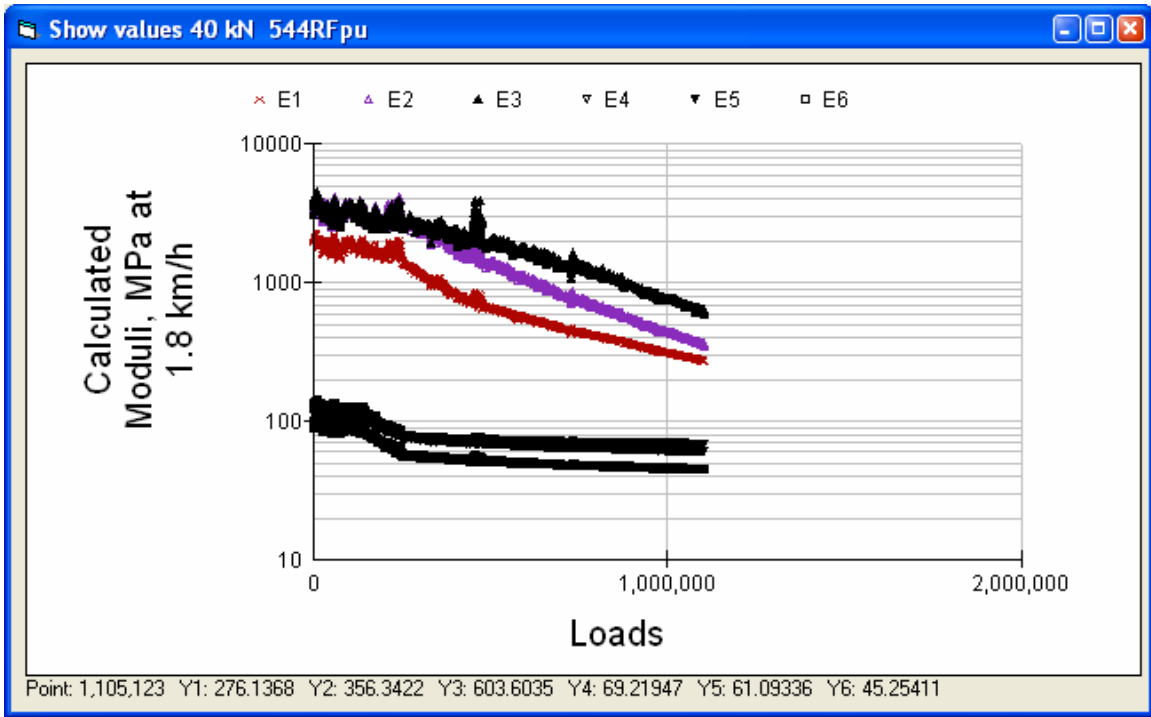


Figure 206. Section 544RF calculated moduli of pavement layers.

5.3 Section 545RF DGAC Overlay, Undrained

The pavement structure for Section 545RF is shown in Figure 207. Slip between layer 2 and layer 3 was assumed to develop at 200,000 ESALs (corresponding to approximately 200,000 load repetitions).

545RFpu structural data

Design methods Tools Change WIM Parameters

S mm MPa

Layer	Material	Thick	Modulus	Poisson	R	GF	Cost/m3
1	DGACVHVS3Rg	90	7653	0.35	0	1.46	114
2	DGACVHVS1TRg	71	9055	0.35	0	1.46	114
3	DGACVHVS1BRg	72	11189	0.35	0	1.46	114
4	ABHVS5	259	245	0.35	78	1.1	57
5	AS2HVS5	243	275	0.35	50	1	30
6	ClayHVS5	0	186	0.35	20	0	0

Figure 207. Section 545RF pavement structure.

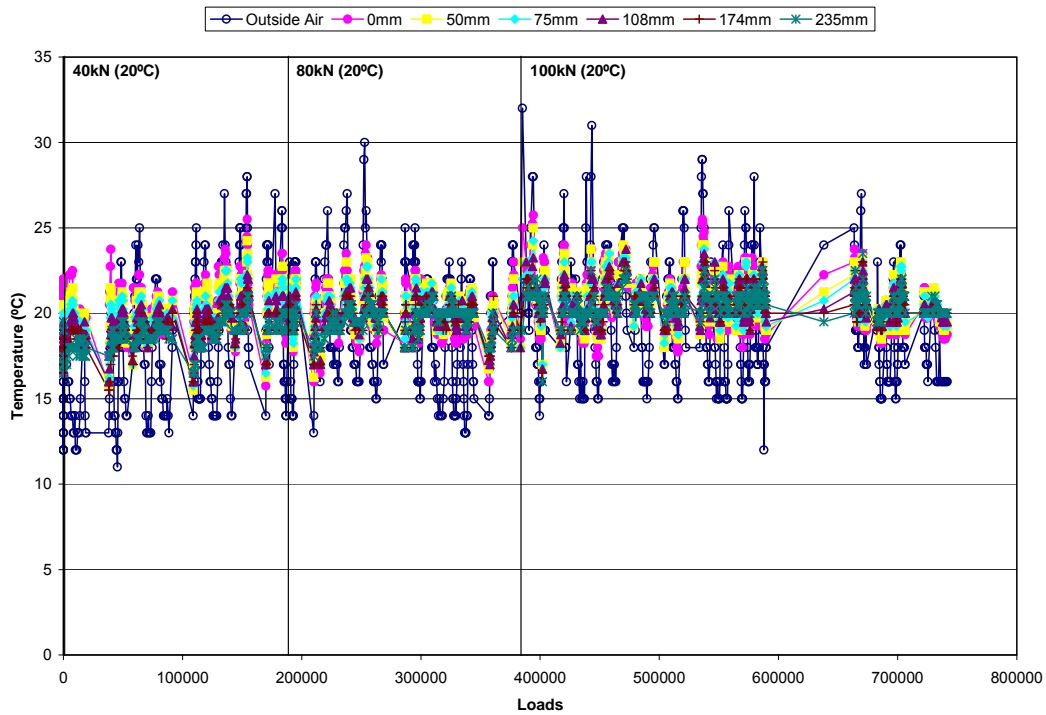


Figure 208. Section 545RF temperatures during testing.

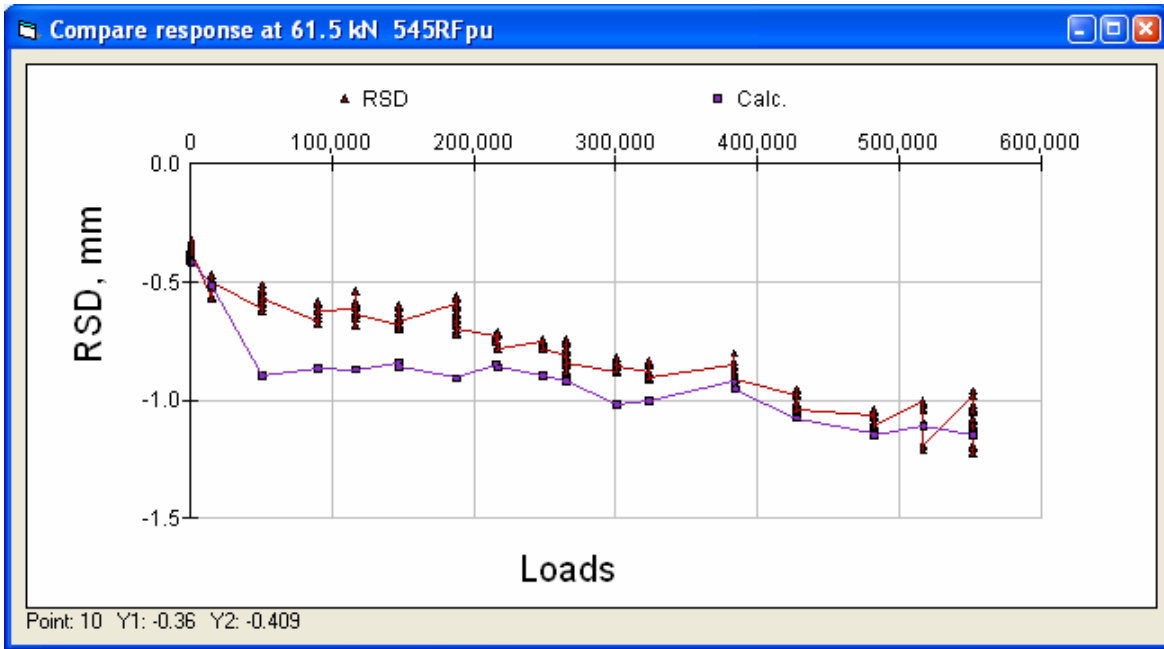


Figure 209. Section 545RF Road Surface Deflectometer, at 40 kN.

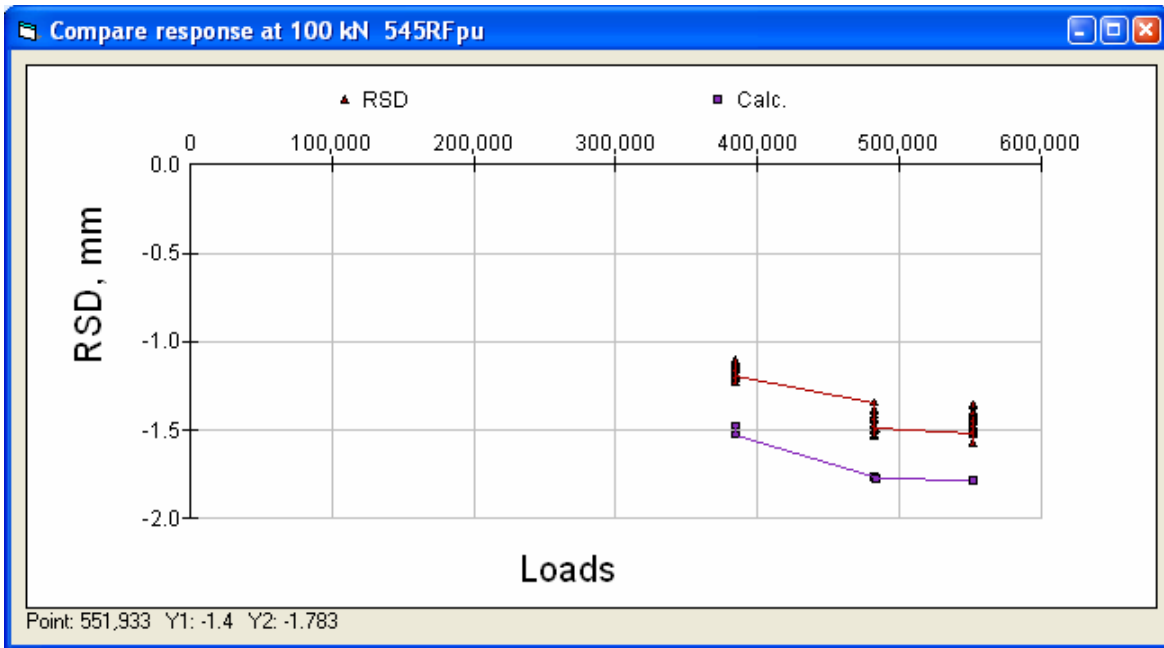


Figure 210. Section 545RF Road Surface Deflectometer, 100 kN.

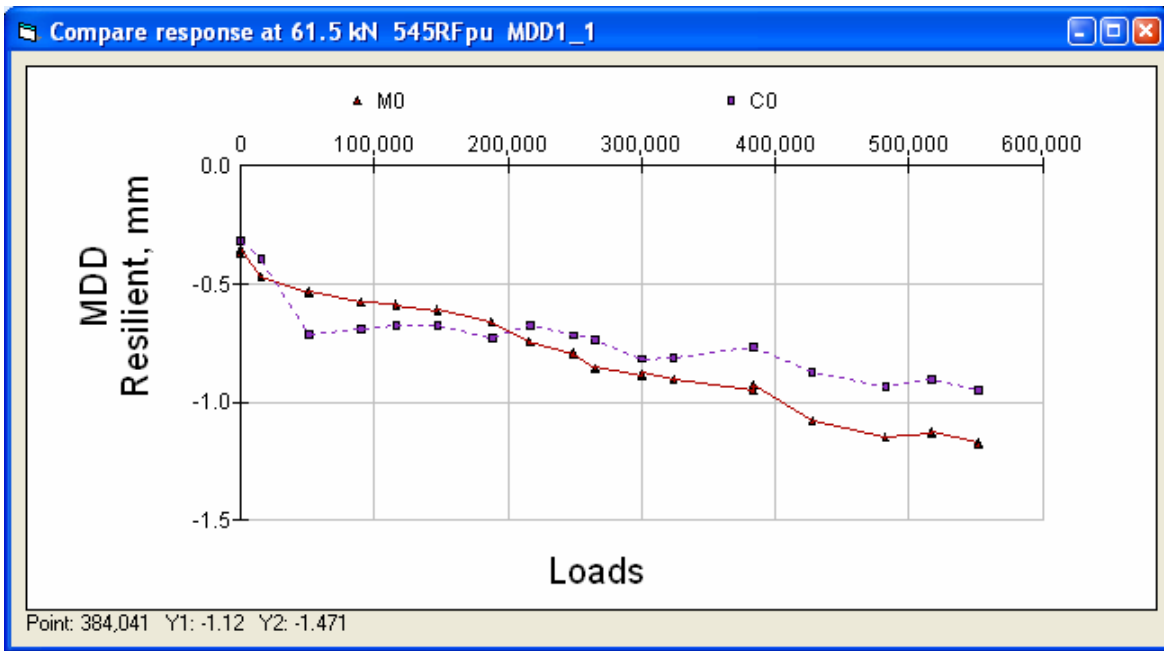


Figure 211. Section 545RF 40 kN top module.

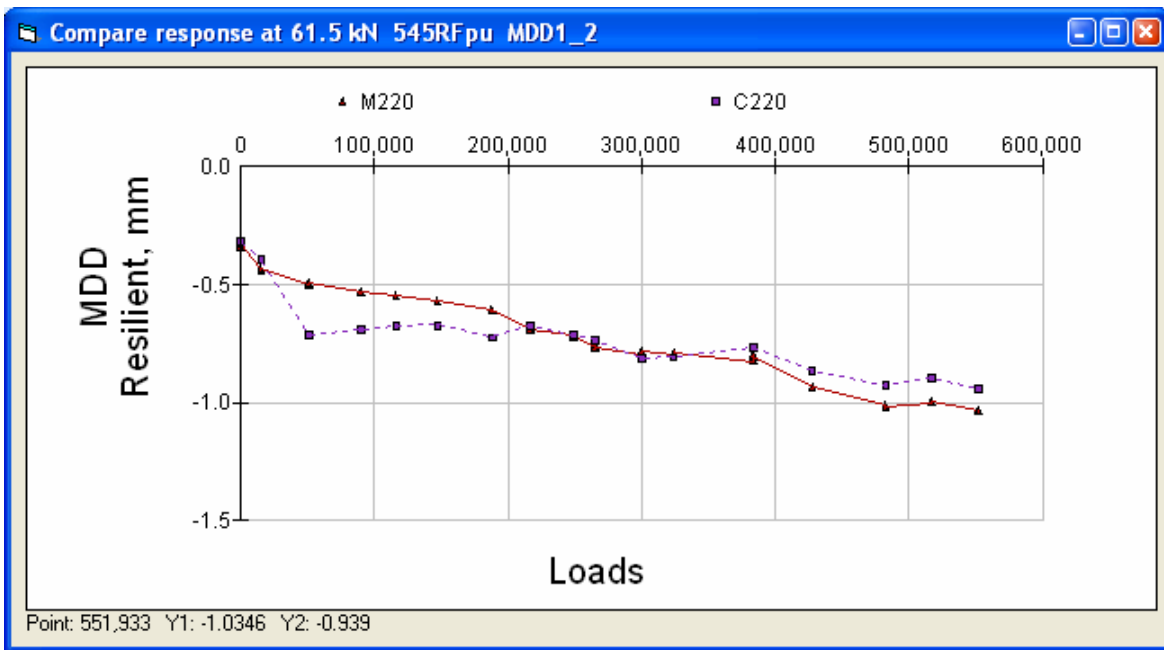


Figure 212. Section 545RF 40 kN top of aggregate base.

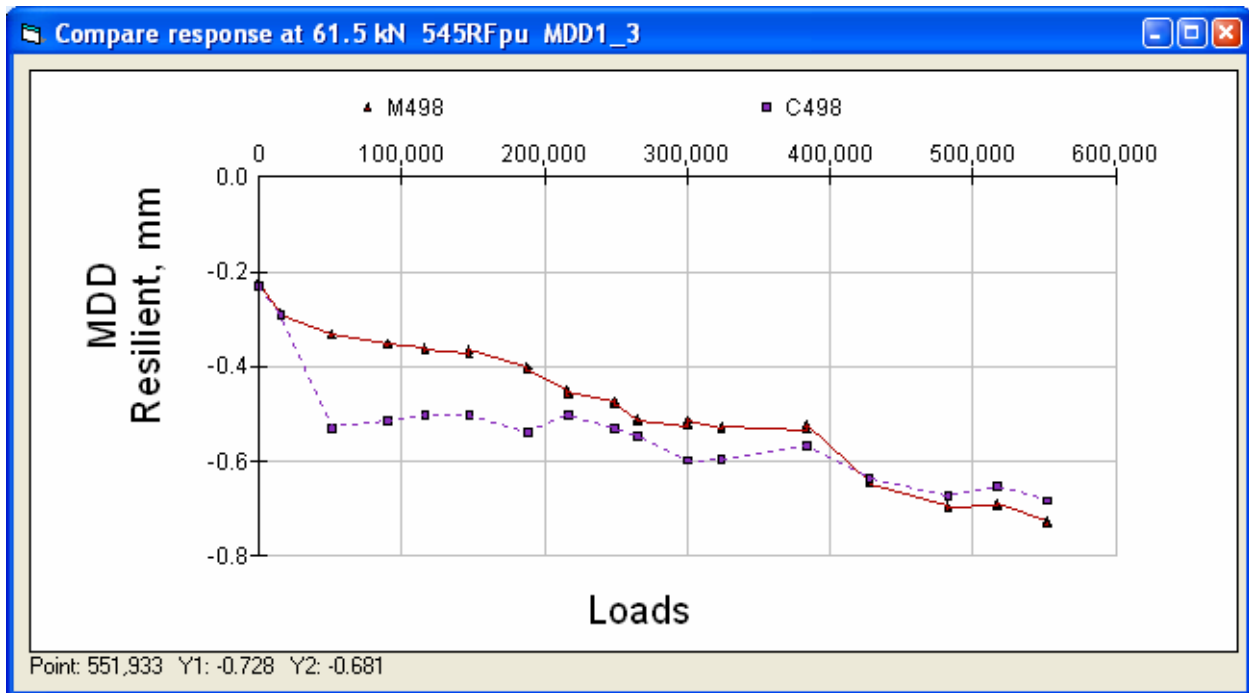


Figure 213. Section 545RF 40 kN top of aggregate subbase.

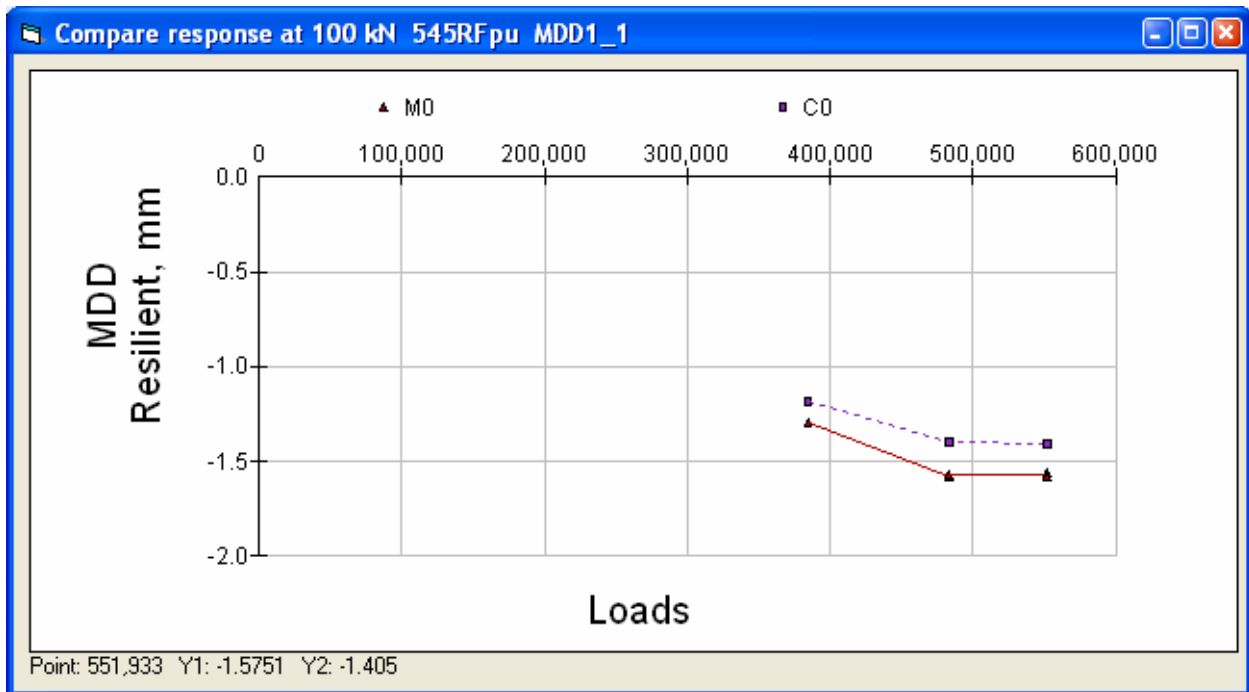


Figure 214. Section 545RF 100 kN top module.

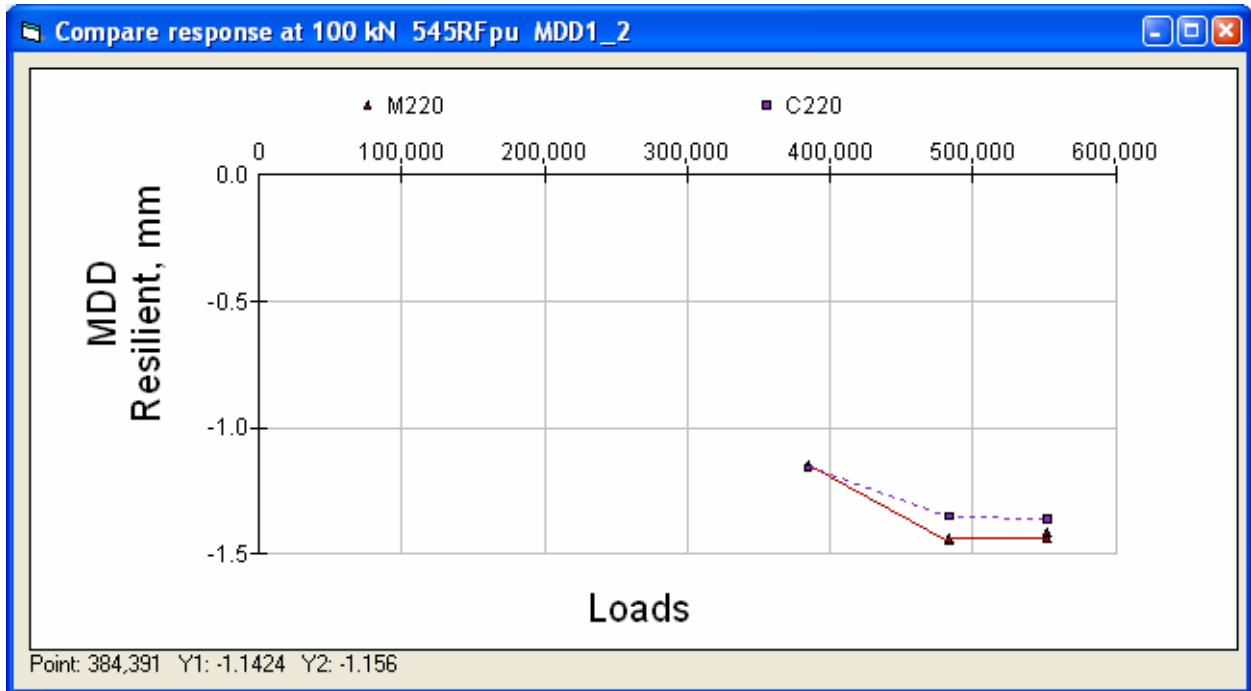


Figure 215. Section 545RF 100 kN top of aggregate base.

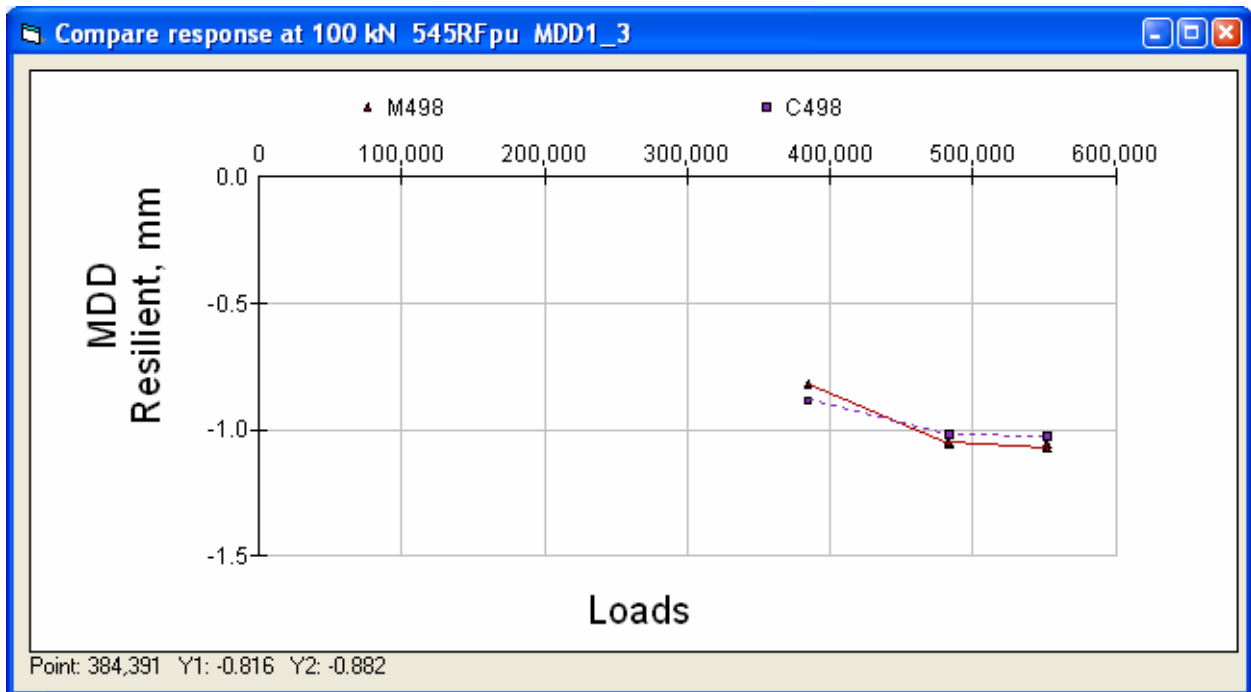


Figure 216. Section 545RF 100 kN top of aggregate subbase.

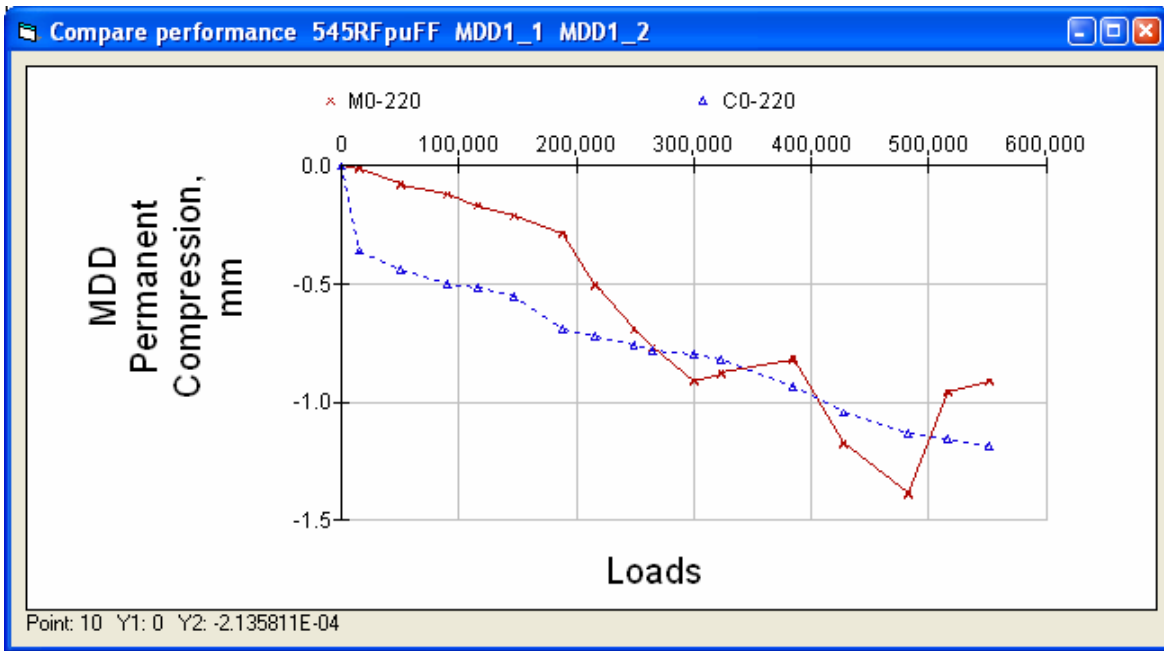


Figure 217. Section 545RF permanent deformation of asphalt layers.

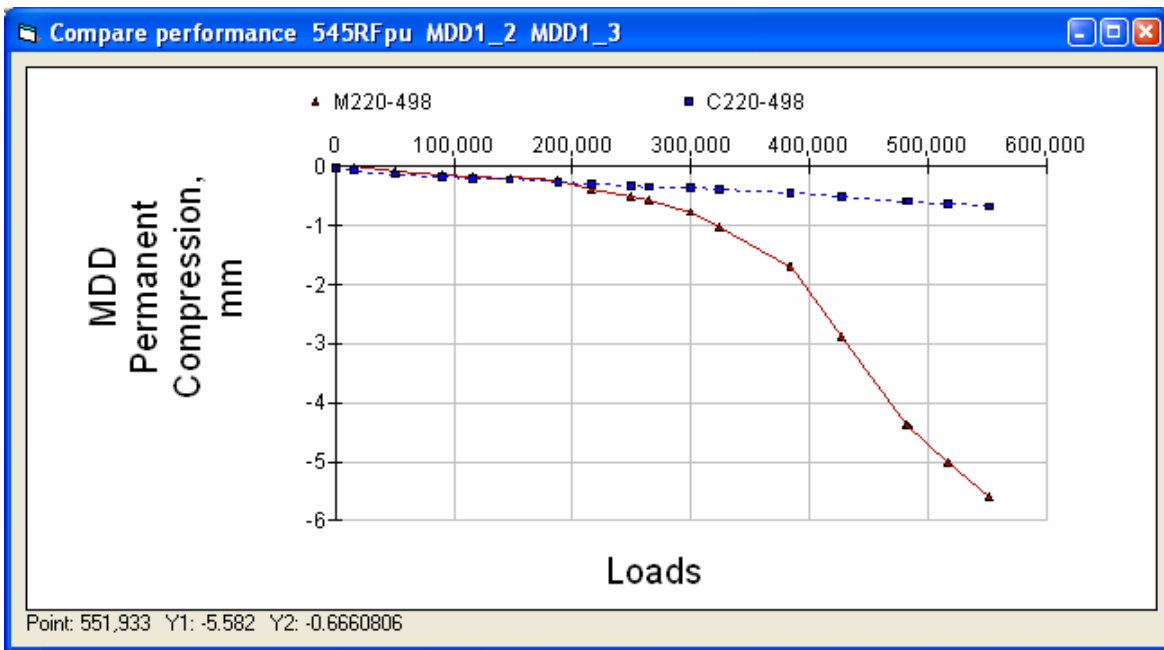


Figure 218. Section 545RF permanent deformation of aggregate base.

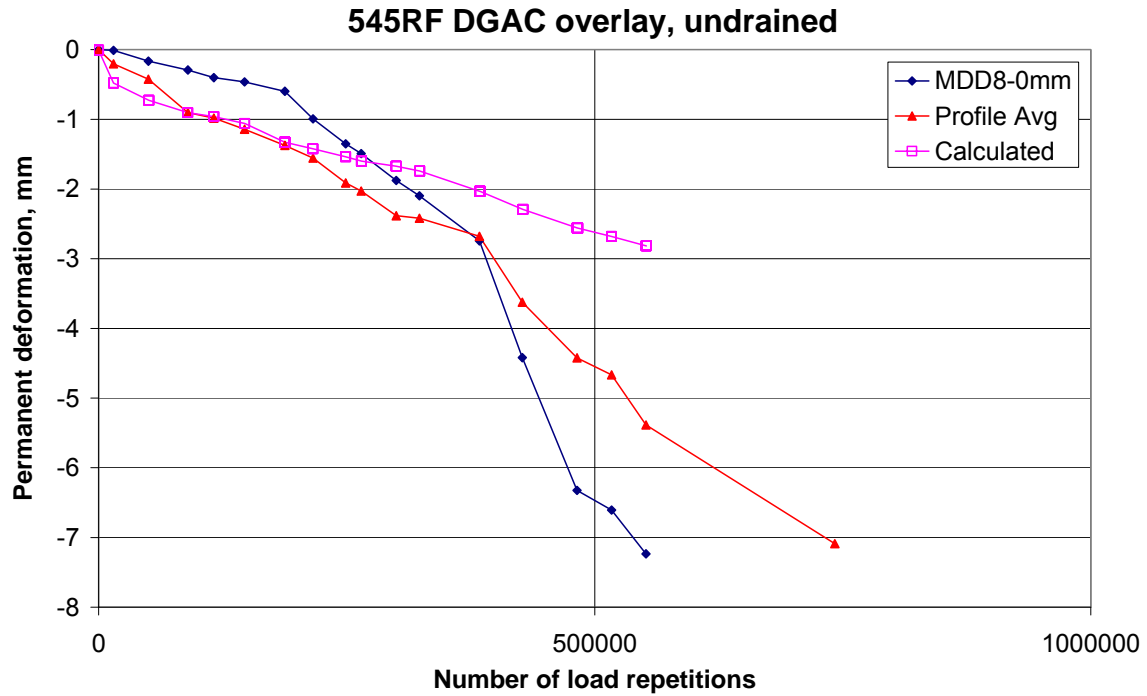


Figure 219. Section 545RF permanent deformation at pavement surface.

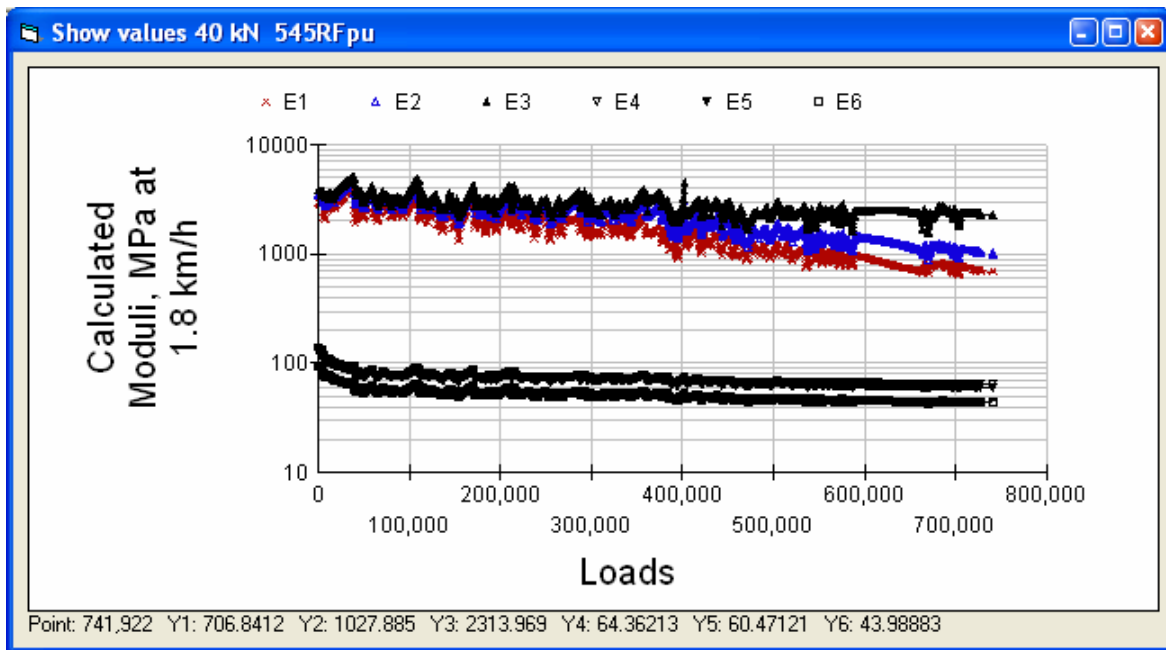


Figure 220. Section 545RF calculated moduli of pavement layers.

5.4 Visual Cracking versus Damage of the Top Asphalt Layer, Goal 5

Figure 221 shows visual cracking (in m/m^2) versus the relative decrease in the modulus of the overlay. As was the case for the previous simulations, visual cracking was not observed before the calculated modulus of the overlay had dropped by 50–60 percent. The difference between drained and undrained sections is similar to the difference in Goal 1, with the drained sections showing cracking at a greater loss of stiffness than the undrained sections.

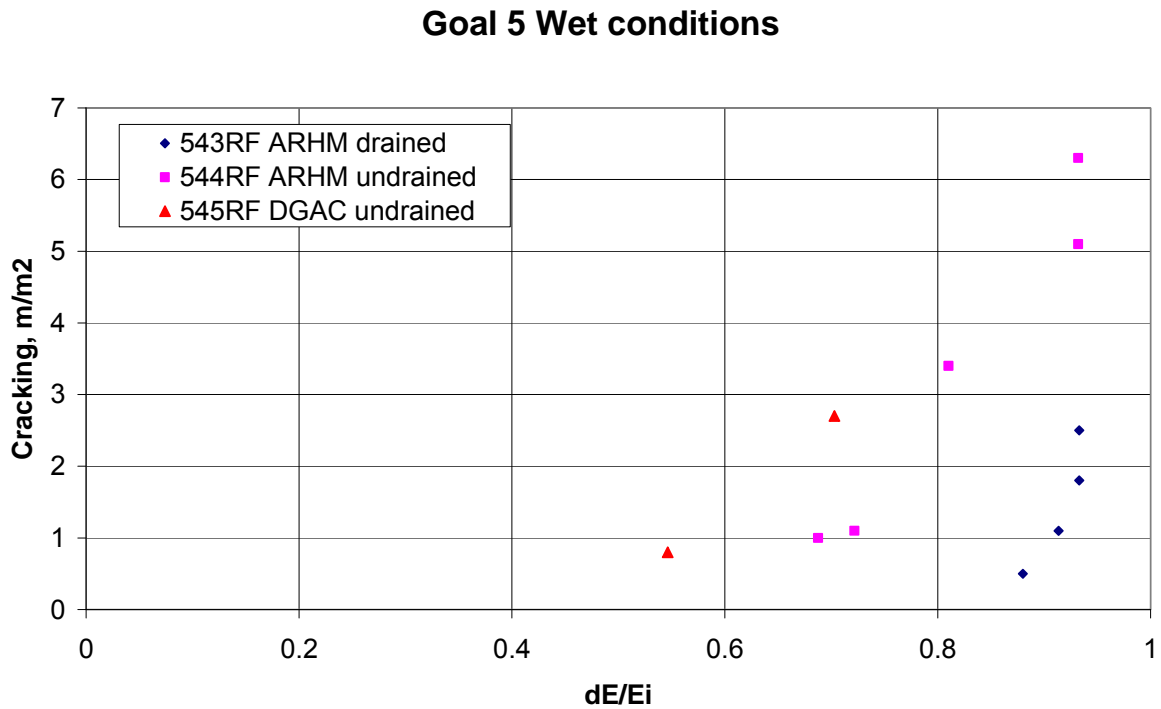


Figure 221. Visual cracking versus relative decrease in modulus of layer 1, Goal 5 Wet conditions.

Cracking versus relative deflection

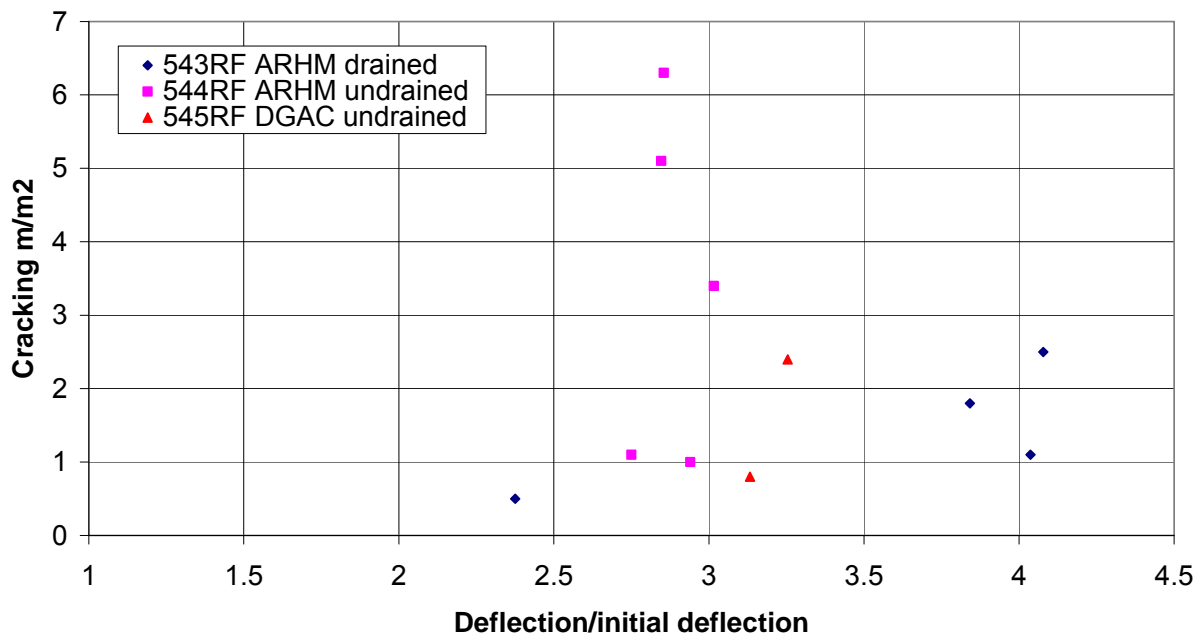


Figure 222. Goal 5, cracking versus increase in deflection.

6.0 GOAL 9 MODIFIED BINDER (MB) ROAD, INITIAL TESTS

6.1 Materials Characterization

Modulus parameters for the Goal 9 asphalt concrete (AC) are shown in Figure 223. It should be noted that the binder for the asphalt concrete in these sections is conventional and unmodified. Modified binders (MB) were used for the subsequent overlays, for which testing is still underway, and they are not considered in this report.

Material parameters

Name: DGACVHVS99 R value: 0 Gravel factor: 1.46

Modulus Classical Incremental Recursive Environment

Reference modulus, MPa: 7371 Reference temperature, C: 20 Poisson's ratio: 0.35

$\log(E) = \text{delta} + \text{alfa} / (\exp(\text{beta} + \text{gamma} * \log(\text{tr})))$

delta: 2.30103 beta: -0.3032 gamma: 0.8931 alfa: 1.79338609454

reduced time, $\text{tr} = \text{It} * (\text{reference viscosity} / \text{viscosity})^{aT}$, reference loading time, $\text{It} = 0.015 \text{ sec}$

aT: 1.337

$\log(\log(\text{viscosity, cPoise})) = A + \text{VTS} * \log(T \text{ K})$, T temperature degree Kelvin

A: 9.6307 VTS: -3.5047

Standard deviation factor (sdf) on modulus: 1.05

Figure 223. MB road, AC modulus-versus-reduced time parameters from frequency sweep.

The modulus-versus-reduced time parameters were determined from frequency sweep testing and are shown in Figure 223. These were the parameters used in the CalME simulations.

FWD testing was carried out at different intervals during the HVS experiments. The moduli of the layers were determined from backcalculation using *Elmod5* software. The tests were done at the center line of the road from September 2001 to May 2003. The asphalt layer moduli are influenced by both temperature and aging effects.

Modulus of asphalt, Goal 9

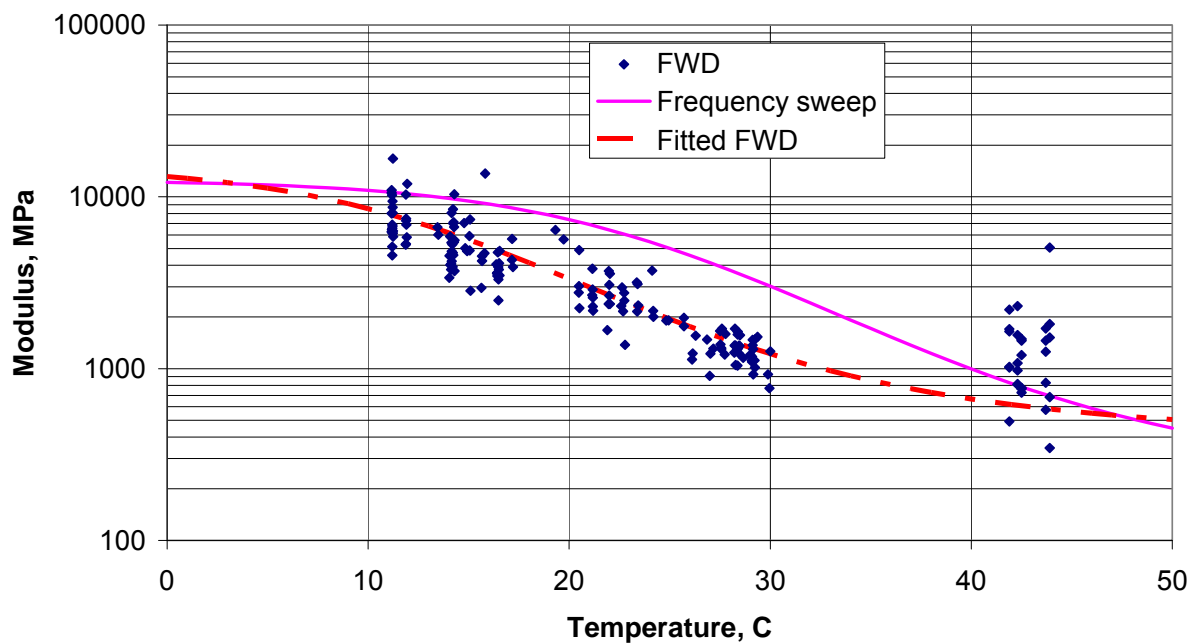


Figure 224. Moduli from FWD compared to frequency sweep tests, Goal 9 (MB road).

Although there is a large scatter in the backcalculated moduli (as seen in Figure 224), the values appear to be considerably lower than those from frequency sweep tests, at intermediate temperatures. It should be noted that the thickness of the asphalt layer is close to the lower limit for backcalculation of the modulus. However, the tendency is the same as for Goal 1 (where it could have been influenced by slip between the two asphalt layers). The parameters for the best fit to the FWD data are shown in Table 26.

Another possible explanation for the difference in moduli is a difference in strain level. Laboratory tests have shown that greater strain levels result in lower stiffnesses. At 20°C and a frequency of 5 Hz, shear frequency sweep data showed a decrease in shear stiffness from 668 to 1666 to 1918 MPa for shear strains of 1000, 500, and 100 μ strain, respectively (Harvey, Guada, and Long, AAPT 2000). The FWD has greater strain (about 300 μ strain) than the flexural frequency sweep tests (about 200 μ strain), which helps explain the difference.

Table 26. Parameters for FWD Moduli versus Reduced Time, Goal 9

Reference Modulus	3333 MPa
Reference Temperature	20°C
δ	2.6021
β	1.1266
γ	0.8059
α	1.5740
aT	1.3370
A	9.6307
VTS	-3.5047

Damage parameters for the AC were determined from laboratory beam controlled-strain fatigue testing. The parameters are shown in the first column of Figure 225. A shift factor of 3 was used, as for the previous simulations.

The same parameters used for the conventional Goal 3 simulations were used (column 2 of Figure 225) for permanent deformation of the AC layer.

The aggregate base (AB) was 100 percent recycled material with a high content of recycled portland cement concrete. Figure 226 shows the backcalculated moduli plotted against time. The moduli are average values for the full test line using drop 2, corresponding to a load level of approximately 40 kN. The first six points were determined during autumn of 2001 and early winter of 2002, and the last two tests were done after the summer of 2002. Some of the moduli variation may be due to changes in the temperature of the AC layer but some must be due to self-cementing of the PCC in the AB layer. A purely granular material, without any cohesion, cannot achieve layer moduli of 800–1200 MPa.

Material parameters

Name: DGACVHVSG9 R value: 0 Gravel factor: 1.46

Modulus Classical Incremental **Recursive** Environment

Damage = $A * MN^{\alpha} * (\text{response}/\text{reference response})^{\beta} * (E/\text{reference modulus})^{\gamma}$, MN million passages
 AC shear, rd mm = $A * MN^{\alpha} * \exp(\beta * \text{shear stress MPa}/\text{reference shear stress}) * (\text{elastic shear microstrain})^{\gamma}$

	Fatigue, dE/Ei	Permanent deformation, mm	Crushing, dE/Ei	Roughness, IRI m/km	
Response type	e	t	z	e	
A	0.007357	A*K	7	A	0
Sdf A	1.1	Sdf A	1.1	Sdf A	1.1
alfa	0.4945	alfa	0.208	alfa	0.6
Respref	-200	Respref	0.1	Respref	1.53
beta	2.0612	beta	1.03	beta	7.69
Eref	3000			Eref	10000
gamma	1.0306	gamma	1	gamma	-15.4
delta	0.1263				
Shift factor	3				

Figure 225. MB road, damage parameters for AC in first column.

MB road, AB modulus

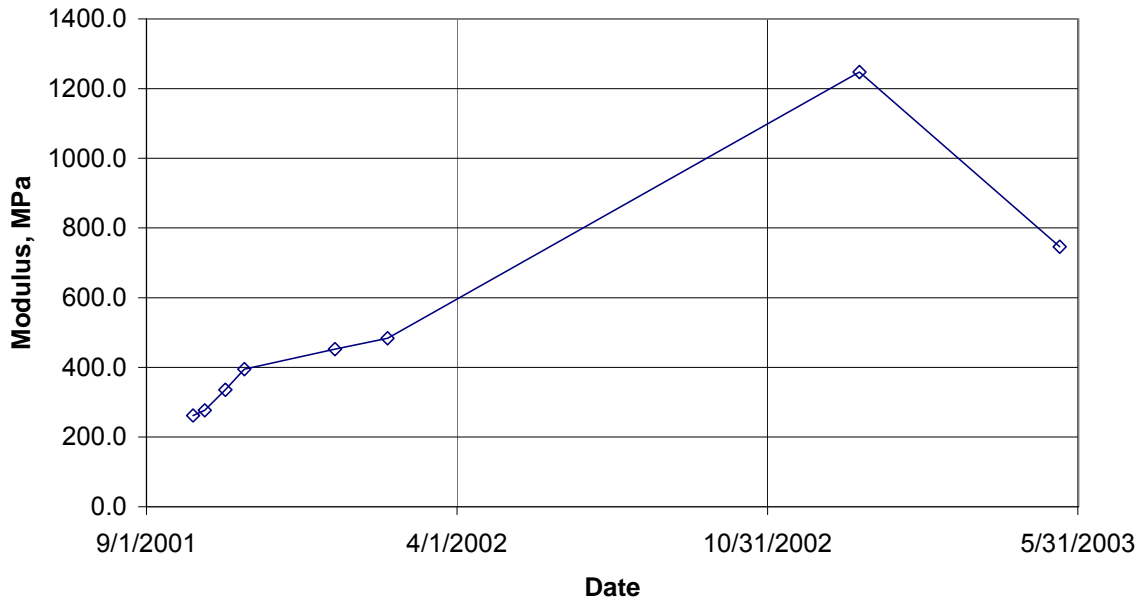


Figure 226. MB road, backcalculated modulus of AB versus time.

MB road, modulus of AB

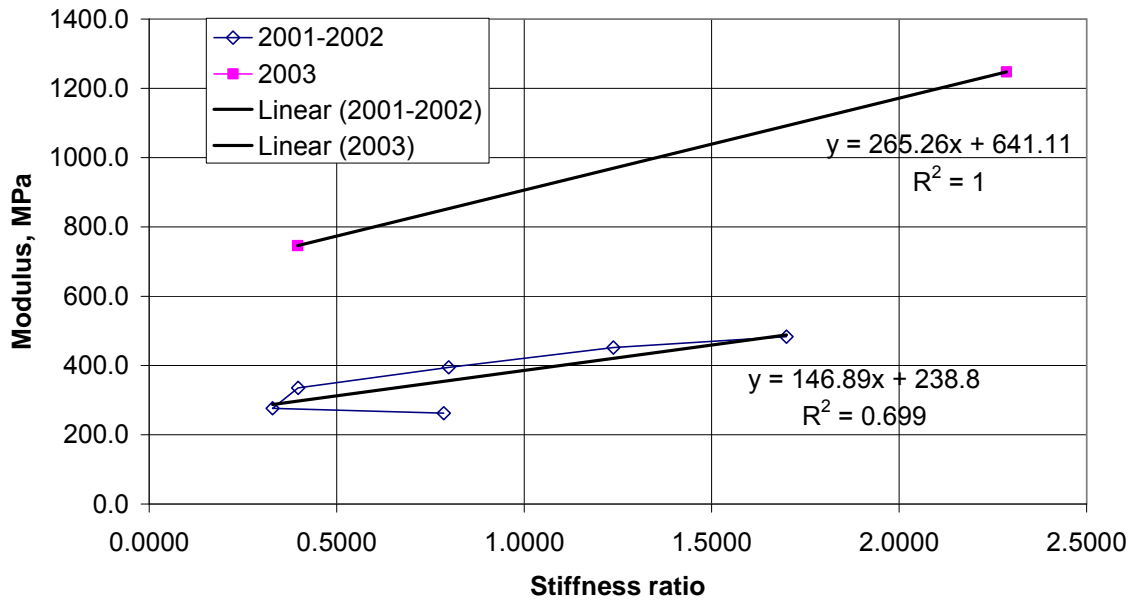


Figure 227. MB road, modulus of AB versus stiffness of AC.

In Figure 227, the modulus of the AB is plotted versus the stiffness ratio calculated as:

$$Stiffness\ ratio = \frac{h_{AC}^3 \times E_{AC}}{1000^3} \tag{32}$$

where h_{AC} is the thickness of the AC (80 mm in the backcalculation), and E_{AC} is the modulus of the AC.

From the two regression lines in Figure 227 the parameters of Equation (18) may be determined:

Table 27. MB Road, Stiffness Parameters for AB

	Eo	Stiffness Factor
2001-2002	344	0.23
2003	795	0.19

MB road, Subgrade modulus

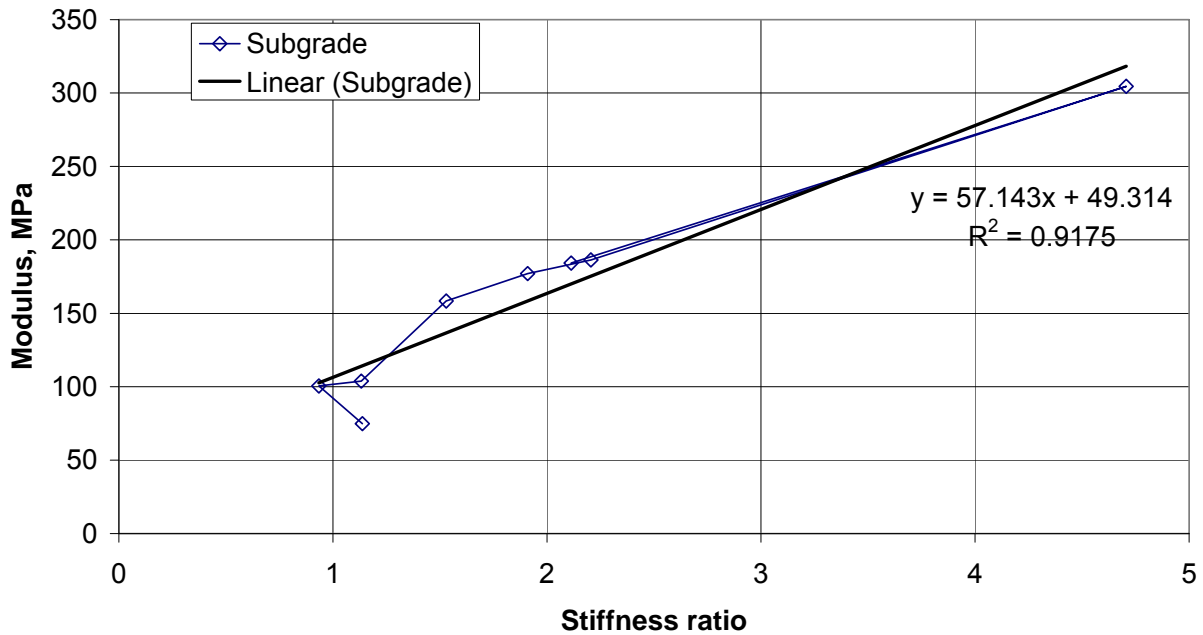


Figure 228. MB road, subgrade modulus versus stiffness of pavement layers.

For the subgrade modulus it is not necessary to distinguish between the tests done before and after the summer of 2002. All the test points are plotted in Figure 228 versus the stiffness ratio calculated as:

$$\text{Stiffness ratio} = \left(\frac{h_{AC} \times \sqrt[3]{E_{AC}} + h_{AB} \times \sqrt[3]{E_{AB}}}{3500} \right)^3 \quad (33)$$

where h_{AB} is the thickness of AB (398 mm in the backcalculation), and E_{AB} is the modulus of the AB.

The regression line for the subgrade in Figure 228 results in:

- $E_o = 116$ MPa and
- Stiffness factor = 0.46

The stiffness factors given above have been used in the simulations, whereas the moduli of AB and subgrade have been selected to give initial deflections that correspond reasonably well to those measured with the RSD or the MDDs (where available).

When calculating the permanent deformation of AB and subgrade, the same parameters were used as in the previous simulations.

A 61.5 kN dual wheel load was used for all of the testing, except for the part of Section 567RF where a 38.4 kN wheel load was used. The results of the HVS tests are given in chronological order in the following subsection.

6.2 Section 567RF MB Road

The test was carried out from December 21, 2001, to January 20, 2002. The pavement section is shown in Figure 229. Cracking was only recorded at the end of the test, when it had reached 8.2 m/m².

567RF structural data

Design methods Tools Change WIM Parameters

S

mm MPa

Layer	Material	Thick	Modulus	Poisson	R	GF	Cost/m3
1	DGACVHVSG9	78	7371	0.35	0	1.46	114
2	ABHVS9	398	120	0.35	78	1.1	57
3	ClayHVS9	0	120	0.35	5	0	0

Figure 229. Section 567RF pavement structure.

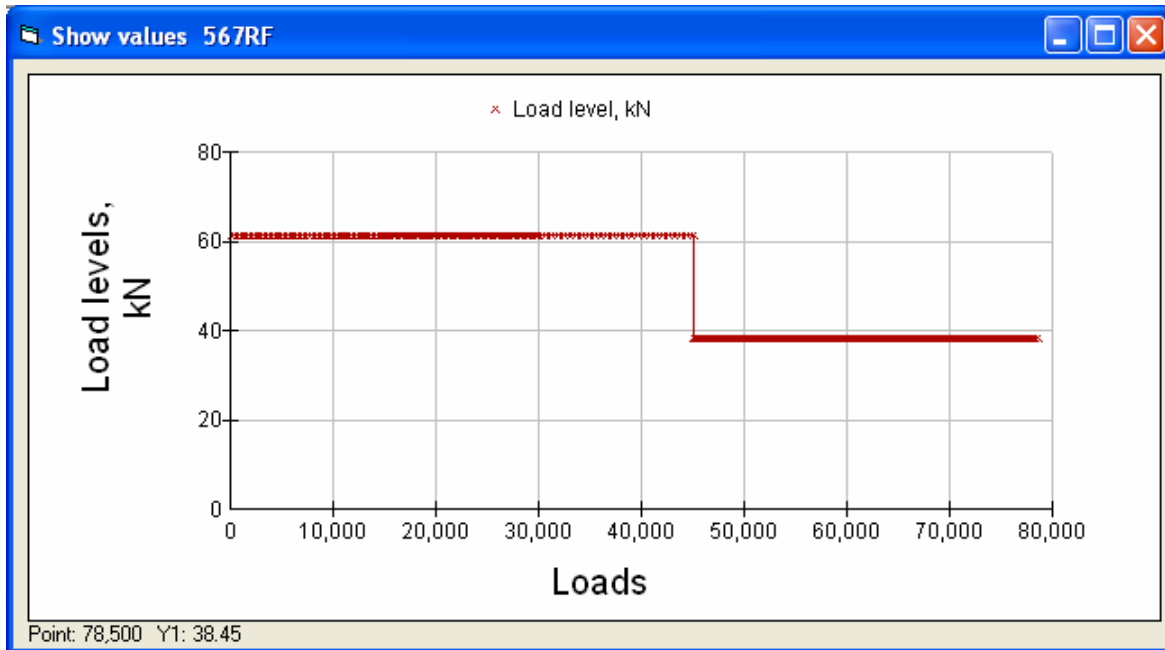


Figure 230. Section 567RF load levels.

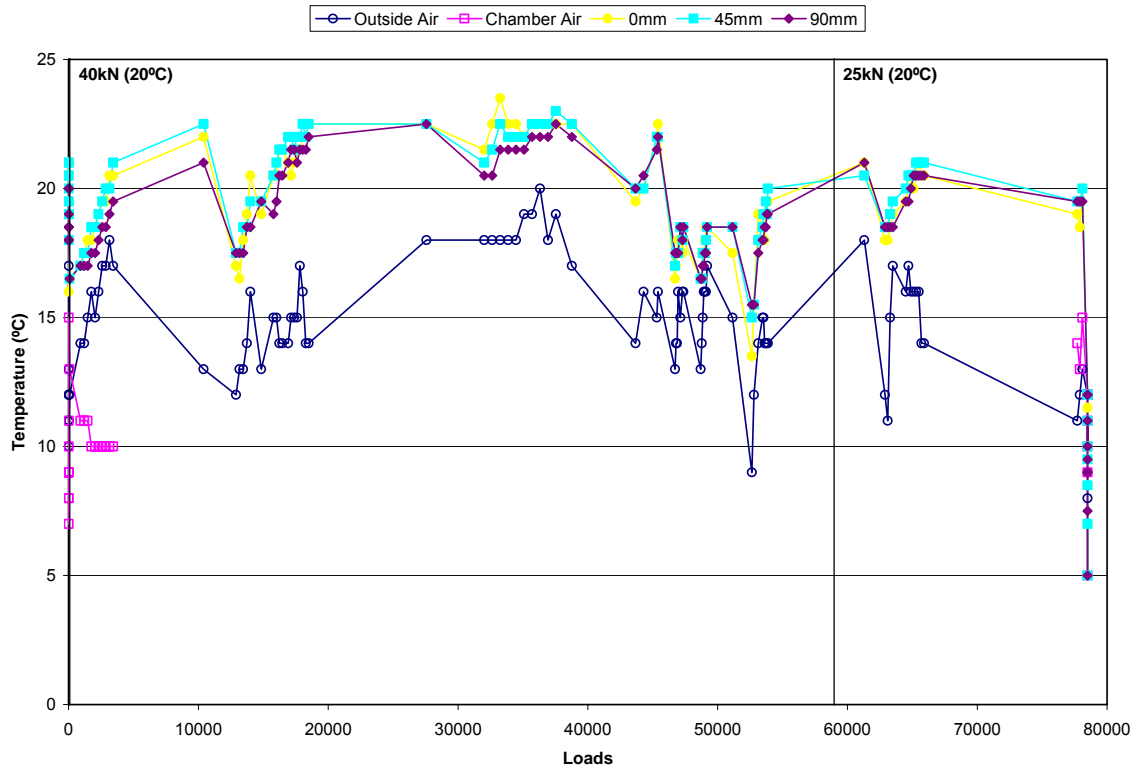


Figure 231. Section 567RF temperatures during testing.

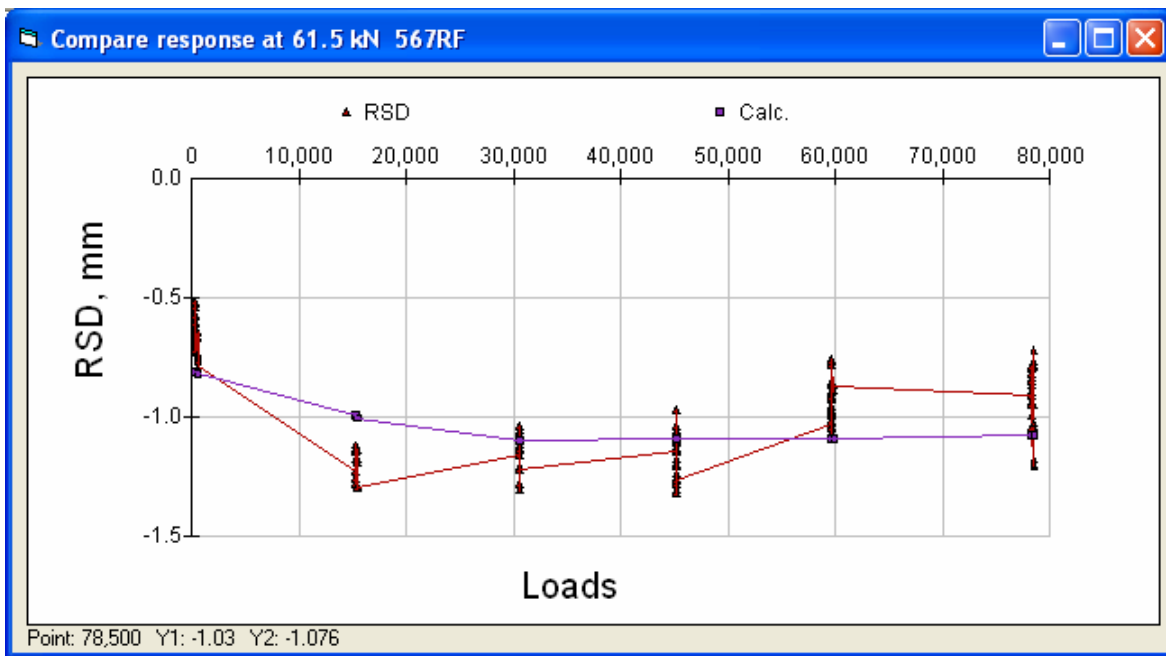


Figure 232. Section 567RF Road Surface Deflectometer.

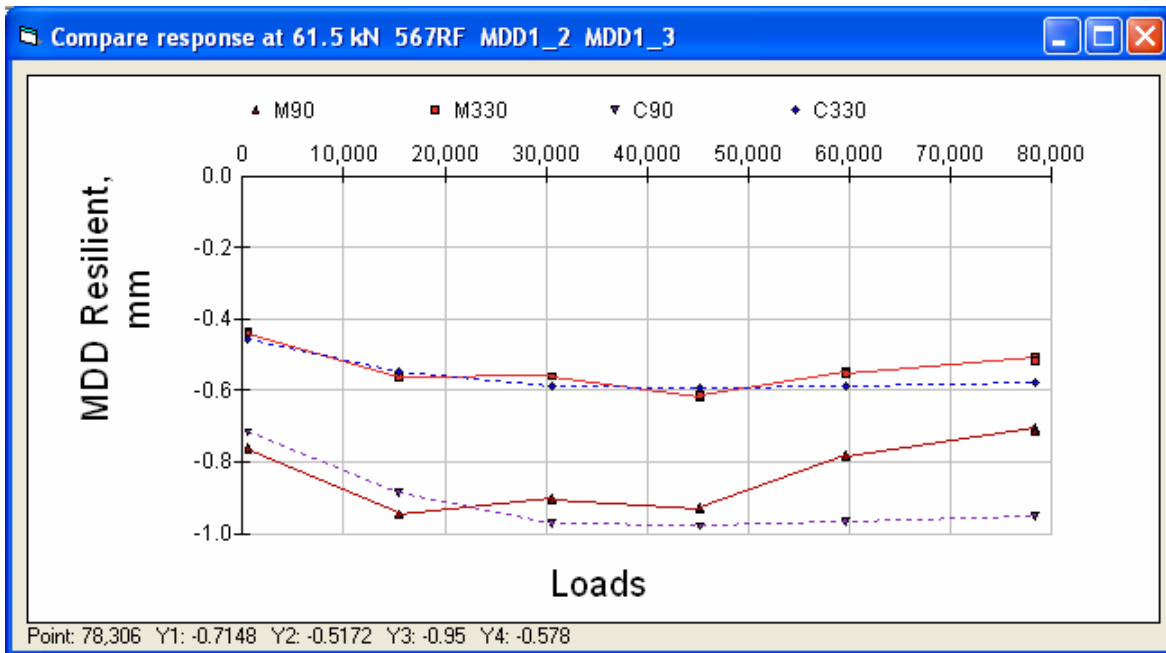


Figure 233. Section 567RF MDDs at 90mm and 330 mm.

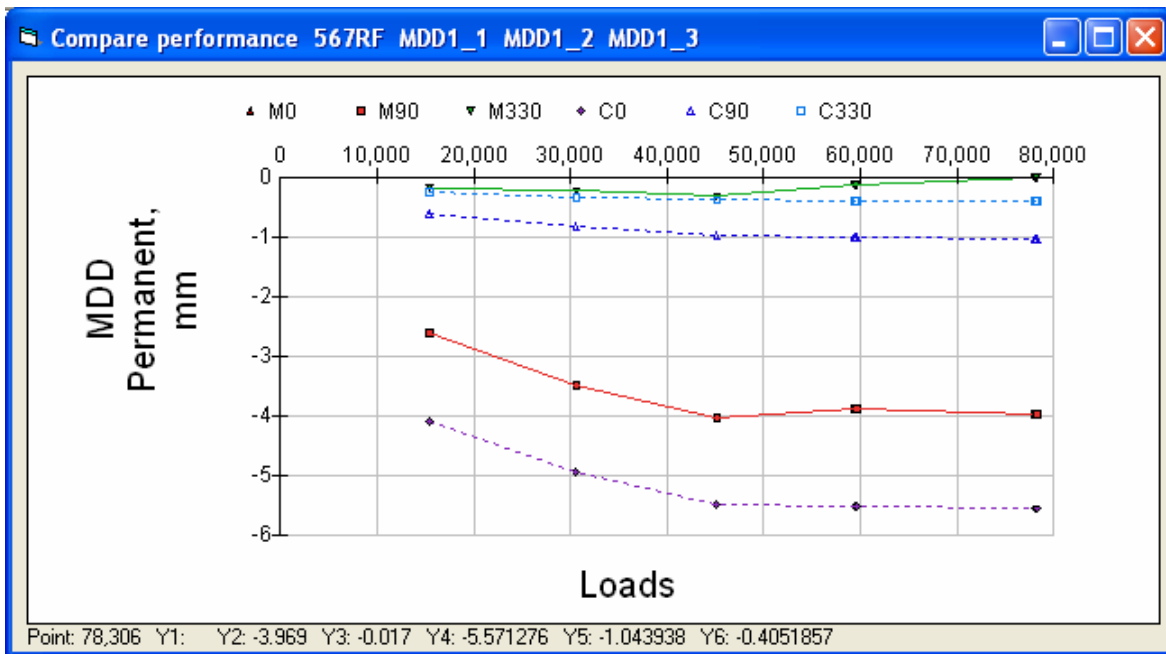


Figure 234. Section 567RF permanent deformation of MDDs.

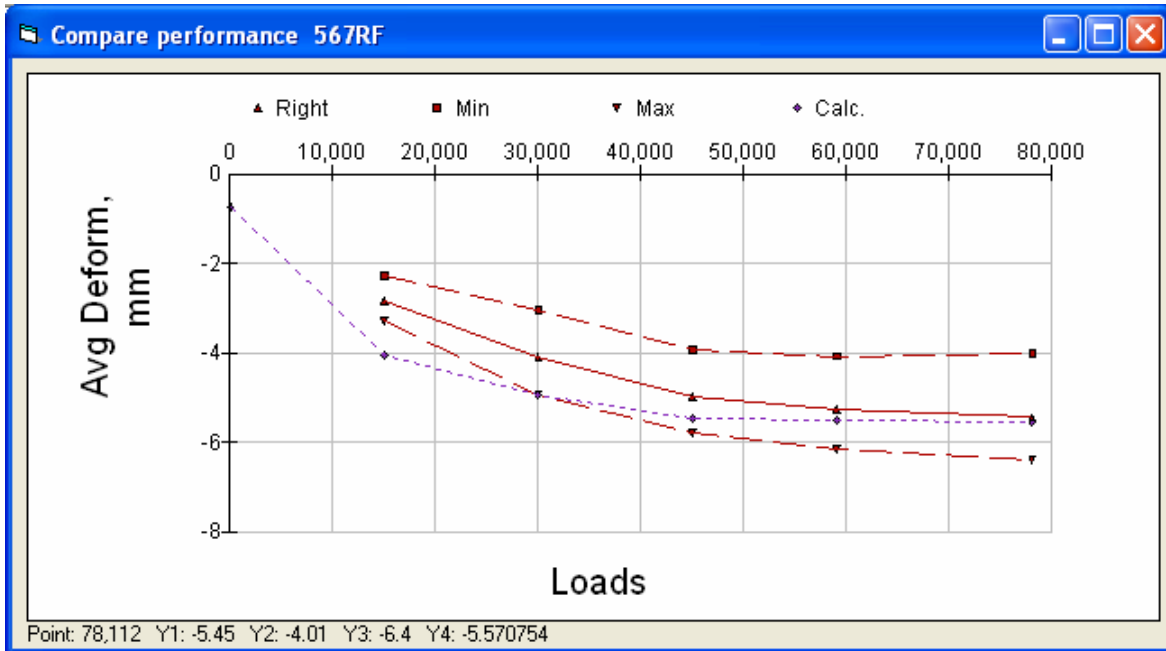


Figure 235. Section 567RF permanent deformation at pavement surface from profilometer.

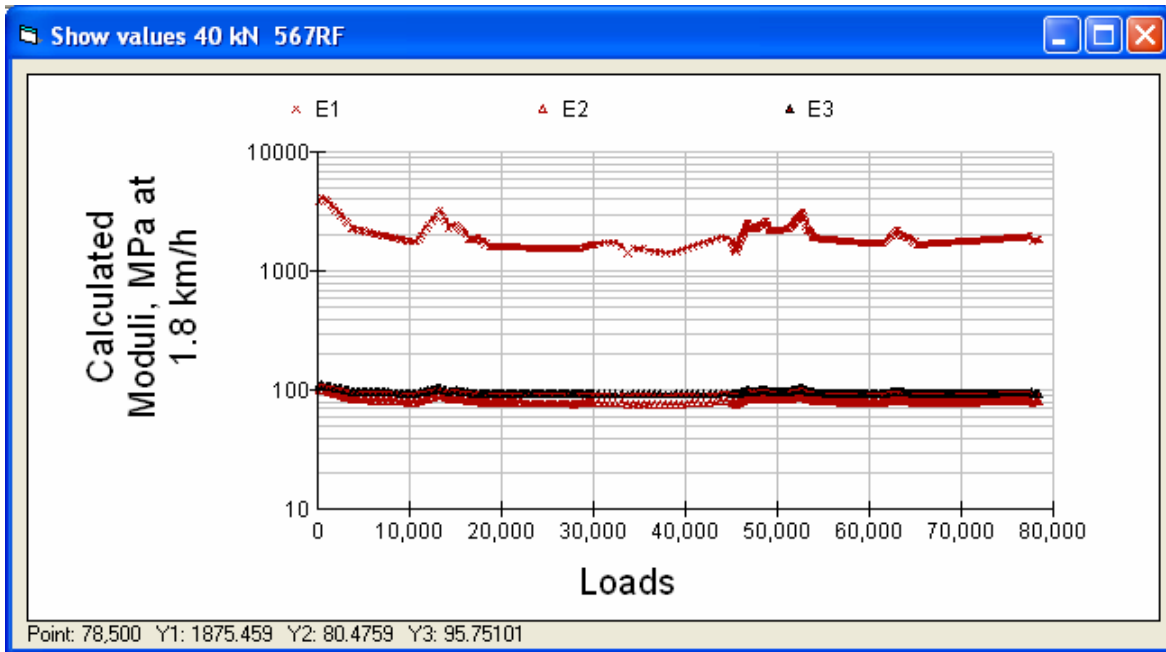


Figure 236. Section 567RF calculated moduli at 40 kN and actual temperature.

6.3 Section 568RF MB Road

The test was carried out from January 14, 2002, to February 5, 2002. The pavement structure is shown in Figure 237. The first visible cracking was recorded at approximately 198,000 load repetitions.

568RF structural data

Design methods Tools Change WIM Parameters

S

mm MPa

Layer	Material	Thick	Modulus	Poisson	R	GF	Cost/m3
1	DGACVHVSG9	80	7371	0.35	0	1.46	114
2	ABHVS9	398	150	0.35	78	1.1	57
3	ClayHVS9	0	150	0.35	20	0	0

Figure 237. Section 568RF pavement structure.

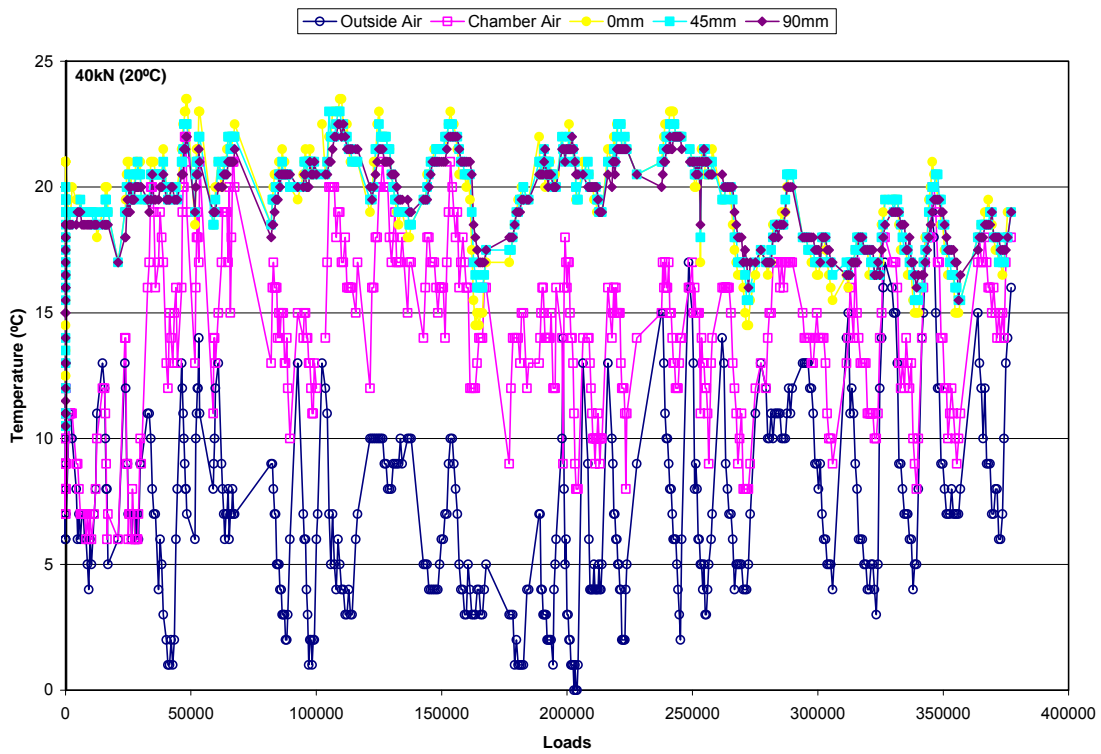


Figure 238. Section 568RF temperatures during testing.



Figure 239. Section 568RF Road Surface Deflectometer.

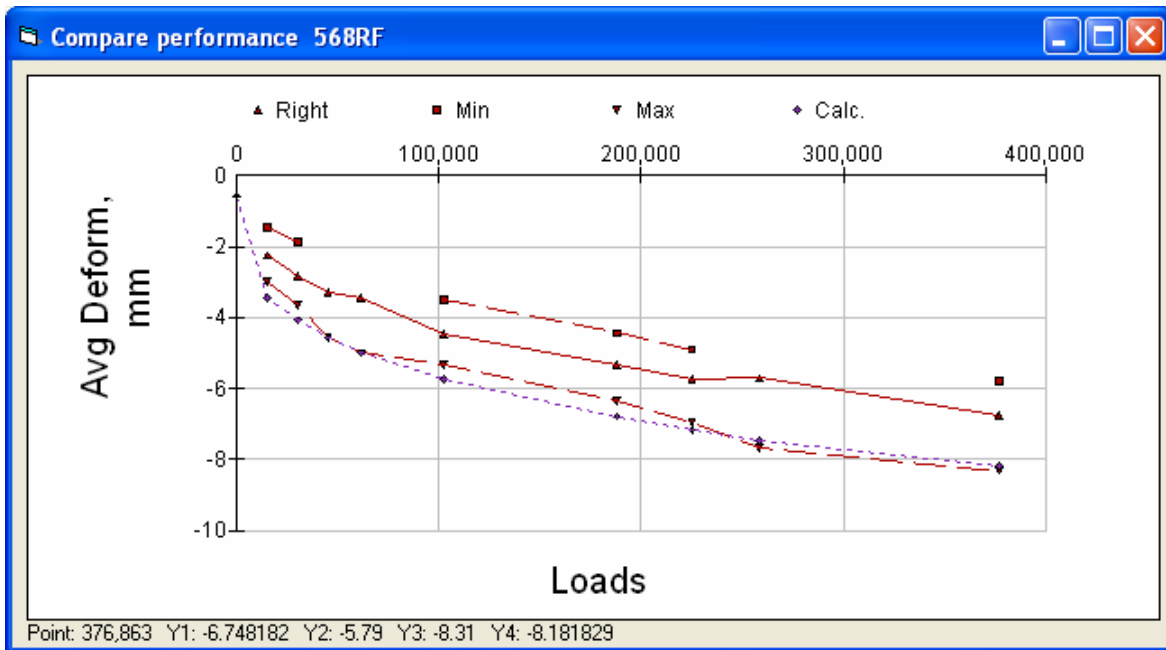


Figure 240. Section 568RF permanent deformation at pavement surface from profilometer.

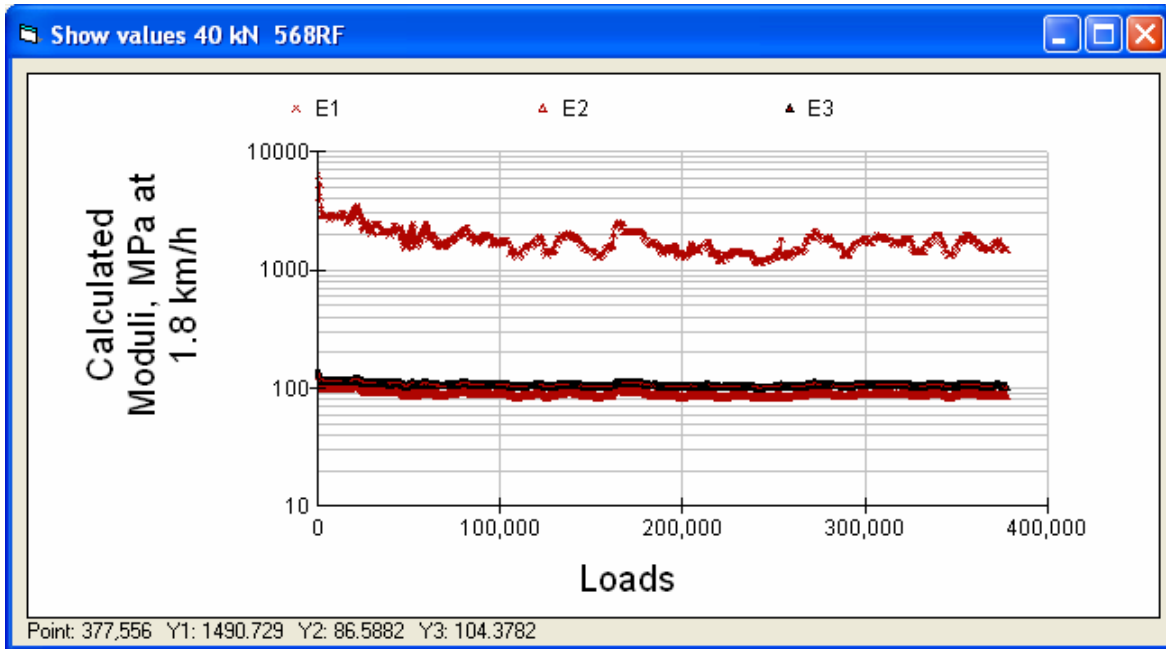


Figure 241. Section 568RF calculated layer moduli at 40 kN and actual temperature.

6.4 Section 573RF MB Road

The test was carried out from March 20, 2002, to July 8, 2002. The pavement structure is shown in Figure 242. Cracking was only recorded at the end of the test, where it had reached 4.2 m/m².

573RF structural data

Design methods Tools Change WIM Parameters

S mm MPa

Layer	Material	Thick	Modulus	Poisson	R	GF	Cost/m3
1	DGACVHVSG9	78	7371	0.35	0	1.46	114
2	ABHVS9	398	180	0.35	78	1.1	57
3	ClayHVS9	0	120	0.35	20	0	0

Figure 242. Section 573RF pavement structure.

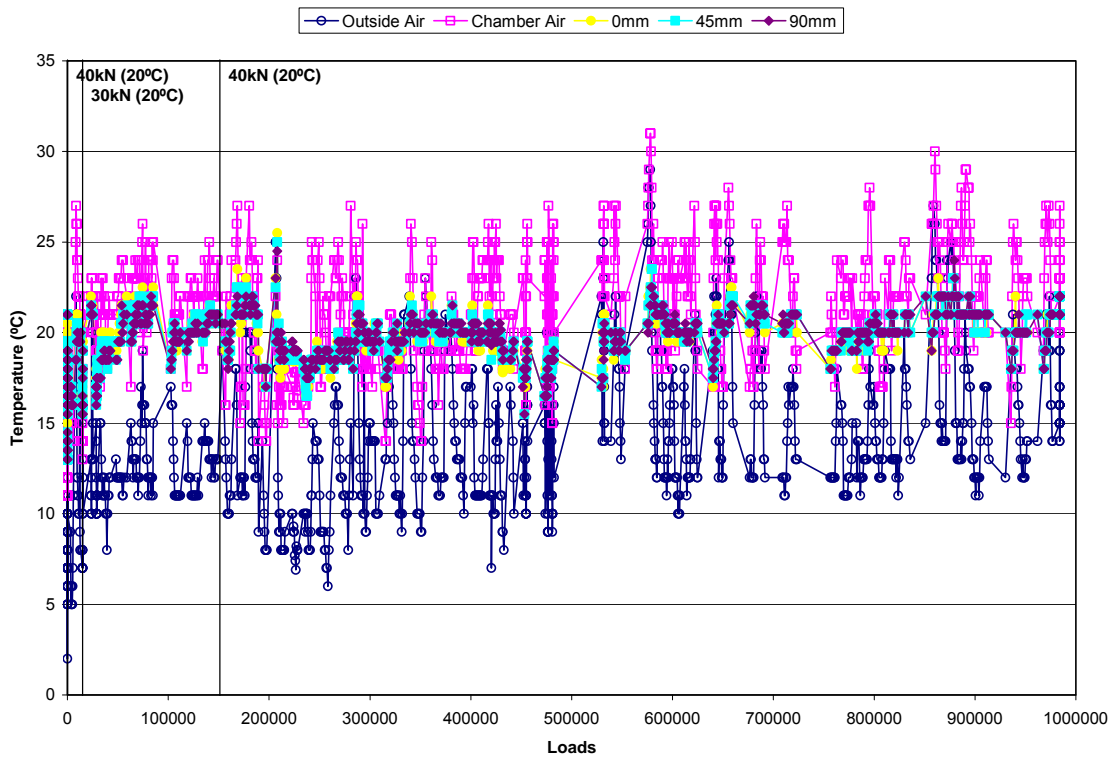


Figure 243. Section 573RF temperatures during testing.

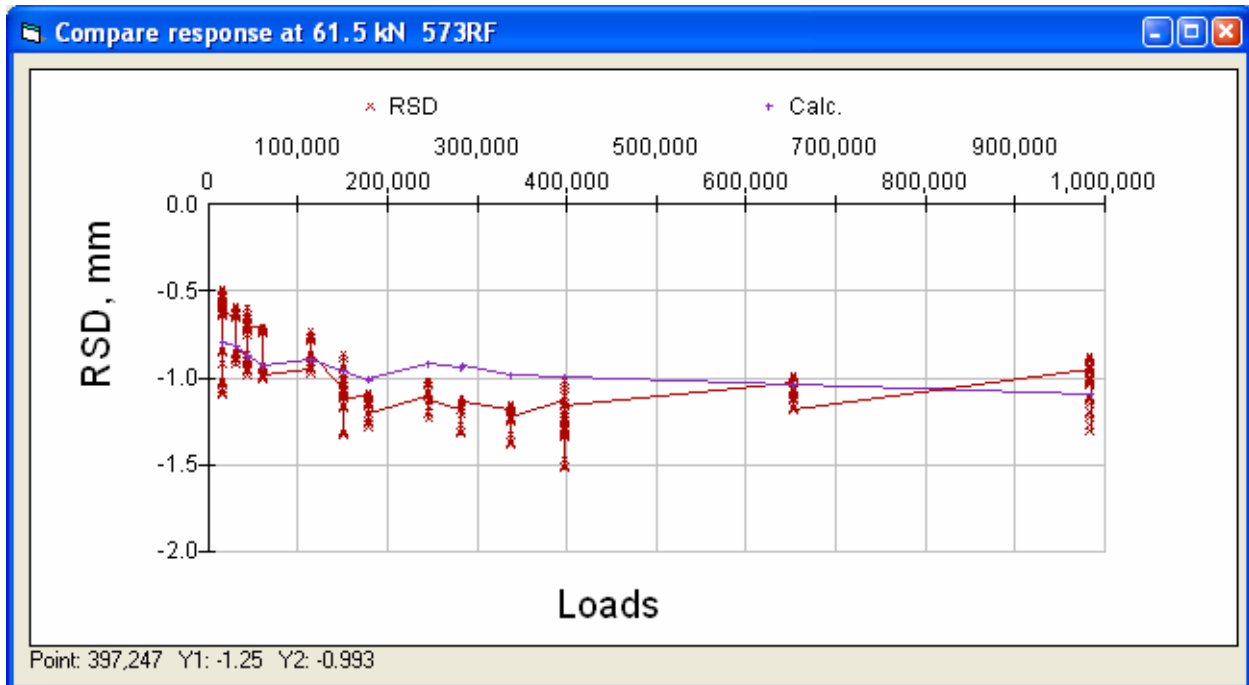


Figure 244. Section 573RF Road Surface Deflectometer.

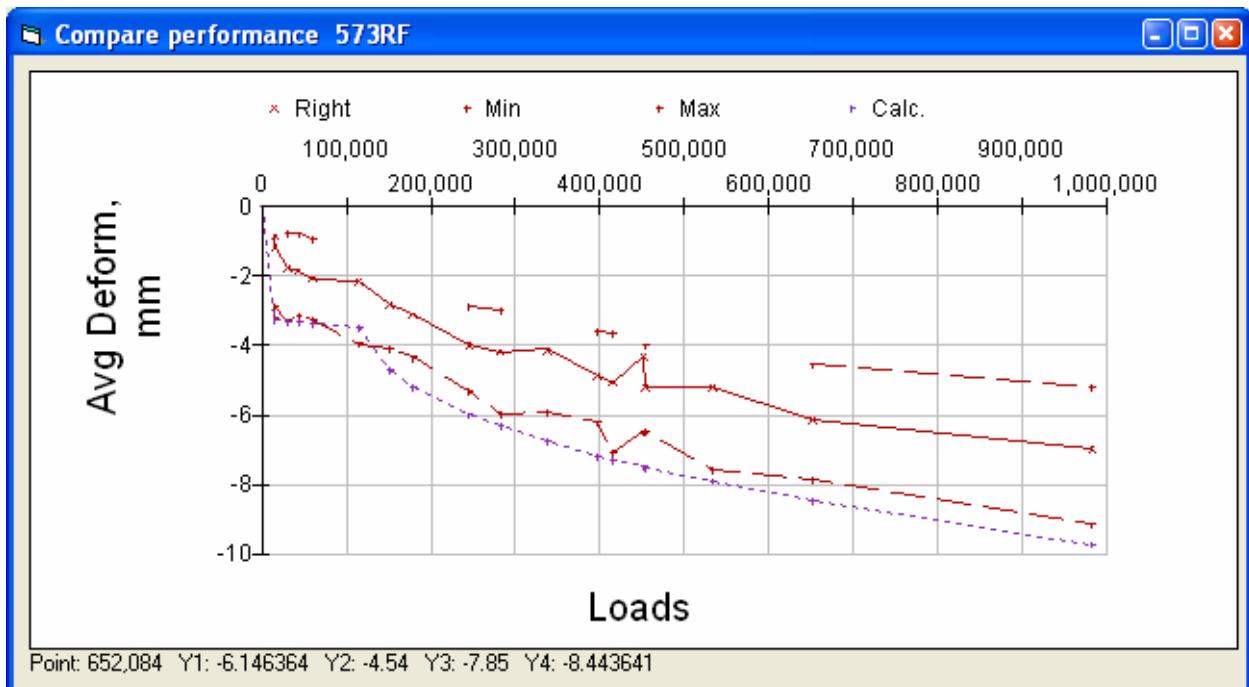


Figure 245. Section 573RF permanent deformation at pavement surface from profilometer.

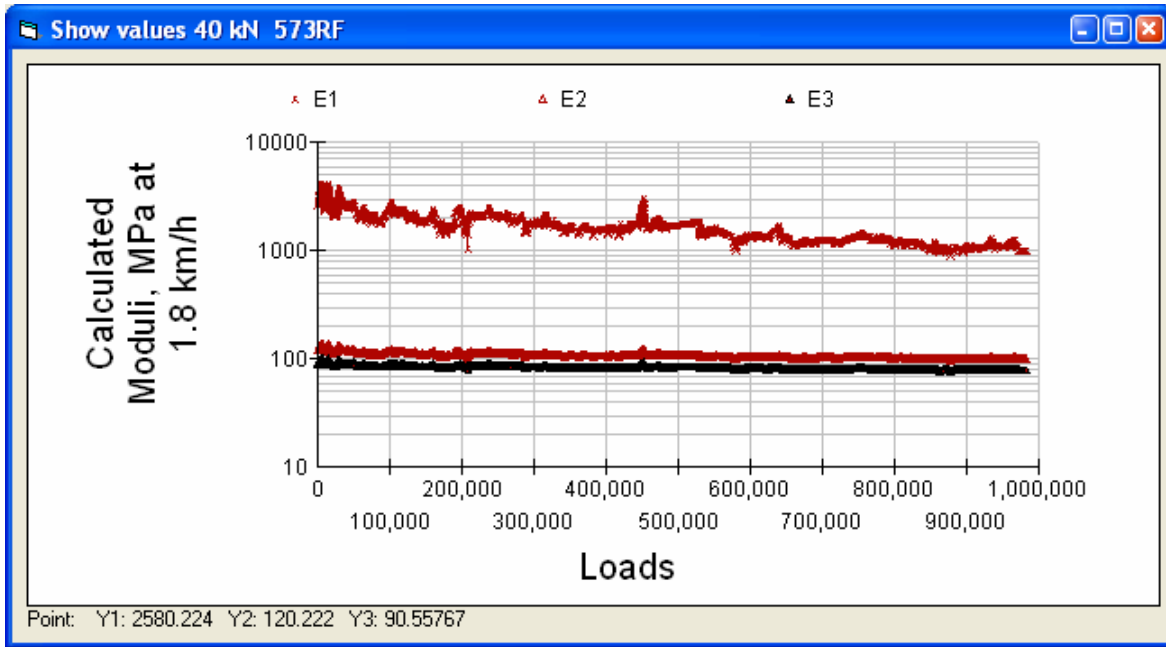


Figure 246. Section 573RF calculated layer moduli at 40 kN and actual temperature.

6.5 Section 571RF MB Road

The test was carried out from July 12, 2002, to October 2, 2002. The pavement structure is shown in Figure 247. The first visible cracking was recorded at approximately 480,000 load repetitions.

571RF structural data

Design methods Tools Change WIM Parameters

S mm MPa

Layer	Material	Thick	Modulus	Poisson	R	GF	Cost/m3
1	DGACVHVSG9	82	7371	0.35	0	1.46	114
2	ABHVS9	398	220	0.35	78	1.1	57
3	ClayHVS9	0	110	0.35	20	0	0

Figure 247. Section 571RF pavement structure.

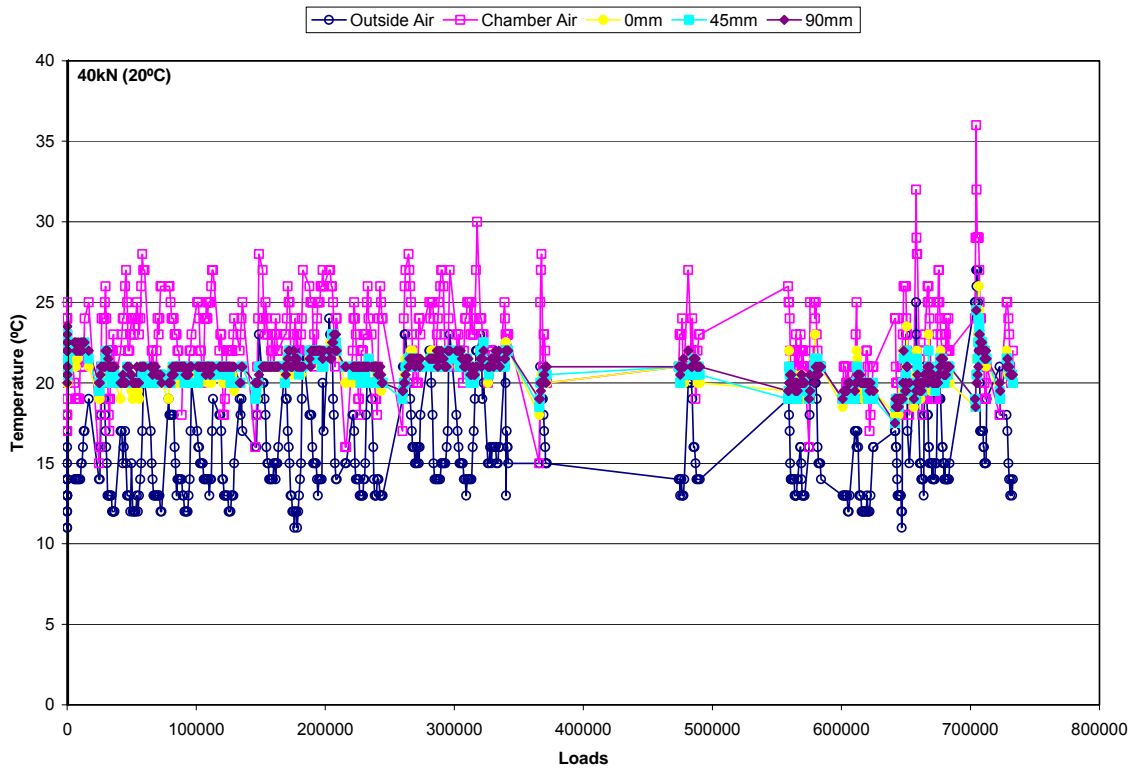


Figure 248. Section 571RF temperatures during testing.

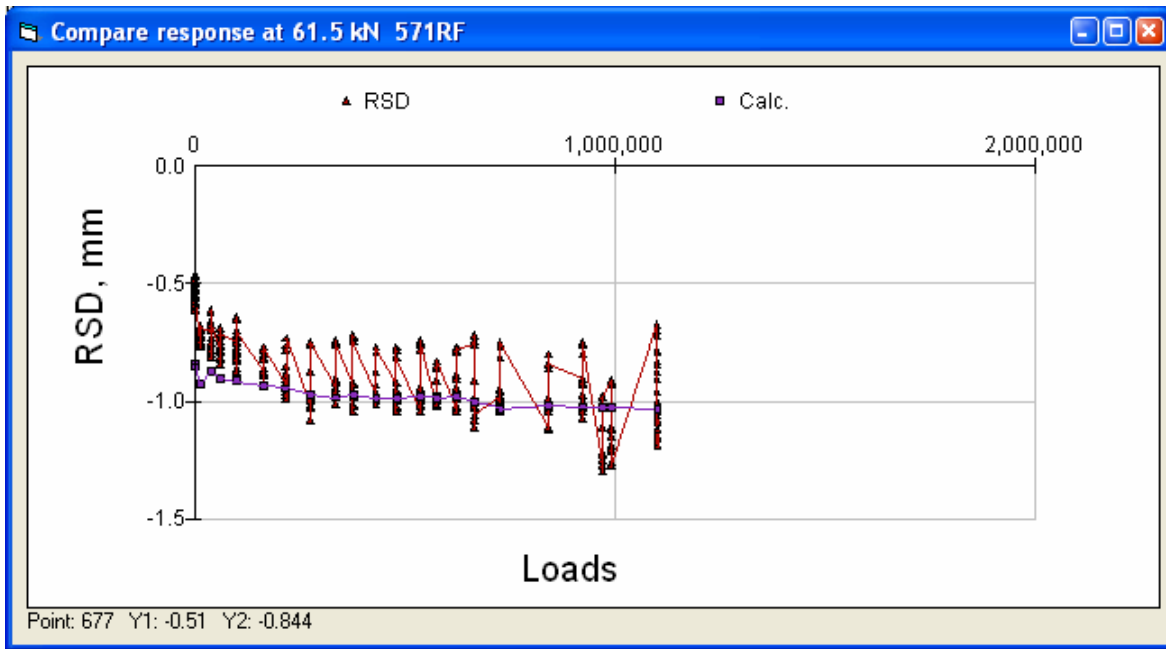


Figure 249. Section 571RF Road Surface Deflectometer.

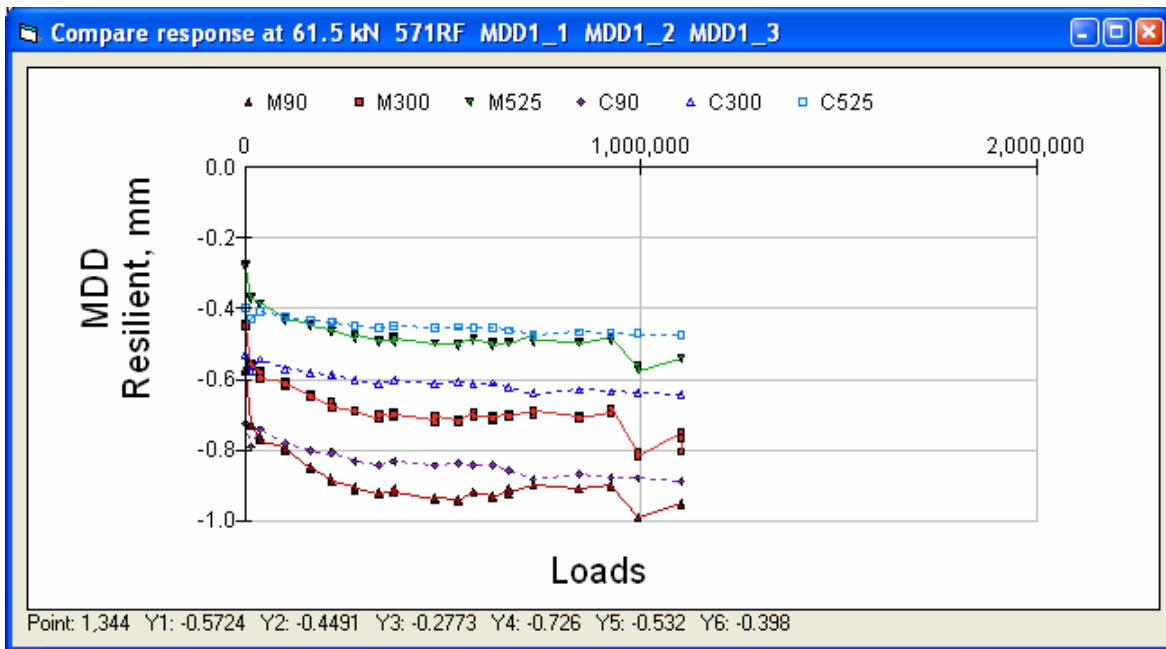


Figure 250. Section 571RF MDDs at 90 mm, 300 mm, and 525 mm.

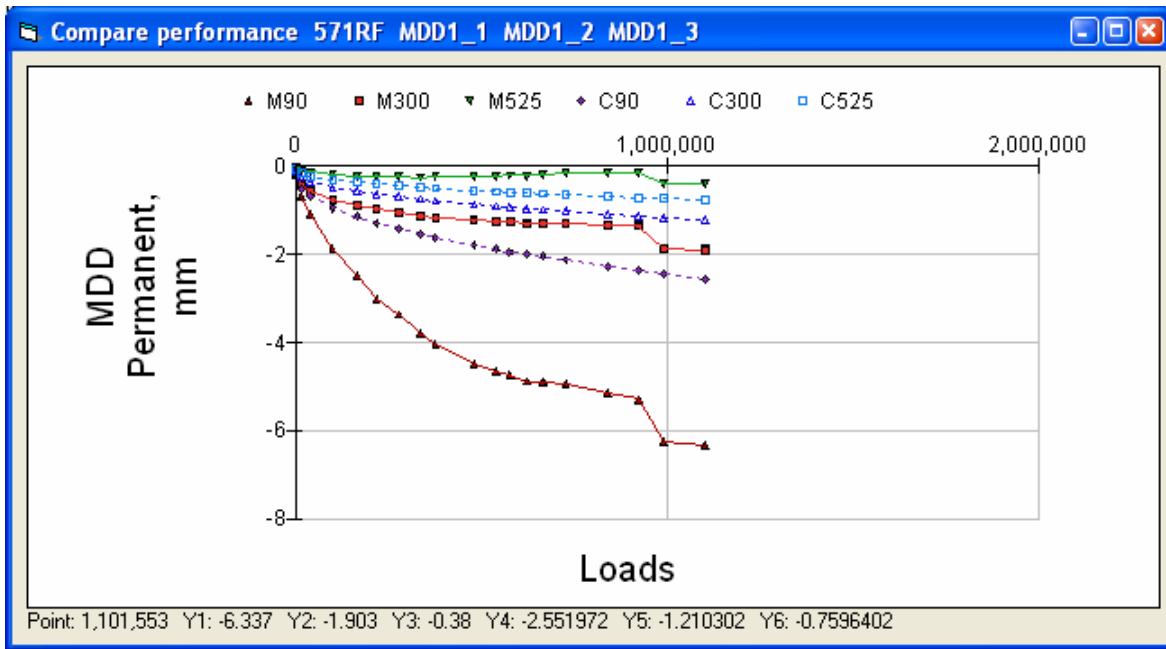


Figure 251. Section 571RF permanent deformation of MDDs.

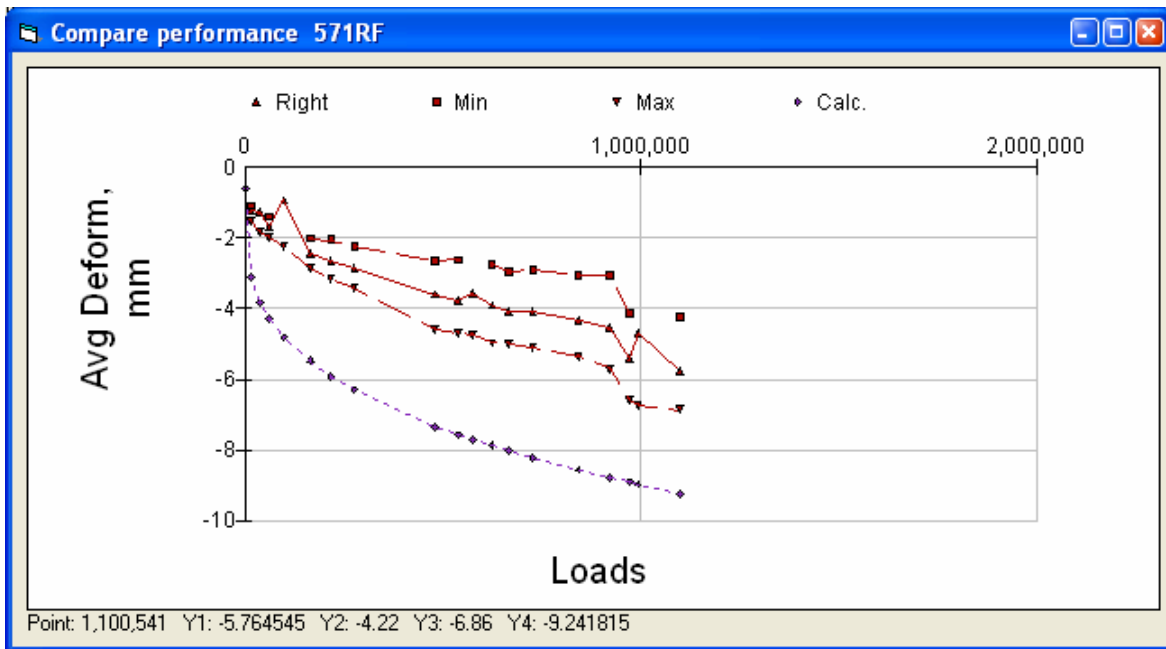


Figure 252. Section 571RF permanent deformation at the pavement surface.

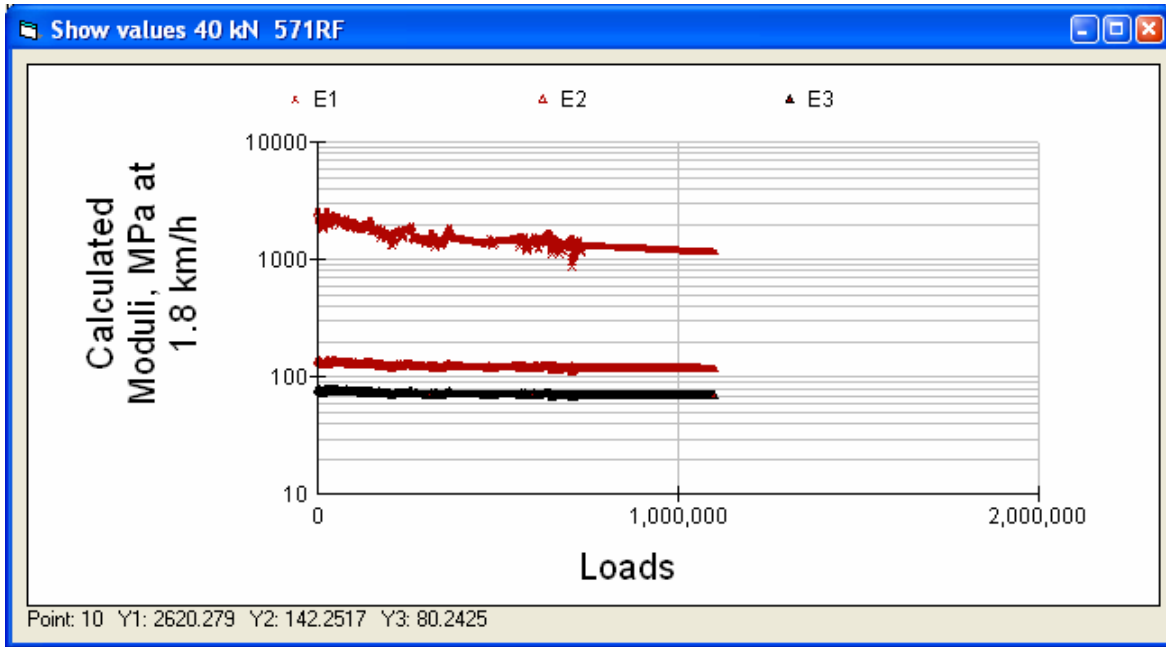


Figure 253. Section 571RF calculated layer moduli at 40 kN and actual temperature.

6.6 Section 572RF MB Road

The test was carried out from January 24, 2003, to March 12, 2003. The pavement structure is shown in Figure 254. The first visible cracking was recorded at approximately 220,000 load repetitions.

572RF structural data

Design methods Tools Change WIM Parameters

S mm MPa

Layer	Material	Thick	Modulus	Poisson	R	GF	Cost/m3
1	DGACVHVSG9	76	7371	0.35	0	1.46	114
2	ABHVS9	398	160	0.35	78	1.1	57
3	ClayHVS9	0	100	0.35	20	0	0

Figure 254. Section 572RF pavement structure.

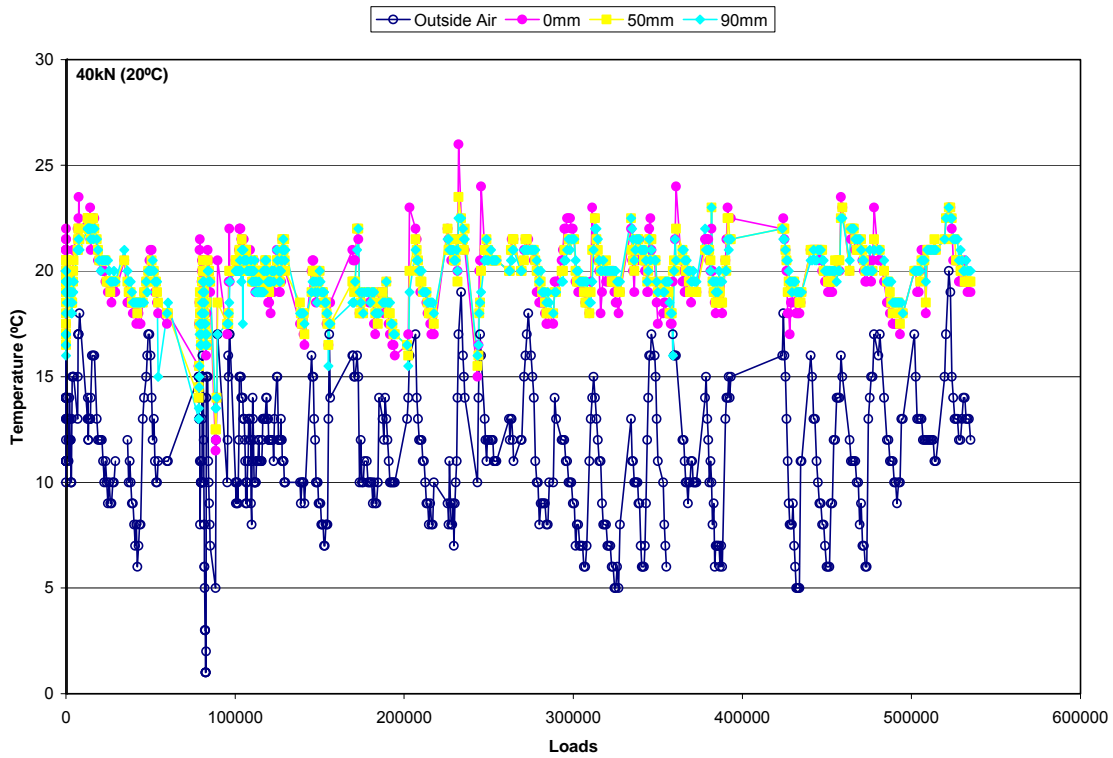


Figure 255. Section 572RF temperatures during testing.

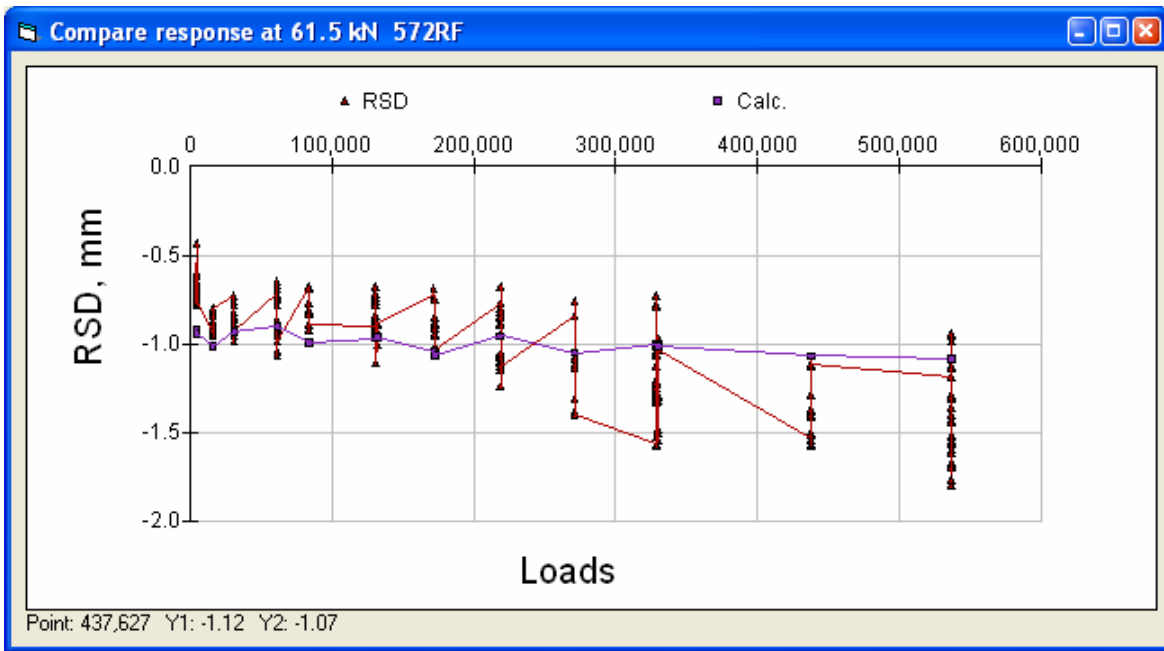


Figure 256. Section 572RF Road Surface Deflectometer.

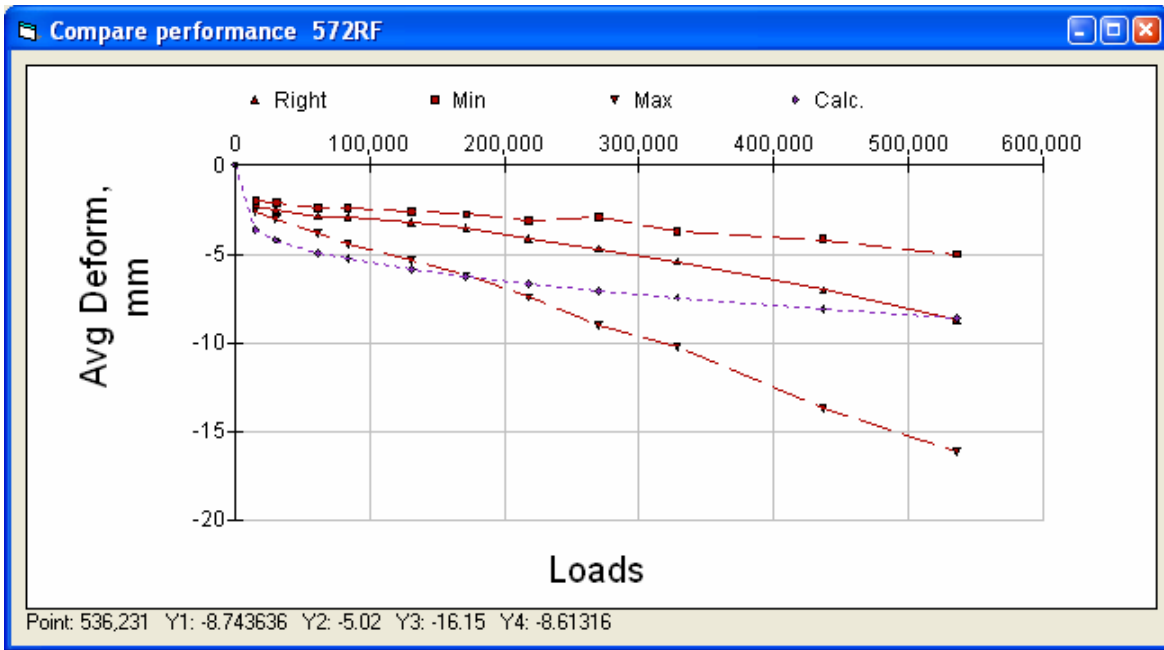


Figure 257. Section 572RF permanent deformation at the pavement surface.

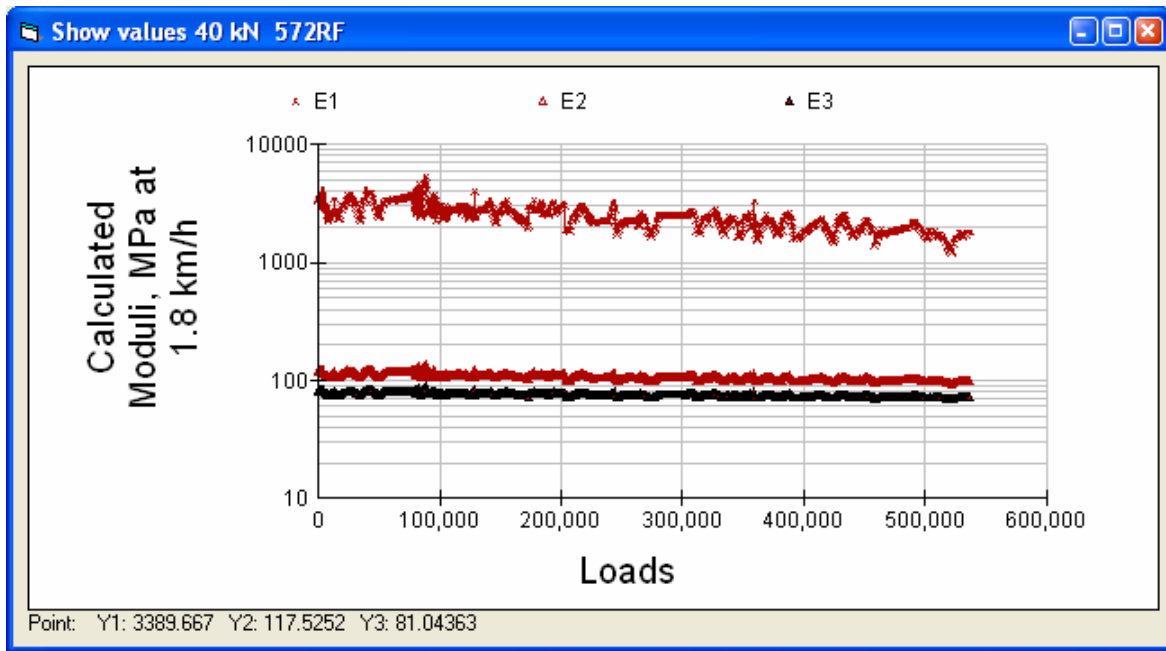


Figure 258. Section 572RF calculated layer moduli at 40 kN and actual temperature.

6.7 Section 569RF MB Road

The test was carried out from March 25, 2003, to April 7, 2003. The pavement structure is shown in Figure 259. Cracking was only recorded at 150,000 load repetitions, where it had reached 5.9 m/m².

Layer	Material	Thick	Modulus	Poisson	R	GF	Cost/m3
1	DGACVHVSG9	104	7371	0.35	0	1.46	114
2	CTB-A-HVS	398	800	0.2	0	1.7	80
3	ClayHVS9	0	200	0.35	20	0	0

Figure 259. Section 569RF pavement structure.

To obtain an increase in resilient deflection comparable to the measured increase, a weak CTB layer was introduced as the base layer with a damage function $\omega = MN \times (\mu\epsilon/(-35 \mu\text{strain}))^{5.6} \times (E/E_i)^{5.6}$. There is no independent evidence for this damage function. The parameters were chosen in order to match the measured resilient deflections. (see the appendix for an alternative simulation)

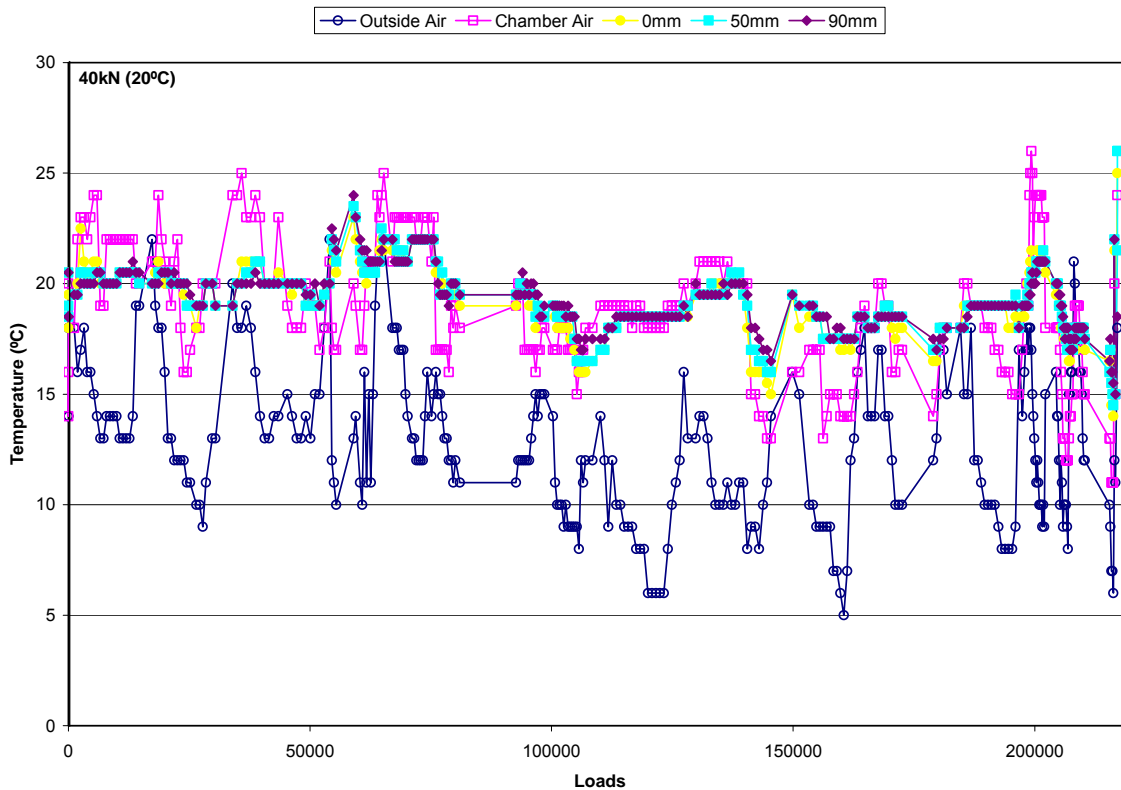


Figure 260. Section 569RF temperatures during testing.

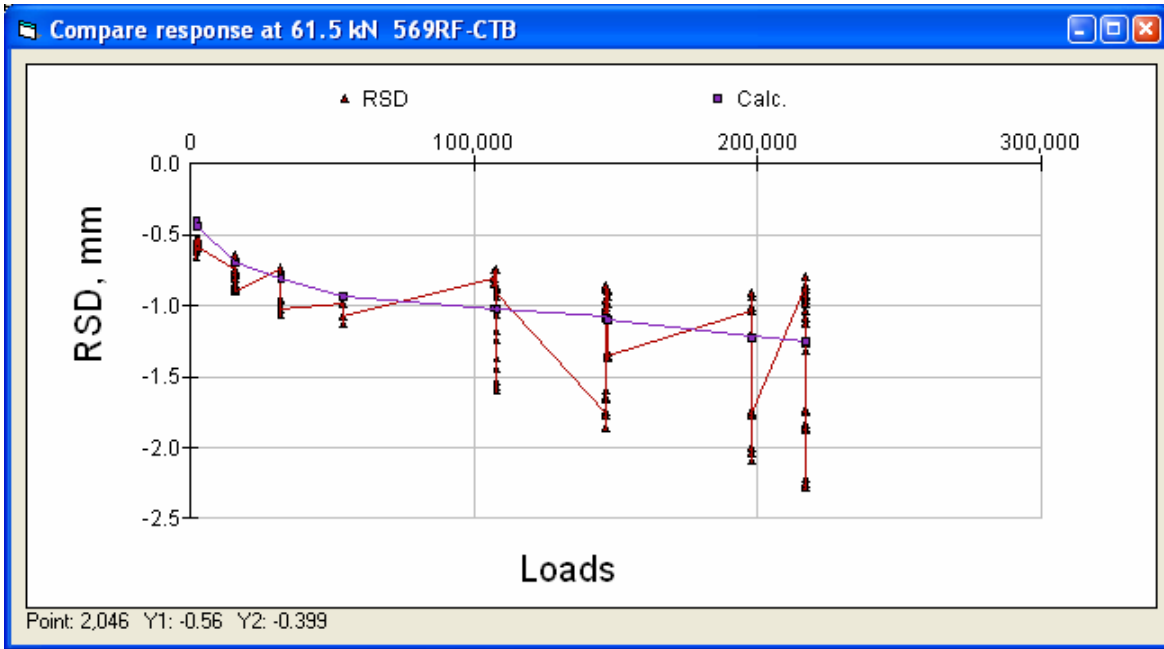


Figure 261. Section 569RF Road Surface Deflectometer.

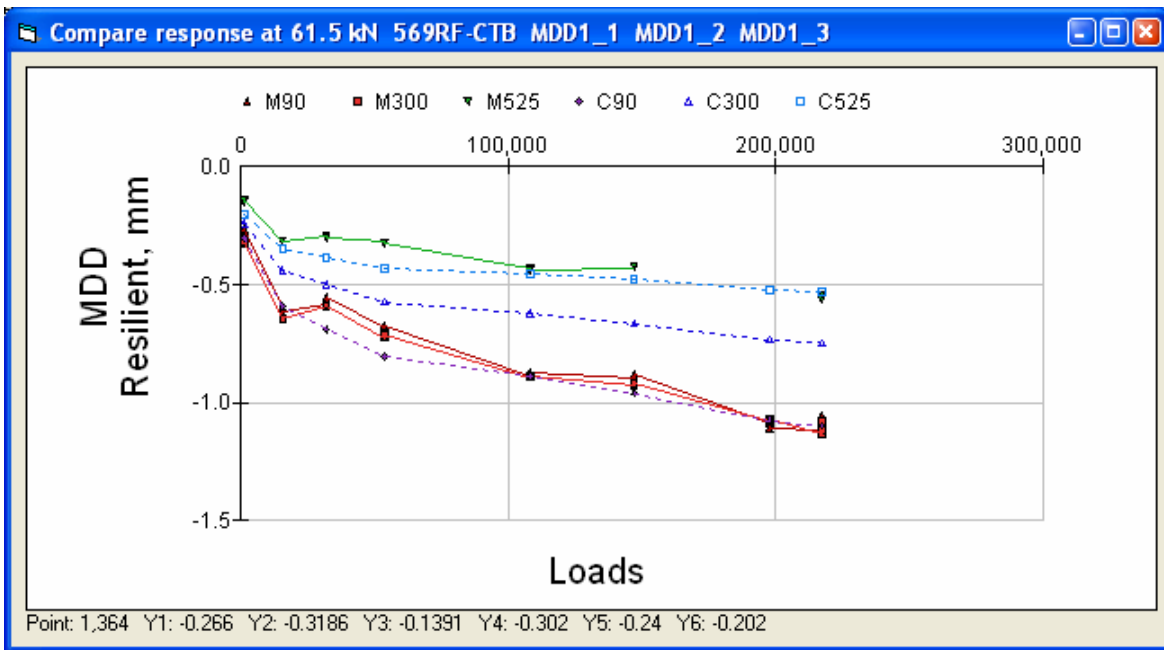


Figure 262. Section 569RF MDDs at 90 mm, 300 mm, and 525 mm

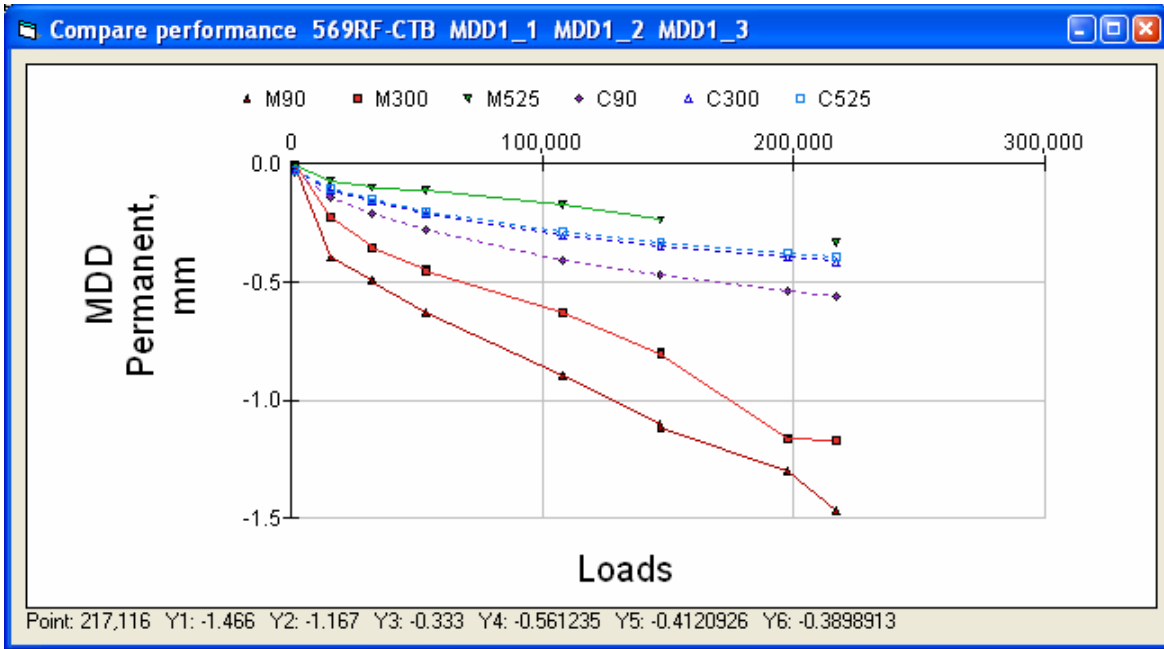


Figure 263. Section 569RF permanent deformation of MDDs.

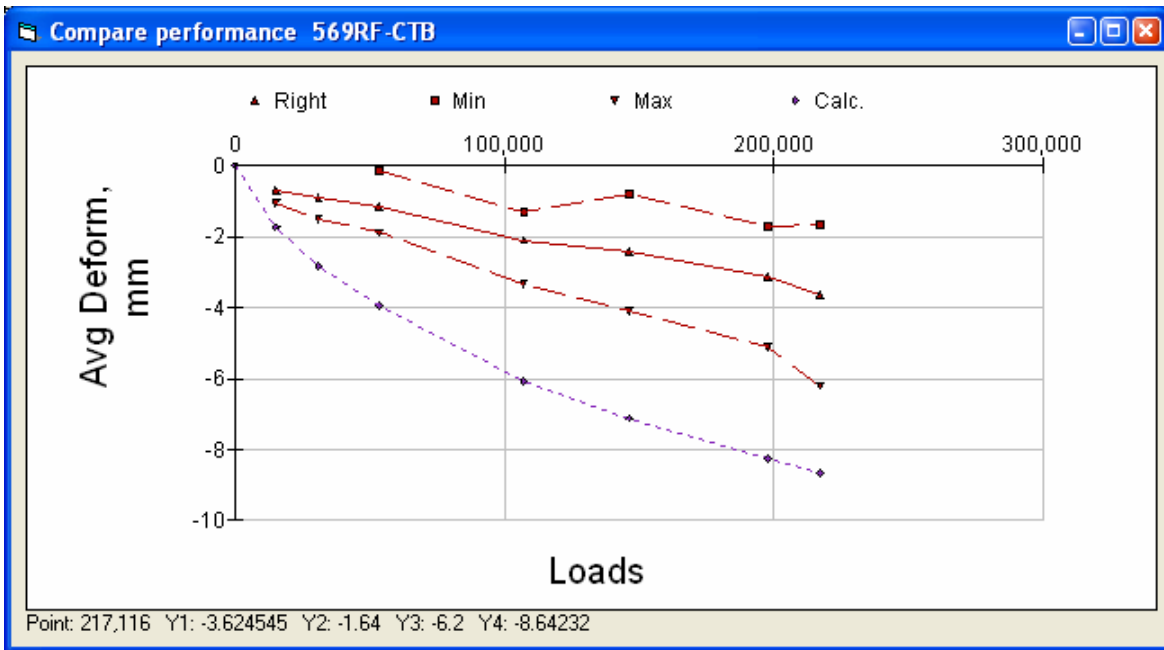


Figure 264. Section 569RF permanent deformation at pavement surface from profilometer.

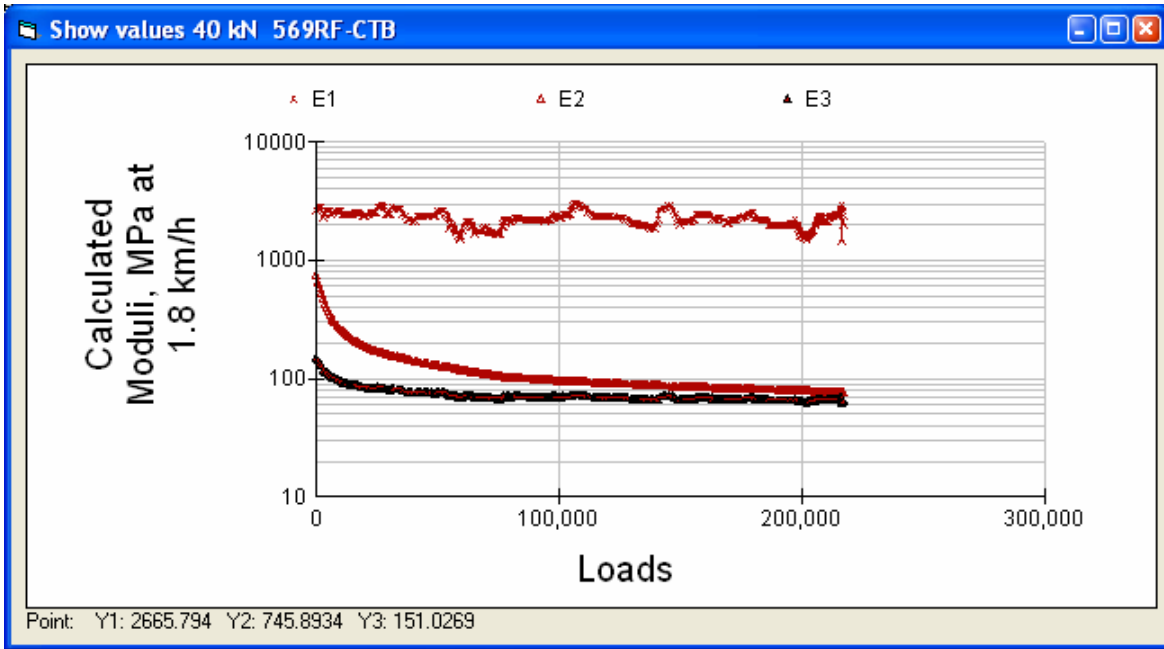


Figure 265. Section 569RF calculated layer moduli at 40 kN and actual temperature.

6.8 Visual Cracking Versus Damage of the Top Asphalt Layer, Goal 9

In Figure 266, cracking at the surface of the pavement (in m/m^2) is shown as a function of the calculated relative decrease in modulus of the AC layer.

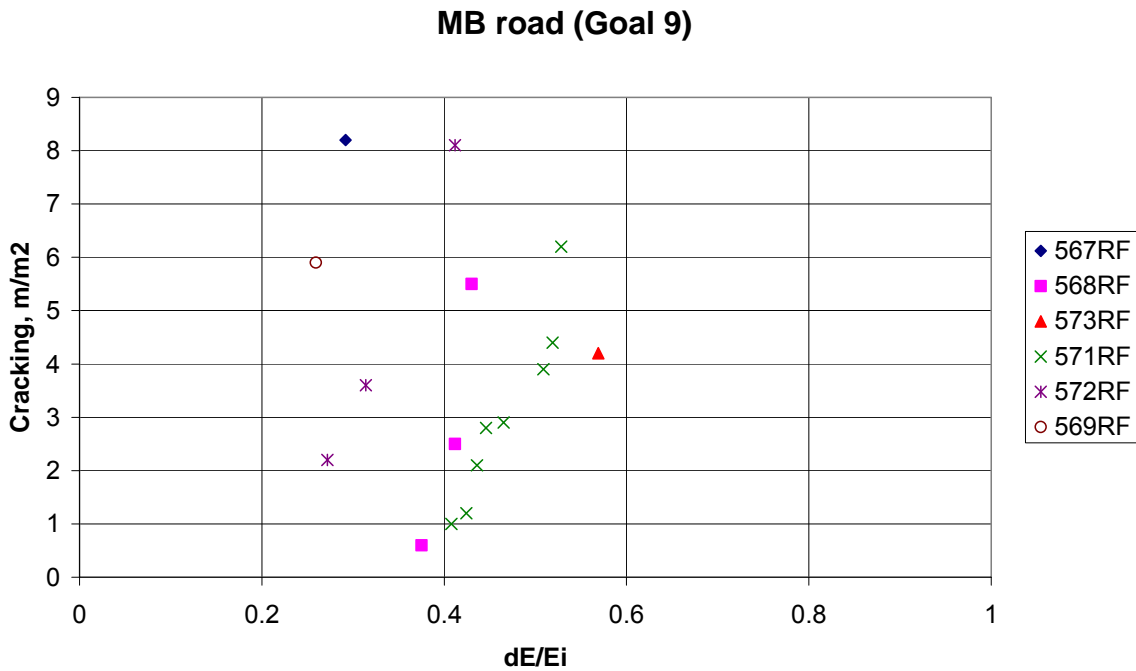


Figure 266. Cracking versus relative decrease in modulus of AC layer for Goal 9 (MB road).

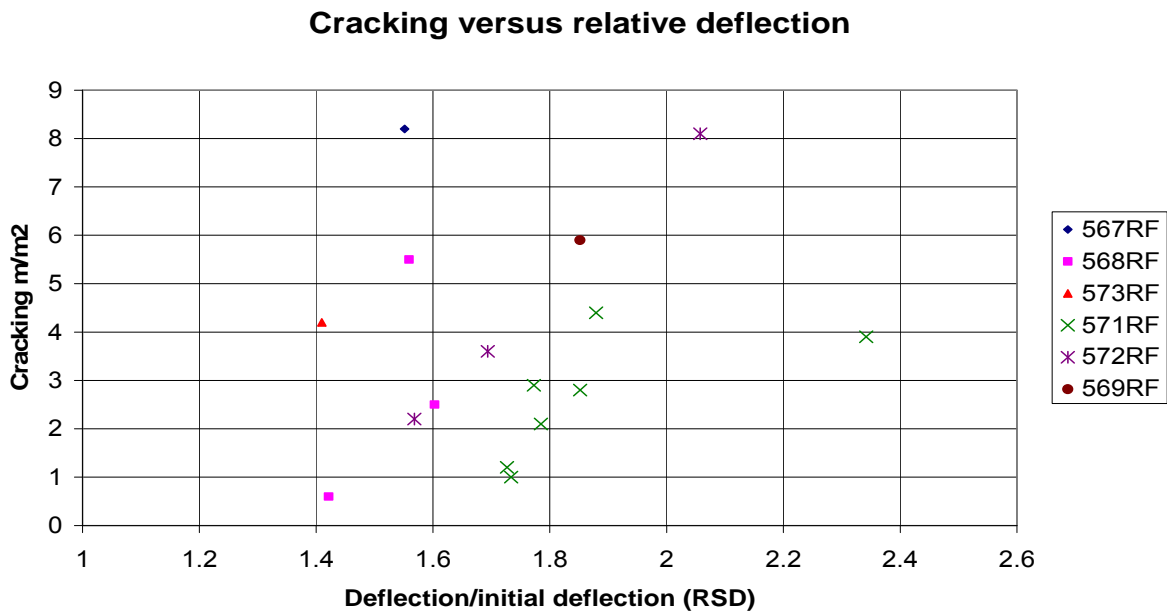


Figure 267. Goal 9 (MB road), Cracking versus increase in deflection (RSD)

7.0 SUMMARY AND RECOMMENDATIONS

CalME software provides users with four approaches for evaluating or designing a flexible pavement structure:

- Caltrans' current methods: the R-value method for new flexible structures and the deflection reduction method for overlay thickness design for existing flexible pavements.
- "Classical" Mechanistic-Empirical (ME) Design, which is based largely on the Asphalt Institute Method, which uses very simple methods to characterize materials, climate and traffic inputs.
- Incremental Design, a standard Miner's Law approach that permits damage calculation for the axle load spectrum and expected temperature regimes, but without updating of the material's properties through the life of the project.
- An Incremental-Recursive approach in which the materials properties of the pavement — in terms of damage and aging — are updated as the pavement life simulation progresses.

The Incremental-Recursive approach was used for the simulations included in this report; it is the only approach that can accurately indicate pavement condition at different points during the pavement's life.

CalME includes a set of models developed for predicting flexible pavement performance operating in an Incremental-Recursive model. They include:

- A stiffness model for asphalt concrete modulus that is derived from the model used in NCHRP 1-37A, with adjustments based on field observations;
- An asphalt concrete fatigue model that predicts damage as a function of load repetition, tensile strain, and stiffness, using parameters from flexural beam testing;
- An ability to model partial bonding between asphalt concrete layers;
- A model that adjusts the stiffness of unbound layers as a function of the combined bending resistance (a function of their stiffness and thickness) of the bound layers above them, and as a function of load level;
- A permanent deformation model for asphalt concrete as a function of permanent shear strain near the pavement surface beneath the edge of a tire, with permanent shear strain predicted by the calculated elastic shear strain and elastic shear stress
- A permanent deformation model for unbound layers as a function of the vertical strain at the top of each layer;
- A reflection cracking model based on tensile strain calculated using a regression equation developed from a large number of Finite Element analyses, and use of the same damage parameters developed for asphalt concrete fatigue.

These models were used to simulate pavement response for 27 flexible pavement tests under HVS trafficking performed for Caltrans since 1995. Detailed results have been shown in this report, section by section. A summary comparison of the results across all the sections of this report follows.

7.1 Shift Factors and Damage Equations Used in Simulations

Fatigue damage and rutting equations, and shift factors for fatigue and unbound layers rutting used in all the simulations presented in this report are shown in the following table. It can be seen that the same equations and shift factors were used for all of the simulations, except for the shift factor for the damage function for the underlying asphalt concrete in Goal 3. Equation number refers to the equation number in the report.

Table 28. Summary of Damage Equations and Shift Factors Used in All Simulations

	Fatigue Damage Equation No.	Unbound Layers Rutting Equation No.	Fatigue Shift Factor	Unbound Layers Shift Factor
Goal 1	6	29	3	1
Goal 3 medium temp overlay	6	29	3	1
Goal 3 medium temp underlying	6	29	0.6	1
Goal 3 high temp	6	29	3	1
Goal 5	6	29	3	1
Goal 9 underlying	6	29	3	1

Parameter values for equations used in the simulations are presented in Section 9.4 of this report.

7.2 Response Model

Resilient deflections were measured during 17 of the HVS tests. The deflections showed a considerable increase during the tests. For the Road Surface Deflectometer (RSD), the increase was between 38 and 304 percent, with an average value of 136 percent. The initial and final RSD deflections are shown in Table 29 and for the top MDD in Table 30.

Table 29. Measured and Calculated Road Surface Deflectometer Deflections (RSD), in mm

	RSD	Measured		Calculated		Ratio Final/Initial	
		Initial	Final	Initial	Final	Measured	Calculated
Goal 1	501RF	0.333	0.761	0.398	0.916	2.29	2.30
	503RF	0.250	0.826	0.338	0.919	3.30	2.72
	500RF	0.396	0.756	0.331	0.961	1.91	2.90
	502CT	0.234	0.693	0.297	0.649	2.96	2.19
Goal 3, 20°C	517RF	0.395	0.717	0.454	0.930	1.82	2.05
	518RF	0.439	0.814	0.480	0.936	1.85	1.95
	514RF	0.314	0.879	0.373	0.874	2.80	2.34
	515RF	0.346	0.758	0.318	0.761	2.19	2.39
Goal 5	543RF	0.255	1.031	0.304	0.973	4.04	3.20
	544RF	0.355	0.986	0.332	1.200	2.78	3.61
	545RF	0.367	1.125	0.409	1.144	3.07	2.80
Goal 9	567RF	0.722	0.997	0.810	1.076	1.38	1.33
	568RF	0.714	1.145	0.650	1.019	1.60	1.57
	573RF	0.790	1.128	0.791	1.093	1.43	1.38
	571RF	0.618	1.088	0.844	1.036	1.76	1.23
	572RF	0.740	1.530	0.924	1.089	2.07	1.18
	569RF	0.591	1.376	0.399	1.246	2.33	3.12

Table 30. Measured and Calculated Deflections of the Top Multi-depth Deflectometer (MDD), in mm

	MDD0	Measured		Calculated		Ratio Final/Initial	
		Initial	Final	Initial	Final	Measured	Calculated
Goal 1	501RF	0.364	0.852	0.343	0.813	2.34	2.37
	503RF	0.277	0.916	0.283	0.816	3.31	2.88
	500RF	0.358	0.668	0.324	0.849	1.87	2.62
	502CT	0.195	0.673	0.259	0.672	3.45	2.59
Goal 3, 20°C	517RF	0.463	0.768	0.385	0.823	1.66	2.14
	518RF	0.400	0.742	0.413	0.839	1.86	2.03
	514RF	0.232	0.879	0.342	0.770	3.79	2.25
	515RF	0.390	0.688	0.279	0.694	1.76	2.49
Goal 5	543RF	0.258	1.015	0.286	0.976	3.93	3.41
	544RF	0.385	1.049	0.317	1.211	2.72	3.82
	545RF	0.355	1.213	0.385	1.243	3.42	3.23
Goal 9	567RF	0.805	0.752	0.732	0.972	0.93	1.33
	571RF	0.728	1.000	0.726	0.889	1.37	1.22
	569RF	0.266	1.092	0.302	1.097	4.11	3.63

The test sections are listed in the tables in the same order that they are presented in the report. Variation in temperature of the AC and the position of the RSD will influence deflection, so the deflections are average values at the beginning and end of the HVS testing based on measurements at all RSD positions and uncorrected for the expected minor differences in temperature at time of measurement. All deflections were measured at the centerline of a 40 kN dual wheel load.

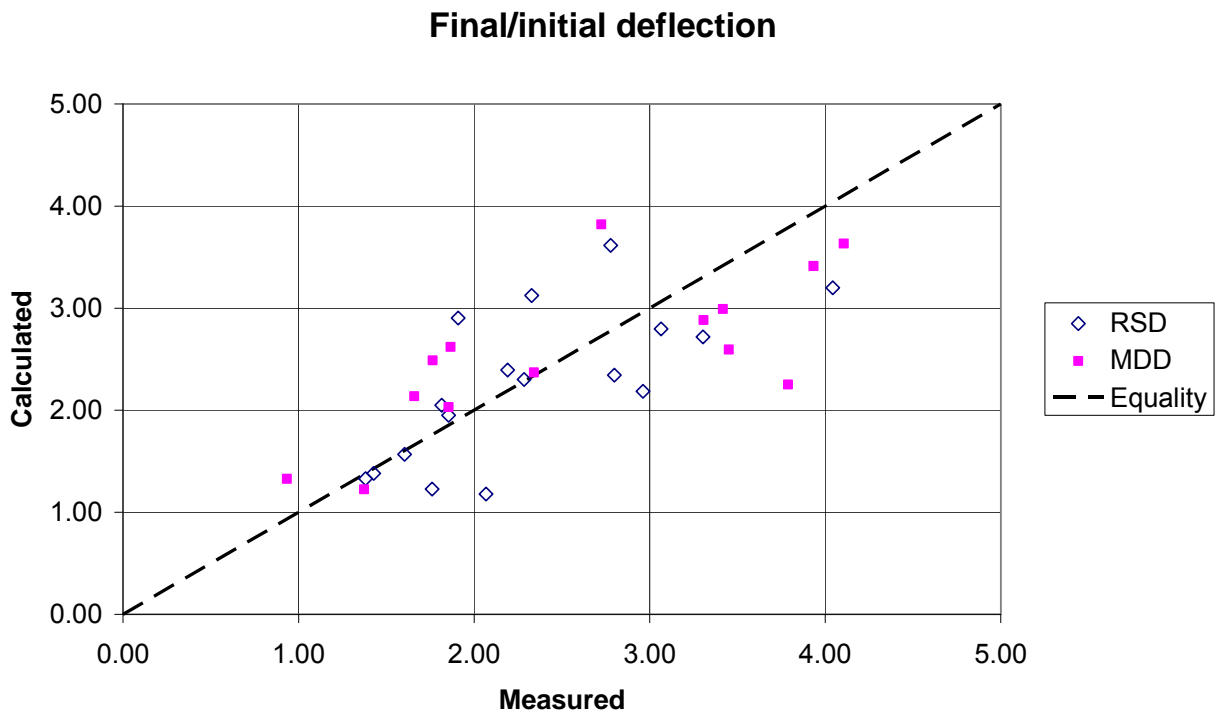


Figure 268. Ratio of final over initial deflection.

The ratios of the final over the initial deflections are shown in Figure 268. On average the deflections increased by a factor of 2.4 during the HVS testing.

If the response model (the mechanistic model) could not correctly predict this development in resilient deflection, then its calculation of response — in terms of stresses and strains — would also be incorrect. If that were the case, it would not be possible to calibrate the empirical models between response and damage. Therefore, it was crucial that the calculated resilient deflections be reasonable correct.

It is not presently possible to predict the increase in resilient deflections with the NCHRP 1-37A Design Guide because in it the layer moduli do not change with increased damage, with the exception of cement-bound materials. The Guide calculates damage, but it is not used to adjust moduli. Therefore, only the new unloaded pavement and its final state of distress can be checked and used for calibration with APT (Accelerated Pavement Testing) or field data. This makes it very difficult to check the reasonableness of the individual effects of the different models operating in the program, such as aging, damage, permanent deformation, temperature, load duration, etc. A change to the ME Pavement Design Guide — to allow layer moduli to change with increasing damage — is very desirable.

To obtain reasonable agreement between measured and calculated resilient deflections with *CalME*, a number of assumptions were made:

1. Frequency sweep tests on laboratory specimens can be used to determine the moduli of the asphalt bound layers as a function of reduced time. A minimum asphalt modulus of 200 MPa was assumed when determining the model's parameters from frequency sweep data. AC moduli determined from FWD testing tended to be lower than the frequency sweep moduli.
2. The moduli of the unbound materials can be determined from the initial RSD and MDD deflections. The moduli of the granular materials were generally lower than the corresponding moduli from FWD testing and of the same order of magnitude as the triaxial moduli for saturated

- material. For the subgrade, MDD moduli were similar to FWD moduli and larger than triaxial moduli.
3. Poisson's ratio was 0.35 for all layers.
 4. Laboratory fatigue tests (controlled strain tests on beams) can be used to assess the damage to asphalt bound materials (in terms of the decrease in their modulus). A constant shift factor of 3 was used between the HVS tests and the laboratory tests for original material for 16 of the 17 test sections where resilient deflections were measured. This means that three load repetitions during HVS testing caused the same damage as one laboratory load, given the same conditions of strain, modulus, and temperature.
 5. A simple model can be used to calculate the strain in an overlay covering existing cracks, and this calculation can be used with parameters derived from laboratory fatigue testing to calculate the reduction in modulus of the overlay, again using a shift factor of three.
 6. To obtain reasonable initial deflections on overlaid sections that had previously been loaded to cracking, a certain amount of "pseudo-healing" had to be assumed, a reasonable assumption based on observation of APT and laboratory testing. Under pavement reloading the material deteriorated quickly with a shift factor of 0.6 (i.e., a rate of deterioration five times that of the original material), similar to what was observed in APT and laboratory testing.
 7. In certain test sections a slip developed between some asphalt layers. In these cases a full slip was used with the Layered Elastic Analysis Program (LEAP) response model (except for calculation of the permanent deformation of the asphalt layers). The actual effect of a slip between layers probably cannot be correctly modeled with LEAP, but would require a Finite Element model.
 8. FWD tests and MDD resilient deflections both showed that the moduli of the unbound layers varied with the stiffness of the layers above the one under consideration. The effect observed from the measured data was that the stiffness of unbound granular and clay materials decreased as the stiffness of the layers above them decreased. The "effective" stiffness of the layers above was modeled as the material stiffness times the thickness cubed. This observed effect contradicts the commonly accepted wisdom for granular materials, which is based primarily on triaxial testing and suggests that the stiffness of granular materials should increase as the stiffness of the layers above decreases because of the increased sum of the principal stresses or first stress invariant. The research team continues to investigate this phenomenon and the hypothesis that the stiffer layers above provide greater confinement to the unbound particulate material in the granular layer. The boundary conditions differ considerably between triaxial testing and the placement of a stiff plate such as a layer of cold asphalt concrete across a layer of loose particles. Despite the lack of theoretical or numerical analysis to completely explain the cause, the empirical evidence is irrefutable and has not been contradicted by a single example, regardless of whether the asphalt layer lost stiffness because of increased temperature or increased damage. Stiffness factors derived from FWD tests were used to model these changes. Neither the NCHRP 1-37A Design Guide nor any other known mechanistic-empirical design procedure considers this effect, which has an important influence on resilient deflections and requires detailed study. Here the phenomenon is modeled by adjusting the modulus of the unbound materials as a function of the "effective" sub-plate bending stiffness of the overlaying plate.
 9. The unbound layers are non-linear elastic. This is the well known non-linearity, which the NCHRP 1-37A Design Guide also considers, with the modulus of granular materials increasing with the bulk stress (to a power of 0.6, in all tests) and the modulus of the subgrade decreasing with deviator stress (to a power of -0.3). The phenomenon is modeled here by adjusting the modulus of the unbound layers as a function of the load level. This phenomenon is different than the one described above, and both are considered here.

Using these assumptions, it was possible to model resilient deflections reasonably well for the full history of all of HVS test sections using the LEAP response model. To model HVS test sections using the NCHRP 1-37A Design Guide several important changes are required to the Design Guide models.

7.3 Damage of Asphalt Materials

Controlled strain fatigue tests on beams were used to derive model parameters for the decrease in asphalt modulus for all the asphalt materials — except for the ATPB, for which laboratory tests were unavailable.

Using these damage models (and the other assumptions mentioned above) with a shift factor of 3 produced the correct changes to resilient deflections during all the HVS tests.

For reflection cracking, a simple model was used to calculate the strains in an overlay caused by existing cracking in the original top layer. With this model and the laboratory fatigue model, reasonably correct resilient deflections were also predicted. It should be noted, however, that the resilient deflections, at the center of a dual wheel, are not very sensitive to the modulus of the overlay.

Relating visual cracking to calculated asphalt damage proved to be difficult. No single relationship could be derived. Goal 1 and Goal 5 showed differences between the drained and the undrained sections, for Goal 3 (reflection cracking) the increase in visual cracking was much steeper than for Goal 1 and Goal 3, and for Goal 9 (MB road) visual cracking occurred at much less calculated damage than for the other experiments.

It is possible that the relationship between visual cracking and calculated damage depends on the thickness of the asphalt layers, and that reflection cracking develops differently from cracks in the original structure. It is also possible that the development of visual cracking depends on factors that were not considered during the simulations.

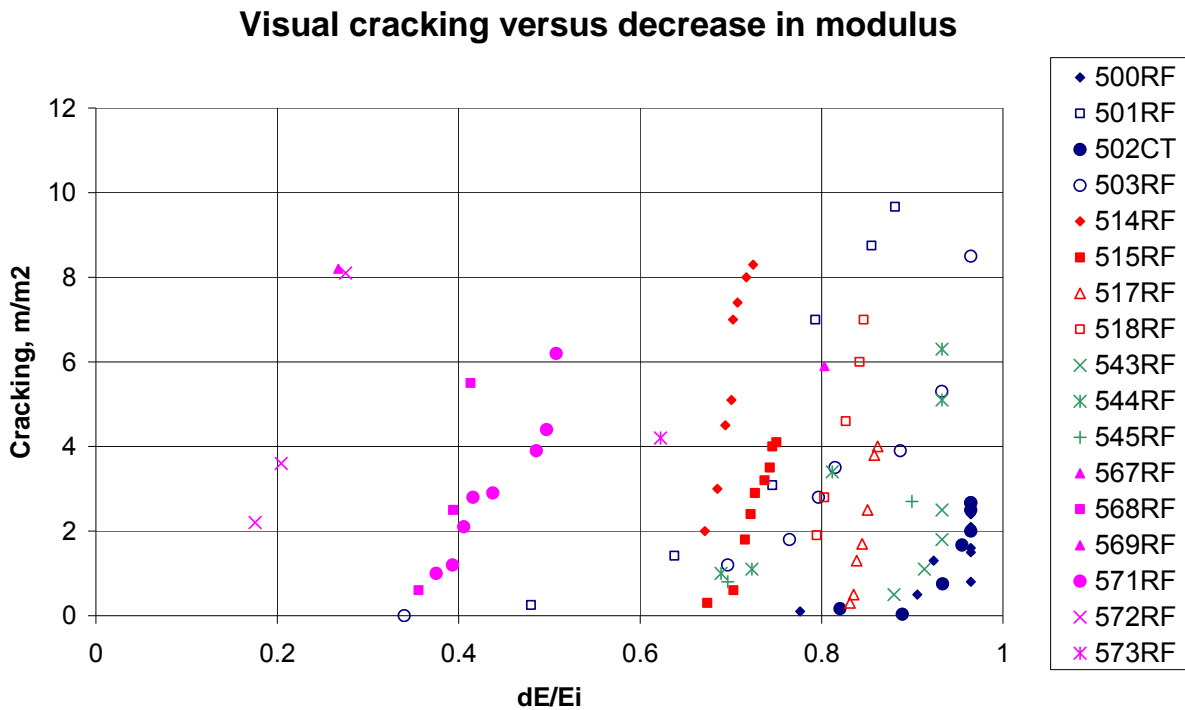


Figure 269. Cracking versus calculated decrease in modulus of top layer.

No single relationship could be established between the relative increase in deflection and the amount of surface cracking, Figure 270, but it may be noted that visible cracking was not observed until the deflection had increased by 50 percent or more. For the pavements with thin asphalt layers (Sections 567RF–573RF) and for rehabilitated pavements (Sections 514RF-518RF) the relative increase in deflection is lower, 50–100 percent, than for the thicker, original pavements (Sections 500RF-503RF) where it is 100–200 percent. The largest increase in deflection is for the wet tests (Sections 543RF–545RF).

Cracking versus relative deflection

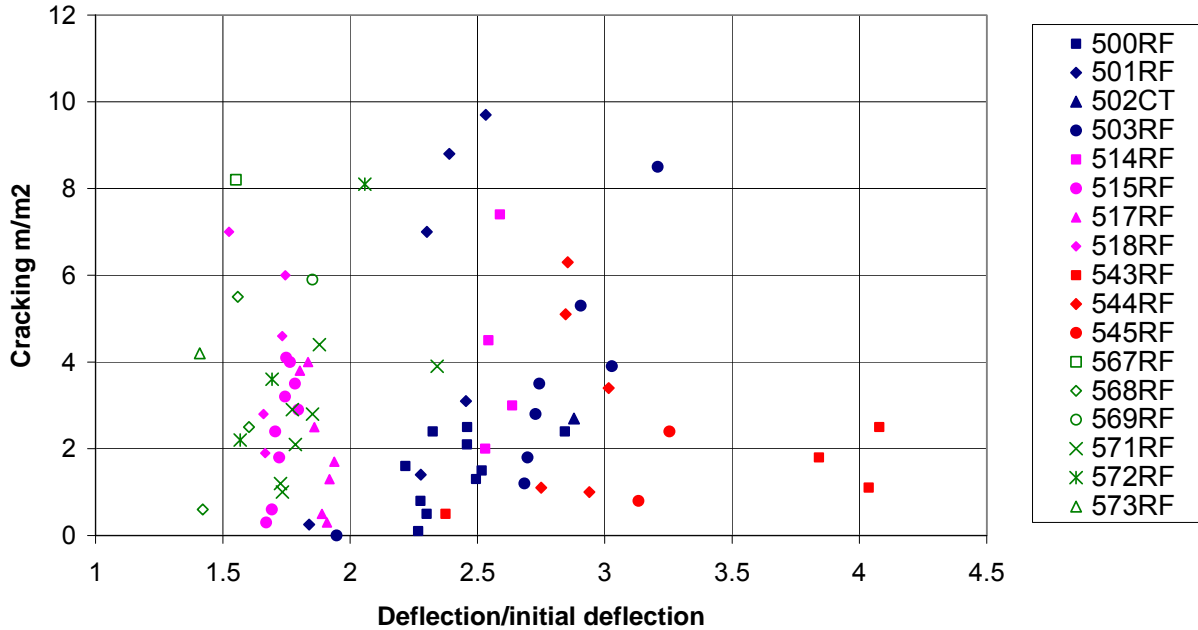


Figure 270. Cracking versus increase in deflection.

7.4 Permanent Deformation of Asphalt

Figure 271 shows the measured and predicted final permanent deformation of the asphalt layers from Goal 1, Goal 3 and Goal 5, where data on the permanent deformation of the asphalt were available. For the rutting tests of Goal 3 (45–55°C), permanent deformation (measured and calculated) was the total deformation of all layers but it was completely dominated by the asphalt deformation. (The values are also shown in mm in Table 31.)

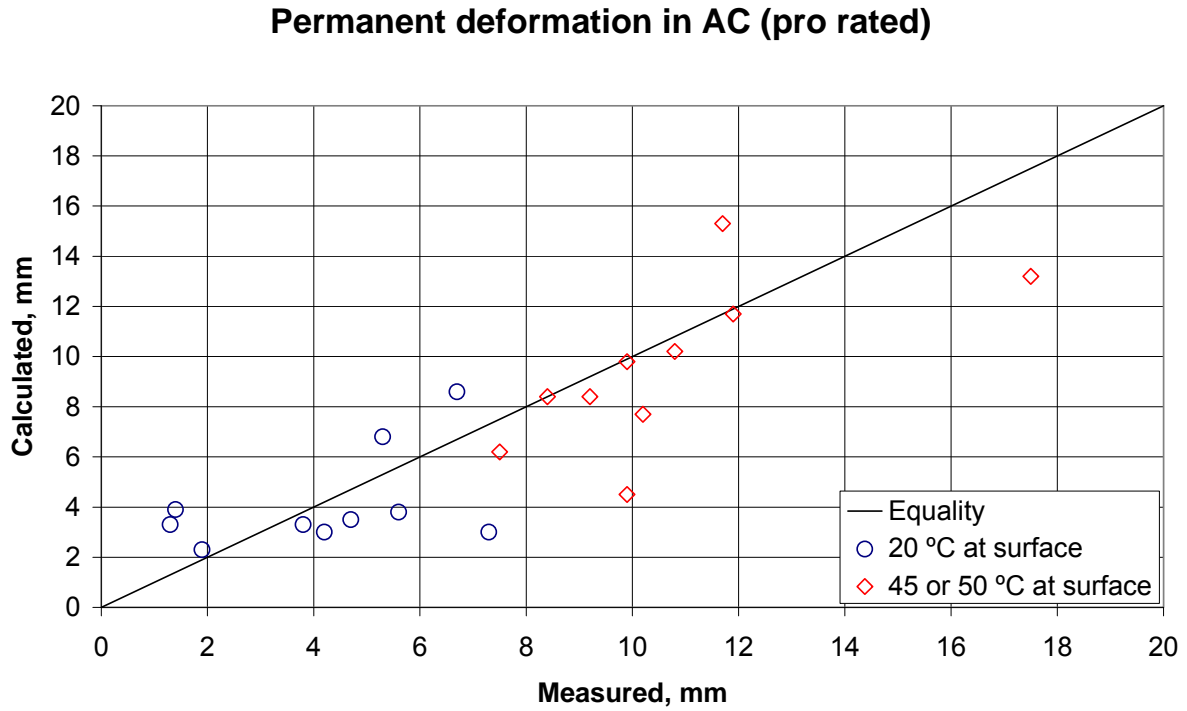


Figure 271. Measured and predicted final permanent deformation of asphalt.

The correlation coefficient between measured and calculated deformations was 0.82 and the standard error of estimate was 2.2 mm.

Table 31. Final Permanent Deformation of Asphalt, in mm

	Section	Measured	Calculated	Ratio = Measured/Calculated
Goal 1	501RF	4.7	3.6	1.3
	503RF	3.8	3.4	1.1
	500RF	5.6	3.9	1.4
	502CT	4.2	3.2	1.3
Goal 3, 20°C	517RF	5.3	4.9	1.1
	518RF	1.4	2.4	0.6
	514RF	1.9	2.1	0.9
	515RF	1.4	2.4	0.6
Goal 5	543RF	7.2	2.6	2.8
	544RF	1.3	2.6	0.5
Goal 3, Rutting (45– 55°C)	504RF	7.5	6.2	1.2
	505RF	9.9	4.5	2.2
	506RF	10.2	7.7	1.3
	507RF	11.9	11.7	1.0
	508RF	11.7	15.3	0.8
	509RF	10.8	10.2	1.1
	510RF	9.2	8.4	1.1
	511RF	9.9	9.8	1.0
	512RF	8.4	8.4	1.0
	513RF	17.5	13.2	1.3

The asphalt layers of Section 543RF, which was a wet drained test where the ATPB apparently collapsed, had a high measured permanent deformation. The permanent deformation was measured between elevation 0 mm and 250 mm, comprising 47 mm of the ATPB layer that may have caused the 4.6-mm difference between measured and calculated permanent deformation.

The high temperature tests with the bias-ply dual tire and with the aircraft tire both resulted in smaller calculated than measured values.

7.5 Permanent Deformation of Granular Layers

The permanent deformation of the granular layers for Goal 1, Goal 3, and Goal 5 are shown in Figure 272. It should be noted that the permanent deformations are rather small, except for Section 543RF, the wet drained section, where the permanent deformation includes part of the ATPB, which completely stripped and collapsed after 600,000 repetitions (which the models cannot capture).

Permanent deformation of granular layers

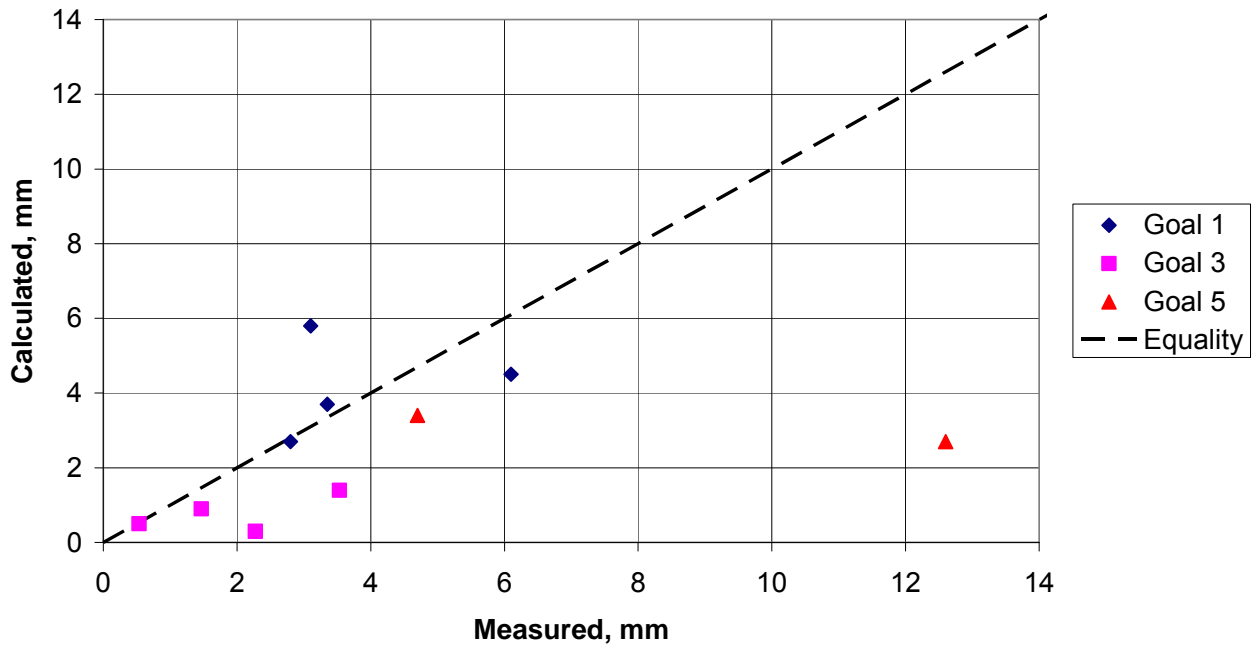


Figure 272. Final permanent deformation of granular layers.

The scatter of the data is very large, as may be seen in the plots in this report. The average coefficient of variation is 58 percent. The measured values shown in Figure 272 are averages. The values are also shown (in mm) in Table 32.

Table 32. Final Permanent Deformation of Granular Layer, in mm

	Section	Measured	Calculated
Goal 1	501RF	3.4	3.7
	503RF	6.1	4.5
	500RF	3.1	5.8
	502CT	2.8	2.7
Goal 3, 20°C	517RF	3.5	1.4
	518RF	1.5	0.9
	514RF	2.3	0.3
	515RF	0.5	0.5
Goal 5	543RF	12.6	2.7
	544RF	4.7	3.4

For Goal 3 the predicted permanent deformations tended to underestimate the measured values. It is possible that some recovery from permanent deformation took place from Goal 1 to Goal 3. Assuming a full recovery, however, would have resulted in overpredictions of the deformations.

The permanent deformations of the granular materials were predicted using Equation (29) with the following parameters:

Table 33. Parameters used for Granular Materials in Equation (29)

Parameter	Value
A	0.8 mm
α	0.333
$resp_{ref}$	1000 μ strain
β	1.333
E_{ref}	40 MPa
γ	0.333

Permanent deformation was calculated both at the top of the AB (aggregate base) and at the top of the ASB. The two materials are rather similar and might have been treated as a single layer. In that case, the parameter A should have been increased to 1.1 mm, the value used for the subgrade.

7.6 Permanent Deformation of Subgrade

The final permanent deformation of the subgrade was even smaller than that of the granular layers, with a maximum measured value of less than 2 mm. In addition the scatter of the data was as large as for the granular layers, with an average coefficient of variation of 70 percent. This is far from ideal for the calibration of a permanent deformation model for the subgrade.

The mean measured and predicted final deformations are shown in Figure 273 and (in mm) Table 34.

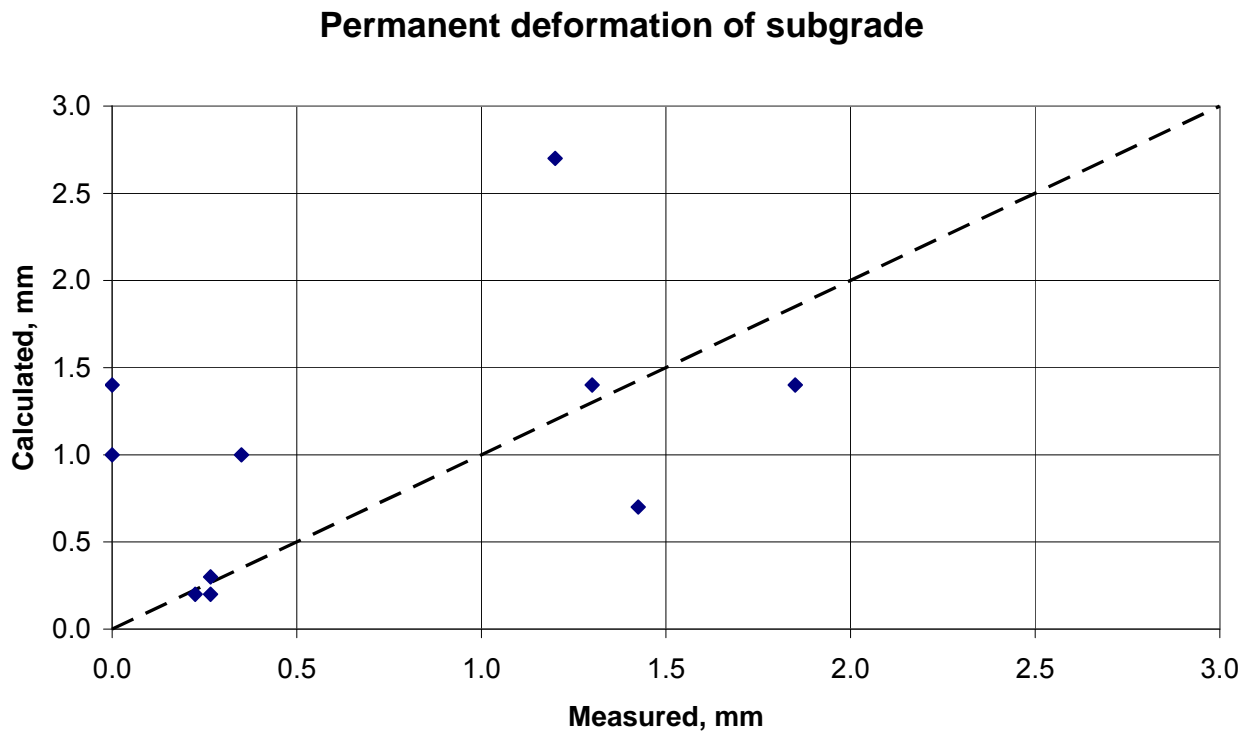


Figure 273. Final permanent deformation of the subgrade.

Table 34. Final Permanent Deformation of Subgrade, in mm

	Section	Measured	Calculated
Goal 1	501RF	1.3	1.4
	503RF	1.9	1.4
	500RF	1.2	2.7
	502CT	0.4	1.0
Goal 3, 20°C	517RF	1.4	0.7
	518RF	0.3	0.3
	514RF	0.2	0.2
	515RF	0.3	0.2
Goal 5	543RF	0.0	1.0
	544RF	0.0	1.4

The permanent deformations of the subgrade were predicted using Equation (29) with the following parameters:

Table 35. Parameters Used for Subgrade in Equation (29)

Parameter	Value
A	1.1 mm
α	0.333
$resp_{ref}$	1000 μ strain
β	1.333
E_{ref}	40 MPa
γ	0.333

7.7 Total Permanent Deformation at Pavement Surface

Figure 274 shows the final calculated permanent deformation at the pavement surface versus the mean value of the measured final average deformation over the test area, determined from profile data. It should be noted that the permanent deformation often showed considerable variation over the test area, as also indicated by the minimum and maximum values shown in some of this report's graphs.

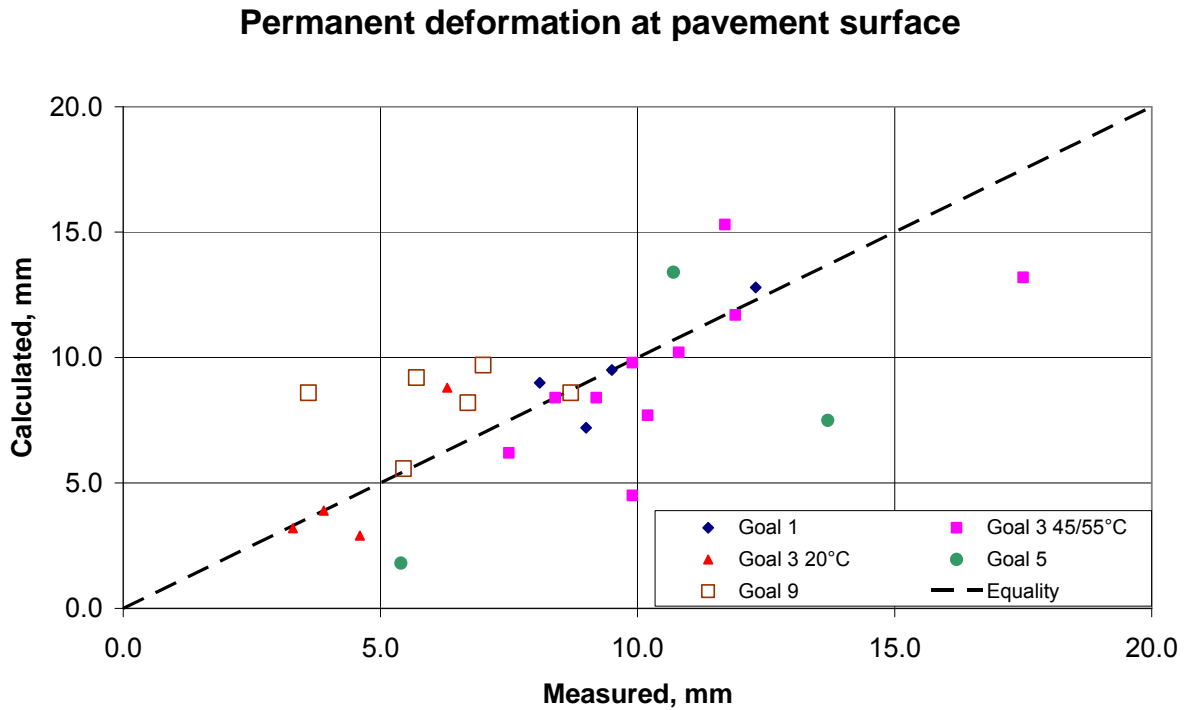


Figure 274. Final permanent deformation at the pavement surface (profile data).

For the wet experiment in Goal 5, the predicted final deformation was underestimated for the drained Section 543RF because of the collapse of the ATPB layer after it stripped under heavy loading and large amounts of water drained through it.

The final permanent deformations are also shown (in mm) in Table 36.

Table 36. Final Permanent Deformation at the Pavement Surface, in mm

	Section	Measured	Calculated
Goal 1	500RF	12.3	12.8
	501RF	9.0	7.2
	502CT	9.5	9.5
	503RF	8.1	9.0
Goal 3, 45-55°C	504RF	7.5	6.2
	505RF	9.9	4.5
	506RF	10.2	7.7
	507RF	11.9	11.7
	508RF	11.7	15.3
	509RF	10.8	10.2
	510RF	9.2	8.4
	511RF	9.9	9.8
	512RF	8.4	8.4
	513RF	17.5	13.2
Goal 3, 20°C	514RF	4.6	2.9
	515RF	3.9	3.9
	517RF	6.3	8.8
	518RF	3.3	3.2
Goal 5 Wet	543RF	13.7	7.5
	544RF	10.7	13.4
	545RF	5.4	1.8
Goal 9 MB road	567RF	5.5	5.1
	568RF	6.7	7.5
	569RF	3.6	5.6
	571RF	5.7	7.6
	572RF	8.7	5.4
	573RF	7.0	9.7

The correlation coefficient between measured and calculated total permanent deformation was 0.61 and the standard error of estimate was 2.6 mm.

7.8 Recommendations

The overall results from this study indicate that Incremental-Recursive models provide reasonable results when predicting the response and performance of pavements under HVS loading. However, now that the models have been shown to match the mechanics of the pavements under these conditions, additional work remains before the models can be used for pavement design and performance prediction.

There are significant differences between HVS testing and the field, and the approach used in this study has limitations because of those differences.

First, the effects of aging and of seasonal variations have not been quantified in the results included in this report because the models were calibrated using HVS tests of relatively short duration. Seasonal variation of unbound layers' stiffness can be input in *CalME* by the user, and can be taken from typical patterns measured in the field. Aging and seasonal variation affect asphalt concrete stiffnesses at the same time that damage is occurring. Aging increases stiffness, although deflection measurements in the field show that the net effect of aging and damage is an overall decrease in stiffness with accumulating traffic loads. Field calibration is required to evaluate the difference in response between the field pavement and the incremental-recursive simulation that should be attributed to aging. It is likely that the effect of aging can be dealt with through shift factors.

Second, neither the effects of rest periods between loadings nor of faster traffic have been included in the calibration. It is expected that rest periods and different trafficking patterns will result in different shift factors.

Third, moduli from frequency sweep data, triaxial tests, FWD tests, and MDD deflections used in this study are similar but not identical. The NCHRP 1-37A study proposes relying primarily on triaxial testing to characterize stiffnesses for flexible pavement layers and for permanent deformation parameters for asphaltic materials. Because the majority of work to be performed by Caltrans over the next several decades will involve rehabilitation and reconstruction, with some addition of lane capacity, the research team recommends that the most practical and economical methods for characterizing materials for Caltrans will be:

1. Backcalculating stiffnesses of existing pavement layers using FWD data,
2. Using flexural frequency sweep data to develop master stiffness curves of new asphaltic materials and for default values of materials for which test data are already available,
3. Using flexural fatigue data for damage parameters, for fatigue and reflection cracking of new asphaltic materials, and for default values of materials for which test data are already available,
4. Using repeated shear test data for permanent deformation parameters for new asphaltic materials, or default values of materials for which test data are already available, and
5. Using default values from previous backcalculation for stiffnesses of new unbound layers based on soil classification and achievement of required compaction.

Use of these methods to predict stiffnesses in field pavements in order to simulate field pavements needs to be evaluated with the *CalME* Incremental-Recursive models.

Following are the recommended next steps to develop these models:

1. Perform a sensitivity analysis using "typical" values for properties and climate in the database established to date, and tie these results to *CalME* with the Classical (Asphalt Institute MS-1 equations), Incremental (Miner's Law), and Incremental-Recursive methods to evaluate reasonableness of sensitivity.
2. Validate the recommended methods for characterizing flexible pavement materials, listed above, in conjunction with the models described in this report by comparing simulated and actual performance from mainline highway case studies and full-speed, test track data, such as WesTrack and NCAT track.

3. Address the variability of the input parameters (moduli, thicknesses, traffic loading, etc.) and uncertainty on the damage models. It is expected that the sensitivity analyses will identify the most important variables controlling expected performance. Employing a Monte Carlo simulation using those critical variables is one possibility that should be explored. An alternative is to estimate typical variability of performance in the field by drawing on available literature, then incorporating a factor for the uncertainty of design life. The NCHRP 1-37A report takes this approach. Another possible alternative would be a combined approach that uses simulation for the truly unknown variables, including traffic and weather, and a statistically derived distribution for the within project variables created by variations in materials and construction.
4. Make final decisions regarding use of cemented layers in the flexible pavement structure, then calibrate. It is generally recommended that “semi-rigid” pavements, in which asphalt concrete is placed directly on cement-treated base (CTB) or lean concrete base (LCB), not be used because of the relatively quick reflection of shrinkage cracks. However, because Caltrans has used semi-rigid pavements in the past and they remain in the current design method, it is therefore important to have models for the response and performance of these layers. Models for fatigue and crushing of these materials can be evaluated using APT data from Louisiana and from field data taken at mainline sections in California. The models in the NCHRP 1-37A report can be the starting point for such a validation-and-calibration exercise.

8.0 REFERENCES

1. Bejarano, M. O., Harvey, J. T., Ali, A., Mahama, D., Hung, D., and Preedonant, P. December 2001 (Revision December 2004). Performance of drained and undrained flexible pavement structures under wet conditions: Accelerated test data, test section 545, undrained. (Draft report prepared for the California Department of Transportation.) UC Pavement Research Center, Institute of Transportation Studies, University of California: Davis and Berkeley.
2. Bejarano, M. O., Harvey, J. T., Ali, A., Mahama, D., Hung, D., and Preedonant, P. December 2001 (Revision May 2004). Performance of drained and undrained flexible pavement structures under wet conditions: Test data from accelerated pavement test section 544, undrained. (Draft report prepared for the California Department of Transportation.) UC Pavement Research Center, Institute of Transportation Studies, University of California: Davis and Berkeley.
3. Bejarano, M. O., Harvey, J. T., Ali, A., Mahama, D., Hung, D., and Preedonant, P. March 2003. Performance of drained and undrained flexible pavement structures in accelerated loading under wet conditions. Summary Report, Goal 5 Partnered Pavement Performance Program. (Draft report prepared for the California Department of Transportation.) UC Pavement Research Center, Institute of Transportation Studies. University of California: Davis and Berkeley.
4. Bejarano, M. O., Harvey, J. T., Ali, A., Russo, M., Mahama, D., Hung, D., and Preedonant, P. December 2001 (Revision February 2004). Performance of drained and undrained flexible pavement structures under wet conditions: Test data from accelerated pavement test section 543, drained. (Draft report prepared for the California Department of Transportation.) UC Pavement Research Center, Institute of Transportation Studies, University of California: Davis and Berkeley.
5. Bejarano, M., Morton, B., and Scheffy, C. August 2005. Summary of construction activities and results from six initial accelerated pavement tests conducted on asphalt concrete pavement section for modified-binder overlay. (Draft report prepared for the California Department of Transportation.) UC Pavement Research Center, Institute of Transportation Studies, University of California: Davis and Berkeley.
6. Deacon, J.A, Harvey, J.T., Guada, I., Popescu, L., and Monismith, C.L. 2002. Analytically based approach to rutting prediction. *Transportation Research Record 1806*. Washington D.C.
7. de Beer, M., and Fisher, C. 1997 Contact stresses of pneumatic tires measured with the vehicle-road surface pressure transducer array (VRSPTA) system. Report for the University of California at Berkeley (UCB) and the Nevada Automotive Test Center (NATC). Transportek, CSIR. Pretoria, South Africa.
8. Harvey, J. T., Bejarano, M., Fantoni, A., Heath, A., Shin, H. C. December 2000. Performance of Caltrans asphalt concrete and asphalt-rubber hot mix overlays at moderate temperatures: Accelerated pavement testing evaluation. Draft report prepared for the California Department of Transportation. UC Pavement Research Center, Institute of Transportation Studies, University of California: Berkeley and Davis.
9. Harvey, J., Coetzee, N., and Louw, L. November 1999. CAL/APT Program: Construction of the goal 3 overlays and recommendations for improved overlay performance in California. Report prepared for the California Department of Transportation. UC Pavement Research Center, CAL/APT Program, Institute of Transportation Studies, University of California: Davis and Berkeley.
10. Harvey, J. T., du Plessis, L., Long, F., Deacon, J. A., Guada, I., Hung, D. and Scheffy, C. June 1997. CAL/APT Program: Test results from accelerated pavement test on pavement structure containing asphalt treated permeable base (ATPB), section 500RF. Report No. RTA-65W485-3, prepared for

- the California Department of Transportation. UC Pavement Research Center, CAL/APT Program, Institute of Transportation Studies, University of California: Davis and Berkeley.
11. Harvey, J. T., du Plessis, L., Long, F., Shatnawi, S., Scheffy, C., Tsai, B-W., Guada, I., Hung, D., Coetzee, N., Reimer, M., and Monismith, C. L. June 1996. Initial CAL/APT Program: Site information, test pavement construction, pavement materials characterizations, initial CAL/APT test results, and performance estimates. Report no. RTA-65W485-3, prepared for the California Department of Transportation. UC Pavement Research Center, CAL/APT Program, Institute of Transportation Studies, University of California: Davis and Berkeley.
 12. Harvey, J., Guada, I., and Long, F. 2000. Effects of material properties, specimen geometry, and specimen preparation variables on asphalt concrete tests for rutting. *Asphalt Paving Technology* 69: 236.
 13. Harvey, J., Guada, I., Scheffy, C., Louw, L., Prozzi, J., and Hung, D. February 1998. CAL/APT Program: Test results from accelerated pavement test on pavement structure containing asphalt treated permeable base, section 502CT. Draft report submitted to California Department of Transportation. UC Pavement Research Center, CAL/APT Program, Institute of Transportation Studies, University of California: Davis and Berkeley.
 14. Harvey, J., Hung, D., Prozzi, J., Louw, L., Scheffy, C., and Guada, I. December 1997. CAL/APT Program: Test results from accelerated pavement test on pavement structure containing untreated aggregate base, section 503RF. Draft report submitted to California Department of Transportation. UC Pavement Research Center, CAL/APT Program, Institute of Transportation Studies, University of California: Davis and Berkeley.
 15. Harvey, J., Long, F., and Prozzi, J. A. 1999. Application of CAL/APT results to long life flexible pavement reconstruction. 1999 Accelerated Pavement Testing International Conference. Nevada: Reno.
 16. Harvey, J. and Popescu, L. January 2000. Rutting of Caltrans asphalt concrete and asphalt-rubber hot mix under different wheels, tires, and temperatures: Accelerated pavement testing evaluation. Draft report prepared for California Department of Transportation. UC Pavement Research Center, CAL/APT Program, Institute of Transportation Studies, University of California: Davis and Berkeley.
 17. Harvey, J., Prozzi, J., Deacon, D., Hung, D., Guada, I., du Plessis, L., Long, F., and Scheffy, C. April 1999. CAL/APT Program: Test results from accelerated pavement test on pavement structure containing aggregate base (AB), section 501RF. Report prepared for the California Department of Transportation. Pavement Research Center, CAL/APT Program, Institute of Transportation Studies, University of California: Davis and Berkeley.
 18. Harvey, J. T., Roesler, J., Coetzee, N. F., and Monismith, C. L. June 2000. CAL/APT Program Summary Report: Six Year Period, 1994-2000. Report number FHWA/CA/RM-2000/15. Prepared for California Department of Transportation. UC Pavement Research Center, CAL/APT Program, Institute of Transportation Studies, University of California: Davis and Berkeley.
 19. Harvey, J., Tsai, B-W., Long, F., and Hung, D. June 1999. CAL/APT Program: Asphalt treated permeable base (ATPB), laboratory tests, performance predictions and evaluation of Caltrans and other agencies' experience. Report prepared for the California Department of Transportation. UC Pavement Research Center, CAL/APT Program, Institute of Transportation Studies, University of California: Davis and Berkeley.
 20. Hornyk, P. and Gérard, A. January 1999. *A pneumatic repeated load triaxial apparatus for unbound granular materials and subgrade soils*. Proceedings of an International Workshop on Modelling and Advanced Testing for Unbound Granular Materials. Gomes Correia, A. and Balkema, A.A., eds. Lisbon.

21. National Cooperative Highway Research Program (NCHRP). July 1985. *Proposed AASHTO Guide for Design of Pavement Structures*. Project 20-7/24.
22. National Cooperative Highway Research Program (NCHRP). March 2004. *Guide for Mechanistic-Empirical Design of New and Rehabilitated Pavement Structures*. National Cooperative Highway Research Program, Report 1-37A.
23. Tsai, B., Harvey, J., and Monismith, C. 2002. *WesTrack Fatigue Performance Prediction Using Miner's Law*. Transportation Research Record 1809: 137–147.
24. Tsai, B., Harvey, J., and Monismith, C. 2002. *High Temperature Fatigue and Fatigue Damage Process of Aggregate-Asphalt Mixes*. Asphalt Paving Technology: Vol. 71, pp 345-385.
25. Ullidtz, P. 2002. Analytical tools for pavement design. Proceedings of the Ninth International Conference on Asphalt Pavements. Copenhagen.
26. Ullidtz, P. 2005. A Simple Model for Pavement Damage. Paper accepted for publication by the Transportation Research Board, National Research Council, Washington, D.C., 2005.
27. Wu, R-Z. 2005. Finite Element Analyses of Reflective Cracking in Asphalt Concrete Overlays. Doctoral dissertation. Department of Civil and Environmental Engineering, University of California, Berkeley.
28. Tia, M., Rogue, R., Sirin, O. and Kim, H-J. 2002 “Evaluation of Superpave Mixtures with and without Polymer Modification by Means of Accelerated Pavement Testing.” Final report, University of Florida.

9.0 APPENDIX

9.1 Glossary

A

Accelerated Pavement Testing (APT)
aggregate base (AB)
aggregate subbase (ASB)
asphalt concrete (AC)
asphalt rubber hot-mix gap-graded (ARHM-GG)
asphalt-treated permeable base (ATPB)

C

California Department of Transportation (Caltrans)
cement-treated base (CTB)

D

dense-graded asphalt concrete (DGAC)
Distinct Element Method (DEM)

E

Equivalent Single Axle Load (ESAL)

F

Falling Weight Deflectometer (FWD)

Finite Element Method (FEM)

Field Mix Field Compacted (FMFC)

H

Heavy Vehicle Simulator (HVS)

L

Layered Elastic Analysis Program (LEAP)

lean concrete base (LCB)

ln logarithm to base e (natural logarithm)

log logarithm to base 10

M

Mechanistic-Empirical (ME)

Mechanistic-Empirical (ME) design

Mechanistic-Empirical Design Guide (MEPDG)

moisture content (MC)

modified binder (MB)

Multi-depth Deflectometer (MDD)

N

NCHRP 1-37A Design Guide (NCHRP 2004)

P

Pavement Management System (PMS)

R

Road Surface Deflectometer (RSD)

Repeated Simple Shear Tests at Constant Height (RSST-CH)

root-mean square (RMS)

S

sdf standard deviation factor (10 raised to the standard deviation of the logarithms of the values)

U

Unified Soil Classification System (USCS)

University of California Pavement Research Center (UCPRC)

9.2 List of Units

°C degree Celcius, centigrade
cm centimeter (0.001 m)
cPoise centi Poise (0.1 Pa×sec)
g/cm³ gram per cubic cm
Hz Hertz, oscillations per second
°K degree Kelvin (as °C but counted from absolute zero)
km/h kilometer per hour
kN kilo Newton (1,000 N)
kPa kilo Pascal (1,000 Pa)
MPa Mega Pascal (one million Pa)
msec millisecond
μstrain micro strain (10⁻⁶ m/m)
N Newton
°R degree Rankine (as Fahrenheit but counted from absolute zero)
sec second

9.3 List of Parameters in Equations

α , β , γ , δ , λ , α_A , α_B , α_C , α_D , β_A , β_B , and β_C are used to denote constants, which may be different from one equation to another (in CalME forms the Greek letters are spelled alfa, beta, gamma, delta, and lambda)

γ^e elastic shear strain

γ^i inelastic (plastic) shear strain

θ bulk stress

σ_d deviator stress

τ shear stress

τ_{oct} octahedral shear stress

$\mu\epsilon$ strain in μstrain

ν Poisson's ratio

ω damage

A constant in viscosity versus temperature relationship

aTg power on viscosity in reduced time relationship

C constant in non-linear modulus relation for cohesive soils

d deflection

E modulus
 E_{AC} modulus of AC
 E_i initial modulus (with no damage), or modulus of layer i
 E_{max} maximum modulus
 E_{min} minimum modulus
 E_o modulus of unbound layer at reference stiffness of above layers
 $E_{40\text{ kN}}$ modulus at a wheel load of 40 kN
 E_p modulus at a wheel load of P
 h_i thickness of layer i
 I_1 first stress invariant
 J_2 second deviator stress invariant
K calibration factor between rut depth and inelastic shear strain
 k_1 , k_2 , and k_3 constants in non-linear relation for unbound materials
 t loading time, corresponding to creep test
MN number of load applications in million
N number of load applications
n power in non-linear modulus relation for cohesive soils
P wheel load
p mean normal stress ($I_1/3 = \theta/3$)
 p_a atmospheric pressure
q mean deviator stress
 $resp_{ref}$ reference response
 rd_{AC} rut depth in AC
S stiffness
 S_{ref} reference stiffness
SR stiffness ratio (E/E_i)
 t_r reduced time
visc viscosity
 $visc_{ref}$ viscosity at reference temperature
VTS viscosity temperature susceptibility
w internal energy density

9.4 Parameter Values Used in Simulations

Master curve $\log(E)=\delta+\alpha/(1+\exp(\beta+\gamma*\log(tr)))$

Reference temperature 20°C, frequency sweep data. Viscosity parameters $A = 9.6307$ (in °K) and $VTS = -3.5047$.

Name	E delta	E beta	E gamma	aT g	Reference modulus
ATPB	2.3010	-0.2400	1.0000	1.0000	1144
DGAC-G1-Bot	2.3010	-0.4007	0.9807	1.2824	11172
DGAC-G1-Top	2.3010	-0.3987	0.9436	1.3529	9038
DGAC-G3	2.3010	-0.1790	0.8840	1.1770	7653
DGAC-G9	2.3010	-0.3032	0.8931	1.3370	7371
RAC-G	2.3010	-0.0841	0.9890	1.0080	4755

Fatigue and unbound layers rutting parameters

$dam = A*MN^{\alpha}*(\epsilon/200)^{\beta}*(E/3000)^{\gamma}*\exp(\delta*t)$

where dam is the damage, either fatigue damage or vertical rut depth.

Name	Ft A	Ft alfa	Ft beta	Ft gamma	Ft delta
DGAC-G1-Top	0.001536	0.8695	4.1968	2.0984	0.1619
DGAC-G1-Bot	0.001245	0.8399	3.9718	1.9859	0.1913
DGAC-G3	0.008700	0.6874	3.2920	1.6460	0.1453
DGAC-G9	0.007357	0.4945	2.0612	1.0306	0.1263
RAC-G	0.018560	0.5911	2.9198	1.4599	0.1371

For the permanent deformation of the unbound layers the parameters were: $A = 1.1$ for subgrade and 0.8 for base and subbase, $\alpha = 0.333$, $Respref = 1000$ μ strain instead of 200, $\beta = 1.333$, $Eref = 40$ MPa instead of 3000, and $\gamma = 0.333$.

Permanent deformation of asphalt concrete

For Goal 1 and Goal 3 simulations a Gamma function was used, with parameters shown below.

Name	Pd A	Pd alfa	Pd beta	Pd gamma
DGAC-G1-Top	-1.316	5.218	1.03	2.86
DGAC-G1-Bot	-1.316	5.218	1.03	2.86
DGAC-G3	-0.568	4.208	1.03	2.47

For Goal 9 a power function was used:

$rd = 7*layer\ thickness\ mm*MN^{0.208}*\exp(1.03*shear\ stress/0.1\ MPa)*elastic\ shear\ strain.$

9.5 Section 569RF Simulated with a CTB Model from an HVS Nordic Experiment.

In the Goal 9 experiments the aggregate base was 100 percent recycled material with a high content of recycled portland cement concrete. The backcalculated moduli of the base layer were shown in Figure 226, which has been reproduced below for convenience.

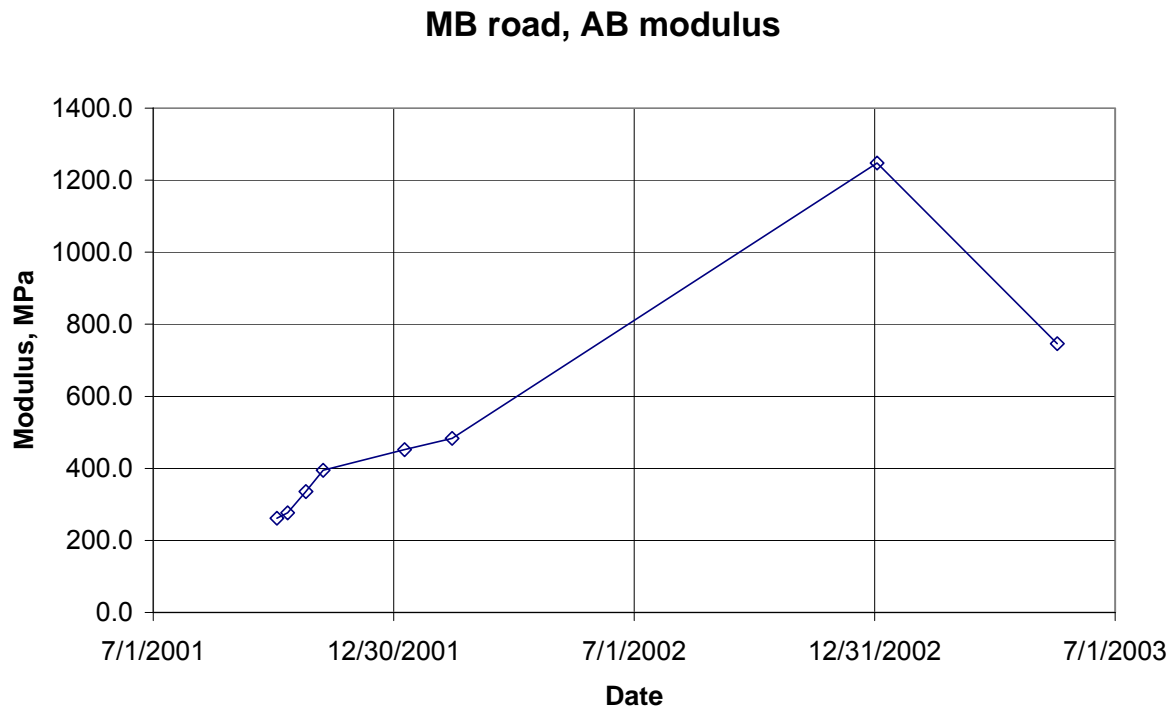


Figure 275. Modulus of AB layer backcalculated from FWD tests in center line.

The HVS test on Section 569RF was carried out from 03/25/2003 to 04/07/2003. During this period the backcalculated modulus of the AB was between 800 MPa and 1,200 MPa. Such a high modulus must be due to self-cementing of the layer. During the HVS test the surface deflection dropped rapidly, indicating that it might be necessary to simulate the layer as a lightly cemented aggregate base.

An incremental-recursive model for cement-treated base (CTB) materials was developed by C. Busch (Thogersen et al. 2004). The model is based on six HVS tests carried out in Southern Sweden using the HVS Nordic equipment, on three different CTB materials. Replicate sections were available for each material and one of the sections, for each material, was instrumented with stress and strain gauges for monitoring the response during the test. FWD tests were carried out before and after the tests and LWD (Light Weight Deflectometer) tests were done during the HVS testing. Two of the materials were based on a 0/16 mm gravel with target strengths (28 days, unconfined compressive) of 8 MPa and 4 MPa, respectively, and the third was based on a 0/8 mm sand, with a target strength of 4 MPa. The cement content ranged from 60 kg/m³ to 100 kg/m³. All materials had an addition of 331 kg/m³ of limestone powder.

The model developed is described as (quotation from page 41):

The final incremental-recursive model then becomes

$$\omega = \left(\frac{N}{10^6} \right)^\alpha \times \left(\frac{\varepsilon}{\varepsilon_{REF}} \right)^\beta \times (1 - \omega)^\gamma$$

where:

N is the number of load repetitions,

ε is the maximum horizontal strain in the bottom of the stabilised layer

and the constants are as follows:

$$\alpha = 0.25$$

$$\beta = 0.25 + 0.90 \times (E_{INITIAL}/10,000 \text{ MPa})$$

$$\gamma = 0.05 + 0.90 \times (E_{INITIAL}/10,000 \text{ MPa})$$

$$\varepsilon_{REF} = 45 \text{ } \mu\text{str}$$

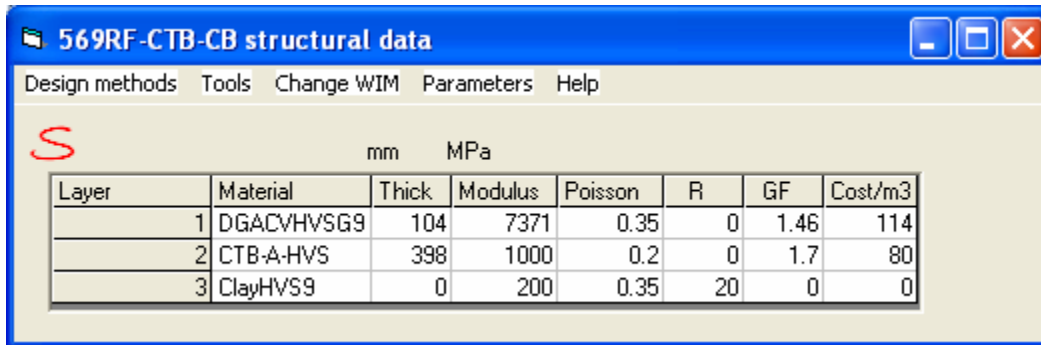
For deterministic design purposes (see section 8), a central model is not always satisfactory, since some measure of safety is normally required. Normal Danish design models are based on 25% percentiles of E-moduli for the pavement layers, i.e 75% of the initial E-moduli will be above the design values. If a similar line of reasoning is applied to the incremental-recursive model, it should predict values, where only 25% of the measurements from the FWS sections fall below the prediction. This objective can be achieved by reducing the α -value to 0.19.

With an initial CTB modulus assumed to be 1,000 MPa one gets $\beta = 0.34$ and $\gamma = 0.14$. The best agreement with the measured response was obtained using the α -value of 0.19 corresponding to the 25th percentile modulus. Equation 6 can then be written as:

$$\omega = MN^{0.19} \times \left(\frac{\mu\varepsilon}{-45 \text{ } \mu\text{strain}} \right)^{0.34} \times \left(\frac{E}{1000 \text{ MPa}} \right)^{0.14} \quad (34)$$

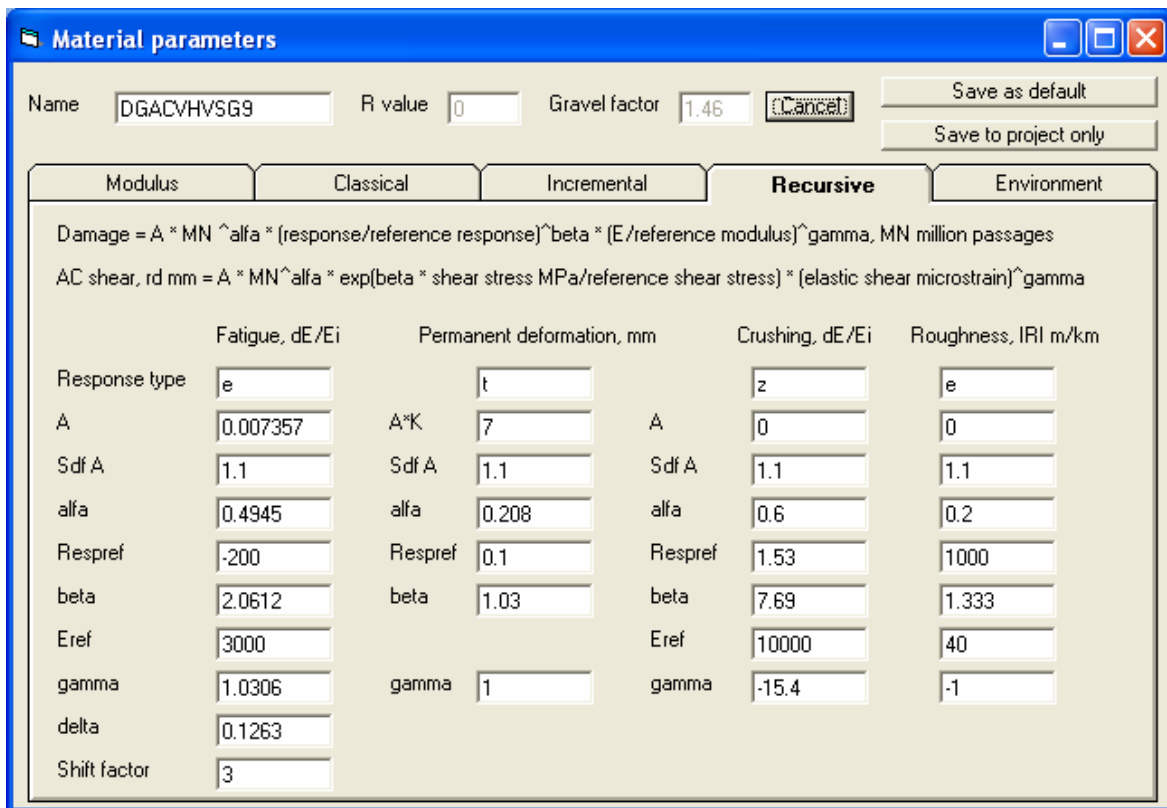
Equation 34

The pavement structure used in the simulation is shown in Figure 276, and the parameters for DGAC and CTB in Figure 277 Figure 278, respectively.



Layer	Material	Thick	Modulus	Poisson	R	GF	Cost/m3
1	DGACVHVSG9	104	7371	0.35	0	1.46	114
2	CTB-A-HVS	398	1000	0.2	0	1.7	80
3	ClayHVS9	0	200	0.35	20	0	0

Figure 276. Pavement structure for Section 569RF.



Name: DGACVHVSG9 R value: 0 Gravel factor: 1.46

Modulus Classical Incremental **Recursive** Environment

Damage = $A * MN^{\alpha} * (\text{response/reference response})^{\beta} * (E/\text{reference modulus})^{\gamma}$, MN million passages
 AC shear, rd mm = $A * MN^{\alpha} * \exp(\beta * \text{shear stress MPa}/\text{reference shear stress}) * (\text{elastic shear microstrain})^{\gamma}$

	Fatigue, dE/Ei	Permanent deformation, mm	Crushing, dE/Ei	Roughness, IRI m/km
Response type	e	t	z	e
A	0.007357	A*K 7	A 0	0
Sdf A	1.1	Sdf A 1.1	Sdf A 1.1	1.1
alfa	0.4945	alfa 0.208	alfa 0.6	0.2
Respref	-200	Respref 0.1	Respref 1.53	1000
beta	2.0612	beta 1.03	beta 7.69	1.333
Eref	3000		Eref 10000	40
gamma	1.0306	gamma 1	gamma -15.4	-1
delta	0.1263			
Shift factor	3			

Figure 277. Damage parameters used for DGAC of Section 569RF.

Material parameters

Name: R value: Gravel factor:

	Modulus	Classical	Incremental	Recursive	Environment
Damage = $A * MN^{\alpha} * (\text{response}/\text{reference response})^{\beta} * (E/\text{reference modulus})^{\gamma}$, MN million passages					
AC shear, rd mm = $A * MN^{\alpha} * \exp(\beta * \text{shear stress MPa}/\text{reference shear stress}) * (\text{elastic shear microstrain})^{\gamma}$					
	Fatigue, dE/Ei	Permanent deformation, mm		Crushing, dE/Ei	Roughness, IRI m/km
Response type	<input type="text" value="e"/>	<input type="text" value="z"/>		<input type="text" value="z"/>	<input type="text" value="e"/>
A	<input type="text" value="1"/>	A*K <input type="text" value="0.8"/>	A	<input type="text" value="0"/>	<input type="text" value="0"/>
Sdf A	<input type="text" value="1.1"/>	Sdf A <input type="text" value="1.1"/>	Sdf A	<input type="text" value="1.1"/>	<input type="text" value="1.1"/>
alfa	<input type="text" value="0.19"/>	alfa <input type="text" value="0.333"/>	alfa	<input type="text" value="1"/>	<input type="text" value="1"/>
Respref	<input type="text" value="-45"/>	Respref <input type="text" value="1000"/>	Respref	<input type="text" value="1.7"/>	<input type="text" value="664"/>
beta	<input type="text" value="0.34"/>	beta <input type="text" value="1.333"/>	beta	<input type="text" value="7.69"/>	<input type="text" value="4"/>
Eref	<input type="text" value="1000"/>	Eref <input type="text" value="40"/>	Eref	<input type="text" value="2000"/>	<input type="text" value="160"/>
gamma	<input type="text" value="0.14"/>	gamma <input type="text" value="0.333"/>	gamma	<input type="text" value="-15.4"/>	<input type="text" value="0"/>
delta	<input type="text" value="0"/>				
Shift factor	<input type="text" value="1"/>				

Figure 278. Damage parameters used for CTB of Section 569RF.

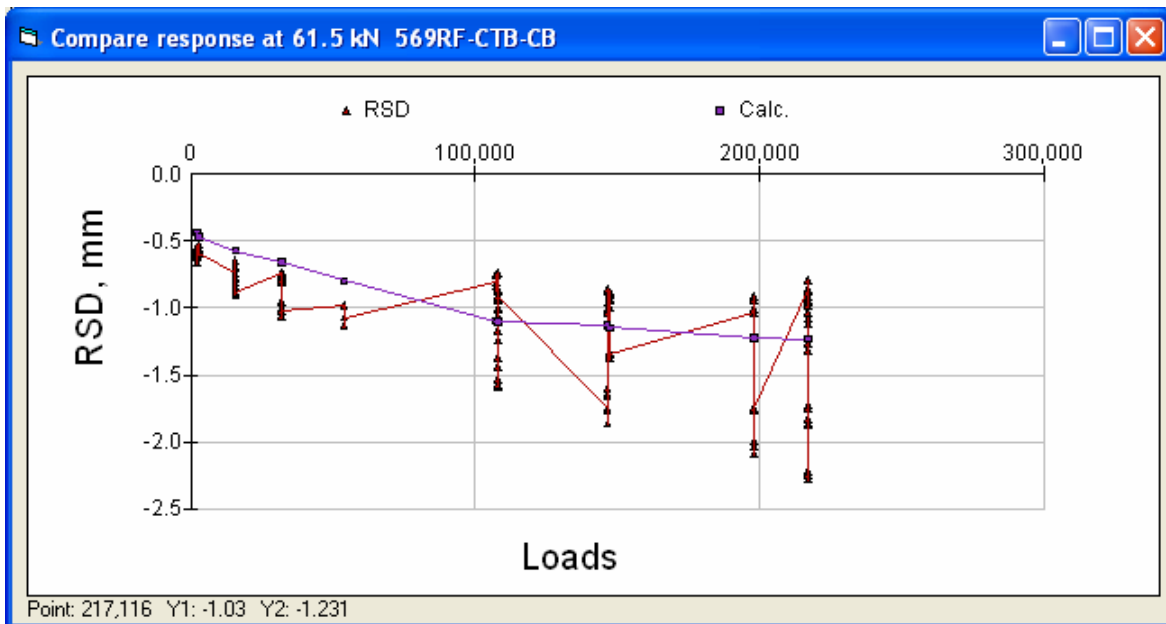


Figure 279. Section 569RF Road Surface Deflectometer.

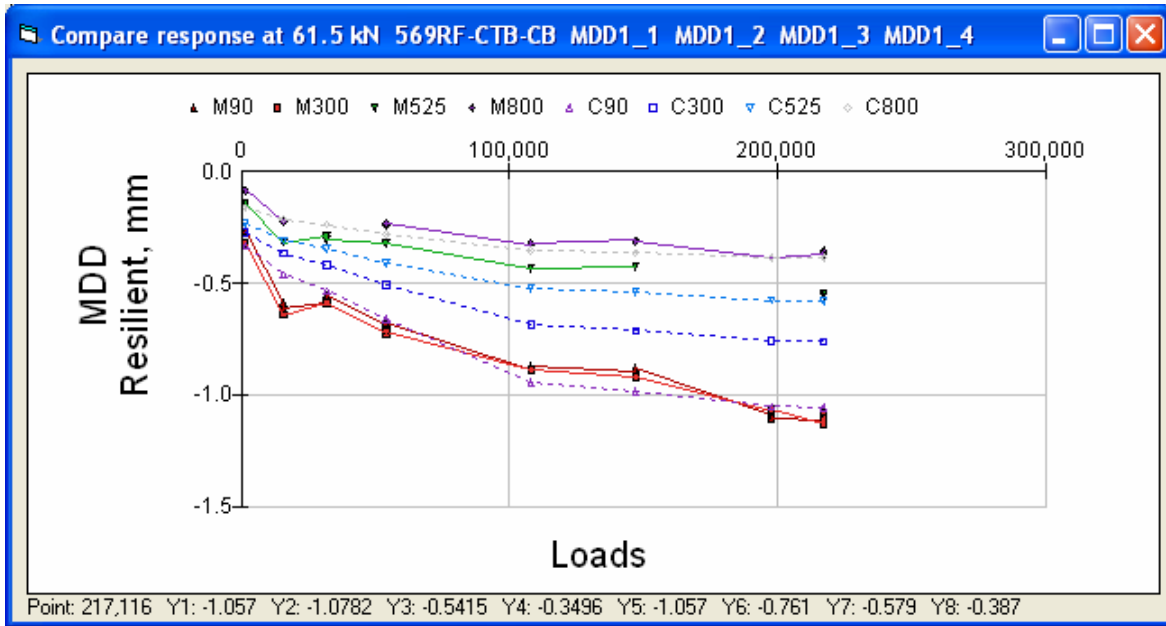


Figure 280. Section 569RF MDD resilient deflections.

The simulated response is seen to be surprisingly close to the measured response in Figure 279 and Figure 280, except for the MDD at a depth of 300 mm where the measured value is slightly higher than the deflection measured at a depth of 90 mm.

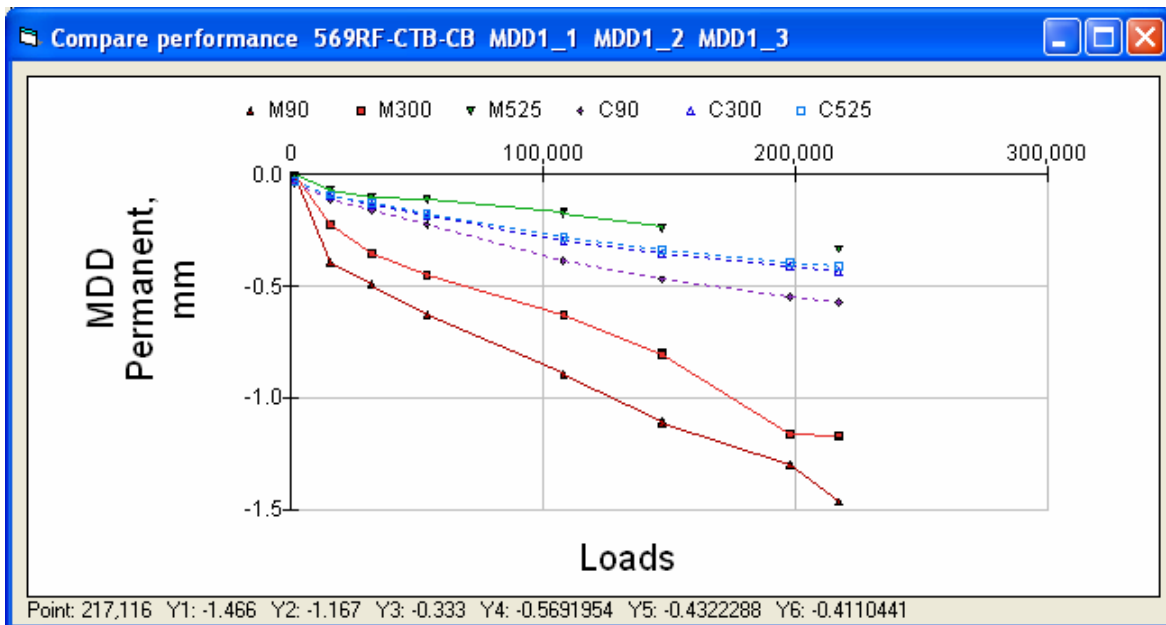


Figure 281. Section 569RF permanent MDD deformations.

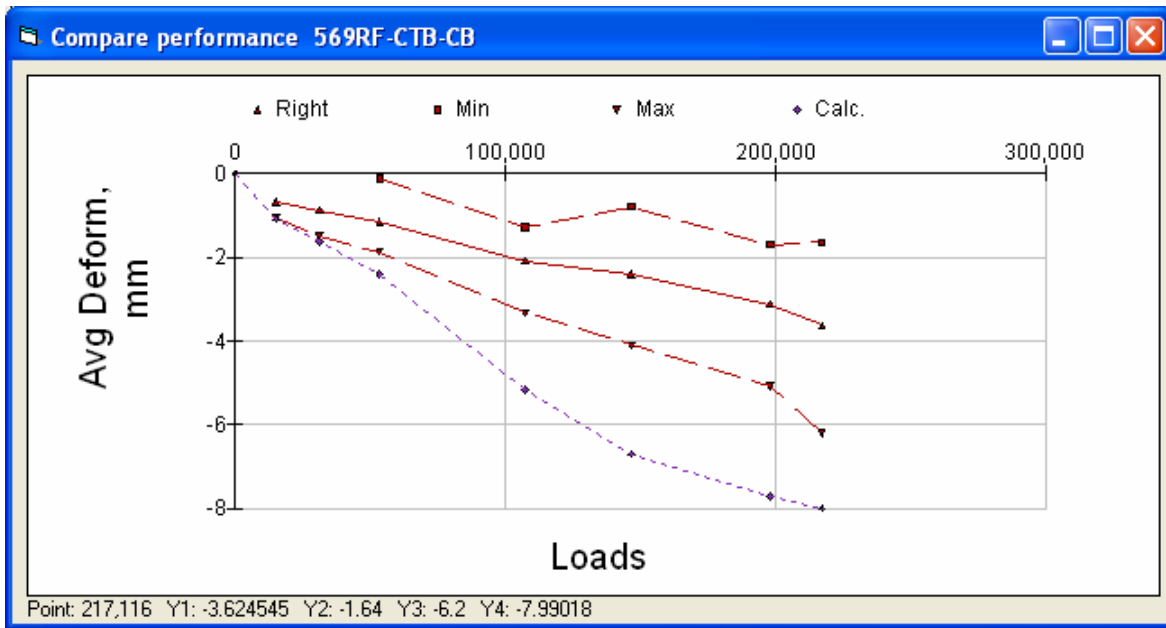


Figure 282. Section 569RF average permanent deformation from pavement profile.

The permanent deformation on top of the CTB is underestimated whereas it is overestimated on the top of the asphalt, as shown in Figure 281 Figure 282. Had the gamma function derived for the Goal 3 DGAC for prediction of the AC permanent deformation been used instead of the power function, then the predicted permanent deformation of the asphalt would have been even larger.

Reference:

Thogersen, F., Busch, C., and Henrichsen, A. "Mechanistic Design of Semi-Rigid Pavements – An Incremental Approach," Report 138, Danish Road Institute, 2004.

<http://www.vejdirektoratet.dk/publikationer.asp?page=document&objno=73973>